

APPENDIX D

SUMMARIES

PVHA FIELD TRIPS

9607100283 -
PART 2

APPENDIX D

SUMMARY - CRATER FLAT FIELD TRIP D-1

SUMMARY - SLEEPING BUTTE/LATHROP WELLS FIELD TRIP D-4

**SUMMARY
CRATER FLAT FIELD TRIP
PROBABILISTIC VOLCANIC HAZARD ANALYSIS PROJECT
YUCCA MOUNTAIN, NEVADA**

March 29, 1995

The field trip to Crater Flat was organized at the request of the expert panel members, who wanted to observe first hand the volcanic geology and structural elements of the Crater Flat basin. The primary goal of the field trip was to provide the expert panel members an opportunity to form their own interpretations regarding the spatial, temporal, and physical aspects of the Crater Flat volcanic centers. The field trip was led by several earth scientists who have carried out extensive mapping and/or research of the geology in the Crater Flat area. The field trip stops and presentations were made at locations where key outcrops of the local geology could be observed. The presentations given by the field trip leaders focused on their interpretations of the spatial, temporal, and structural aspects of the local and/or regional geology of the Crater Flat basin. A copy of the field trip itinerary is included with this summary. This itinerary was modified slightly during the course of the day.

A meeting was held the evening before the field trip to review the geologic setting of the region, and to discuss the field trip itinerary.

Stop 1: I-95 (near the southern end of Bare Mountain)

Chris Fridrich (U.S. Geological Survey [USGS]) presented an overview of Basin and Range extensional tectonics. He discussed the Cenozoic tectonic evolution of the Yucca Mountain region, and the implications for structural controls on volcanism in the Crater Flat basin.

Frank Perry (Los Alamos National Laboratory [LANL]) then gave a brief presentation on the late Cenozoic basalt chronology of the region.

Stop 2: Steve's Pass

Chris Fridrich presented an overview of his tectonic pull-apart model of the Crater Flat basin. George Thompson (Stanford University) then reviewed the USGS seismic line across the Crater Flat basin. He discussed the structural character of the basin based on his interpretation of the seismic line, and he also discussed the significance of the Bare Mountain fault.

Stop 3: Red Cone

Gene Smith (University of Nevada, Las Vegas) presented his geologic mapping of Red Cone. He led the field trip participants to a number of outcrops on and adjacent to the cone, and discussed his geologic interpretations at each. Included in the discussions was his interpretation of vents, and vent alignments on the cone. Frank Perry then presented and discussed $^{40}\text{Ar}/^{39}\text{Ar}$ age dates and geochemical data from the cone. Chuck Connor (Center for Nuclear Waste Regulatory

Analyses [CNWRA]) gave a brief presentation on the results of a ground magnetometer experiment by the CNWRA to explore the existence of subsurface dike connecting Red and Black cones. He stated that the resolution of their data did not allow an interpretation for or against the presence of a dike.

Stop 4: Black Cone

Gene Smith presented his geologic mapping and interpretations of Black Cone. He also presented geochemical data that he interprets as evidence that Black Cone and Red Cone were derived from different magma sources. Frank Perry presented and discussed the $^{40}\text{Ar}/^{39}\text{Ar}$ age dates and geochemical data from Black Cone.

Stop 5: Trench 8 (Solitario Canyon fault)

Chris Menges (USGS) gave an overview of the stratigraphy and structures exposed in the exploratory trench excavated across the Solitario Canyon fault. His discussion focused on the significance of an ash deposit that was discovered in a fissure adjacent to the main fault in the trench exposure, and the temporal relationship between faulting events and volcanic activity in the region. Frank Perry, along with Chris Menges, discussed the age and chemistry of the ash, and its correlation with the volcanic centers in Crater Flat.

Stop 6: Southeast (3.7 Ma) Crater Flat

Frank Perry and Bruce Crowe (LANL) gave an overview of the basalts in southeast Crater Flat. Frank Perry discussed the geochemistry and how it differs from the younger centers in Crater Flat. Bruce Crowe discussed dike geometry and orientations of the 3.7 Ma area.

**CRATER FLAT
 MARCH 29, 1995 FIELD TRIP PARTICIPANTS**

NAME	AFFILIATION
Lynn Bowker	Los Alamos National Laboratory
Richard W. Carlson	Carnegie Institution of Washington
Karen Carter	Los Alamos National Laboratory
Chuck B. Connor	Center for Nuclear Waste Regulatory Analyses
Kevin Coppersmith	Geomatrix
Todd Crampton	Geomatrix
Bruce Crowe	Los Alamos National Laboratory
Terry Crump	TRW
Wendell A. Duffield	U.S. Geological Survey
Kean Finnegan	Los Alamos National Laboratory
Richard V. Fisher	University of California
Chris Fridrich	U.S. Geological Survey
Sandra Green	Eureka County Information Center
William R. Hackett	WRH Associates
Brittain E. Hill	Center for Nuclear Waste Regulatory Analyses
William J. Hinze	ACNW/Nuclear Regulatory Commission
Mel A. Kuntz	U.S. Geological Survey
Alexander R. McBirney	University of Oregon (Emeritus)
Chris Menges	U.S. Geological Survey
Peter A. Morris	Applied Decision Analysis
Stephen T. Nelson	Woodward-Clyde Federal Services
Jeanne C. Nesbit	U.S. Department of Energy
Roseanne C. Perman	Geomatrix
Frank Perry	Los Alamos National Laboratory
John Perry	Nye County
Michael F. Sheridan	State University of New York, Buffalo
Eugene I. Smith	University of Nevada
Richard P. Smith	Idaho National Engineering Laboratory
J. Carl Stepp	Woodward-Clyde Federal Services
George A. Thompson	Stanford University
John Trapp	U.S. Nuclear Regulatory Commission
George P.L. Walker	University of Hawaii
Gene Yogodzinski	University of Nevada

SUMMARY
SLEEPING BUTTE/LATHROP WELLS FIELD TRIP
PROBABILISTIC VOLCANIC HAZARD ANALYSIS PROJECT
YUCCA MOUNTAIN, NEVADA

April 25 and 26, 1995

A two day field trip to the Sleeping Butte and Lathrop Wells volcanoes was organized at the request of the expert panel members, who wanted to observe first hand the volcanic geology at each of the volcanic centers, particularly at the Lathrop Wells cone. The primary goal of the field trip was to provide the expert panel members an opportunity to form their own interpretations regarding the spatial, temporal, and physical aspects of the Sleeping Butte and Lathrop Wells volcanic centers. The Lathrop Wells volcano was visited on the first day of the trip and the Sleeping Butte volcanoes on the second day. The field trip was led by several earth scientists who have carried out extensive mapping and/or research of the geology of the two areas. The field trip stops and presentations were made at locations where key outcrops of the local geology could be observed. The presentations given by the field trip leaders focused on their interpretations of the spatial, temporal, and physical aspects of the local and/or regional geology of the Sleeping Butte or Lathrop Wells area. A copy of the Lathrop Wells scheduled field itinerary is included with this summary; a printed itinerary for the Sleeping Butte field trip was not prepared.

A meeting was held the evening before the Lathrop Wells field trip to review the geologic investigations conducted at the Lathrop Wells volcanic center. Several short presentations were made in preparation for the field visit.

DAY 1 - LATHROP WELLS VOLCANIC CENTER

Stop 1: East Quarry

Bruce Crowe and Frank Perry (Los Alamos National Laboratory) gave an overview of the chemical and physical properties of their Qs3 and Qs4 tephra units exposed in a bulldozer cut. The two units are separated by soil horizons, which were identified and described by Les McFadden (University of New Mexico) and Steve Wells (University of California). They described the degree of development and structure of the various soil horizons, and the estimated relative age of the soils based on their physical properties.

Stop 2: South Quarry

Frank Perry briefly described the vent deposits (Qs1) draped by fall sheet deposits (Qs2) mapped and interpreted by Crowe and Perry (1988) at this location.

Stop 3: Southern Margin of Main Cone

Frank Perry briefly described the Qs2 fall sheet remnant mapped and interpreted by Crowe and Perry (1988) overlying the local Miocene bedrock. He also briefly discussed the flow/vent relationships of the Q11d deposit in the area.

Stop 4: West of Main Cone

Les McFadden and Steve Wells discussed the geomorphology of the main cone and the alluvial fan blanketing the northwest margin of the cone. Of particular interest was an erosional geomorphic surface at the base of the main cone that is draped by a relatively thin apron, or fan of alluvial deposits. Also discussed was the lack of rilling, or erosion of the main cone itself, and the estimated age of the cone based on the geomorphic relationships and features present.

Stop 5: North of Main Cone

Les McFadden and Steve Wells continued their discussion of the geomorphology of the main cone and adjacent alluvial fan.

Stop 6: Trench Exposure of Scoria Flow Relationships and Soils

Bruce Crowe and Frank Perry discussed the stratigraphy of the volcanic deposits exposed in the trench. Les McFadden and Steve Wells described the soil horizons between the volcanic units, and discussed their relative ages based on their degree of development and structure.

Stop 7: Scoria Vents East of Main Cone

Bruce Crowe gave a brief overview of his interpretation of the vent/scoria flow relationships on the east side of the main cone.

Stop 8: Main Cone Summit

Frank Perry gave an overview of the volcanic geology at Lathrop Wells. The field trip participants then engaged in an open discussion of the day's field observations.

DAY 2 - SLEEPING BUTTE

The Sleeping Butte visit was led by Scott Minor, Robert Fleck, Duane Champion, and Paul Orkild, all of the U.S. Geological Survey. Scott Minor began the trip by presenting an overview of the preliminary geologic mapping of the Pahute Mesa 30'x 60' quadrangle. The first stop was at the summit of Thirsty Mountain, from which Scott Minor pointed out the edge of the Timber Mountain - Oasis Valley caldera complex. Robert Fleck then presented some of his age dates for the Thirsty Mountain basalt. The next stop was at Hidden Cone, where various volcanic features along the southeast side of the cone were examined. Scott Minor described the geologic mapping of the surrounding area, noting that a fault occurs at the south end of the cone. Robert Fleck presented age dates for the Hidden Cone basalts, and Duane Champion presented paleomagnetic data for the basalt flows at the northern end of the cone. The final stop of the day was at Little Black Peak, where several outcrops were examined.

**LATHROP WELLS AND SLEEPING BUTTE AREA
 APRIL 25-26, 1995 FIELD TRIP PARTICIPANTS**

NAME	AFFILIATION
Duane Champion	U.S. Geological Survey
Chuck Connor	Center for Nuclear Waste Regulatory Analyses
Kevin J. Coppersmith	Geomatrix
Todd Crampton	Geomatrix
Bruce Crowe	Los Alamos National Laboratory
Terry Crump	TRW
Wendell A. Duffield	U.S. Geological Survey
Richard V. Fisher	University of California, Santa Barbara
Robert Fleck	U.S. Geological Survey
Sandra Green	Eureka County
William R. Hackett	WRH Associates
Brittain E. Hill	Center for Nuclear Waste Regulatory Analyses
Mel A. Kuntz	U.S. Geological Survey
Alexander R. McBirney	University of Oregon
Steve McDuffie	Nuclear Regulatory Commission
Les McFadden	University of New Mexico
Scott Minor	U.S. Geological Survey
Stephen T. Nelson	Woodward-Clyde Federal Services
Paul Orkild	U.S. Geological Survey
Roseanne C. Perman	Geomatrix
Frank Perry	Los Alamos National Laboratory
John Perry	Nye County
Leon Reiter	Nuclear Regulatory Commission
Michael F. Sheridan	State University of New York, Buffalo
Eugene I. Smith	University of Nevada, Las Vegas
Richard P. Smith	Idaho National Engineering Laboratory
Engelbrecht von Tiesenhausen	Clark County
George P.L. Walker	University of Hawaii
Steve Wells	University of California, Riverside
John Whitney	U.S. Geological Survey
Gene Yogodzinski	University of Nevada, Las Vegas

APPENDIX E

ELICITATION INTERVIEW SUMMARIES

APPENDIX E

Dr. Richard W. Carlson	RC-1
Dr. Bruce M. Crowe	BC-1
Dr. Wendell A. Duffield	WD-1
Dr. Richard V. Fisher	RF-1
Dr. William R. Hackett	WH-1
Dr. Mel A. Kuntz	MK-1
Dr. Alexander R. McBirney	AM-1
Dr. Michael F. Sheridan	MS-1
Dr. George A. Thompson	GT-1
Dr. George P.L. Walker	GW-1

RICHARD W. CARLSON
ELICITATION INTERVIEW FOR PVHA PROJECT

VOLCANIC/TECTONIC SETTING

In the broadest sense, volcanism in the Yucca Mountain region (YMR) (for the purposes of this elicitation "Yucca Mountain region" is defined as the circular area 50 km in radius centered on the proposed repository site) is an expression of the same volcanic/tectonic process occurring throughout the Basin and Range/western U.S. Miocene and younger volcanism and extension in the Basin and Range most likely represents the reaction of the western part of continental North America to the change from subduction along its western margin to the overriding of the various oceanic spreading centers (Atwater, 1970; Christiansen and Lipman, 1972; Cross and Pilger, 1978; Eaton, 1982). This led to a considerably different temperature structure in the mantle beneath the western U.S. (Severinghaus and Atwater, 1990), which is expressed by the changing character of volcanism. During the pre-Miocene subduction interval, the lithospheric mantle beneath the western U.S. was cooled by the cold subducting oceanic slab, but also was charged with volatiles by fluids rising from the dehydrating subducting plate. When subduction ceased, the overridden oceanic spreading center brought hot asthenospheric mantle directly beneath the volatile-charged lithosphere. This gave rise to the first burst of volcanism, manifest in the YMR by early caldera-forming silicic volcanism and associated basaltic activity beginning roughly at 15 Ma (Christiansen et al., 1977). The large volumes associated with this early volcanism probably reflect the diapiric ascent of asthenosphere that filled in the void as the subducting slabs detached and sank into the deeper mantle, with an additional contribution from the easily melted, hydrous mantle beneath the area formed as a result of the long history of subduction-induced metasomatism (Carlson and Hart, 1987). Volcanism following this initial burst is expressed differently, both compositionally and volumetrically, in various parts of the Basin and Range (Jones et al., 1992). In the YMR, the volume erupted decreases dramatically with time and the volcanism becomes more alkalic, reflecting increasingly smaller degrees of partial melting (Crowe et al., 1995).

In the author's opinion, the continuing volcanism in the YMR reflects conductive heating of the lithospheric mantle by the underlying asthenosphere, perhaps assisted by mantle ascent accompanying lithosphere extension. In the geological, geophysical, and volcanological data reviewed during the course of the PVHA project, the author does not see a clear connection between the tectonic history of post-Miocene extension in the YMR and the post-8 Ma volcanism.

suggesting that melting is primarily accomplished by conductive heating of the lithosphere rather than by diapiric ascent. Isotopic compositions of Sr and Nd in the Yucca Mountain basalts are extreme for Basin and Range lavas and point strongly to a magma source in Proterozoic lithospheric mantle (G. Yogodzinski presentation at PVHA Workshop 3). Thus, the YMR has much less potential to generate partial melts compared to most of the Basin and Range, where hot asthenospheric mantle appears to have displaced whatever lithospheric mantle was present prior to inception of Basin and Range activity.

REGION OF INTEREST

The main cause of Miocene and younger volcanism in the Basin and Range appears to be replacement of cold subducting slabs with hot asthenospheric mantle beneath the western North American lithosphere (Atwater, 1970). This represents a broad and more-or-less constant "flame," capable of causing melting and volcanism across the entire Cordilleran U.S. Clearly, however, all of the Basin and Range has not responded similarly to this "flame" (Christiansen and Lipman, 1972; Jones et al., 1992). In the Basin and Range, Yucca Mountain sits in a heat flow low, has minimal signs of present-day extensional stress, and lies at the northern boundary of the so-called "amagmatic gap," distinguished by the absence of Mesozoic and Cenozoic magmatic activity (Christiansen and Lipman, 1972; Farmer et al., 1989; Jones et al., 1992). The explanation for this may be indicated by the extreme isotopic composition (G. Yogodzinski presentation at PVHA Workshop 3) of the magmas of the YMR: the YMR is underlain by an unusually thick/persistent/non-extended section of Proterozoic lithospheric mantle (this author's extension of the concepts and data presented by G. Yogodzinski at PVHA Workshop 3). Trace element characteristics of the post-5 Ma YMR basalts (Crowe et al., 1995; Vaniman et al., 1982; F.V. Perry, pers. comm., 1995) indicate a source that contained garnet (garnet is stable in a peridotitic assemblage only at depths greater than approximately 60 km) and possibly a hydrous phase, such as amphibole and/or phlogopite, the presence of which would constrain the maximum depth of magma generation to on the order of 100-150 km because these phases are not stable at higher pressures. Nd isotopic compositions of YMR basalts provide minimum depleted mantle model ages of 1-1.5 Ga (calculated from data provided by F.V. Perry, pers. comm., 1995), suggesting that the source of these lavas is Proterozoic lithospheric mantle of an age approaching that of the continental basement in this area (Bennett and DePaolo, 1987; Farmer and DePaolo, 1983; Farmer et al., 1989). The constancy of Sr and Nd isotopic compositions of post-8 Ma basalts from the YMR and some nearby areas (G. Yogodzinski presentation at PVHA Workshop 3) indicate that this 100-150+ km thick section of Proterozoic lithospheric mantle has not been displaced or thinned significantly by Basin and Range extension, as appears to have occurred in many other

areas of the Basin and Range (Carlson and Hart, 1987; Leeman and Fitton, 1989; Perry et al., 1987).

Assuming that this feature of the YMR has influenced its volcanic history, the relevant region of interest for calculating volcanic probabilities in the YMR should include nearby areas that have the same isotopic signature of Proterozoic lithosphere: the area within the Amargosa Valley Isotopic Province (AVIP) proposed by G. Yogodzinski (presentation at PVHA Workshop 3). The AVIP includes the area of Yucca Mountain volcanism (northern border to include Sleeping Butte, Thirsty Mesa, and Buckboard Mesa extending south to Crater Flat and Lathrop Wells), and then extends south to include the buried Amargosa Valley centers and the volcanic centers in northern Death Valley that are isotopically similar to the Yucca Mountain basalts. The Death Valley activity is included to increase the number of events from an area whose lithospheric compositional and thermal structure may be similar to the YMR and, hence, may have responded similarly to the broad heat source behind Basin and Range volcanism. Post-Miocene volcanism outside the AVIP is not considered significant by this author in terms of its impact on calculating volcanic event probabilities in the YMR.

The possibility of subdividing the AVIP on the basis of caldera locations and tomography was examined. Tomographic data examined by Evans and Smith (1992) were resolved and interpreted to show high velocities under the Timber Mountain caldera and low velocities (indicating melt) below Crater Flat. (The presence of partial melt is not necessarily correlated with future volcanism, but its absence is a good explanation for why volcanism has not occurred.) The Evans and Smith (1992) map was superimposed on the AVIP, but no clear associations were observed between tomography and the record of young volcanism. The distribution of volcanoes within the AVIP appears to be random. Evidence for clustering of centers is very weak (in part due to the small data set) and the author concludes that there is no good basis for subdividing the area.

EVENT DEFINITION

Temporal Aspects

A volcanic event is defined herein as an eruption or series of eruptions related to the same magmatic conduit system that transfers magma from a diffuse zone of partial melting in the mantle to a volcanic edifice. An event could be an eruption from a single feeder dike at a single time, or it could be related to an en echelon dike set or a branch from a major dike. An event is controlled by the process of magma ascent and crystallization. Thin (thicknesses of a meter or less) dikes filled with magma will be cooled rapidly by the lower temperatures present in surrounding upper crust wall rocks. This cooling will lead to crystallization of the magma in the dike. When the

magma has solidified to the point that it reaches a yield strength similar to that of surrounding rock, the "event," as defined here, is over. A new event will be initiated by the next propagation of magma from the mantle source towards the surface. In areas of high magmatic output, this event definition is blurred because individual conduits, and hence volcanoes, may be fed with a more-or-less continuous stream of new, hot, magma. In such situations, "events" may last many thousands of years. The volcanoes and dikes in the YMR are very small, such that an event most likely occurs on the order of tens to hundreds of years.

Spatial Aspects

The expected spatial dimensions of an event are on the order of a basaltic dike: 1 to 5 km (Delaney and Gartner, 1995; Walker, 1987). The maximum might be represented by a set of dikes giving rise to an event having dimensions of 10 to 20 km. A possible example of an event near the maximum size would be the case where the cones in northern Crater Flat are assumed to represent a single event.

Geochemical Affinity

Geochemical affinities need not discriminate individual events because substantial variations can occur in single flows from the same event, but they can provide supporting information to other data that suggest separate events. The volumes of the YMR basaltic volcanoes are low, and they sample a very small region of the mantle (Crowe et al., 1995). Their chemical compositions (Crowe et al., 1995; Vaniman et al., 1982) indicate that the magmas have experienced fractional crystallization since leaving the mantle, but, on the basis of no evidence for crystallization of plagioclase, the magmas do not appear to have undergone storage and fractionation in crustal-depth magma chambers (Crowe et al., 1995). Such magma chambers might be expected to promote mixing and homogenization of magmas prior to eruption. Without such mixing chambers, differences in the degree of partial melting for individual batches of magma extracted from the source rock, the extent of crystallization, and the degree of interaction and incorporation of wall rock by these magmas on route to the surface could lead to chemical variations in magmas erupted at different times during one event.

Note: The following elements of the PVHA model are summarized in the form of a logic tree in Figure RC-1.

SPATIAL MODELS

The future spatial distribution of volcanoes is modeled using two basic models: a model assuming a uniform distribution of events within the AVIP zone (termed the "uniform" model), and a model

of the type proposed by Connor and Hill (1993), where the spatial distribution of observed events is smoothed to represent the probability of future event locations (termed the "spatial smoothing" model). The weights assigned to these models are: uniform (0.4) and spatial smoothing (0.6). The "field shape" approach of Sheridan (1992) was considered but not used in this case because the author is uncomfortable with assigning a "field" shape to individual volcanic centers as sparse as those in the YMR. Nevertheless, guided by the general field shape trends displayed by Basin and Range volcanism (M. Sheridan presentation at PVHA Workshop 3), the author selected "smoothing" kernels that, at the larger of the smoothing distances examined here, cause the "spatial smoothing" model solutions to approach those that would be produced by "field shape" models in terms of the volcanic event contours calculated.

On the basis of his previous studies of volcanic centers in the western U.S. and elsewhere around the world, the author has a strong bias towards believing that the exact location of volcanism is structurally controlled. This bias is reflected in the 60% weight assigned to the spatial smoothing approach, but structural control is poorly supported by volcanism in the YMR, leading to the 40% weight assigned to the uniform model. The Crater Flat cones clearly are aligned, but this may represent a shallow stress condition that was present when the dike feeding these eruptions extended close to the surface. Lathrop Wells does not lie along this alignment, nor do the volcanic centers to the north. In the author's opinion, the strongest evidence for structural control is that the Crater Flat centers, including Lathrop Wells, formed in the area that displays the most evidence for extension in the Quaternary (B. Crowe and G. Thompson presentations at PVHA Workshop 4). Larger-scale alignments, such as along the Walker Lane, were reviewed, but the author does not see a particularly compelling reason to believe that the Walker Lane has had much effect on the YMR volcanic centers.

The spatial control typically observed is that basaltic centers seem to avoid erupting through the center of calderas, presumably because the presence of subsurface silicic magma beneath the caldera impedes ascent of basaltic magma. After the silicic magma crystallizes and cools to the point that it can fracture, basaltic magmas can erupt through calderas. Given the occurrence of Buckboard Mesa, it appears this point has been reached at Yucca Mountain, so there is no longer a good reason to exclude an intra-caldera basaltic center.

In general, there does not appear to be any particular area in the YMR that has either a strongly enhanced or diminished probability of being the site of the next eruptive center. Therefore, spatially homogenous probability models are only slightly less weighted (40% to 60%) compared to structure controlled models such as the spatial smoothing model used here.

The uniform model is implemented by assuming that the probability distribution of future events is uniform within the AVIP (see discussion of AVIP in "Region of Interest" section).

The spatial smoothing approach is implemented using an Epanechnikov smoothing operator that is elliptically shaped, with a 2:1 aspect ratio, and oriented to the northwest parallel to the Crater Flat volcanic zone of Crowe and Perry (1989). Where a single event is represented by multiple cones, the mid-point of the cones is used as the point estimate for the event. The elliptical shape is intended to elongate the probability contours in the northwest direction to reflect this structural trend. This elongation is similar to the "field shape" approach proposed by Sheridan (1992), although the spatial smoothing approach is driven more by the distribution of events than by a parametric form. Two alternative smoothing distances (long dimension of operator) are considered, and their relative weights are: 10 km (0.5), and 20 km (0.5). Smoothing is used for post-5 Ma events within the northern half of the AVIP.

EVENT COUNTS

Based on the definition of volcanic "events" given earlier, the number of events—and their uncertainties—are assessed for each of the centers in the AVIP (Figure RC-2). The event counts and rates of occurrence for various time periods are summarized in Tables RC-1 and RC-2.

Lathrop Wells

The available data at Lathrop Wells suggest that a single event is most likely, but more than 1 event may have occurred (Crowe et al., 1995). Each of the geochronology data sets has its own set of problems and leads to large uncertainties. The paleomagnetic data argue for a single event (Champion, 1991). However, the evidence for a soil horizon, and other observations, lead to problems with the single-event interpretation (Wells et al., 1992; 1990). Although unlikely, it is possible to envision a process where a monogenetic center is reactivated by a second period of activity due to a "random" hit at the same place.

The following event counts and their relative weights are assigned for the Lathrop Wells center: 1 (0.95), and 2 (0.05).

Sleeping Butte

One to 3 events may be represented by the geologic relationships at Sleeping Butte, with 1 event most likely. Little Black Peak and Hidden Cone are closely spaced (3 km apart) and the geochronology would allow for them to be essentially the same age (Crowe et al., 1995). Little Black Peak and Hidden Cone would be considered separate events for the 2-event scenario, which is given much less weight (Champion, 1991; Crowe et al., 1995). For the 3-event scenario,

Hidden Cone is interpreted to consist of 2 events, which was suggested at the PVHA Sleeping Butte field trip based on paleomagnetic and geomorphic data.

The event counts and their relative weights for the Sleeping Butte area are: 1 (0.7), 2 (0.2), and 3 (0.1).

Death Valley

The <0.7 Ma Split Cone deposits in Death Valley represent the only post-1 Ma event in this area (informal PVHA memo by B. Crowe).

A single event at Split Cone is assigned a weight of 1.0.

1.0 Ma Crater Flat

The 1.0 Ma basalts in northern Crater Flat represent 1 to 5 events, with 1 event most likely. The single-event scenario is preferred on the basis of age-dating information, although the uncertainties are probably on the order of 50,000 yr (Crowe et al., 1995). Paleomagnetic data indicate the cones are of similar age (Champion, 1991), and available isotopic dates, while less reliable for these relatively young rocks, also allow the interpretation that the cones are of similar age (Crowe et al., 1995). The possible evidence for multiple events at Red Cone reviewed on the PVHA Crater Flat field trip (e.g., scoria mounds, possible dikes, geochemical differences) is not convincing. If the age-dates are not accurate, 3 events could be represented on the basis of geochemical differences between the cones (Red and Black cones formed in a single event, Makani and Little Cones are each separate events) (Crowe et al., 1995). Based on counts of mapped cones, a maximum of 5 events may have occurred (Little Cones consists of two mapped cones).

The following event counts and their relative weights are assigned for northern Crater Flat: 1 (0.6), 3 (0.3), and 5 (0.1).

Buckboard Mesa

Buckboard Mesa basalts appear to be related to a single fissure flow. However, if the two cones are considered separate events, 2 events might be represented (Crowe et al., 1995).

The event counts and their relative weights assigned to the Buckboard Mesa area are: 1 (0.9), and 2 (0.1).

3.7 Ma Crater Flat

The 3.7 Ma basalts in southeastern Crater Flat may represent 1 to as many as 6 events, with 1 event most likely (Crowe et al., 1995). Evidence for multiple events is not convincing, and age-

dates have overlapping uncertainties that suggest that a single event may have occurred (Crowe et al., 1995). Discontinuities in the outcrops could be related to faulting. Two to 6 events are possible, based on individually mapped dikes and fissures summarized in Crowe et al. (1995).

The following event counts and their relative weights are assigned for the 3.7 Ma area of Crater Flat: 1 (0.8), 2 (0.1), 3 (0.05), 4 (0.02), 5 (0.02), and 6 (0.01).

Amargosa Valley

Three to 6 separate events could be represented by the aeromagnetic anomalies in Amargosa Valley, as discussed and designated by V. Langenheim (presentation at PVHA Workshop 1). Dikes in the 3.7 Ma area of Crater Flat suggest that dike alignments during this general time period should be north-south (Crowe et al., 1995). Anomalies D and C are close together but have different polarities (Langenheim et al., 1993). In the 3-event scenario, anomalies B, C, and D would be separate events, as they are the most believable as buried cones (Langenheim et al., 1993). In the 4-event scenario, anomaly E is also included, which is judged to be a preferred interpretation. Anomalies F and G, which are included in the 5- and 6-event scenarios, have a relatively low probability of representing events, as they have signatures similar to the background noise level (Langenheim et al., 1993). *Note: Anomalies F and G on the aeromagnetic map presented by V. Langenheim at PVHA Workshop 1 correspond to anomaly A in Langenheim et al. (1993).*

The following event counts and their relative weights are assigned to the Amargosa Valley area: 3 (0.3), 4 (0.5), 5 (0.1), and 6 (0.1).

Thirsty Mesa

A single flow sheet appears to be present at Thirsty Mesa that is interpreted to represent simple fissure-fed flows (Crowe et al., 1995). The flow volume is not atypical for the region if it occurred from a single event (Crowe et al., 1995).

The favored number of events at Thirsty Mesa is 1 (0.9), and the possibility of 2 events is included (0.1).

TEMPORAL MODELS AND RATES OF OCCURRENCE

Two temporal models are used: a volume-predictable approach that is applied only to the northern portion of the AVIP, and a homogeneous approach that is applied to the entire AVIP. Because of the small number of events occurring in the northern AVIP, and recognizing the decreasing volume of lava erupted with time throughout this province, a volume predictable approach was

developed to estimate the present-day rate of volcanism based on volume estimates for eruptions occurring only over the past 5 my where the data are reasonably complete and accurate. The author considers the volume predictable approach to offer a more reliable estimate of current eruptive rates in the YMR because the very small number of young-(i.e., <1 Ma) vents in the region leads to large uncertainties in both homogeneous (Crowe et al., 1995; Crowe and Perry, 1989) and non-homogenous approaches (Ho, 1991). This volume predictable approach to a time-varying eruptive rate is considered along with a homogeneous approach that averages the event counts over the last 1 my in the YMR. The relative weights assigned to these two models is 70% for the volume-predictable approach and 30% for the 1 my average homogeneous model. The higher weight given to the volume-predictable approach reflects the author's opinion that this approach provides a slightly more reliable "averaging" method to calculate the present day eruptive rate in the YMR, and acknowledges that this rate has not been constant during the history of post-8 Ma volcanism.

The volume predictable approach is designed to recognize that the volume of eruptions has declined over the past 15 my (Crowe et al., 1995) and uses this information to estimate the expected volume of an eruption at the present time and near future. The data for cumulative volume versus time shown in Figure 7.6 of Crowe et al. (1995) were fit by an equation relating volume to the square root of time, as would be expected if magma production were controlled by a diffusion-limited process such as thermal conduction. A simple two-point fit to the data of volume versus time gives the equation:

$$\text{Cumulative Volume (km}^3\text{)} = 3 \text{ (km}^3\text{)} + 1.33 * (\text{Time [Ma]})^{1.5}$$

where Time=0 at 4.8 Ma and Time=4.8 Ma today. This equation provides the following eruption rates for the integrated time intervals (Time = 0 today) listed below:

<u>Time Interval (Ma)</u>	<u>Eruptive Volume (m³/yr)</u>
0 - 0.1	305
0 - 1.0	321
0 - 2.0	344
4.7 - 4.8	4200

To derive event counts and/or repose times from these volumes requires information on the average volume per event and how this has changed with time. The data for volume per event

versus time from Figure 7.9 of Crowe et al. (1995) show an exponential fall off with time in the volume per event and were fit with an exponential curve of the following form:

$$\text{Volume per Event (km}^3\text{)} = 0.13 * e^{0.65 * \text{Time(Ma)}}$$

where Time=0 today. This curve predicts a current event size of approximately 0.13 km³ and an event size of 2.9 km³ at 4.8 Ma. Given the eruptive volume figures quoted above, these event sizes translate into event rates of 2.3 events per million years (426,000 yr repose time) today and 1.4 events per million years (690,000 yr repose time) at 4.8 Ma. Consequently, this approach predicts that although magma production is declining in the Yucca Mountain area, the frequency of eruptions has increased over the past 5 my because the volume per event has decreased more rapidly than the erupted volume with time.

An attempt was made to fit a periodic function to event rate at Yucca Mountain by a cubic spline fit to the data for event count versus time, given as Figure 3.11 in Crowe et al. (1995). This method is considered to have poor accuracy because of the small number of data points included. Nevertheless, the cubic spline fit extrapolates to an event rate of approximately 1.6 events/my at the present time, which is not greatly different from the present-day value calculated from the volume predicable model. Consequently, the author's choice for present-day eruption rate is 2.3 ± 0.7 events per million years.

Undetected Events

The probability that volcanic events (i.e., dikes) would ascend to shallow depths (300 m, which is the depth of the proposed repository) and not erupt at the surface is considered to be low by the author. Dikes ascend by exsolving volatiles in the shallow crust, gaining eruptive pressure with ascent. Unless they encounter some unusually impenetrable strata, the increasing eruptive pressure in the dike should cause the majority of dikes, if they have made it to the upper 0.5 km of the crust, to continue on to surface eruption. To allow for some failed dikes that might make it to 300 m depth, but not to surface eruption, the author estimates that about 10% more events may exist at shallow depth than have been interpreted at the surface (i.e., the event counts should be multiplied by 1.1 to include the undetected events).

EVENT GEOMETRIES

When an event is defined by two or more features (e.g., cones), the mid-point of the features should be used as the point location of the event.

The length of an event is expected to be the length of a basaltic dike, about 1 to 5 km long (Delaney and Gartner, 1995). In some cases, a set of dikes may occur during a single event and extend the total length to as much as 12 km or more (such as the possible event interpreted for northern Crater Flat). The cumulative distribution for event length is the following:

1 km	(0.1)
3 km	(0.5)
5 km	(0.75)
12 km	(0.95)
20-30 km	(1.0)

The maximum dike length lies within the range of 20 to 30 km. Dikes longer than 30 km are given zero probability because this length would exceed the length of most continuous mapped faults in the area (Scott, 1990). The assessed relative weights on maximum lengths are 20 km (0.6), 25 km (0.3) and 30 km (0.1).

Note: At the request of Dr. Carlson, a smooth interpolation function was fit to his discrete cumulative density estimates for dike length. The resulting cumulative distributions and density functions are shown on Figure RC-3.

The width of an event is essentially the width of a dike, estimated to be 0.5 to 1 m (Delaney and Gartner, 1995). In the case of "ballooning" of dikes near the surface, the maximum width is 2 m.

The expected orientation of events is parallel to the alignment of the 1 Ma Crater Flat cones: N25E, with a 90% confidence bound of ± 30 degrees.

In modeling the geometry of an event, the eruption locality is considered to be randomly placed relative to the location along the dike, i.e., a dike propagating towards the surface is equally likely to reach the surface at any point along its dimension.

HYDROMAGMATIC ACTIVITY AND TYPE OF ERUPTION

Based both on the nature of eruptive activity in the YMR and in other areas of the Basin and Range (M. Sheridan presentation at PVHA Workshop 3), the most likely event (95% probability) would be another small cinder/scoria cone accompanied by small-volume flows, such as at Crater Flat and Lathrop Wells. Dike injection, of course, would accompany an eruption. The post-caldera activity in the YMR shows no particular tendency towards hydromagmatic eruptions; however, the trend towards a decreasing degree of partial melting increases the likelihood of a volatile, charged eruption. Maar-forming events, however, are rather rare in the Basin and Range

(e.g., M. Sheridan presentation at PVHA Workshop 3). The probability of a Plinian event is <5%: 3% of which might be a maar-type eruption (includes hydromagmatic events), 1% large-volume tholeiitic event, and 1% a rhyolitic event.

Richard Carlson
4/12/96

REFERENCES

- Atwater, T., 1970, Implications of plate tectonics for the Cenozoic tectonic evolution of western North America: Geological Society of America Bulletin: v. 81, p. 3513-3535.
- Bennett, V.C., and DePaolo, D.J., 1987, Proterozoic crustal history of the western United States as determined by neodymium isotopic mapping: Geological Society of America Bulletin: v. 99, p. 674-685.
- Carlson, R.W., and Hart, W.K., 1987, Crustal genesis on the Oregon Plateau: Journal of Geophysical Research: v. 92, p. 6191-6206.
- Champion, D.E., 1991, Volcanic episodes near Yucca Mountain as determined by paleomagnetic studies at Lathrop Wells, Crater Flat, and Sleeping Butte, Nevada: Proceedings, High-Level Radioactive Waste Management, Las Vegas, Nevada, American Nuclear Society, v. 1, p. 61-67.
- Christiansen, R.L., and Lipman, P.W., 1972, Cenozoic volcanism and plate-tectonic evolution of the western United States, II, late Cenozoic: Philosophical Transactions Royal Society London Series A, v. 271, p. 249-284.
- Christiansen, R.L., Lipman, P.W., Carr, W.J., Jr., Byers, F.M., Orkild, P.P., and Sargent, K.A., 1977, The Timber Mountain-Oasis caldera complex of southern Nevada: Geological Society of America Bulletin, v. 88, p. 943-959.
- Connor, C.B., and Hill, B.E., 1993, Estimating the probability of volcanic disruption of the candidate Yucca Mountain repository using spatially and temporally non-homogeneous poisson models: Site Characterization and Model Validation Focus '93 Symposium, La Grange, IL, American Nuclear Society.
- Cross, T.A., and Pilger, R.H., 1978, Constraints on absolute motion and plate interaction inferred from Cenozoic igneous activity in the western United States: American Journal of Science, v. 278, p. 865-902.
- Crowe, B., and Perry, F.V., 1989, Volcanic probabilities calculations for the Yucca Mountain site: estimation of volcanic rates: Proceedings, Nuclear Waste Isolation in the Unsaturated Zone, Focus '89, American Nuclear Society, v. 2, p. 326-334.
- Crowe, B.M., Perry, F.V., Geissman, J., McFadden, L., Wells, S., Murrell, M., Poths, J., Valentine, G.A., Bowker, L., and Finnegan, K., 1995, Status of volcanism studies for the Yucca Mountain site characterization project: Los Alamos National Laboratory Report LA-12908-MS, March 1995.

- Delaney, P.T., and Gartner, A.E., 1995. Physical processes of shallow mafic dike emplacement near the San Rafael swell, Utah: U.S. Geological Survey Open-File Report 95-491.
- Eaton, G.P., 1982. The Basin and Range province: origin and tectonic significance: Annual Reviews of Earth Planetary Science, v. 10, p. 409-440.
- Evans, J.R., and Smith, M., III, 1992. Teleseismic tomography of the Yucca Mountain region: volcanism and tectonism: Proceedings, Third International High Level Radioactive Waste Management Conference, American Nuclear Society, v. 2, p. 2371-2380.
- Farmer, G.L., and DePaolo, D.J., 1983, Origin of Mesozoic and Tertiary granite in the western United States and implications for pre-Mesozoic crustal structure: Nd and Sr isotopic studies in the geocline of the northern Great Basin: Journal of Geophysical Research, v. 88, p. 3379-3401.
- Farmer, G.L., Perry, F.V., Semken, S., Crowe, B., Curtis, D., and DePaolo, D.J., 1989. Isotopic evidence on the structure and origin of subcontinental lithospheric mantle in southern Nevada: Journal of Geophysical Research, v. 94, p. 7885-7898.
- Ho, C.H., 1991. Time trend analysis of basaltic volcanism for the Yucca Mountain site: Journal of Volcanology and Geothermal Research, v. 46, p. 61-72.
- Jones, J.H., Wernicke, B.P., Farmer, G.L., Walker, J.D., Colman, D.S., McKenna, L.W., and Perry, F.V., 1992, Variations across and along a major continental rift: an interdisciplinary study of the Basin and Range province, western USA: Tectonophysics, v. 213, p. 57-69.
- Langenheim, V.E., Kirchoff-Stein, K.S., and Oliver, H.W., 1993, Geophysical investigations of buried volcanic centers near Yucca Mountain, southwest Nevada: Proceedings, High-Level Radioactive Waste Management Conference, Las Vegas, NV, American Nuclear Society, v. 2, p. 1840-1846.
- Leeman, W.P., and Fitton, J.G., 1989, Magmatism associated with lithospheric extension: Journal of Geophysical Research, v. 94, p. 7682-7684.
- Perry, F.V., Baldrige, W.S., and DePaolo, D.J., 1987, Role of asthenosphere and lithosphere in the genesis of late Cenozoic basaltic rocks from the Rio Grande Rift and adjacent regions of the southwestern United States: Journal of Geophysical Research, v. 92, p. 9193-9213.
- Scott, R.B., 1990. Tectonic setting of Yucca Mountain, southwest Nevada, *in* B.P. Wernicke (ed.), Basin and Range Extensional Tectonics Near the Latitude of Las Vegas, Nevada: Geological Society of America Memoir 176, p. 251-282.

- Severinghaus, J., and Atwater, T., 1990, Cenozoic geometry and thermal state of the subducting slabs beneath western North America, *in* B.P. Wernicke (ed.), Basin and Range Extensional Tectonics Near the Latitude of Las Vegas, Nevada: Geological Society America Memoir 176, 1022 p.
- Sheridan, M.F., 1992, A Monte Carlo technique to estimate the probability of volcanic dikes: Proceedings, High-Level Radioactive Waste Management, Las Vegas, NV, American Nuclear Society, v. 2, p. 2033-2038.
- Vaniman, D.T., Crowe, B.M., and Gladney, E.S., 1982, Petrology and geochemistry of hawaiite lavas from Crater Flat, Nevada: Contributions to Mineralogy and Petrology, v. 80, p. 341-357.
- Walker, G.P.L., 1987, The dike complex of Koolau volcano, Oahu: internal structure of a Hawaiian rift zone: U.S. Geological Survey Professional Paper 1350, p. 961-993.
- Wells, S.G., Crowe, B.M., and McFadden, L.D., 1992, Measuring the age of the Lathrop Wells volcanic center at Yucca Mountain: Science, v. 257, p. 555-558.
- Wells, S.G., McFadden, L.D., Renault, C.E., Turrin, B.D., and Crowe, B.M., 1990, A geomorphic assessment of Quaternary volcanism in the Yucca Mountain area, Nevada Test Site, southern Nevada: implications for the proposed high-level radioactive waste repository: Geology, v. 18, p. 549-553.

TABLE RC-1
RICHARD W. CARLSON - EVENT COUNTS

LOCATION	COUNTS (CONES)	WEIGHT	NOTES
Lathrop Wells	1	(0.95)	BC: Black Cone B-G: Aeromagnetic anomalies of V. Langenheim, USGS
	2	(0.05)	
Sleeping Butte	1 (LBP+HC)	(0.7)	HC: Hidden Cone 2HC: 2 events at Hidden Cone LBP: Little Black Peak
	2 (LBP, HC)	(0.2)	
	3 (LBP, 2HC)	(0.1)	
1.0 Ma Crater Flat	1 (all)	(0.6)	LC: Little Cones 2LC: 2 events at Little Cones M: Makani Cone
	3 (LC, RC+BC, M)	(0.3)	
	5 (2LC, RC, BC, M)	(0.1)	
Buckboard Mesa	1	(0.9)	RC: Red Cone SC: Split Cone
	2	(0.1)	
3.7 Ma Crater Flat	1	(0.8)	
	2	(0.1)	
	3	(0.05)	
	4	(0.02)	
	5	(0.02)	
	6	(0.01)	
Amargosa Valley	3 (B,C,D)	(0.3)	
	4 (B,C,D,E)	(0.5)	
	5 (B,C,D,E,F)	(0.1)	
	6 (B,C,D,E,F,G)	(0.1)	
Thirsty Mesa	1	(0.9)	
	2	(0.1)	
Death Valley (1 Ma)	1 (SC)	(1.0)	

TABLE RC-2
RICHARD W. CARLSON - RATES OF OCCURRENCE

TIME PERIOD	COUNT METHOD FOR ZONES	NOTES
1.0 Ma (0.3)	AVIP: (LW+SB+NCF+DV)	AVIP: Amargosa Valley Isotopic Province of Yogodzinski (1995) AV: Amargosa Valley BM: Buckboard Mesa DV: Death Valley LW: Lathrop Wells
5.0 Ma (0.7)	NAVIP: (LW+SB+NCF+3.7+AV+TM+BM)	NCF: Northern (1.0 Ma) Crater Flat NAVIP: Northern Amargosa Valley Isotopic Province TM: Thirsty Mesa SB: Sleeping Butte 3.7: 3.7 Ma Crater Flat

<i>Temporal Models</i>	<i>Time Period</i>	<i>Region Of Interest</i>	<i>Spatial Models</i>	<i>Sources</i>
------------------------	--------------------	---------------------------	-----------------------	----------------

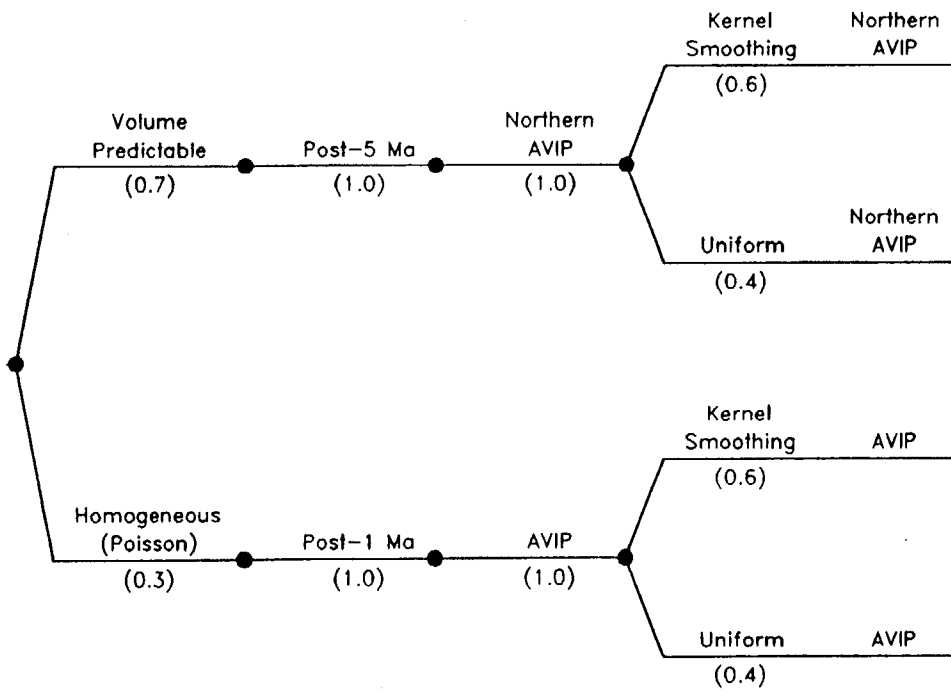
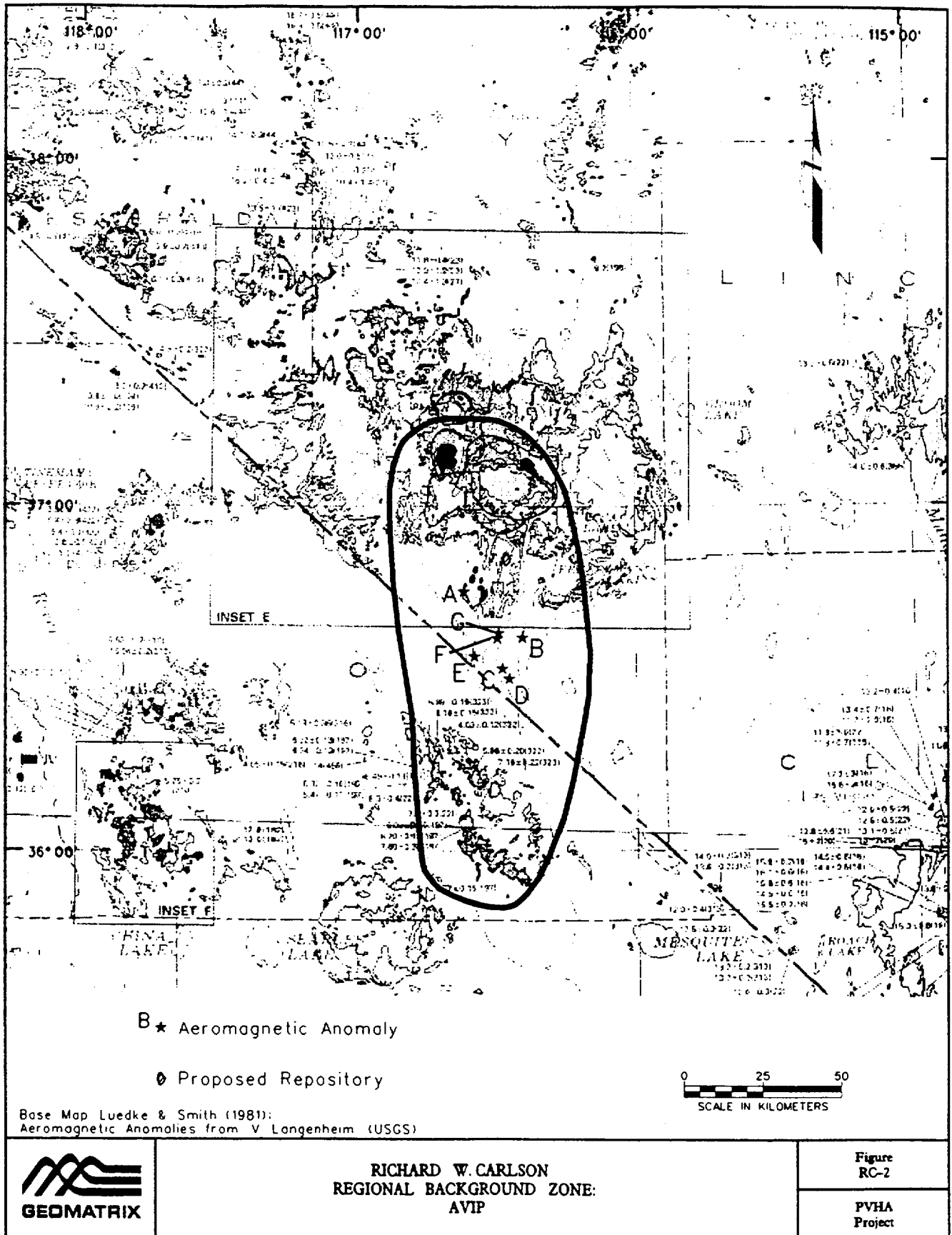


Figure RC-1 PVHA model logic tree developed by Richard W. Carlson.



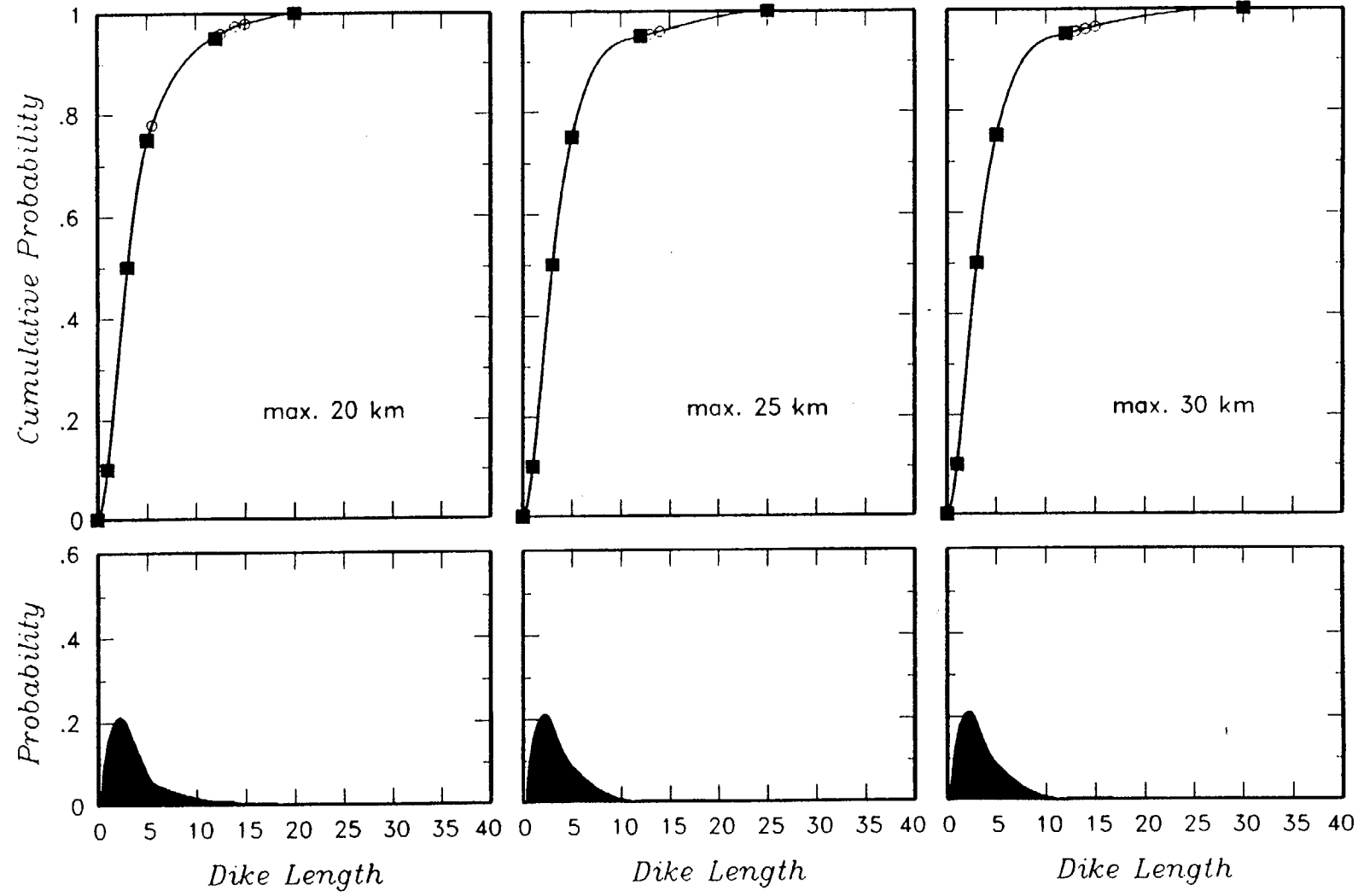


Figure RC-3 Dike length distribution developed by Richard W. Carlson.

BRUCE M. CROWE
ELICITATION INTERVIEW FOR PVHA PROJECT

VOLCANIC/TECTONIC SETTING

The southwest Nevada volcanic field (SWNVF; Christiansen et al., 1977; Byers et al., 1976; 1989) experienced maximum extension and silicic volcanism during the period of about 16 to 11 Ma (Crowe et al., 1995, Chapters 2 and 3). Subsequently, areas of intense tectonism and volcanism migrated outward to the eastern and western edges of the Great Basin. Silicic volcanism ceased in the central and southern part of the SWNVF after eruptive activity of the Black Mountain caldera complex (8-9 Ma; Crowe and Sargent, 1979; Crowe, 1990; Crowe et al., 1995). Voluminous basaltic volcanism accompanied and was probably the driving force (thermally and magmatically) for the generation of the large volume silicic volcanism but basaltic volcanism rarely appeared in the surface eruptions probably because of density trapping beneath the cogenetic silicic magmas. Evidence of cogenetic basaltic and silicic magmas is suggested primarily by the rare occurrences of basalt as very minor components in the strongly compositionally zoned ash-flow sheets (for example as lithic fragments in ash-flow deposits, thin hydrovolcanic layers in the Plinian phases of the ash-flow cycles of the Timber Mountain Tuff). Eruptions of basaltic volcanic rocks became more important volumetrically in the waning phases of activity of the SWNVF (late Miocene) probably as a result of solidification of the silicic magma chambers so that they no longer functioned as density traps for ascending basalt. Subsequent late Miocene and younger volcanic activity was unrelated to the silicic volcanism and consisted of sporadic eruption of small volumes of basalt magma. These eruptions formed volcanic centers and clusters of volcanic centers over widely scattered areas of the Yucca Mountain region (YMR; see Crowe, 1990; Crowe et al., 1995). The YMR, for this elicitation, refers to the area encompassing sites of basaltic volcanism that post-date voluminous silicic volcanism in the central and southern part of the SWNVF. It is identified as the YMR when referencing the distribution area of post-9.15 Ma sites of basaltic volcanism and as the YMR/PQ when referencing the distribution area of post-5.05 Ma sites of basaltic volcanism.

The driving force for the Miocene large volume silicic volcanic activity almost certainly was from upwelling of asthenospheric mantle with generation of basaltic magma from adiabatic decompression and melting of mantle peridotite (Farmer et al., 1991; Perry et al., 1993). The origin of the late Miocene and younger basaltic volcanism in the YMR is less clear but most likely can be attributed to partial melting of a hydrous upper mantle that may or may not be related to low rates of surface extension (Best and Brimhall, 1974; Vaniman et al., 1982; Perry et al., 1987;

1993; Farmer et al., 1989; Perry and Crowe, 1992; see also Crowe, et al., 1995, Chapter 4, and the PVHA Elicitation Interview for R. Carlson, this report).

Two major episodes of Miocene and younger basaltic volcanic activity are recognized in the SWNFV and the YMR following the subdivisions of Crowe (1990). These are basaltic volcanic rocks of the silicic episode (BSE) and postcaldera basalt (PCB). The BSE are judged not to be relevant to probabilistic volcanic hazard assessment (PVHA) because of their Miocene age and their formation during a different tectonic setting than the modern setting for the YMR (Crowe, et al., 1995, Chapter 3). The PCB are divided into two cycles (Crowe, 1990) and include the older postcaldera basalt (OPB) and younger postcaldera basalt (YPB). The OPB are judged to be of limited significance to PVHA for several reasons: (1) they range in age from 9 to 6.5 Ma and because of their age are judged to be at best weak predictors of future rates and/or sites of volcanic activity, (2) they occur primarily in the north and northeast parts of the YMR away from the Yucca Mountain site, and (3) there has been time-space migration of volcanic activity recorded in the patterns of basaltic volcanism associated with the PCB (Crowe et al., 1995; Golder Associates, 1995). The OPB are considered in some aspects of PVHA (see following sections) but their inclusion leads to estimated disruption probabilities that are as low as some regional background estimates (Crowe, 1995). They therefore are assigned small weights in the PVHA. The YPB are judged to be the most important record of basaltic volcanic events for PVHA for the Yucca Mountain site and as used, include all Pliocene and Quaternary (post-5.05 Ma) basaltic volcanic centers and inferred buried volcanic centers identified from aeromagnetic data. Subintervals of the YPB are recognized that correspond to the concept of volcanic cycles (Crowe, 1990; Crowe et al., 1995) and these intervals are emphasized in the PVHA.

Working Assumptions for the PVHA

Several observations concerning the tectonic and volcanic history of the Yucca Mountain region are considered to be especially relevant to the PVHA. These include:

1. The intensity of tectonic activity has waned in the YMR since the Miocene. The detailed history of waning tectonism cannot be established since there is a gap in the preserved record of datable rocks between about 11 Ma and the Pliocene (3.7 Ma basalt of southeastern Crater Flat). However, rates of extension in the Pliocene and Quaternary are dramatically less than extension rates in the Miocene (Carr, 1984; Scott, 1990; Fridrich, 1995).
2. The source region for generation of basaltic magmas during the Miocene, Pliocene, and Quaternary is the lithospheric mantle based on inferences from

- isotopic and geochemical data for basaltic volcanic rocks (Vaniman et al., 1982; Farmer et al., 1989; Crowe et al., 1995, Chapter 4).
3. Geophysical data show that the upper mantle in the continental interior including the southern Great Basin is of higher temperature with decreased density compared to coastal areas to the west and cratonal areas to the east (Humphreys and Dueker, 1994). The upper mantle rocks of the southern Great Basin and perhaps many areas of the Basin and Range province probably contain a small degree of partial melt and are capable of generating small volumes of basalt magma (Crowe et al., 1995, Chapters 3 and 4).
 4. The YMR is located at the north edge of an amagmatic gap, an area that experienced no or very limited Cenozoic volcanic activity during extensional deformation (Farmer et al., 1989; Jones et al., 1992; Crowe et al., 1995). The amagmatic gap coincides spatially with and may be associated with an area of preserved ancient lithospheric mantle (Farmer et al., 1989).
 5. The most active areas of volcanism in the southern Great Basin (recurrence rates, erupted volumes) are at the eastern and western margins of the province (Suppe et al., 1975; Smith and Luedke, 1984). Rates of basaltic volcanic activity in the interior and less active parts of the southern Great Basin are much lower and it is more difficult to relate the location of basalt centers in the less active areas to individual faults or tectonic features (Crowe et al., 1986; 1995).
 6. There has been time-space migration of post-9.15 Ma basaltic volcanism in the YMR and this migration is characterized by a southwest stepping or southwest drift of areas of activity (Crowe et al., 1995; Golder Associates, 1995). The region and age of volcanic activity of most relevance to PVHA for the Yucca Mountain site is the area defined by the distribution of basaltic volcanic centers 5.05 Ma and younger. This area can be defined in different ways dependent on geologic interpretations of the volcanic record. Examples of alternative areal definitions include the Crater Flat volcanic zone (CFVZ; Crowe and Perry, 1989), the Area of Most Recent Volcanism (Smith et al., 1990) and the YMR/PQ (defined above, also see Crowe et al., 1995, Chapters 2 and 3).
 7. Ascent of basaltic magma in the YMR may follow deeper seated structural features such as buried strike-slip faults of the Walker Lane system (Crowe and Perry, 1989; Schweickert, 1989), or ring-fracture systems of Miocene caldera complexes (Crowe and Carr, 1980).
 8. Quaternary basaltic volcanic centers in the YMR/PQ and interior areas of the Basin and Range province tend to occur more commonly in alluvial basins than range interiors. This may be because the alluvial basins represent areas of low

but continuing extension (Fridrich, 1995) and/or they are generally the areas of lowest topographic elevation.

9. The volume of erupted magma in the YMR/PQ has declined from the Pliocene to the Quaternary but there may be a slight increase in the frequency of volcanic events in the late Quaternary (Vaniman and Crowe, 1981; Perry and Crowe, 1992; Crowe et al., 1995).
10. The generation, ascent and eruption of basaltic magma represents a composite of multiple interacting processes. While individual processes may be episodic or deterministic, the composite distribution of multiple interacting processes is probably best represented as a Poisson process (Tuckwell, 1988; Ash, 1993; Olkin et al., 1994). This assumption is verified by examining the sequence of volcanic events (Crowe et al., 1995, Chapter 7; Golder Associates, 1995). These analyses show that there are no consistent patterns in the location of individual volcanic events relative to the location of the immediately preceding volcanic event. The only general tendencies are for volcanic events to remain within a defined zone and a slight southwestward drift in the location of volcanic events through time. The rate of southwest drift is not significant for 10,000 years but could become significant for assessing volcanic hazards for intervals of hundreds of thousand of years (Golder Associates, 1995).

EVENT DEFINITION

A spatially and temporally discrete basaltic volcanic feature is termed a *volcanic center*, and for the purposes of PVHA, a volcanic center is considered equivalent to a volcanic *event*. A volcanic center is defined as a spatially and temporally related sequence of basaltic volcanic rocks that consists generally of a main scoria cone or cones, smaller satellite vents and associated lava flows. While this is a simple definition, there can be uncertainty in identifying and/or separating volcanic centers when, for example, a center consists of more than one spatially separate scoria cone. Generally, the uncertainty in identifying volcanic events is bounded in this elicitation through treating volcanic events as a probability distribution and using varying assumptions and alternative models in constructing the probability distributions.

Temporal Aspects

Small volume basaltic volcanic centers are generally regarded as monogenetic volcanic centers that are inferred to have formed during relatively brief intervals (months to years; e.g., see Wood and Kienle, 1990). Alternatively, detailed geologic, geochronology and geochemical studies of basalt centers in the YMR suggest that some may have formed during brief volcanic events separated by intervals of as much as several tens of thousands of years and would be classified as

polygenetic volcanic centers (Crowe et al., 1989; Wells et al., 1990, 1992; Crowe et al., 1995). A polygenetic classification for some volcanic centers in the YMR is regarded as permissive but unproved given current data for the volcanic centers of the YMR, and the model is not accepted by most volcanologists. Moreover, polygenetic volcanic events are not significant to PVHA primarily because the event of concern is the formation of a new volcanic center not the recurrence of eruptive events at an existing center. The polygenetic model is mentioned in this elicitation primarily because some researchers have incorporated this model in their definition of volcanic events used in PVHA (e.g., Ho et al., 1991; Ho, 1992). However, the polygenetic model, as used in this elicitation, only affects the maximum estimates of event counts (see following sections that describe event counts). A more significant uncertainty in the definition of volcanic events is the uncertainty in the chronology of the volcanic centers. This uncertainty varies with the age of an individual volcanic center and is strongly dependent on the quantity of collected data and the number of alternative geochronology methods used to establish the age of the center. Generally, the uncertainty in age determinations is within about 100 to 150 Ka of the cited age of volcanic events.

Spatial Aspects

The separation distances of volcanic events should correspond to the lengths of feeder dikes. Fedotov (1978) suggested that the width-to-length ratio of basalt dikes is about 10^{-2} to 10^{-3} corresponding to dike lengths of < 1 to 4 km using measured dike widths of 0.3 to 4 m (Crowe et al., 1983a). If several centers are aligned, as for example the Quaternary basalt centers of Crater Flat, the dimensions of an event could be as long as the alignment length and would probably be formed by multiple dikes (12.6 km in Crater Flat). Using these dimensions as guidelines, a separation of two volcanic centers by > 4-5 km would suggest the centers represent separate volcanic events; separation of centers by 10-12 km would strongly suggest separate events, regardless of chronology or geochemical data.

Geochemical Aspects

Conceptually, an individual volcanic event should be formed by a single pulse or batch of magma and the geochemical characteristics of the deposits of the event should be similar or be related by processes of fractionation or contamination. Alternatively, if there are significant differences in the geochemical composition of the volcanic deposits that cannot be explained by magmatic processes, the deposits could be judged to be formed from two volcanic events. In practice however, there may not be a complete understanding of all possible mechanisms of geochemical diversity in a basalt center and geochemical differences by themselves may not be sufficient evidence to define separate volcanic events. Thus interpretations based on geochemical data must

be used somewhat cautiously and these data are used in the elicitation primarily to define alternative approaches to minimum, maximum and most likely event counts.

Note: The elements of the PVHA model are summarized in the form of a logic tree in Figure BC-1.

UNDETECTED EVENTS

In addition to volcanic events defined from chronology, spatial and geochemical data, there is the potential for hidden or undetected events. These events would be represented by intrusive events that might exist at depths of about 300 m (repository depth) but did not erupt magma to the surface. Because these events could contribute to the cumulative event counts, they are considered in assessment of maximum event models. Consideration of the number of hidden or undetected events is dependent on the age and geologic setting of the events. Quaternary volcanic centers are too young to be completely buried by surficial processes. This is demonstrated by the relatively unmodified character and limited burial of Quaternary volcanic centers in the YMR (Crowe et al., 1995). In contrast, some Pliocene and Miocene centers are known to be buried beneath alluvium (Crowe et al., 1995). The geologic setting of basaltic centers also affects the likelihood of the possible presence of undetected events. Basalt centers located in alluvial fill or most rock types of Paleozoic age are readily detectable using aeromagnetic data because of the strong contrast in magnetic susceptibility between basalt and these deposits. The likelihood of undetected events would be higher where basalt centers are situated in volcanic country rock because of decreased contrasts in magnetic susceptibility. Geologic setting is probably important only for the basalt of Thirsty Mesa, the Hidden Cone and possibly the Lathrop Wells center; all other Pliocene and Quaternary basalt centers are in alluvial deposits. A working assumption of the elicitation is the inference that there are no major undetected events. That is, undetected events are of concern only for assessing the maximum event count models. It is judged to be highly unlikely that volcanic events like a cluster of centers or a center with the dimensions of the Lathrop Wells volcano would be undetected. This judgment is based on two observations. First, high quality low altitude drape aeromagnetic data have been obtained for the YMR (for example Kane and Bracken, 1983; Langenheim, in press) and these data are ideal for detection of basalt centers in the extensive alluvial fill of valleys in the YMR. Further, the quality of data interpretations has been investigated at some sites through exploratory drilling that verified the presence of inferred buried basalt (Carr, 1982; Carr and Parish, 1985). Second, it is judged to be highly unlikely for basalt magma to ascend as a dike to depths as shallow as 300 m (repository depth) and not erupt at some point along the length of the dike. Dike ascent at shallow depths should be controlled by release of volatiles as the magma approaches the surface of the earth (Wilson and Head, 1981).

REGION OF INTEREST

The region of interest for the PVHA is the southern Great Basin, and it is subdivided into two partly overlapping sets for this elicitation. The first set includes regional models that are used to assess background rates of volcanic activity for the southern Great Basin; PVHA estimates are used from these models to compare and cross-check results of PVHA applied to the second set. The second set includes the distribution and structural-tectonic models of volcanic events in the YMR and the YMR/PQ, and these models form the primary basis for the PVHA.

The subdivisions of the southern Great Basin are based on two concepts. First, there is a background level of low recurrence rates of the formation of small volume basalt centers of Quaternary age within the relatively inactive areas of the *interior* parts of the southern Great Basin (generally east of Death Valley, south of the south end of the Reville range, north of Las Vegas and west of the eastern border of the State of Nevada). Recurrence rates and disruption probabilities for volcanic zones in the YMR and YMR/PQ should be greater than these background rates. Second, higher recurrence rates and disruption probabilities should apply to volcanic zones that are demarcated by the spatial distribution of Pliocene and Quaternary volcanic centers, by structural, tectonic or topographic features, or by combinations of these features. The Yucca Mountain site is located near but outside most of the defined volcanic zones (see following sections). Logically, the recurrence rates and disruption probabilities for the Yucca Mountain site must be greater than the bounds established from regional background models (minimum bounds) and somewhat less than estimates obtained assuming location of a repository in volcanic zones (maximum bounds). These bounds are listed in Tables BC-1 and BC-2.

REGIONAL MODELS AND PROBABILITY BOUNDS

Three regional zones are described and illustrated on Figures BC-2 through BC-4. The first zone is the southern Great Basin region and it includes all significant sites of Pliocene and Quaternary volcanic centers within the area outlined on Figure BC-2. The area does not include the Lunar Crater or Reville areas, areas west of the west side of Death Valley, and areas east of the Nevada Test Site. The second region (Figure BC-3) is a modified version of the Armagosa Valley Isotopic Province (AVIP) as defined by G. Yogodzinski (presentation at PVHA Workshop 3). The AVIP zone is modified slightly to include the basaltic andesite of Skull Mountain and the basalt of Pahute Mesa, sites with isotopic ratios of Sr and Nd that correspond to the AVIP (Crowe et al., 1986; Farmer et al., 1989; G. Yogodzinski presentation at PVHA Workshop 3). The third regional zone is the distribution area of the Postcaldera basalt (PCB) of the YMR including the Older postcaldera basalt, the Younger postcaldera basalt and all aeromagnetic anomalies suspected to represent buried basalt

centers (Crowe et al., 1995, Chapter 2). This third regional zone (Figure BC-4) is the only model where event counts, recurrence rates and disruption ratios are assessed for Miocene basaltic volcanic rocks (post-9.05 Ma).

Simple logic requires that the probability of disruption of the Yucca Mountain site must be greater than regional background models and less than the disruption probabilities *within* local volcanic zones. The first step followed in this elicitation is to estimate recurrence rates and disruption ratios for the regional-background models. The minimum probability bounds for the regional models are summarized in Table BC-1. These estimates use the map areas for the three regional zones from the outlines shown on Figures BC-2 through BC-4. The event counts used for the recurrence rates are the *most likely* event counts from the data presented in the following sections. The Quaternary event counts are for the post-1.8 Ma (current definition of the Quaternary) and the Plio-Quaternary are for the post-5.05 Ma (to be consistent with the interval used for spatial models, described below. A post-9.15 Ma interval is estimated for the PCB zone only because there are insufficient data for late Miocene event counts for most regions outside of the PCB zone. The estimated disruption probability assumes random location of a repository with dimensions appropriate to the Yucca Mountain site *in* the regional-background zones. The maximum probability bounds listed in Table BC-2 are for volcanic zones in the PCB zone. The zone definitions and event counts used in Table BC-2 are presented in following sections.

SPATIAL MODELS

The approach developed to assess the future locations of volcanic activity in the YMR is based on subdividing the region of interest into zones, or the *zonation* approach. This approach also incorporates a *uniform* approach, as the future distribution of events is assumed to be uniform within each designated zone.

Three alternative time intervals are considered for the analysis that are established from the ages of volcanic centers in the YMR. These intervals are adjusted for uncertainty in establishing the age of volcanic events, defined as 150 ka to encompass the uncertainty of all geochronology measurements (see section above on temporal aspects of event definitions). The intervals used are:

Post-1.15 Ma Interval

This interval extends from the present ($t = 0$) to the eruption of the 1.0 Ma Quaternary basalt of Crater Flat (Crowe et al., 1995). Its upper bound is marked by the approximately 1.9 Ma hiatus between the basalt of the 2.9 Ma Buckboard Mesa and the 1.0 Ma Quaternary basalt of Crater Flat.

Post-5.05 Ma Interval

This interval extends from the present ($t = 0$) to the 4.95 Ma age of the basalt of Thirsty Mesa. The upper limit of the interval is marked by the approximately 1.25 Ma hiatus between the basalt of Thirsty Mesa (age established from chronology data presented by F. Perry at PVHA Workshop 1) and the youngest age for the basalt of Nye Canyon (Crowe et al., 1995). This interval coincides with the timing of a major change in the spatial patterns of basalt centers that occurred between the OPB and YPB cycles (Crowe et al., 1995, see Chapter 3).

Post-9.15 Ma Interval

This interval extends from the present ($t = 0$) to the 9.0 Ma age of the oldest basalt center of the Older postcaldera basalt, the basalt of Pahute Mesa (Crowe et al., 1995, Chapter 2). Two alternative approaches are used to subdivide the region into zones: the pattern of observed volcanic centers and structural considerations. These zone types and their weights for the hazard analysis are as follows:

- | | |
|----------------------------------|--------|
| Set 1. Event-Distribution Zones | (0.40) |
| Set 2. Structural-Tectonic Zones | (0.60) |

Event-Distribution Zones

Event-distribution zones are established through systematic examination of different combinations of the distribution areas of volcanic events in the YMR. The geometry of the zones is allowed to vary according to the distribution of events, and it is controlled by both the interval chosen for the event rates and by geologic assumptions concerning the volcanic record of the chosen interval. For event-distribution zones, the geometry of the individual zones varies as a direct function of the included volcanic centers. The intervals used for the distribution zones correspond to gaps or breaks in the distribution of ages of the volcanic centers and/or changes in the spatial distribution of volcanic events.

Distribution zones were developed for different combinations of volcanic events using the chronology intervals listed above; the zones shown on Figures BC-4, BC-5, BC-6, and BC-7. Three event-distribution zones are used in the PVHA including variations of the CFVZ of Crowe and Perry (1989), the Younger Postcaldera model, which corresponds geographically to the YMR/PQ, and the distribution area of the PCB, which corresponds geographically to the YMR. The PCB zone is somewhat difficult to apply to PVHA because the added Miocene events are weak predictors of future volcanic activity and the added distribution area does not include the Yucca Mountain site. However, this zone was included in the PVHA for two reasons. First, there was considerable discussion concerning the inclusion of the OPB in probability estimates during PVHA workshops

and field trips. Second, developing probability estimates for the distribution areas and event counts of the YPB and the OPB was judged to be useful for comparison with other probability estimates.

The following event-distribution zones are used:

The Quaternary and Plio-Quaternary CFVZ

Two zones are defined that encompass the Quaternary CFVZ (Figure BC-5) and the Plio-Quaternary CFVZ (Figure BC-6).

The Younger Postcaldera Zone

This zone is defined by the distribution of all Pliocene and Quaternary basalt centers in the YMR (Figure BC-7) and includes the basalt of Buckboard Mesa and the aeromagnetic anomalies of the Crater Flat and the Amargosa Valley basins. The Younger Postcaldera zone is identical geometrically to the YMR/PQ. The Quaternary CFVZ (Figure BC-5) is identical to the Quaternary portion of the Younger Postcaldera Zone.

The Postcaldera Basalt Zone

This zone is defined by the distribution of the Miocene and younger basalt units of the Postcaldera basalt episode (Figure BC-4), and is identical to the third regional-background model.

The relative weights assigned to these zones are as follows:

Plio-Quaternary and Quaternary CFVZ	(0.80)
Younger Postcaldera Zone	(0.15)
Postcaldera Basalt Zone	(0.05)

The Plio-Quaternary and Quaternary models are judged to best reflect likely patterns of future volcanism. These distribution areas do not include the basalt of Buckboard Mesa because this basalt site is located 35 km N-NE of Yucca Mountain and is judged not to be part of the Walker Lane setting associated with Yucca Mountain (described below). Moreover, the geochemical composition of the basalt of Buckboard Mesa is different than all other basalt units of the CFVZ (Vaniman and Crowe, 1981; Vaniman et al., 1982; Crowe et al., 1986). The distribution area of the Postcaldera basalt is given a lower weight because of the older age of the basalt units of the OPB and the distribution area added by including the volcanic events of the OPB does not include the Yucca Mountain site.

Structural-Tectonic Zones

Structural-tectonic zones are based on the assumption that Pliocene and Quaternary basalt centers of the YMR occur in zones that can be defined through assessment of controlling structural and tectonic features of the geologic setting of the YMR. Basalt centers are inferred to occur preferentially within these zones so that there are higher rates of event recurrence in the zones than outside the zones. There are two important inferences associated with the selection of structural-tectonic zones. First, structural-tectonic features probably provide ascent pathways for basalt magmas primarily through the occurrence of fractured rock. The features do not control the generation of basalt magma, but instead provide passive but preferential pathways that permit or facilitate the ascent of basalt magma. There is a greater likelihood, therefore, of future volcanic events within the structural-tectonic zones than outside of the zones. Second, basalt magma may divert at shallow levels within the zones and form basalt dikes oriented in N-NE trending directions following the maximum compressive stress direction (Crowe et al., 1995, Chapters 3 and 5).

The following structural-tectonic zones are used:

The Plio-Quaternary and Quaternary Pull-Apart Zone

These zones are based on the work of Fridrich (1995) who concludes that the Crater Flat structural basin was formed by a combination of east-west to southeast-northwest extension and northwest-directed right slip. The boundaries of the basin changed through time and included the Yucca Mountain site during the Miocene, the Amargosa and Crater Flat basins during the Pliocene, and only the Crater Flat basin during the Quaternary. The following subsets are used for this model: (a) Quaternary model consisting of the Crater Flat topographic basin (Figure BC-8), (b) subdivisions of the Quaternary model that correspond to the fault models of the Crater Flat basin developed by G. Thompson (presentation at PVHA Workshop 4) (Figure BC-9), and (c) Plio-Quaternary model consisting of the Crater Flat topographic basin and the area of the Amargosa Valley containing aeromagnetic anomalies assumed to be buried basalt centers (Figure BC-10). These three subsets are weighted equally (0.33, 0.33, 0.33) in the elicitation.

The Northwest-Trending Walker Lane Zone (WLZ)

This zone is based on the assumption that largely buried structural features of the Walker Lane structural system control the distribution of volcanic events in the YMR. The system is inferred to extend from the Amargosa basin on the southeast to a sub-basin of Sarcobatus Flat on the northwest (Figure BC-11). Two intervals are used for the events count for the WLZ (1.15 and 5.05 Ma), but the geometry/area of the zone is held constant for both intervals.

The Northeast-Trending Structural Zone (NESZ)

This zone is based on the assumption that a northeast-trending structural zone, defined by parallel sets of west-down, closely spaced normal faults, extends from Pahute Mesa through Yucca Mountain to the Amargosa Valley (Figure BC-12). The model is a composite of the structural models of Carr (1990), Smith et al. (1990), and the en echelon pull-apart basin models of Wright (1987) and Carr (1990). The NESZ, like the WLZ, is evaluated for two intervals (1.15 and 5.05 Ma) with the geometry/area of the zone held constant for both intervals.

The relative weights assigned to these zones are as follows:

Plio-Quaternary and Quaternary Pull-Apart Zones	(0.60)
Walker Lane Zone	(0.25)
Northeast-Trending Structural Zone	(0.15)

The basalt centers of the YMR are assumed to occur primarily in alluvial basins at sites of continuing extension and thus the pull-apart basin models are given the highest weights. This is supported both by the distribution of the basalt centers and the observation from the T. Brocher seismic refraction/reflection line (G. Thompson presentation at PVHA Workshop 4) that the basalt centers of Crater Flat occur mostly above the deepest parts of the Crater Flat basin. The Walker Lane model is judged to be important but it is a buried structure, there is limited evidence of through-going Walker Lane structures, and its expression in the regional geology of the YMR appears primarily to be in the location and development of en echelon, pull-apart basins. Thus the pull-apart basin models are favored over a through-going Walker Lane structure. The justification for the northeast-trending structural zone is dependent on the location of only one center (basalt of Buckboard Mesa) in the Plio-Quaternary record of the YMR. The normal faults that define the zone do not appear to be preferred pathways for ascent and eruption of basalt magma, and the model of Wright (1987) has more direct application to the Amargosa Valley and areas to the south than to Yucca Mountain and areas to the north.

Distribution of Events Within Zones

Two questions must be considered for the distribution of events in defined zones. These are: (1) what constraints can be placed on the distribution of events within zones?, and (2) what is the nature of the boundaries of the zones?

The distribution of events within zones cannot be strongly constrained using the data sets of Plio-Quaternary volcanic events in the YMR. This is based on the observation that while there are broad patterns to the distribution of events, the sequence of events jumps randomly with respect to jump lengths and jump directions (Crowe et al., 1995, see Chapter 7; Golder Associates, 1995). There

may be a slight tendency for a southwest drift of event locations through time and an oscillation of center locations between northwest and southeast poles (Golder Associates, 1995). However, the location of any one volcanic event does not provide significant constraints on the location of a succeeding event. Thus smoothing or clustering models that are based on event locations are not used in this elicitation. Instead, event locations are allowed to vary randomly within distribution and structural-tectonic zones.

The boundaries of zones are defined based on topographic criteria (e.g., topographic basins) or on the distribution of volcanic events. No simple generalizations can be made on the nature of the boundaries for individual zones and there is uncertainty in their locations. To incorporate this uncertainty in the modeling, volcanic events are confined within zones but feeder dikes associated with the events are allowed to extend beyond the zone boundaries. Thus the uncertainty of zone boundaries is captured in the assigned dimensions of basalt feeder dikes.

Background Zones

The zonation models considered for the post-1.15 Ma and post-5.05 Ma time periods include cases where the repository does not lie within a source zone. The rate of events in the immediate vicinity of the site is then determined by a background rate computed for the region of interest. As described previously, these alternative regions of interest are considered the SGB, AVIP, and PCB zones (Figures BC-2 through BC-4). Zones SGB and AVIP are considered equally acceptable for providing estimates of background rates. The PCB zone is considered less likely because it contains very few events, except for the post-9.05 Ma time period. The relative weights assigned to these zones depend upon the time period. For the post-1.15 Ma time period the SGB and AVIP zones are considered with weights of (0.5) and (0.5). The PCB zone is excluded because it contains no events. For the post-5.05 Ma time period, the weighting is: SGB (0.4), AVIP (0.4), and PCB (0.2). For the post-9.05 Ma time period, the site lies within the large PCB zone and no consideration of a background zone is needed.

EVENT COUNTS

Using the event definitions provided above, the number of events are described as probability distributions that are designed to encompass the uncertainty of the event definitions for individual basaltic centers in the YMR and for the regional zones. The event counts are listed for the YMR in order of decreasing age and are divided into basalt cycles (OPB and YPB). These data are followed by event counts for the surrounding regions of the southern Great Basin. The latter sites are described by geographic locality and not in order of age. The level of information available for the event counts is greatest for the YMR and generally decreases with increasing distance from

the YMR (except for Ubehebe Craters, described by Crowe and Fisher, 1973). A summary of event counts is provided in Table BC-3. Rates of occurrence based on the event counts are shown in Table BC-4.

OLDER POSTCALDERA BASALT

Basalt of Pahute Mesa

The geology and chronology of the basalt of Pahute Mesa are described in Crowe et al. (1995). The basalt sites consist of three spatially separate basalt centers that are partly to deeply dissected. Their separate locations and somewhat different K-Ar ages require a 3-event minimum model. The western and central centers expose large and somewhat complex conduit plugs, vent scoria and multiple feeder dikes and could represent more than one event; these observations provide the basis for the 4-event and 5-event scenarios. The addition of two undetected events is permissible given the deep degree of dissection of all the volcanic centers.

Event counts and relative weights: 3 (0.50), 4 (0.20), 5 (0.15), 6 (0.10), 7 (0.05)

Basalt of Paiute Ridge

The basalt of Paiute Ridge was mapped by Byers and Barnes (1967) and described by Crowe et al. (1983b) and Valentine et al. (1992). The site consists of multiple sill-and-dike complexes centered in a graben in the interior of the Half Pint range. Ratcliff et al. (1994) showed that the mafic intrusions and lava flows of the center record a geomagnetic field reversal of probable short duration, a compelling argument that the center formed during a single brief magmatic event. However, an equally convincing argument can be made that the length and spacing of the mapped intrusions probably requires at least 2 separate feeder dike systems. Accordingly, the 1-event and 2-event scenarios are given equal weights and are treated as the most likely events. As many as 3-to-4 events can be identified if vent areas, marked by plugs and eroded scoria deposits, are equated to individual cones and each spatially separate cone is defined as a volcanic event. A 5-event scenario is used to account for undetected events.

Event counts and relative weights: 1 (0.35), 2 (0.35), 3 (0.15), 4 (0.10), 5 (0.05)

Basalt of Scarp Canyon

A separate basalt site crops out southeast of the basalt of Paiute Ridge and west of Nye Canyon. This site was included with the basalt of Paiute Ridge in Crowe et al. (1995), but is classified as a separate unit for this elicitation. The site consists of a 3-to-4 km basalt dike and two small plug masses. A second spatially separate site intersected in a drillhole in alluvium in Frenchman Flat

was dated at 8.6 Ma and is probably correlative with the basalt of Scarp Canyon (Crowe et al., 1995). The spatial separation of the two sites suggests that a 2-event scenario is preferred for the most likely model. A 3-event model is assigned an equal probability because there is limited information on the extent of the basalt encountered in the drillhole site in Frenchman Flat and geophysical data for Frenchman Flat have not been examined by the author. A 1-event scenario is assigned a low weight but is considered possible and assumes the age and correlation of the basalt site in Frenchman Flat are incorrect. The 4-event and 5-event scenarios are allowed for the maximum model assuming the possible presence of one or two undetected events.

Event counts and relative weights: 1 (0.05), 2 (0.40), 3 (0.40), 4 (0.10), 5 (0.05)

Basalt of Yucca Flat

A basalt unit was intersected in drillhole UE1-8 and a basalt sample from the unit was dated at 8.1 Ma (Carr, 1984). Event scenarios of 1 to 3 events are assigned to the site and include the possibility of undetected events.

Event counts and relative weights: 1 (0.40), 2 (0.40), 3 (0.20)

Basalt of Rocket Wash

The basalt of Rocket Wash consists of one eroded vent, the source of a single lava flow that upholds a small mesa along the west edge of the ring-fracture zone of the Timber Mountain caldera (Crowe et al., 1995). The preferred event count for the site is a 1-event scenario based on the limited extent of the scoria-cone deposits and the simple geometry of the vent and flow complex. As many as three events may be possible (including undetected events) primarily because geophysical data for the site have not been examined by the author. However, multi-event models are given lower weights because the lava flow upholds topography (inverse topography) and the unit has not been buried by younger deposits.

Event counts and relative weights: 1 (0.75), 2 (0.20), 3 (0.05)

Basalt of Nye Canyon

The geology and chronology of the basalt of Nye Canyon were summarized by Crowe et al., (1986; 1995). The site consists of an alignment of three surface centers and a buried center in the northeast edge of Frenchman Flat (Carr, 1974). The number of possible volcanic events at Nye Canyon ranges from 1 to as many as 9. A 1-event scenario is given a small weight because the length of the alignment of the four centers exceeds the probable length of a single feeder dike. Scenarios

of 2-to-3 events are given near-equal weights and are treated as the most likely scenarios because the spacing of the centers probably requires two dikes (two-event model) and the middle Nye center (surface center) is petrologically distinct, contains nodules of mantle periodite and has a high Mg number (Crowe et al., 1986; Farmer et al., 1989). The models of 4 and 5 events respectively, are given equal weights because each center could be treated as a single event, and the southern Nye Center (surface center) is associated with a complex arcuate dike that could represent more than one event. As many as 4 additional events are permissible as undetected events given the complexity of the arcuate dike, and because geophysical data for the buried basalt center in Frenchman Flat have not been examined by the author.

Event counts and relative weights: 1 (0.02), 2 (0.20), 3 (0.20), 4 (0.16), 5 (0.16), 6 (0.12), 7 (0.08), 8 (0.04), 9 (0.02)

YOUNGER POSTCALDERA BASALT

Basalt of Thirsty Mesa

The geology of the basalt of Thirsty Mesa has been summarized by Crowe et al., (1995). The center consists of a lava mesa surmounting an ignimbrite plateau upheld by the Thirsty Canyon Tuff. The center is modeled as one to three events based on existing geologic information. A 1-event model is supported by the similarity in age determinations of samples collected from basal lava flows and a feeder dike from the summit vent of Thirsty Mesa (Crowe et al., 1995). Paleomagnetic data presented by D. Champion (PVHA field trip to Sleeping Butte) are consistent with a single short duration event. Geochemical data show no evidence of compositional variation that cannot be explained by a 1-event eruptive history (Crowe et al., 1986; 1995; F. Perry presentations at PVHA Workshops 1 and 3). The 2- and 3-event models are based on reconnaissance geologic mapping that shows the vent area for the center consists of three partly coalesced scoria/spatter cones. The likelihood of undetected events from burial is judged to be extremely low because the center is a high-standing topographic feature.

Event counts and relative weights: 1 (0.85), 2 (0.09), 3 (0.06)

Amargosa Valley

The aeromagnetic anomalies of the Amargosa Valley have been described by Kane and Bracken (1983), Langenheim (in press) and Crowe et al., (1995). Only one of the aeromagnetic anomalies (anomaly B of Langenheim, in press) has been drilled and dated at about 3.9 Ma (Crowe et al., 1995). Its age is consistent with burial through time of a former surface volcanic center by over 100 meters of alluvial fill. This amount of burial is consistent with the location of the anomaly

near the trace of the Fortymile Wash which empties into and ends in the Amargosa Valley. Anomaly D may be related to a basalt intersected in a water well at 190-m depth (Langenheim, in press). Modeling of anomaly C suggests a 1- to 1.5-km-wide body at a depth of 200 m, presumably a subaerial scoria cone and lava flow that were buried by alluvial fill. None of the anomalies can be modeled reasonably as buried dikes (V. Langenheim, pers. comm. during the elicitation on 13-June-95). Three to 12 volcanic events are judged to be possible in the Amargosa Valley with the 6-event scenario assigned as the most likely event count. The 3-event scenario consists of anomaly B, a single combined event for anomalies C and D, and anomaly E. Two of these events have been identified from borehole data (Langenheim, in press), anomaly B has a shape consistent with the presence of a single center with a lava flow extending from the center to the south, anomalies C and D are closely spaced and could be a single event, and anomaly E is a small anomaly and is probably a single center. Anomalies F and G are inferred to be produced by local ash-flow tuff or lava and are judged not to be of Pliocene age. The 6-event scenario infers that anomalies A, B, C, D, E each represents individual events with anomalies F and G combined into a single event because of their close spacing. The separation of anomalies C and D into individual events is based on their different magnetic polarities inferred from aeromagnetic data (Langenheim, in press). The maximum event model assumes anomalies F and G are separate events, assigns 3 events to anomaly B because of its large size, and allows for 2 hidden events. A larger number of undetected events are assigned to the anomaly sites of Amargosa Valley because of the complete burial of all sites by alluvium and the limited exploratory drilling of the anomaly sites.

Event counts and relative weights: 3 (0.05), 4 (0.12), 5 (0.20), 6 (0.20), 7 (0.20), 8 (0.10), 9 (0.07), 10 (0.03), 11 (0.02) and 12 (0.01).

3.7 Ma Basalt of Southeast Crater Flat

The 3.7 Ma basalt of southeast Crater Flat has been described by Vaniman and Crowe (1981), Vaniman et al. (1982), and is summarized in Crowe et al. (1995). The basaltic unit is inferred to represent 1 to 8 events with the most likely event counts being 2-to-3 events. The 1-event model is based on uniform, but incompletely documented, field magnetic directions for the deposits (Champion, 1991). The 2-event model is judged the most likely model because a minimum of two dike feeders are needed to explain the vent distribution and the vents occur over a length of 4.8 km. A 3-event model is given equal weighting because of the presence of a large eroded center at the north end of the vent alignment (Vaniman and Crowe, 1981) coupled with the geometric requirement of two feeder dikes. Four to as many as 6 events are required if each identified vent area is judged to represent a volcanic event; each event-count is given equal weighting (4-events, 5-events and 6-events) because there is no basis to discriminate the different counts. However, each of the events are weighted lower than the 2- and 3-event scenarios on the basis of the alignment

of the centers, the uniformity of chronology data for samples along the length of the alignment (Crowe et al., 1995) and the apparent uniformity of field magnetization directions (Champion, 1991). The 7-event and 8-event models assume up to two undetected events and are given somewhat higher weightings than undetected events for other sites in the YMR because of the extensive alluvial cover of the eastern outcrops of the basalt unit.

Event counts and relative weights: 1 (0.10), 2 (0.25), 3 (0.25), 4 (0.10), 5 (0.10), 6 (0.10), 7 (0.05), 8 (0.05).

Basalt of Buckboard Mesa

The basalt of Buckboard Mesa has been mapped by the U.S. Geological Survey and the data compiled at a scale of 1:24,000 on geologic quadrangle maps and summarized on the geologic map of the Timber Mountain caldera (Byers et al., 1976). The geology of the center was described by Lutton (1968) and summarized in Crowe et al., (1995) and Crowe and Perry (1995). The preferred event model for the center is the single-event model. This is based on uniformity in age determinations (2.9 to 3.1 Ma; Crowe et al., 1995; Crowe and Perry, 1995), the compositional uniformity of the basalt lavas in outcrop and in drillholes (Lutton, 1968; Crowe et al., 1986; 1995), and the presence of only a single scoria cone and fissure system at the center (Scrugham Peak; Lutton, 1968; Crowe et al., 1995). A 2-event scenario is possible based on the presence of a second, kaersutite-bearing lava flow northwest of Scrugham Peak. However, this lava is similar in age and composition to the other lavas (Crowe and Perry, 1995) and accordingly the 2-event scenario is given a lower weighting. A 3-event model allows for an undetected event but is given a low weighting because of the observation that the basalt of Buckboard Mesa filled a topographic low and is now a topographic high (inverse topography).

Event counts and relative weighting: 1 (0.70), 2 (0.25), 3 (0.05)

Quaternary Basalt of Crater Flat

The Quaternary basalt of Crater Flat has been described by Vaniman and Crowe (1981), Vaniman et al. 1982), Smith et al. (1990), Ho et al. (1991), and the data are summarized in Crowe et al. (1995). One to 7 volcanic events are required to explain the centers, with the 3-event scenario given the highest weighting (most likely estimate). The 1-event scenario is based on the alignment of the centers, the inferred uniformity of their field magnetic directions (Champion, 1991) and the general consistency in the results of age determinations obtained for the centers (Crowe et al., 1995, Chapter 2). Weaknesses of this interpretation are measurement uncertainty in paleomagnetic data, uncertainty concerning the nature of secular variation during the time of eruption of the Quaternary basalt of Crater Flat and some divergence in the results of geochronology data (F. Perry presentation

at PVHA Workshop 1), and the alignment length (12.6 km) exceeds likely dimensions of a single feeder dike. The 2-event scenario assumes that Red Cone and Little Cones, and Black Cone and Makani Cone, were each formed by a single and separate feeder dike. This model is based on a somewhat arbitrary subdivision of the centers and it is given a lower weighting. The preferred three-event scenario assumes that Red Cone and Black Cone formed from a single pulse of magma (1-event; see geochemical data of Bradshaw and Smith, 1994), and the Little Cones and Makani centers each formed as separate events. This is supported by the observation that the Little Cones center can be discriminated geochemically from the Red Cone and Black Cone centers (F. Perry presentation at PVHA Workshop 1), and both Little Cones and Makani cone are spatially separate (3-4 km separation) between the Red Cone and Black Cone centers, respectively. The 4-event scenario assumes each center represents a separate volcanic event. This scenario also assumes that there is sufficient uncertainty in geochronology data to permit this interpretation and that the paleomagnetic data may not represent the temporal complexity of the volcanic events. The 5-event scenario assumes Little Cones consists of two centers (Connor and Hill, 1993), but this scenario is given a low weighting because of the small spacing between the two scoria cones of the center. The 6-event and 7-event scenarios assume 1 or 2 undetected events primarily because the Little Cones site has been partly buried and there is an unexplained positive aeromagnetic anomaly about 1 km south of the Little Cones (Crowe and Carr, 1980; Crowe et al., 1986; 1995). The possibility of other undetected events is given a low weighting because of the high quality of aeromagnetic data for the basin, the location of the basalt centers in alluvium deposits, the availability of subsurface control from two nearby drill holes (VH-1 and VH-2), and the high quality seismic reflection/refraction data near the centers.

Event counts and relative weights: 1 (0.10), 2 (0.10), 3 (0.45), 4 (0.20), 5 (0.10), 6 (0.025), 7 (0.025)

Basalt of Sleeping Butte

The basalt of Sleeping Butte has been described by Crowe and Perry (1991), and the geology of the center is summarized in Crowe et al. (1995). The latter summary does not include the results of recent geologic mapping (Crowe and Perry, 1995) that has verified the presence of a second lava flow lobe from the Hidden Cone center. One to as many as 3 events could be represented by the deposits of the Sleeping Butte center. In the 1-event scenario, Little Black Peak and Hidden Cone are assumed to be fed by a single feeder dike, an inference that is supported by paleomagnetic data (Champion, 1991). The 2-event scenario assumes each center is a separate event based on the 2.6 km separation of the centers, the different field magnetic directions obtained at the northwest flow lobe of the Hidden Cone center (D. Champion presentation at PVHA Sleeping Butte field trip), and the evidence of significant differences in geochemical composition of the centers (F. Perry

presentation at PVHA Workshop 1). The 3-event scenario assumes an undetected event could be associated with the Hidden Cone center, a permissive interpretation given the combination of the location of the center in country rock of Miocene tuff and the center is flanked to the north by extensive outcrops of basaltic lava flows and plugs of Miocene age. -

Event counts and relative weights: 1 (0.35), 2 (0.45), and 3 (0.20)

Lathrop Wells

The Lathrop Wells center has been described by Crowe and Carr (1990), Vaniman and Crowe (1981), Vaniman et al. (1982), Crowe et al. (1986), Wells et al. (1990), Turrin et al. (1991), Crowe et al. (1992), and is summarized in Crowe et al. (1995). One to as many as 4 events could be represented at the Lathrop Wells center. One event is given high preference partly because the polygenetic model for the center is not well accepted by the scientific community, but more importantly because polygenetic events are not significant to the PVHA. As many as three undetected events are possible but are given low weights. The possibility of undetected events is based on the complex structural setting of the center and local presence of Miocene tuff beneath the center. The low event-weightings for undetected events are because of the high quality of aeromagnetic coverage for the center, and at least part of the center overlies alluvial deposits.

Event counts and relative weights: 1 (0.90), 2 (0.06), 3 (0.03), 4 (0.01)

SOUTHERN GREAT BASIN REGION

Death Valley

The Death Valley area has not been mapped at the same level of detail as the basalt centers of the YMR. Basaltic volcanic rocks in the Death Valley area of most relevance to PVHA range in age from Pliocene to Quaternary (Crowe et al., 1986). The Quaternary centers include the Split Cone and the basalt of Shoreline Butte and the Quaternary event models range from 2- to 6-event scenarios. The two-event scenario is based on the age differences in the Quaternary events (0.7 and 1.7 Ma; Crowe et al., 1986), the different degree of geomorphic dissection of the centers and their geographic separation (> 5 km separation). The 3-event and 4-event scenarios are based on the observation of multiple vent areas, marked by accumulation of basaltic scoria, for the basalt of Shoreline Butte. The 5-event and 6-event scenarios allow for the possibility of hidden events because of possibly high sedimentation rates in the valley and the presence of pyroclastic surge deposits of unknown origin in drainages on the east side of the valley (Crowe et al., 1986).

Event counts and relative weights (Quaternary Death Valley): 2 (0.30), 3 (0.30), 4 (0.25), 5 (0.10) and 6 (0.05)

Event counts for Pliocene deposits are based on estimations of vent densities for outcrop areas of basaltic volcanic rocks of the 4-4.5 Ma Funeral Formation. Reconnaissance field studies were conducted on these rocks (Crowe et al., 1986) and their outcrop distribution was obtained from geologic maps of Loren Wright (B. Crowe, informal PVHA memo). The number of events is estimated by measuring the approximate surface area of the volcanic rocks, relating them to event densities observed at other basaltic fields (Crowe et al., 1986, 1995) and adding corrections for extensional deformation. The assigned vent densities vary from 0.10 to 0.40 events km^{-2} and are treated as a triangular distribution with the following parameters:

Event counts for the Pliocene Death Valley: minimum model 22 events (0.1 vent km^{-2}), most likely model 44 events (0.2 vent km^{-2}), and maximum model 88 events (0.4 vent km^{-2}).

Clayton Valley

There are no geochronology data for the basalt of Clayton Valley. The author examined the area briefly in a field visit in the early 1980s that included an assessment of its geomorphic state and measurements of magnetic polarity (reversed). The preservation of the center is consistent with a Quaternary age and it is probably > 700 ka based on its reversed polarity. There is only a single cone so the 1-event scenario is preferred. Additional events are added to account for undetected events.

Event counts and relative weights: 1 (0.85), 2 (0.10), 3 (0.05)

Ubehebe Craters

The Quaternary event counts in the Ubehebe area range from 1 to 6 events, with 1 event assigned as the most likely model. The 1-event scenario assumes Ubehebe is a monogenetic center formed during a single eruptive episode. Geologic mapping of the center (Crowe and Fisher, 1973) shows that it can be divided into eruptive sequences including an early scoria cone (Strombolian eruptions) that was partly destroyed by hydrovolcanic eruptions that formed Ubehebe Crater on the north flank of the scoria cone. The 1-event scenario is given a relatively high weighting because there is no evidence of a time break between the eruptive sequences. The 2-event model assumes simply that the strombolian and hydrovolcanic eruptive phases represent separate events. The 3-event and 4-event models allow for additional events to explain clusters of tuff rings/tuff cones and explosion craters on the south and west flanks of the center; these event counts are assigned decreasing weights with increasing event counts. The 5-event and 6-event models allow for undetected events.

Ubehebe event counts and relative weights: 1 (0.60), 2 (0.15), 3 (0.10), 4 (0.10), 5 (0.025), 6 (0.025)

Grapevine Canyon

Geologic mapping of Grapevine Canyon near its intersection with northern Death Valley is insufficient to establish individual event counts. The event-density method used for the southern Death Valley region is applied to an estimated exposure area of 60 km² but no corrections are made for extension.

Event counts for Grapevine Canyon treating the data as a triangular distribution: minimum model, 6 events (0.1 vent km⁻²); most likely model, 12 events (0.2 vent km⁻²); maximum model 24 events (0.4 vent km⁻²)

Basaltic Andesite of Towne Pass

The basaltic andesite of Towne Pass has been described in Crowe (1983) and Crowe et al. (1986) and is estimated to be about 5.0 Ma. The unit has not been mapped in detail and the event assignments are based on estimations of vent densities from an outcrop area of 110 km².

Event Counts for Towne Pass treating the data as a triangular distribution: minimum model 11 events (0.1 events km⁻²); most likely model, 22 events (0.2 events km⁻²); maximum model 44 events (0.4 events km⁻²)

TEMPORAL MODELS

The preferred temporal model is the homogeneous Poisson model (weight 0.7). A nonhomogeneous Poisson model has been considered by several workers (Ho, 1991; Connor and Hill, 1993; 1995), but gives nearly identical results as the homogeneous Poisson model (Crowe et al., 1995). The sensitivities of time-dependent models, varying ages, and uncertainty for volcanic centers and event counts are judged to be captured largely by choosing observation intervals that correspond to volcanic cycles (Crowe et al., 1995) and assigning probability distributions to the event counts.

Event ages and alternative event ages are summarized in a spreadsheet immediately following this text for all minimum, most likely, and maximum models. These ages are from Crowe et al. (1995), Crowe and Perry (1995) and data presented by F. Perry (presentation at PVHA Workshop 1). These ages are used to calculate β factors for nonstationary temporal models (weight 0.3).

EVENT GEOMETRIES

Dike Dimensions

Data for dike lengths are modified from Crowe et al. (1983b), Maaloe (1987), Barnard et al. (1992), Lister (1990), Lister and Kerr (1991), Sheridan (1992), Wallmann (1993), and Delaney and Gartner

(1995), with modifications for the YMR using observed cluster lengths of centers summarized below. Using theoretical constraints, dike lengths should range from about 0.5 to 10 km (Fedotov, 1978; Crowe et al., 1983b; Maaloe, 1987; Lister and Kerr, 1991). The maximum length of a cluster in the YMR is 12.6 km (Quaternary basalt of Crater Flat). Some constraints on dike lengths may be provided by map data for the Plio-Quaternary basalt centers of the YMR and from considerations of the dimensions of feeder dikes of volcanic centers using geochemical data to identify magma batches at volcanic centers. The following data provide constraints:

Cluster lengths:

(1) 3.7 Ma basalt centers	longest single fissure = 3.2 km en echelon dike length = 4.8 km
(2) Thirsty Mesa cluster	2.0 km
(3) Fissure system for the basalt of Buckboard Mesa	3.6 km
(4) Sleeping Butte cluster	2.6 km
(5) Red Cone-Black Cone alignment	3.2 km
(6) Longest fissure at the Lathrop Wells basalt center	< 2.0 km

Clearly some additional length of feeder dikes extends in the subsurface beyond surface outcrops so the data provide minimum constraints. Using all the above data sources, dike-length distributions assigned for the elicitation are:

(1) Triangular Distribution	minimum	=	0.3 km
	most likely	=	3.5 km
	maximum	=	7.0 km
(2) Normal Distribution	mean	=	3.5 km
	standard deviation	=	3.0 km

The weightings for the dike lengths are 0.60 for the triangular distribution and 0.40 for the normal distribution. The preferred location of events on the dike is near the center, and a triangular distribution is used to model event location.

Note: The resulting cumulative distributions and density functions are shown on Figure BC-15.

Dike Orientations

Dike orientations are based on the direction of the maximum compressive stress direction and the orientation of basalt clusters and groups of basalt centers in the YMR. Based on the presentation by G. Walker (PVHA Workshop 4), I judge that the dike orientations should be bimodal with a N-NE mode and a N-NW mode. The relative frequencies are 0.80 for the N-NE

set and 0.20 for the N-NW set and are assigned on the basis of the observed predominant alignment of vent clusters in the N-NE direction.

Distribution models for the dike orientations are:

- | | | | | |
|-------------------|-------------------------|-------------|---|-------|
| (1) N-NE Dike Set | Triangular Distribution | minimum | = | N-S |
| | | most likely | = | N20°E |
| | | maximum | = | N40°E |
| (2) N-NW Dike Set | Triangular Distribution | minimum | = | N40°W |
| | | most likely | = | N20°W |
| | | maximum | = | N05°E |

Eruption Types

Eruption types are based on the fragment types and sizes in the Pliocene and Quaternary basalt centers of the YMR as summarized in Crowe (1986) and Crowe et al. (1983a; 1983b; 1986; and 1995). The weights for the volcanic events in alluvial basins are:

Mixed Strombolian/Hawaiian	=	0.90
Hydrovolcanic	=	0.10

The weights for volcanic events in range interiors given the deeper depths to the ground water table than alluvial basins are:

Mixed Strombolian/Hawaiian	=	0.95
Hydrovolcanic	=	0.05

Probability of a Return to Silicic Eruptions

There have been no silicic eruptions in the YMR for the last 8.0 Ma. The probability of a future silicic volcanic event must be $\sim 1/8,000,000$ or $1.2 \times 10^{-7} \text{ yr}^{-1}$. This estimate combined with the cessation of silicic volcanism and migration of sites of silicic volcanism to the margins of the southern Great Basin suggests that the probability of a future silicic volcanic eruption must be $< 10^{-10} \text{ yr}^{-1}$.

Bruce Crowe
April 29, 1996

Nonhomogeneous Models: Event Chronology for E1 Incorporating Multiple Alternative Geochronology Models with the Most Likely Models						
EVENT-DISTRIBUTION MODELS	Event Categories	Minimum	Most Likely A	Most Likely B	Most Likely C	Maximum
		(Ma)	(Ma)	(Ma)	(Ma)	(Ma)
Model 1						
Plio-Quaternary and Quaternary Distribution Models Quaternary Cycle						
Event Ages						
	Quat CF	1.00	1.00	1.00	1.20	1.00
			1.00	1.00	1.00	1.00
			1.00	1.00	1.00	1.00
				0.75	0.75	1.00
						0.75
	Sleeping Butte	0.35	0.43	0.35	0.43	0.35
			0.43	0.35	0.35	0.35
	Lathrop	0.13	0.13	0.70	0.70	0.13
	Thirsty Mesa	4.90	4.90	4.90	4.90	4.90
						4.90
						4.90
	Amargosa	3.90	3.90	4.40	3.90	3.90
		3.90	3.90	4.40	3.90	3.90
		3.90	3.90	4.40	3.90	3.90
		3.90	3.90	4.40	3.90	3.90
			3.50	3.50	3.50	3.90
						3.50
	3.7 basalt CF	3.70	3.70	3.70	3.70	3.70
			3.70	3.70	3.70	3.70
			3.70	3.70	3.70	3.70
			3.70	3.70	3.70	3.70
			3.70	3.70	3.70	3.70
			3.70	3.70	3.70	3.70
						3.70
						3.70
	Buckboard	(not included in CFVZ)				
	Quat CF	1.00	1.00	1.00	1.20	1.00
			1.00	1.00	1.00	1.00
			1.00	1.00	1.00	1.00
				0.75	0.75	1.00
						0.75
	Sleeping Butte	0.35	0.43	0.35	0.43	0.35
			0.43	0.35	0.35	0.35
	Lathrop	0.13	0.13	0.70	0.70	0.13

	Event Categories	Minimum	Most Likely A	Most Likely B	Most Likely C	Maximum
		(Ma)	(Ma)	(Ma)	(Ma)	(Ma)
Model 2						
Younger Postcaldera Basalt						
Quaternary Cycle						
Event Ages	Quat CF	1.00	1.00	1.00	1.20	1.00
			1.00	1.00	1.00	1.00
			1.00	1.00	1.00	1.00
				0.75	0.75	1.00
						0.75
	Sleeping Butte	0.35	0.43	0.35	0.43	0.35
			0.43	0.35	0.35	0.35
	Lathrop	0.13	0.13	0.70	0.70	0.13
Plio-Quaternary						
Event Ages	Thirsty Mesa	4.90	4.90	4.90	4.90	4.90
						4.90
						4.90
	Amargosa	3.90	3.90	4.40	3.90	3.90
		3.90	3.90	4.40	3.90	3.90
		3.90	3.90	4.40	3.90	3.90
		3.90	3.90	4.40	3.90	3.90
			3.50	3.50	3.50	3.90
						3.50
	3.7 Basalt CF	3.70	3.70	3.70	3.70	3.70
			3.70	3.70	3.70	3.70
			3.70	3.70	3.70	3.70
			3.70	3.70	3.70	3.70
			3.70	3.70	3.70	3.70
				3.70	3.70	3.70
						3.70
						3.70
	Buckboard	2.90	2.90	3.10	3.10	2.90
	Quat CF	1.00	1.00	1.00	1.20	1.00
			1.00	1.00	1.00	1.00
			1.00	1.00	1.00	1.00
				0.75	0.75	1.00
						0.75
	Sleeping Butte	0.35	0.43	0.35	0.43	0.35
			0.43	0.35	0.35	0.35
	Lathrop	0.13	0.13	0.70	0.70	0.13

Model 3	Event Categories	Minimum	Most Likely A	Most Likely B	Most Likely C	Maximum
Postcaldera Basalt		(Ma)	(Ma)	(Ma)	(Ma)	(Ma)
Mio-Quaternary						
Event Ages	Rocket Wash	8.00	8.00			8.00
	Silent Canyon	9.10	9.10	9.10	9.10	9.10
		8.80	8.80	8.80	8.80	9.10
		8.80	8.80	8.80	8.80	9.10
						8.80
						8.80
						8.80
	Yucca Flat	8.10	8.10	8.10	8.10	8.10
						8.10
						8.10
	Paiute Ridge	8.60	8.60	8.60	8.60	8.60
		8.60	8.60	8.60	8.60	8.60
			8.60	8.60	8.60	8.60
						8.60
	Scarp Canyon	8.70	8.70	8.70	8.70	8.70
		8.60	8.60	8.60	8.60	8.70
						8.60
						8.60
	Nye Canyon	6.60	6.30	6.30	6.30	6.30
		7.20	6.80	6.80	6.80	6.80
			7.20	7.20	7.20	7.20
			7.20	7.20	7.20	7.20
			7.00	7.00	7.00	7.20
						7.00
						7.00
	Quat CF	1.00	1.00	1.00	1.20	1.00
			1.00	1.00	1.00	1.00
			1.00	1.00	1.00	1.00
				0.75	0.75	1.00
						0.80
	Sleeping Butte	0.35	0.43	0.35	0.43	0.38
			0.43	0.35	0.35	0.38
	Lathrop	0.13	0.13	0.70	0.70	0.13
	Thirsty Mesa	4.90	4.90	4.90	4.90	4.90
						4.90
						4.90
	Amargosa	3.90	3.90	4.40	3.90	3.90
		3.90	3.90	4.40	3.90	3.90
		3.90	3.90	4.40	3.90	3.90
		3.90	3.90	4.40	3.90	3.90
			3.50	3.50	3.50	3.90
						3.5

Model 3 (cont.)	Event Categories	Minimum	Most Likely A	Most Likely B	Most Likely C	Maximum
Postcaldera Basalt		(Ma)	(Ma)	(Ma)	(Ma)	(Ma)
Mio-Quaternary						
	3.7 basalt CF	3.70	3.70	3.70	3.70	3.70
			3.70	3.70	3.70	3.70
			3.70	3.70	3.70	3.70
			3.70	3.70	3.70	3.70
			3.70	3.70	3.70	3.70
				3.70	3.70	3.70
					3.70	3.70
						3.70
	Buckboard	2.90	2.90	3.10	3.10	2.90
	Quat CF	1.00	1.00	1.00	1.20	1.00
			1.00	1.00	1.00	1.00
			1.00	1.00	1.00	1.00
				0.75	0.75	1.00
						0.75
	Sleeping Butte	0.35	0.43	0.35	0.43	0.35
			0.43	0.35	0.35	0.35
	Lathrop	0.13	0.13	0.70	0.70	0.13
	Event Categories	Minimum	Most Likely A	Most Likely B	Most Likely C	Maximum
STRUCTURAL-TECTONIC MODELS		(Ma)	(Ma)	(Ma)	(Ma)	(Ma)
Model 1						
Pull Apart Basin						
Quaternary Cycle						
Event ages	Quat CF	1.00	1.00	1.00	1.20	1.00
			1.00	1.00	1.00	1.00
			1.00	1.00	1.00	1.00
				0.75	0.75	1.00
						0.75
	Lathrop Wells	0.13	0.13	0.70	0.70	0.13
Model 1 (cont.)						
Plio-Quaternary Cycle						
Event Ages	Amargosa	3.90	3.90	4.40	3.90	3.90
		3.90	3.90	4.40	3.90	3.90
		3.90	3.90	4.40	3.90	3.90
		3.90	3.90	4.40	3.90	3.90
			3.50	3.50	3.50	3.90
						3.50
	3.7 basalt CF	3.70	3.70	3.70	3.70	3.70
			3.70	3.70	3.70	3.70
			3.70	3.70	3.70	3.70
			3.70	3.70	3.70	3.70
			3.70	3.70	3.70	3.70
				3.70	3.70	3.70
					3.70	3.70
						3.70
	Quat CF	1.00	1.00	1.00	1.20	1.00
			1.00	1.00	1.00	1.00
			1.00	1.00	1.00	1.00
						0.75
	Lathrop Wells	0.13	0.13	0.70	0.70	0.13

	Event Categories	Minimum	Most Likely A	Most Likely B	Most Likely C	Maximum	
Quaternary Volcanic Cycle		(Ma)	(Ma)	(Ma)	(Ma)	(Ma)	
Event Ages	Quat CF	1.00	1.00	1.00	1.20	1.00	
			1.00	1.00	1.00	1.00	
			1.00	1.00	1.00	1.00	
				0.75	0.75	1.00	
						0.75	
	Sleeping Butte	0.35	0.43	0.35	0.43	0.35	
			0.43	0.35	0.35	0.35	
	Lathrop	0.13	0.13	0.70	0.70	0.13	
	Plio-Quaternary Younger Postcaldera Basalt						
	Event Ages	Thirsty Mesa	4.90	4.90	4.90	4.90	4.90
						4.90	
						4.90	
Amargosa		3.90	3.90	4.40	3.90	3.90	
		3.90	3.90	4.40	3.90	3.90	
		3.90	3.90	4.40	3.90	3.90	
		3.90	3.90	4.40	3.90	3.90	
			3.50	3.50	3.50	3.90	
					3.50		
3.7 basalt CF		3.70	3.70	3.70	3.70	3.70	
			3.70	3.70	3.70	3.70	
			3.70	3.70	3.70	3.70	
			3.70	3.70	3.70	3.70	
			3.70	3.70	3.70	3.70	
			3.70	3.70	3.70	3.70	
			3.70	3.70	3.70	3.70	
					3.70		
					3.70		
Buckboard		(not included in WLSZ)					
Quat CF		1.00	1.00	1.00	1.20	1.00	
			1.00	1.00	1.00	1.00	
			1.00	1.00	1.00	1.00	
				0.75	0.75	1.00	
					0.75		
Sleeping Butte	0.35	0.43	0.35	0.43	0.35		
		0.43	0.35	0.35	0.35		
Lathrop	0.13	0.13	0.70	0.70	0.13		

	Event Categories	Minimum	Most Likely A	Most Likely B	Most Likely C	Maximum
Northeast Structural Zone						
Quaternary Cycle						
Event Ages	Quat CF	1.00	1.00	1.00	1.20	1.00
			1.00	1.00	1.00	1.00
			1.00	1.00	1.00	1.00
				0.75	0.75	1.00
						0.75
	Lathrop Wells	0.13	0.13	0.70	0.70	0.13
Model 3 (cont.)						
Quaternary Cycle-KG (includes Death Valley)						
Event Ages	Shoreline Butte	1.70	1.70	1.70	1.70	1.70
		1.70	1.70	1.70	1.70	1.70
			1.70	1.70	1.70	1.70
						1.70
						1.70
	Split Cone	0.70	0.70	0.70	0.70	0.70
	Quat CF	1.00	1.00	1.00	1.20	1.00
			1.00	1.00	1.00	1.00
			1.00	1.00	1.00	1.00
				0.75	0.75	1.00
						0.75
	Lathrop Wells	0.13	0.13	0.70	0.70	0.13
Model 3 (cont.)						
Plio-Quaternary						
Event Ages	Amargosa	3.90	3.90	4.40	3.90	3.90
		3.90	3.90	4.40	3.90	3.90
		3.90	3.90	4.40	3.90	3.90
		3.90	3.90	4.40	3.90	3.90
			3.50	3.50	3.50	3.90
						3.50
	3.7 basalt CF	3.70	3.70	3.70	3.70	3.70
			3.70	3.70	3.70	3.70
			3.70	3.70	3.70	3.70
			3.70	3.70	3.70	3.70
			3.70	3.70	3.70	3.70
				3.70	3.70	3.70
						3.70
						3.70
	Buckboard	2.90	2.90	3.10	3.10	2.90
	Quat CF	1.00	1.00	1.00	1.20	1.00
			1.00	1.00	1.00	1.00
			1.00	1.00	1.00	1.00
				0.75	0.75	1.00
						0.75
	Lathrop Wells	0.13	0.13	0.70	0.70	0.13

	Event Categories	Minimum (Ma)	Most Likely A (Ma)	Most Likely B (Ma)	Most Likely C (Ma)	Maximum (Ma)
Quaternary Cycle						
Event Ages	Clayton Valley	1.70	1.70	1.70	1.70	1.70
	Shoreline Butte	1.70	1.70	1.70	1.70	1.70
			1.70	1.70	1.70	1.70
				1.70	1.70	1.70
	Quat CF	1.00	1.00	1.00	1.20	1.00
			1.00	1.00	1.00	1.00
			1.00	1.00	1.00	1.00
				0.75	0.75	1.00
						0.75
	Split Cone	0.70	0.70	0.70	0.70	0.70
	Sleeping Butte	0.35	0.43	0.35	0.43	0.35
			0.43	0.35	0.35	0.35
	Lathrop Wells	0.13	0.13	0.07	0.07	0.13
	Ubehebe	0.05	0.05	0.02	0.05	0.02
			0.05	0.02	0.05	0.02
						0.02
						0.02

Southern Great Basin (cont)						
Plio-Quaternary Cycle	<i>insufficient geochronology data to make age assignments</i>					
	Event Categories	Minimum (Ma)	Most Likely A (Ma)	Most Likely B (Ma)	Most Likely C (Ma)	Maximum (Ma)
Quaternary Cycle						
Event Ages	Shoreline Butte	1.70	1.70			1.70
			1.70			1.70
						1.70
	Quat CF	1.00	1.00	1.00	1.20	1.00
			1.00	1.00	1.00	1.00
			1.00	1.00	1.00	1.00
				0.75	0.75	1.00
						0.75
	Split Cone	0.70	0.70	0.70	0.70	0.70
	Sleeping Butte	0.35	0.43	0.35	0.43	0.35
			0.43	0.35	0.35	0.35
	Lathrop Wells	0.13	0.13	0.70	0.70	0.13

AVIP (cont)	
Pliocene Cycle	<i>insufficient geochronology data to make age assignments</i>

Postcaldera Basalt Same as the Postcaldera distribution model Regional Model

REFERENCES

- Ash, C., 1993, The probability tutoring book: IEEE Press, New York, New York. 470 p.
- Barnard, R.W., Wilson, M.L., Dockery, H.A., Gauthier, Kaplan, P.G., Eaton, R.R., Bingham, F.W., and Robey, T.H., 1992, An initial total-system performance assessment for Yucca Mountain: Sandia Report SAND91-2795, 11 Chapters.
- Best, M.G., and Brimhall, W.H., 1974, Late Cenozoic alkalic basaltic magmas in the western Colorado Plateau and the Basin and Range transition zone, USA, and their bearing on mantle dynamics: Geological Society of America, v. 85, p. 1677-1690.
- Bradshaw, T.K. and Smith, E.I., 1994, Polygenetic Quaternary volcanism at Crater Flat, Nevada: Journal of Volcanology and Geothermal Research v. 63, p. 165-182.
- Byers, F.M., Jr., and Barnes, H., 1967, Geologic map of the Paiute Ridge Quadrangle, Nye and Lincoln Counties, Nevada: U.S. Geological Survey Map GQ-577.
- Byers, F.M., Carr, W.J., and Orkild, P.P. 1989, Volcanic centers of southwestern Nevada: evolution of understanding 1960-1988: Journal of Geophysical Research, v. 94, p. 5908-5924.
- Byers, F.M., Jr., Carr, W.J., Quinlivan, W.D., and Sargent, K.A., 1976, Volcanic suites and related cauldrons of Timber Mountain-Oasis Valley Caldera complex, Southern Nevada: U.S. Geological Survey Professional Paper 919, 70 p.
- Carr, W.J., 1974, Summary of tectonic and structural evidence for stress orientation at the Nevada test site: U.S. Geological Survey Open-File Report 74-176, 83 p.
- Carr, W.J., 1982, Volcano-tectonic history of Crater Flat, southwestern Nevada, as suggested by new evidence from drill hole US-VH-1 and vicinity: U.S. Geological Survey Open-File Report 82-457, 58 p.
- Carr, W.J., 1984, Regional structural setting of Yucca Mountain, southwestern Nevada, and late Cenozoic rates of tectonic activity in part of the southwestern Great Basin, Nevada and California: U.S. Geological Survey Open-File Report 84-854, 109 p.
- Carr, W.J., 1990, Styles of extension in the Nevada test site region, southern Walker Lane Belt: an Integration of volcano-tectonic and detachment fault models: in B. P. Wernicke (ed.), Basin and Range extensional tectonics near the latitude of Las Vegas, Nevada, Geological Society of America Memoir, p. 283-303.
- Carr, W.J., and Parish, L.D., 1985, Geology of drill hole USW VH-2, and structure of Crater Flat, southwestern Nevada: U.S. Geological Survey Open-File Report 85-475, 41 p.

- Champion, D.E., 1991, Volcanic episodes near Yucca Mountain as determined by paleomagnetic studies at Lathrop Wells, Crater Flat, and Sleeping Butte, Nevada: Proceedings, High Level Radioactive Waste Management Conference, Las Vegas, Nevada, American Nuclear Society, La Grange Park, Illinois, p. 61-67.
- Christiansen, R.L., Lipman, P.W., Carr, W.J., Byers, F.M., Jr., Orkild, P.P., and Sargent, K.A., 1977, The Timber Mountain-Oasis Caldera complex of Southern Nevada: Geological Society of America, v. 88, p. 943-959.
- Connor and Hill, 1995, Estimating the probability of volcanic disruption of the candidate Yucca Mountain Repository using spatially and temporally nonhomogeneous Poisson models: Proceedings, Focus '93 Symposium, American Nuclear Society, La Grange Park, Illinois, p. 174-181
- Crowe, 1986, Volcanic hazard assessment for disposal of high level radioactive waste, *in* Active tectonics: Impact on Society: National Academy Press, Washington, DC, c.16, p. 247-260.
- Crowe, B.M., 1990, Basaltic volcanic episodes of the Yucca Mountain region: Proceedings High-Level Radioactive Waste Management Conference, Las Vegas, Nevada, American Nuclear Society, La Grange Park, Illinois, p. 65-73.
- Crowe, B.M., 1995, Los Alamos letter report: revised probability estimates for the Yucca Mountain region: Los Alamos National Laboratory Milestone Report T056.
- Crowe, B.M., and Carr, W.J., 1980, Preliminary assessment of the risk of volcanism at a proposed nuclear waste repository in the southern Great Basin: U.S. Geological Survey Open-File Report 80-375.
- Crowe, B.M. and Fisher, R.V., 1973, Sedimentary structures in base-surge deposits with special reference to cross-bedding Ubehebe Craters, Death Valley, California: Geological Society of American Bulletin, V.84, p. 663-682.
- Crowe, B., Morley, R., Wells, S., Geissman, J., McDonald, E., McFadden, L., Perry, F., Murrell, M., Poths, J., and Forman, S., 1992, The Lathrop Wells volcanic center: status of field and geochronology studies: Proceedings, High Level Radioactive Waste Management Conference Las Vegas, Nevada, American Nuclear Society, La Grange Park, Illinois, p. 1997-2013.
- Crowe, B.M., and Perry, F.V., 1989, Volcanic probability calculations for the Yucca Mountain site: estimation of volcanic rates: Proceedings, Nuclear Waste Isolation in the Unsaturated Zone, Focus '89, American Nuclear Society, La Grange Park, Illinois, p. 326-334.

- Crowe, B.M., and Perry, F.V., 1991, Preliminary geologic map of the Sleeping Butte volcanic centers: Los Alamos National Laboratory Report. LA-12101-MS, 11 p.
- Crowe, B.M., and Perry, F.V., 1995, Los Alamos letter report: completion of field, geochemistry and geochronology studies at the Sleeping Butte and Buckboard Mesa Basalt Centers: Los Alamos National Laboratory Report.
- Crowe, B., Perry, F., Geissman, J., McFadden, L., Wells, S., Murrell, M., Poths, J., Valentine, G.A., Bowker, L. and Finnegan, K., 1995, Status of volcanism studies for the Yucca Mountain site characterization project: Los Alamos National Laboratory Report LA-12908-MS, 373 p.
- Crowe, B.M., and Sargent, K.A., 1979, Major-element geochemistry of the Silent Canyon-Black Mountain pralkaline volcanic centers, northwestern Nevada test site: applications to an assessment of renewed volcanism: U.S. Geological Survey Open-File Report 79-296, 25 p.
- Crowe, B.M., Self, S., Vaniman, D., Amos, R., and Perry, F., 1983a, Aspects of potential magmatic disruption of a high level radioactive waste repository in southern Nevada: Journal of Geology, v. 91, p. 259-276.
- Crowe, B.M., Turrin, B., Wells, S., Perry, F., McFadden, L., Renault, C., Champion, D., and Harrington, C., 1989, Volcanic hazard studies for the Yucca Mountain project: Waste Management '89 , v. 1, p. 485-492.
- Crowe B.M., Vaniman, D.T., Carr, W.J., 1983b, Status of volcanic hazard studies for the Nevada nuclear waste storage investigations: Los Alamos National Laboratory Report LA-9325-MS..
- Crowe, B.M., Wohletz, K.H., Vaniman, D.T., Gladney, E. and Bower, N., 1986, Status of volcanic hazard studies for the Nevada nuclear waste storage investigations: Los Alamos National Laboratory Report LA-9325-MS, v. II, 101 p.
- Delaney, P.T. and Gartner, A.E., 1995, Physical processes of shallow mafic dike emplacement near the San Rafael Swell, Utah: U.S. Geological Survey Open File Report 95-491, 1-28.
- Farmer, G.L., Broxton, D.E., Warren, R.G., and Pickthorn, W., 1991, Nd, Sr, and O isotopic variations in metaluminous ash-flow tuffs and related volcanic rocks at the TM/Oasis Valley Caldera complex, southwest Nevada: implications for the origin and evolution of large volume silicic magma bodies: Contributions Mineralogy Petrology, v. 109, p. 53-68.
- Farmer, G.L., Perry, F.V., Semken, S., Crowe, B., Curtins, D., and DePaolo, D.J., 1989, Isotopic evidence on the structure and origin of subcontinental lithospheric mantle in southern Nevada: Journal of Geophysical Research, v. 94, p. 7885-7898.

- Fedotov, S.A., 1978, Ascent of basic magmas in the crust and the mechanism of basaltic fissure eruptions: *International Geology Review*, v. 20, p. 33-48.
- Fridrich, C.J., 1995, Characterization of detachment faults in the Yucca Mountain region. *in* Simonds, et al. (eds.), *Final report on detachment faulting: U.S. Geological Survey Administrative Report to DOE (unpublished)*.
- Golder Associates, 1995, Effect of structural controls on basaltic volcanism and eruptive effects at Yucca Mountain, Nevada: prepared for Los Alamos National Laboratory, 101p.
- Ho, C.H., 1991, Time trend analysis of basaltic volcanism for the Yucca Mountain site: *Journal of Volcanology Geothermal Research*, v. 46, 61-72.
- Ho, C.H., 1992, Risk assessment for the Yucca Mountain high level nuclear waste repository site: estimation of volcanic disruption: *Mathematical Geology*, v. 24, p. 347-364.
- Ho, C.H., Smith, E.I., Feurbach, D.L., and Naumann, T.R., 1991, Eruptive probability calculation for the Yucca Mountain site, USA: *Bulletin of Volcanology*, v. 54, p. 50-56.
- Humphreys, E.D., and Dueker, K.G., 1994, Physical state of the western U.S. upper mantle: *Journal of Geophysical Research*, v. 99, p. 9635-9650.
- Jones, J.H., Wernicke, B.P., Farmer, G.L., Walker, J.D., Colman, D.S., Mckenna, L.W., and Perry, F.V., 1992, Variations across and along a major continental rift: an interdisciplinary study of the Basin and Range Province, western USA: *Tectonophysics* v. 213, p. 57-96.
- Kane, M.F., and Bracken, R.E., 1983, Aeromagnetic map of Yucca Mountain and surrounding regions, southwest Nevada: U.S. Geological Survey Open-File Report 83-616.
- Langenheim, V.E., in press, Magnetic and gravity studies of buried volcanic centers in the Amargosa Desert and Crater Flat, southwest Nevada: U.S. Geological Survey Open-File Report.
- Lister, J.R., 1990, Buoyancy-driven fluid fracture: similarity solutions for the horizontal and vertical propagation of fluid-filled cracks: *Journal of Fluid Mechanics*, v. 217, p. 213-219.
- Lister, J.R. and Kerr, R.C., 1991, Fluid-mechanical models of crack propagation and their application to magma transport in dykes: *Journal of Geophysical Research*, v. 96, p. 10,049-10,077.
- Lutton, R.J., 1968, Internal structure of the Buckboard Mesa basalt: *Bulletin of Volcanology*, p. 579-593.
- Maaloe, S., 1987, The generation and shape of feeder dykes from mantle sources: *Contributions Mineralogy Petrology*, v. 96, p. 47-55.

- Olkin, I., Gleser, L.J., and Derman, C., 1994, Probability models and applications: McMillan College Publishing Company, New York, New York, 715 p.
- Perry, F., Baldrige, W.S., and DePaolo, D.J., 1987, Role of asthenosphere and lithosphere in the genesis of late Cenozoic basaltic rocks from the Rio Grande Rift and adjacent regions of the southwestern United States: *Journal of Geophysical Research*, v. 92, p. 9193-9213.
- Perry, F.V., and Crowe, B.M., 1992, Geochemical evidence for waning magmatism and polycyclic volcanism at Crater Flat, Nevada: *Proceedings, High-Level Radioactive Waste Management Conference, Las Vegas, Nevada, American Nuclear Society, La Grange Park, Illinois*, p. 2356-2365.
- Perry, F.V., DePaolo, D.J., and Baldrige, W.S., 1993, Neodymium isotopic evidence for decreasing crustal contributions to Cenozoic ignimbrites of the western United States: implications for the thermal evolution of the Cordilleran crust: *Geological Society of America Bulletin*, v. 105, p. 872-882.
- Ratcliff, C.D., Geissman, J.W., Perry F.V., Crowe, B.M., and Zeitler, P.K., 1994, Paleomagnetic record of a geomagnetic field reversal from late Miocene mafic intrusions, southern Nevada: *Science*, v. 266, p. 412-416.
- Schweickert, R.A., 1989, Evidence for a concealed dextral strike-slip fault beneath Crater Flat, Nevada: *Abstract, Geological Society of America*, v. 20, p. A115.
- Scott, R.B., 1990, Tectonic setting of Yucca Mountain, southwest Nevada, *in* Wernicke, B.P., Ed., *Basin and Range Extensional Tectonics Near the Latitude of Las Vegas, Nevada*, Geological Society America Memoir 176, Boulder, Colorado, p. 251-282.
- Sheridan, M.F., 1992, A Monte Carlo technique to estimate the probability of volcanic dikes, *Proceedings, High-Level Radioactive Waste Management Conference Las Vegas, Nevada, American Nuclear Society, La Grange Park Illinois*, p. 1840-1846.
- Smith, E.I., Feuerbach, D.L., Naumann, T.R., and Faulds, J.E., 1990, The area of most recent volcanism near Yucca Mountain, Nevada: implications for volcanic risk assessment: *Proceedings, High-Level Radioactive Waste Management Conference Las Vegas, Nevada, American Nuclear Society, La Grange Park*, p. 81-90.
- Smith, R.L., and Luedke, R.G., 1984, Potentially active volcanic lineaments and loci in western conterminous United States, *in* *Explosive Volcanism: Inception, Evolution and Hazards*: National Academy Press, Washington, D.C., p. 47-66.
- Suppe, J., Powell, C., and Berry, R., 1975, Regional topography, seismicity, Quaternary volcanism and the present-day tectonics of the western United States: *American Journal of Science*, v. 274-A, p. 397-436.

- Tuckwell, H.C., 1988, *Elementary Applications of Probability Theory*: Champion and Hall, New York, New York, 1988, 255 p.
- Turrin, B.D., Champion, D.E., and Fleck, R.J., 1991, $^{40}\text{Ar}/^{39}\text{Ar}$ age of the Lathrop Wells volcanic center, Yucca Mountain, Nevada: *Science*, v. 257, p. 654-657.
- Valentine, G.A., Crowe, B.M., and Perry, F.V., 1992, Physical processes and effects of magmatism in the Yucca Mountain region: *Proceedings, High Level Radioactive Waste Management Conference, Las Vegas, Nevada, American Nuclear Society, La Grange Park, Illinois*, v. 3, p. 2344-2355.
- Vaniman, D.T., and Crowe, B.M., 1981, Geology and petrology of the basalts of Crater Flat: applications to volcanic risk assessment for the Nevada nuclear waste storage investigations: *Los Alamos National Laboratory Report LA-8845-MS*, 67 p.
- Vaniman, D.T., Crowe, B.M., and Gladney, E.S., 1982, Petrology and geochemistry of Hawaiiite lavas from Crater Flat, Nevada: *Contributions Mineralogy Petrology*, v.80, p. 341-357.
- Wallmann, P.C., 1993, A technique for calculation of the probability of dikes intersecting a repository: *Proceedings, Focus 93 Symposium, American Nuclear Society, La Grange Park, Illinois*, p. 192-199.
- Wells, S.G., Crowe, B.M., and McFadden, L.D., 1992, Measuring the age of the Lathrop Wells volcanic center of Yucca Mountain: *Science*, v. 257, p. 555-558.
- Wells, S.G. McFadden, L.D., Renault, C.E. Renault, and Crowe, B.M., 1990, Geomorphic assessment of late Quaternary volcanism in the Yucca Mountain area, southern Nevada: implications for the proposed high level radioactive waste repository: *Geology*, v. 18, p. 549-553.
- Wilson, L. and Head, J.W., 1981, Ascent and eruption of basaltic magma on the earth and moon: *Journal Geophysical Research*, v. 86, p. 2971-3001.
- Wood, C.A., and Kienle, J., 1990, *Volcanoes of North America*: Cambridge University Press, Cambridge, MA, 384 p.
- Wright, L.A., 1987, Overview of the role of strike-slip and normal faulting in the Neogene history of the region northeast of Death Valley, California: *Nevada Bureau of Mines and Geology Open-File Report*, v. 89-1., p. 1-11.

**TABLE BC-1
 MINIMUM PROBABILITY BOUNDS FROM REGIONAL MODELS**

Zones	Area	Event Counts			Recurrence Rates (events yr ⁻¹ km ²)			Disruption Probability (events yr ⁻¹)		
	km ²	1.8 Ma	5.05 Ma	9.15 Ma	1.8 Ma	5.05 Ma	9.15 Ma	1.8 Ma	5.05 Ma	9.15 Ma
SGB	19874	10	100	9.15	2.8·10 ⁻¹⁰	1.0·10 ⁻⁰⁹	--	1.6·10 ⁻⁹	5.7·10 ⁻⁰⁹	--
AVIP	7636	9	664	--	6.5·10 ⁻¹⁰	1.7·10 ⁻⁰⁸	--	3.7·10 ⁻⁰⁹	9.8·10 ⁻⁰⁸	--
PCB	5649	6	17	31	5.9·10 ⁻¹⁰	6.0·10 ⁻¹⁰	60·10 ⁻¹⁰	3.4·10 ⁻⁰⁹	3.4·10 ⁻⁰⁹	3.4·10 ⁻⁰⁹

**TABLE BC-2
 MAXIMUM PROBABILITY BOUNDS FOR
 VOLCANIC ZONES OF THE PCB
 ASSUMING LOCATION OF A REPOSITORY IN THE ZONES**

Zones	Area	Event Counts			Recurrence Rates (events yr ⁻¹ km ²)			Disruption Probability (events yr ⁻¹)		
	Area km ²	1.15 Ma	5.05 Ma	9.15 Ma	1.15 Ma	5.05 Ma	9.15 Ma	1.15Ma	5.05 Ma	9.15 Ma
CFVZ-Quat	514	6	--	--	1.0·10 ⁻⁰⁸	--	--	5.8·10 ⁻⁰⁸	--	--
CFVZ-Plio-Quat	1068	--	16	--	--	3.0·10 ⁻⁰⁹	--	--	1.7·10 ⁻⁰⁸	--
YPC*	1884	7	17	--	3.2·10 ⁻⁰⁹	1.8·10 ⁻⁰⁹	--	1.8·10 ⁻⁰⁸	1.0·10 ⁻⁰⁸	--
PCB**	5649	--	--	31	--	--	6.0·10 ⁻¹⁰	--	--	3.4·10 ⁻⁰⁹
Pull-Apart/Quat	242	4	--	--	1.4·10 ⁻⁰⁸	--	--	8.2·10 ⁻⁰⁸	--	--
Pull- Apart/Quat***	149	4	--	--	2.3·10 ⁻⁰⁸	--	--	1.3·10 ⁻⁰⁷	--	--
Pull-Apart/Plio- Quat	506	--	10	--	--	3.9·10 ⁻⁰⁹	--	--	2.2·10 ⁻⁰⁸	--
Walker Lane	1452	6	16	--	3.6·10 ⁻⁰⁹	2.2·10 ⁻⁰⁹	--	2.0·10 ⁻⁰⁸	1.2·10 ⁻⁰⁸	--
NESZ	2176	4	14	--	1.6·10 ⁻⁰⁹	1.3·10 ⁻⁰⁹	--	9.1·10 ⁻⁰⁹	7.3·10 ⁻⁰⁹	--

* A Quaternary YPC is not listed because it is identical to the CFVZ-Quaternary
 ** Identical to the YMR Regional Model
 *** A subdivision of the Pull-Apart Quaternary model that uses the fault models of George Thompson

**TABLE BC-3
 BRUCE M. CROWE - EVENT COUNTS**

LOCATION	COUNTS (CONES)	WEIGHT	NOTES
Lathrop Wells	1	(0.9)	A-G: Aeromagnetic anomalies of V. Langenheim, USGS BC: Black Cone HC: Hidden Cone 2HC: 2 events at Hidden Cone LBP: Little Black Peak LC: Little Cones 2LC: 2 events at Little Cone M: Makani Cone RC: Red Cone SC: Split Cone SB: Shoreline Butte 2SB: 2 events at Shoreline Butte 3SB: 3 events at Shoreline Butte u: undetected
	2	(0.06)	
	3	(0.03)	
	4	(0.01)	
Sleeping Butte	1 (LBP+HC)	(0.35)	
	2 (LBP, HC)	(0.45)	
	3 (LBP, 2HC)	(0.2)	
1.0 Ma Crater Flat	1 (all)	(0.1)	
	2 (RC+LC.BC+M)	(0.1)	
	3 (LC, RC+BC, M)	(0.45)	
	4 (LC.RC.BC.M)	(0.2)	
	5 (2LC, RC, BC, M)	(0.1)	
	6 (A, RC, BC, M, 2LC)	(0.025)	
	7 (u)	(0.025)	
Buckboard Mesa	1	(0.7)	
	2	(0.25)	
	3 (u)	(0.05)	
3.7 Ma Crater Flat	1	(0.1)	
	2	(0.25)	
	3	(0.25)	
	4	(0.1)	
	5	(0.1)	
	6	(0.1)	
	7 (u)	(0.05)	
	8 (2u)	(0.05)	
Amargosa Valley	3	(0.05)	
	4	(0.12)	
	5	(0.2)	
	6	(0.2)	
	7 (u)	(0.2)	
	8 (u)	(0.1)	
	9 (2u)	(0.07)	
	10 (3u)	(0.03)	
	11 (4u)	(0.02)	
	12 (5u)	(0.01)	
	Thirsty Mesa	1	(0.85)
		2	(0.09)
3		(0.06)	

TABLE BC-3 (Cont'd)
BRUCE M. CROWE - EVENT COUNTS

LOCATION	COUNTS (CONES)	WEIGHT	NOTES
Death Valley (2 Ma)	2 (SC, SB)	(0.3)	
	3 (2SB, SC)	(0.3)	
	4 (3SB, SC)	(0.25)	
	5 (3SB, SC+u)	(0.1)	
	6 (3SB, SC +2u)	(0.05)	
Death Valley (3-5 Ma)	22 Density Estimates	(0.185)	
	44 " "	(0.63)	
	89 " "	(0.185)	
Clayton Valley	1	(0.85)	
	2 (u)	(0.1)	
	3 (2u)	(0.05)	
Ubehebe	1	(0.6)	
	2	(0.15)	
	3	(0.1)	
	4		
	5 (u)		
	6 (2u)		
Towne Pass	11 Density Estimates	(0.185)	
	22 " "	(0.63)	
	44 " "	(0.185)	
Grapevine Canyon	6 Density Estimates	(0.185)	
	12 " "	(0.63)	
	24 " "	(0.185)	
Nye Canyon	1	(0.02)	
	2	(0.2)	
	3	(0.2)	
	4	(0.16)	
	5	(0.16)	
	6 (u)	(0.12)	
	7 (2u)	(0.08)	
	8 (3u)	(0.04)	
	9 (4u)	(0.02)	

TABLE BC-3 (Cont'd)
BRUCE M. CROWE - EVENT COUNTS

LOCATION	COUNTS (CONES)	WEIGHT	NOTES
Paiute Ridge	1	(0.35)	
	2	(0.35)	
	3	(0.15)	
	4	(0.1)	
	5 (u)	(0.05)	
Yucca Flat	1	(0.4)	
	2	(0.4)	
	3 (u)	(0.2)	
Pahute Mesa	3	(0.5)	
	4	(0.2)	
	5	(0.15)	
	6 (u)	(0.1)	
	7 (u)	(0.05)	

**TABLE BC-4
 BRUCE M. CROWE - RATES OF OCCURRENCE**

TIME PERIOD	COUNT METHOD FOR ZONES	NOTES
Quaternary (post-1.15 Ma)	CF: (LW+NCF+SB) PA: (LW+NCF) WL: (LW+NCF+SB) NE: (LW+NCF) SGB: (DV2+U+CV) AVIP: (DV2)	AV: Amargosa Valley AVIP: Amargosa Valley Isotopic Province of Yogodzinski (1995) BM: Buckboard Mesa CF: Crater Flat CV: Clayton Valley DV2: Death Valley (2 Ma) DV5: Death Valley (3-5 Ma) GV: Grapevine Canyon LW: Lathrop Wells NC: Nye Canyon NCF: Northern (1.0 Ma) Crater Flat NE: North East PCB: Post Caldera Basalts PA: Pull apart and Pull apart with fault PM: Pahute Mesa PR: Paiute Ridge RW: Rocket Wash SB: Sleeping Butte SC: Scarp Canyon SGB: Southern Great Basin TM: Thirsty Mesa TP: Towne Pass U: Ubehebe WL: Walker Lane YF: Yucca Flat YPCB: Younger Post-Caldera Basalts 3.7: 3.7 Ma Crater Flat
Plio-Quaternary (post-5.05 Ma)	CF: (LW+NCF+3.7+AV+SB+TM) YPCB: (LW+NCF+3.7+AV+SB+TM+BM) PA: (LW+NCF+3.7+AV) WL: (LW+NCF+3.7+AV+SB+TM) NE: (LW+NCF+3.7+AV+BM) SGB: (DV2+DV5+U+CV+TP+GV) AVIP: (DV2+DV5)	(Continued from previous row)
Mio-Plio-Quaternary (post-9.05 Ma)	PCB: (LW+NCF+3.7+AV+SB+TM+BM+PM+PR+SC+RW+YF+NC)	(Continued from previous row)

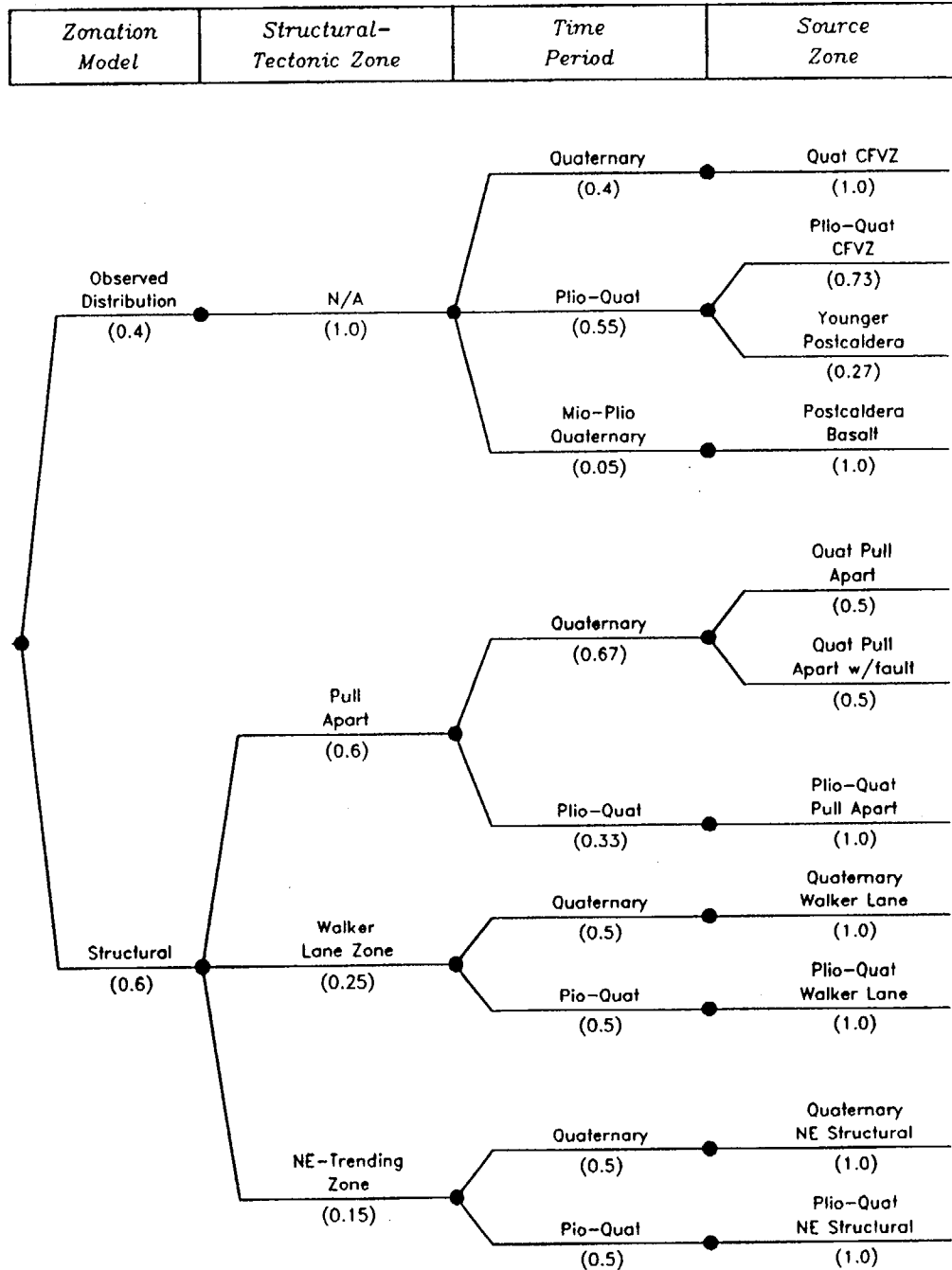
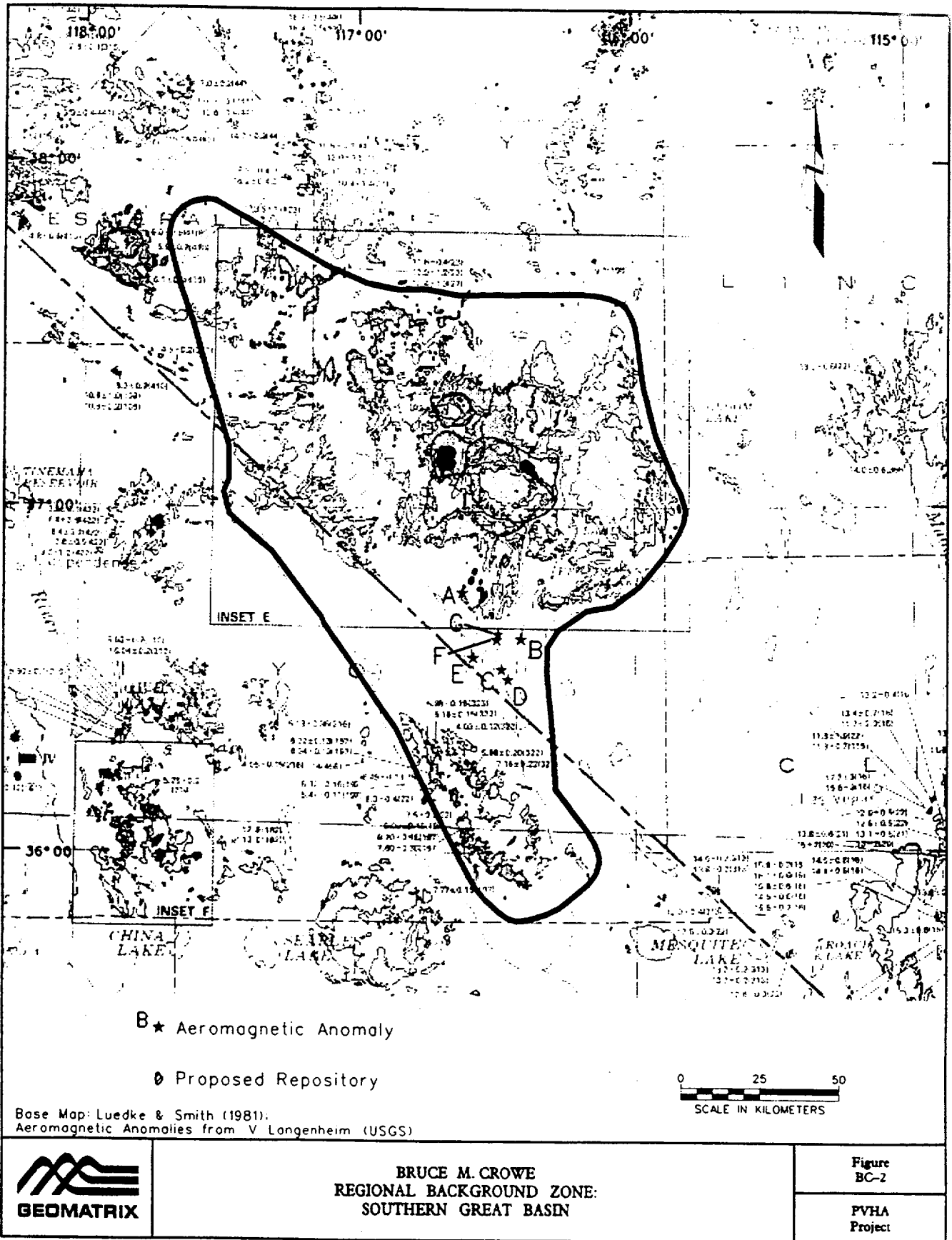
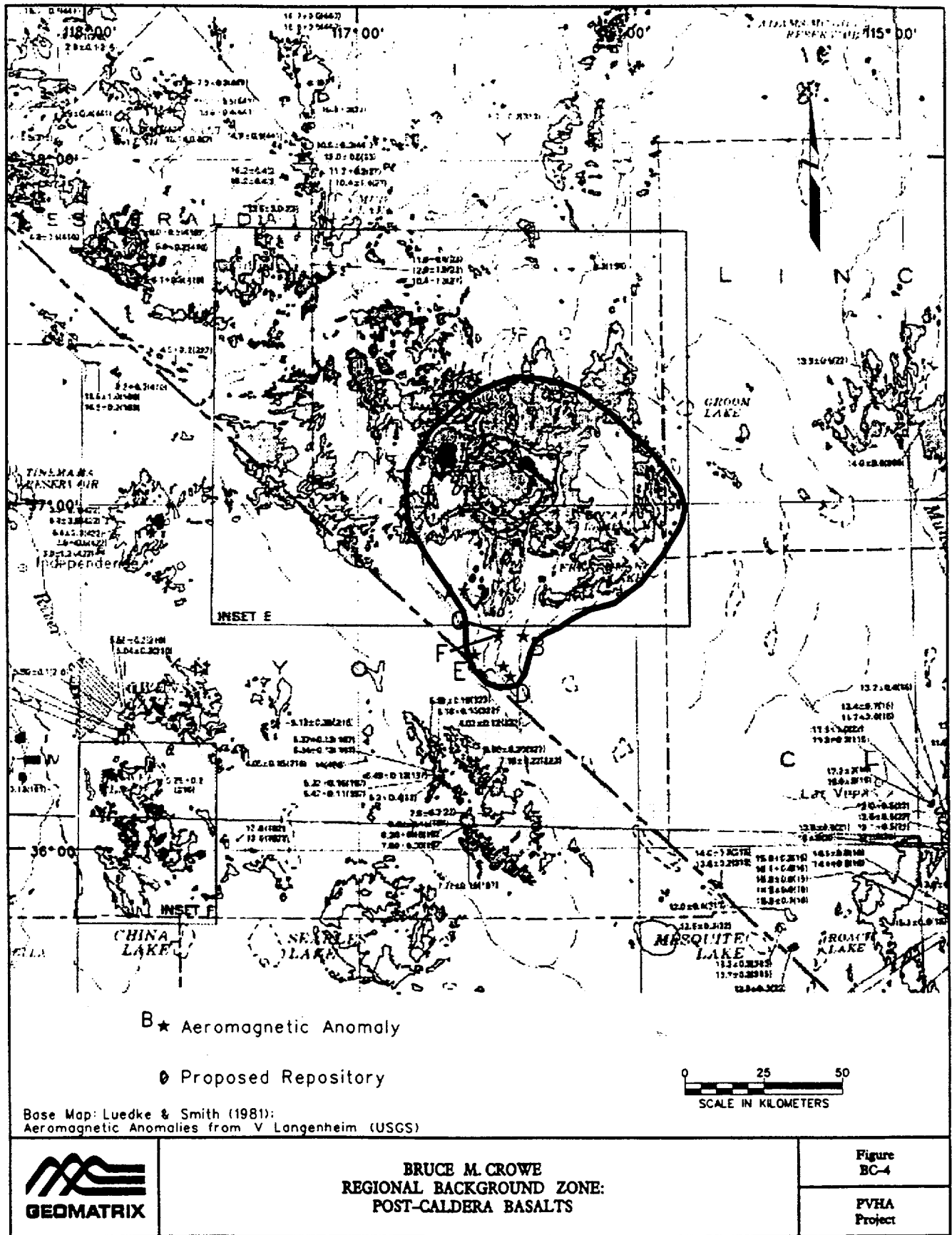
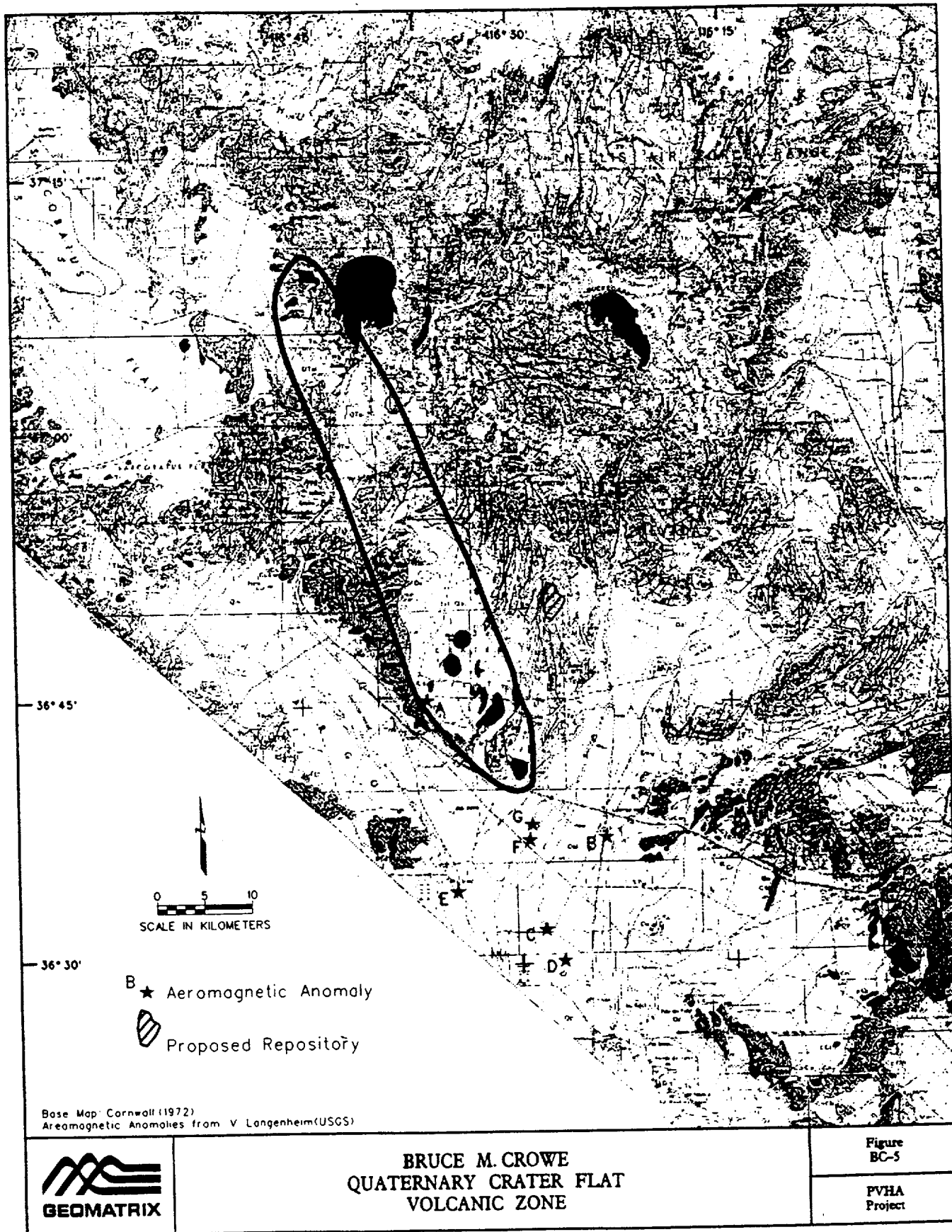


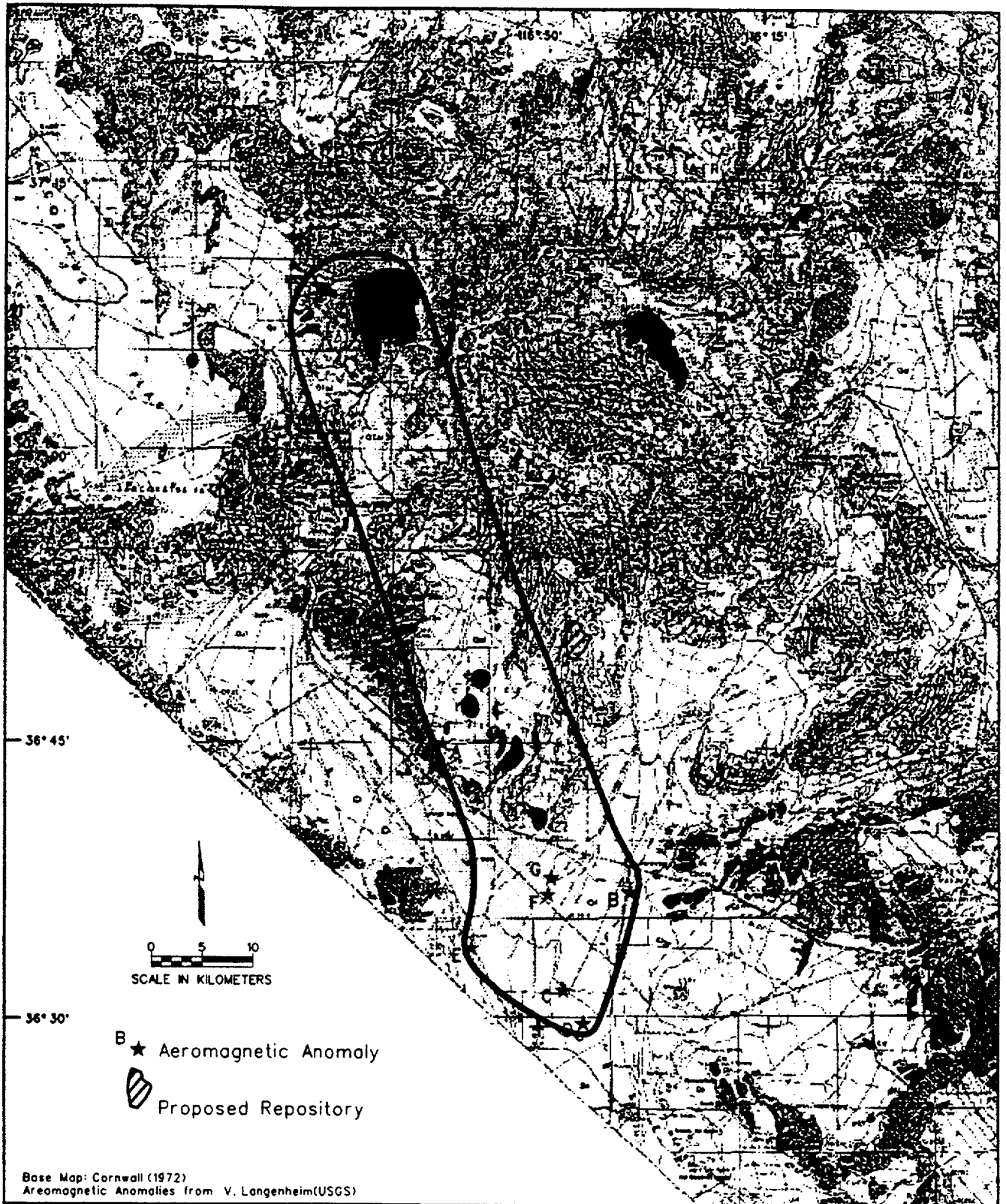
Figure BC-1 PVHA model logic tree developed by Bruce M. Crowe.





H:\p\yucca\qgn\pvha\ludsm\th\bc_04.dgn, Rev. 03-28-96

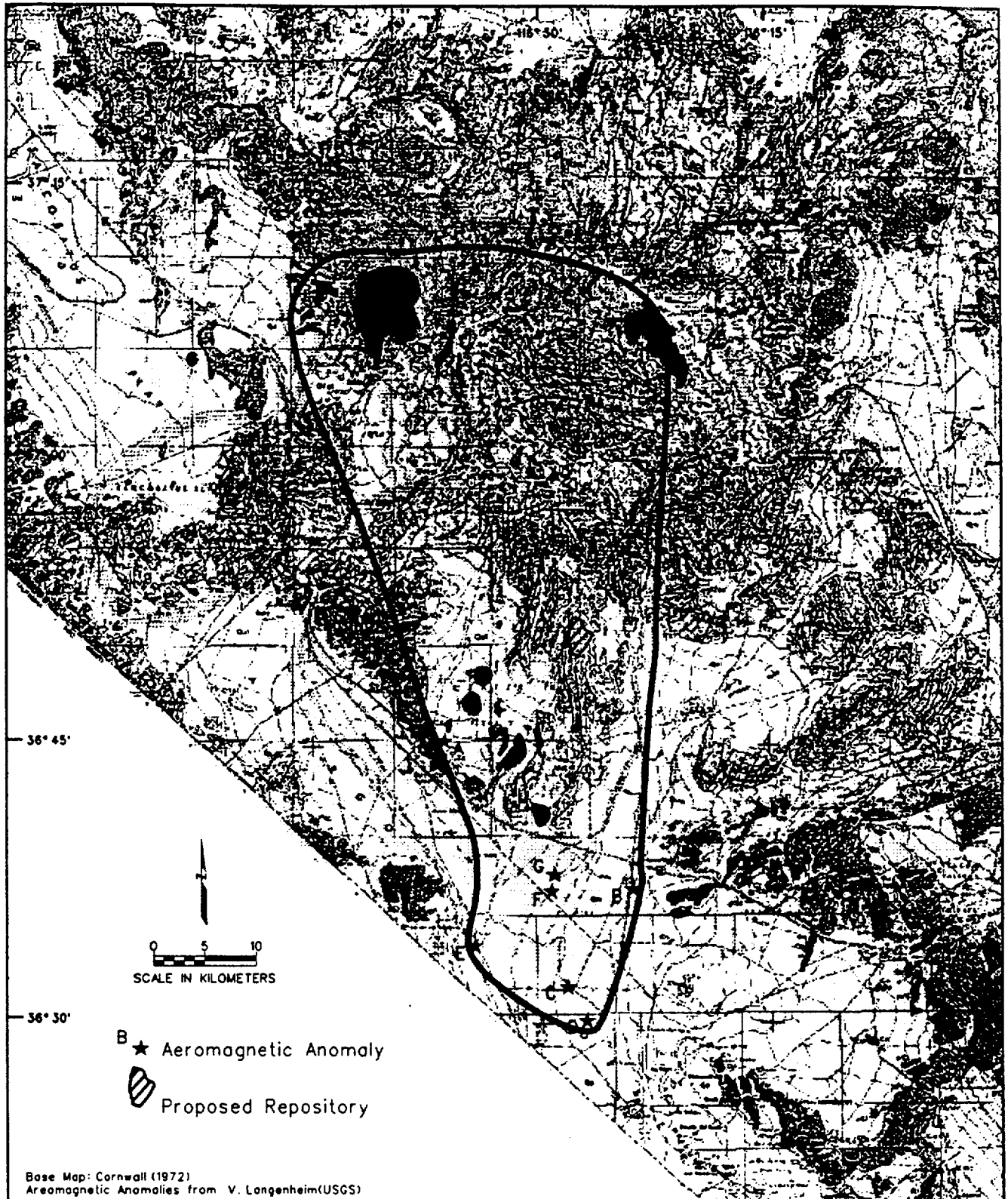




BRUCE M. CROWE
PLIO-QUATERNARY CRATER
FLAT VOLCANIC ZONE

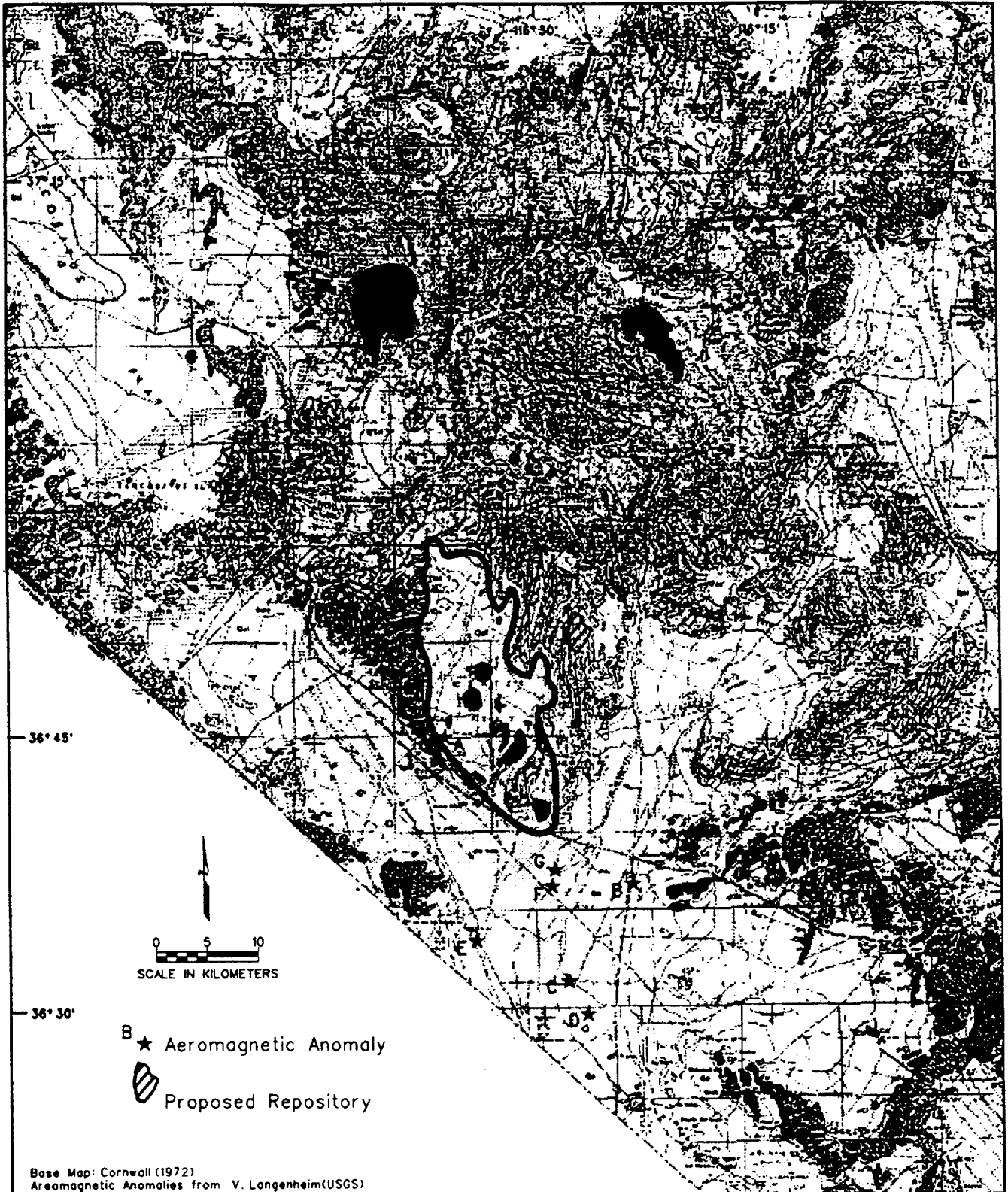
Figure
BC-6

PVHA
Project



**BRUCE M. CROWE
YOUNGER POST-CALDERA ZONE**

**Figure
BC-7**
**PVHA
Project**



Base Map: Cornwall (1972)
Aeromagnetic Anomalies from V. Langenheim (USGS)

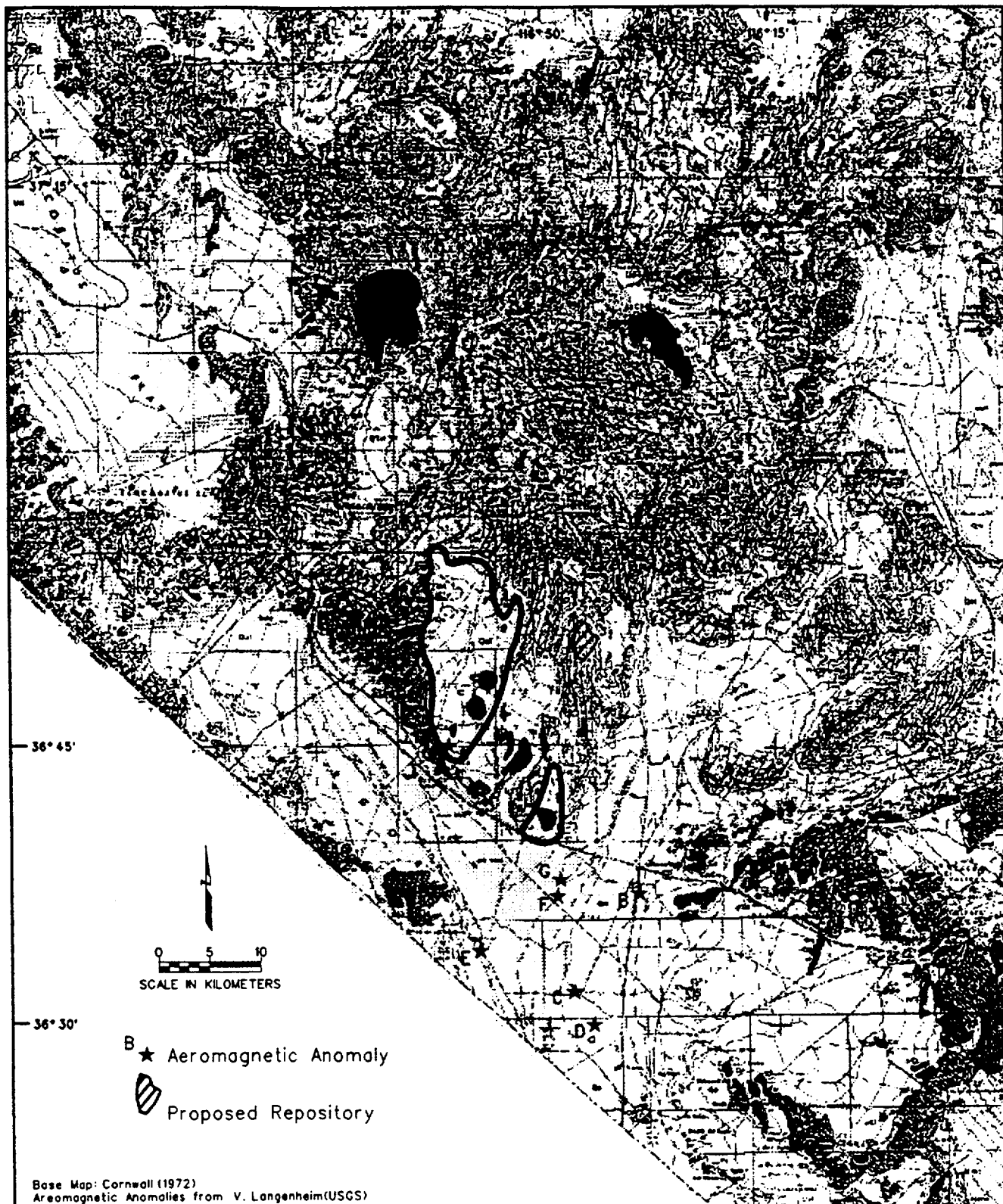


BRUCE M. CROWE
QUATERNARY PULL-APART
ZONE

Figure
BC-8

FVHA
Project

H:\701\yucca\gdn\psho\cornell\bc_08.dgn Rev: 03 28-96



Base Map: Cornwall (1972)
 Aeromagnetic Anomalies from V. Langenheim(USGS)

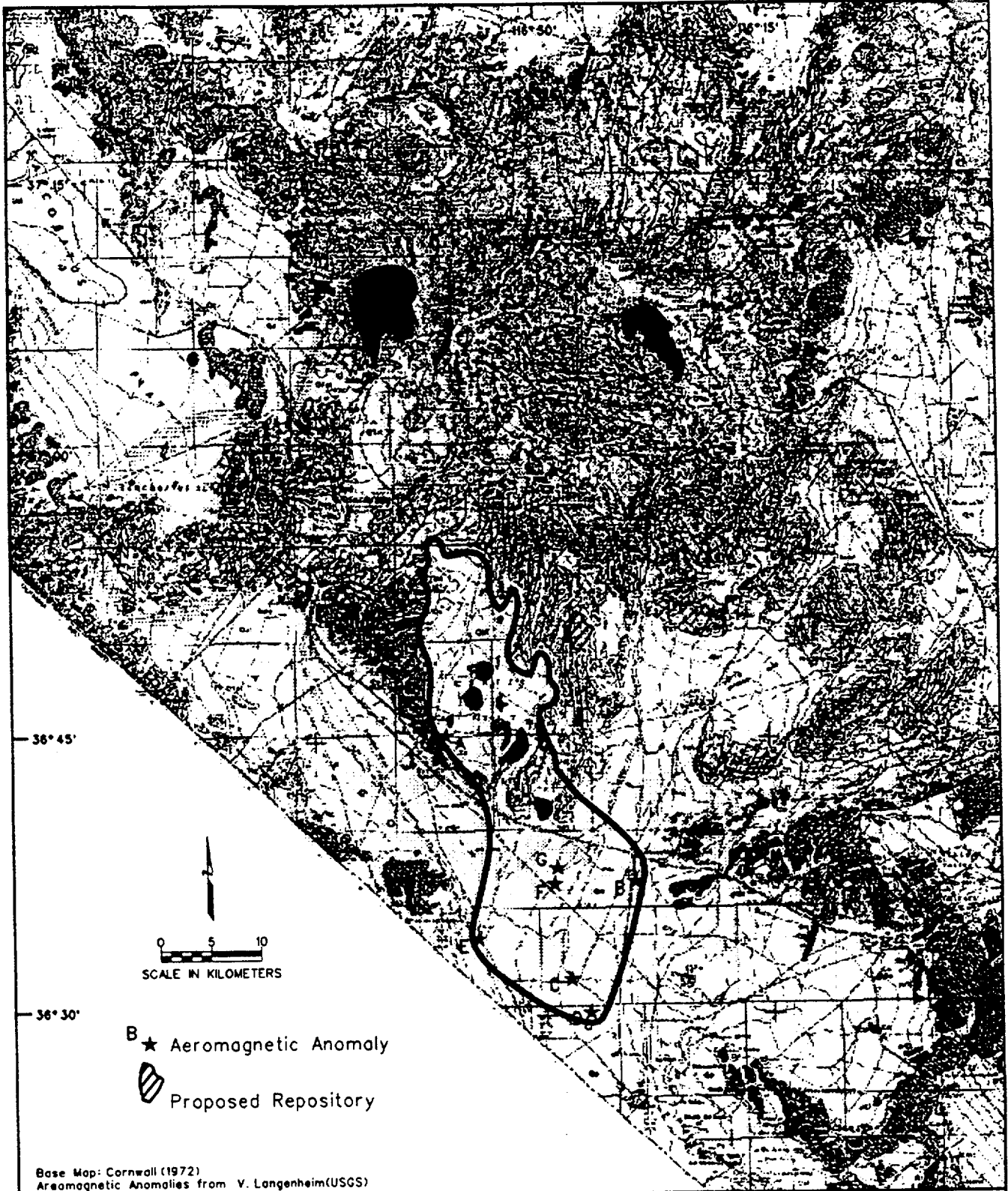


**BRUCE M. CROWE
 QUATERNARY PULL-APART
 ZONE WITH FAULT**

Figure
 BC-9

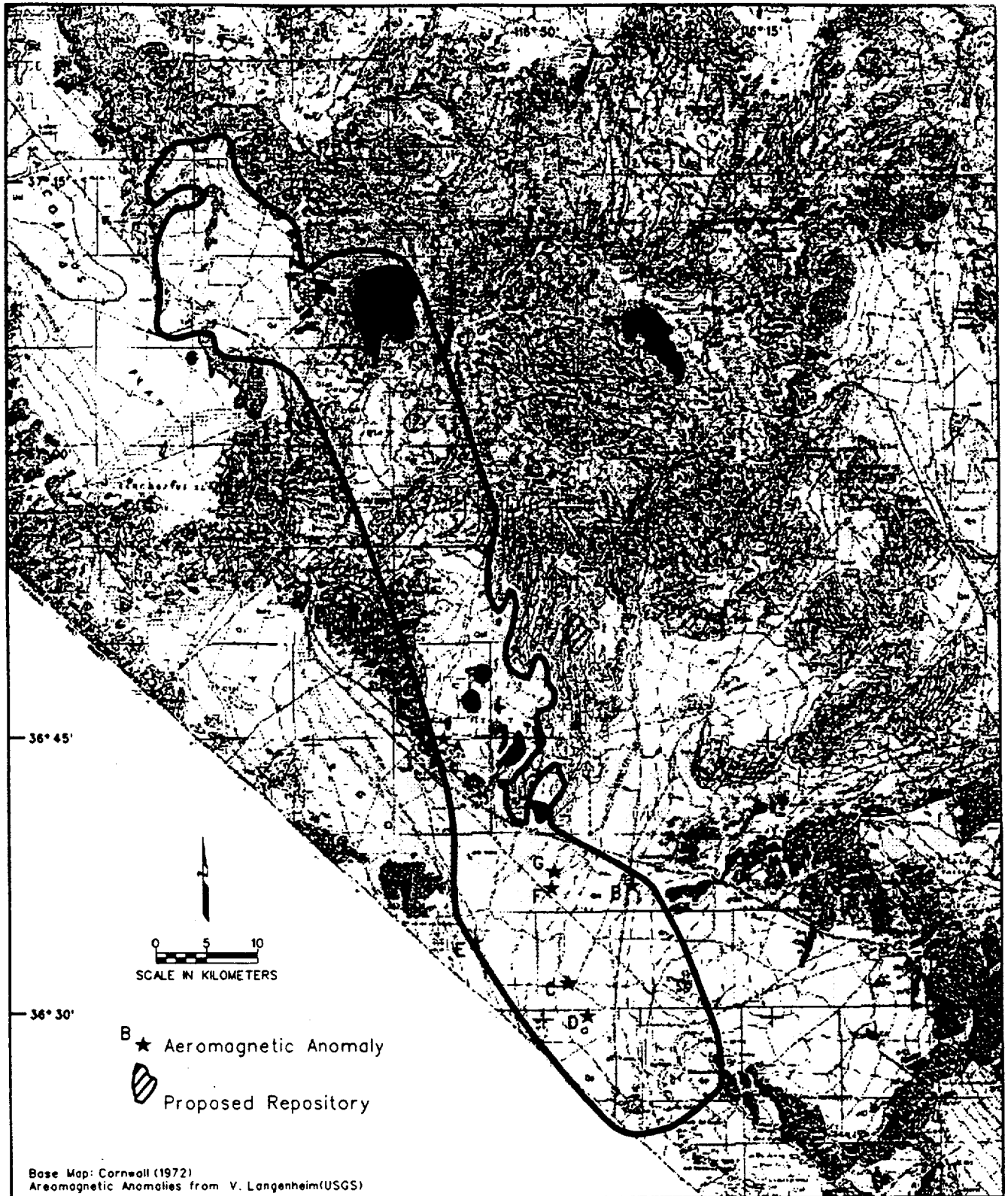
PVHA
 Project

H:\p17\yucca\qgh\p17\cornwall\bc_09.dgn Rev. 03-28-96



	BRUCE M. CROWE PLIO-QUATERNARY PULL-APART ZONE	Figure BC-10
		PVHA Project

\\fp1\yucca\rdg\p-haz\cornwall\bc_10.dgn, Rev. 03-28-96



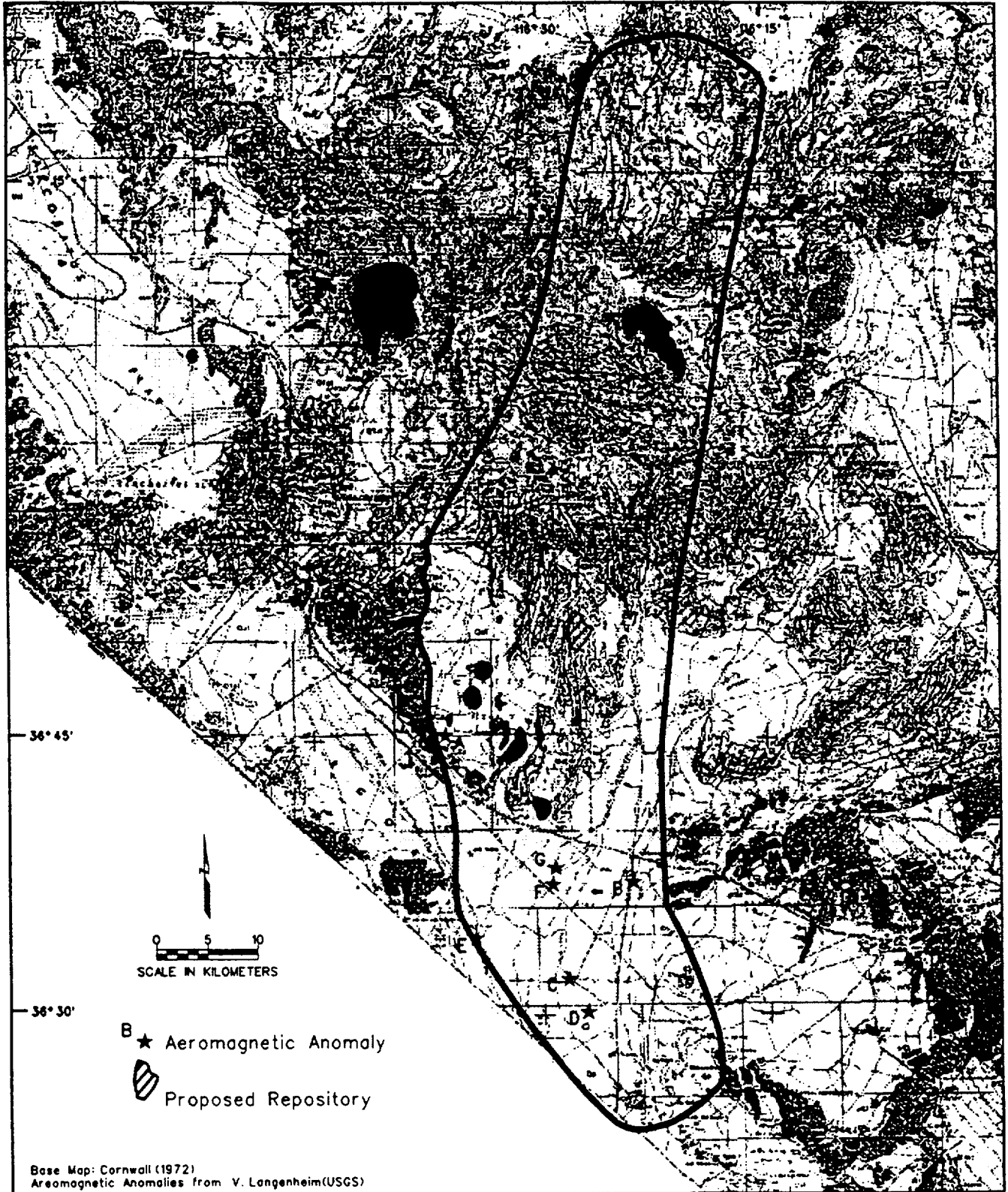
Base Map: Cornwall (1972)
Aeromagnetic Anomalies from V. Langenheim(USGS)



**BRUCE M. CROWE
WALKER LANE STRUCTURAL ZONE**

Figure
BC-II

FVHA
Project



	BRUCE M. CROWE NORTHEAST STRUCTURAL ZONE	Figure BC-12
		PVHA Project

H:\p1\yucca\qgn\pvha\cornwall\bc_12.dgn Rev. 03-28-96

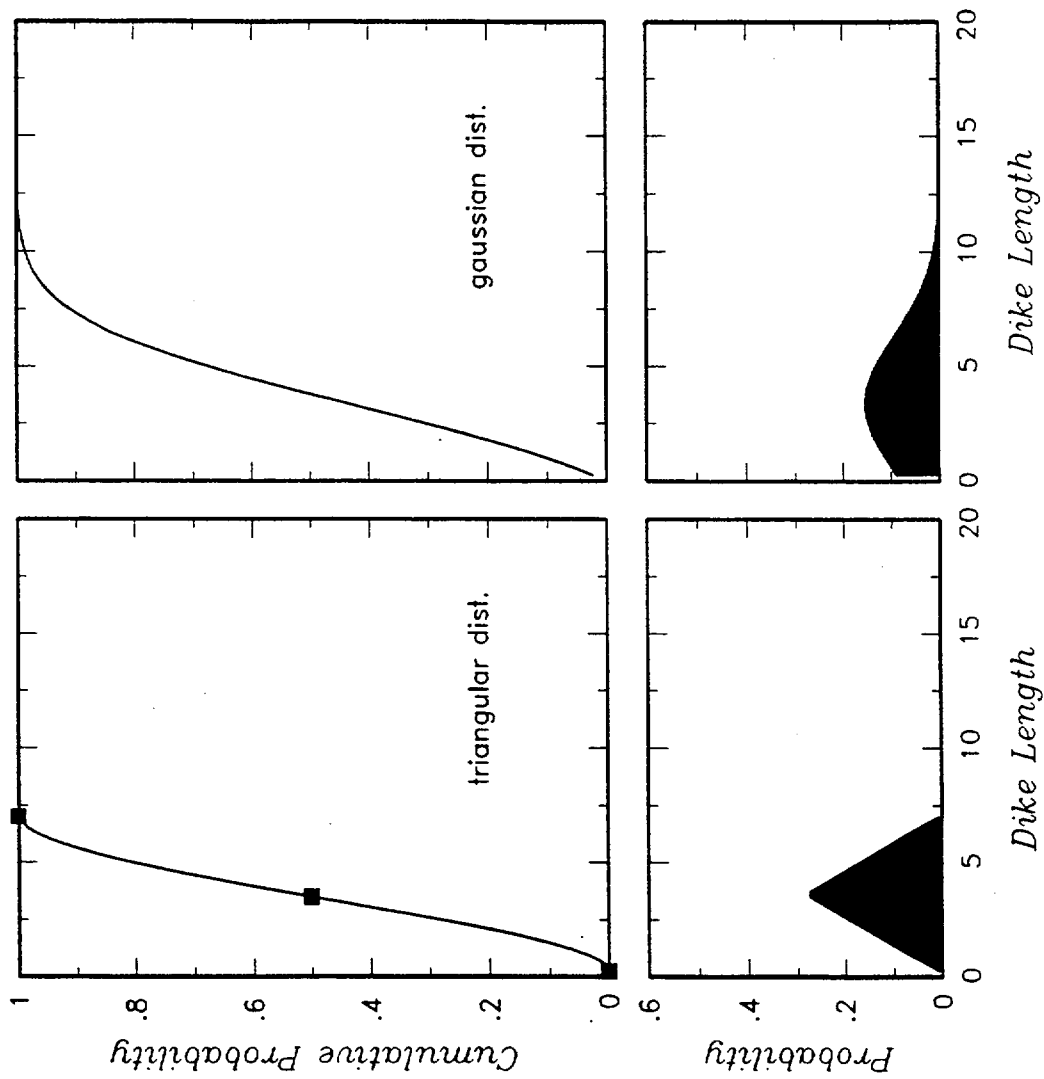


Figure BC-13 Dike length distribution developed by Bruce M. Crowe.

WENDELL A. DUFFIELD

ELICITATION INTERVIEW FOR PVHA PROJECT

INTRODUCTION

My approach to the problem of the volcanic hazard associated with the Yucca Mountain repository site can be described with reference to a target-shoot metaphor. The target is the repository, the "bullets" are dikes, and the "shooters" are represented by volcanic vents, present or future, from which bullets can originate.

My job is to define the positions from which shots might originate, and to define the possible directions and lateral ranges of these shots. The relative frequency with which possible combinations of position, direction, and range produce "hits" is a measure of the volcanic hazard.

VOLCANIC/TECTONIC SETTING

The Great Basin is a region of relatively high heat flow and approximately east-west tectonic extension (Lachenbruch and Sass, 1978), conditions favorable for volcanism. Superimposed on these conditions is the northwest-trending Walker Lane (see Stewart, 1992), which is a structural zone or feature that may favor or focus the occurrence of volcanism. Most Quaternary volcanism of the region is concentrated at or near the margins of the Great Basin (Luedke and Smith, 1981). More locally, near Yucca Mountain, Quaternary volcanics appear to be concentrated along the northeastern edge of the Walker Lane structural zone (Crowe and Perry, 1989). Although the process for generating magma in the Basin and Range is not well known, a knowledge of this process, or processes, is less important than the location of Quaternary volcanic features in assessing where volcanic events may occur in the near geologic future. In addition, knowledge about the volcanic rocks of about 1 Ma or less (all basaltic) in age is far more important to the problem at hand than knowledge of the preceding history of Tertiary silicic volcanism. In the Yucca Mountain region (YMR, defined as the area within a radius of about 100 km of Yucca Mountain), the thermal anomaly that was driving this silicic volcanism has dissipated and does not have much, if any, significance to volcanic processes of the next 10,000 years, the defined period of interest. There has been no silicic volcanism at or near Yucca Mountain for several million years.

There is a finite possibility of a volcanic eruption anywhere within the Great Basin. Thus, allowance should be made for a random occurrence anywhere within the province, although repeated occurrence of events within Quaternary volcanic fields seems far more likely, especially within the 10,000 year time-frame of interest. Volcanoes of Quaternary age and their locations relative to the "striking distance" of the repository site may well be the most significant factors to consider in a volcanic hazard analysis. An event of the type that we are concerned about for the PVHA (a dike intersecting the proposed repository in Yucca Mountain) has not occurred within the past 10 million years (my). Moreover, during the past 4 my, probably fewer than 10 Quaternary eruptions occurred within about 50 km of the repository site. Thus, we are being asked to assess the probability of future recurrence of what has been a very rare event, going back several million years in geologic time.

EVENT DEFINITION

Temporal Aspects

A volcanic event is equivalent to the process of magma ascending to the surface through a dike and erupting, and is limited in duration by the time it takes to crystallize the feeder dike. Once surface eruption ceases, dike solidification probably takes no more than a few decades, based on thermal considerations. Therefore, eruptions that repeat in the same area, or through the same vent, but are separated by more than a few decades, are considered separate events. Having so defined an event, it is worth noting that, with rare exception, current technology does not include geologic clocks capable of resolving prehistoric events of minimum, or even near minimum, duration. In practice, I identify events principally as cinder cones and their lava flows based on the morphology of these features and geologic mapping, and secondarily on the basis of rock chemistry.

Spatial Aspects

The maximum event size is judged to be about 30 km, which is the estimated maximum length of a feeder dike, or dike system, at about 5 to 25 km depths within the crust. At and near the earth's surface, the lengths of most individual dikes might be in the range of about 1 to 7 km (see Delaney and Gartner, 1995). A possible example of a dike, or set of contemporaneous dikes, giving rise to multiple cinder cones is reflected in the roughly north-northeast-aligned volcanoes of Crater Flat. One or multiple cones may form during a single event.

Geochemical Affinities

Time is the key factor in the definition of an event. Differences in chemical composition of volcanic products of a single event may or may not reflect the passage of significant time. There

are many examples of minor to substantial variation in chemistry associated with single volcanic events (e.g., Paracutin). Thus, as a general practice, chemical differences or affinities should not be used to define events, unless independent lines of evidence accurately and precisely constrain timing in a manner consistent with chemical variations.

Note: The elements of the PVHA model are summarized in the form of a logic tree in Figure WD-1.

REGION OF INTEREST

I define the region of interest by a circle with a radius equal to the maximum length of a dike, or contemporaneous set of dikes, that could extend to the repository site from a maximum range "shooting location" (see Zone C in Figure WD-2). Maximum dike length of about 30 km in the middle to upper crust is credible for the YMR, and may be as great as 40 km. These length estimates are based on field experience, review of dike traces on geologic maps, and the hypothesis that a dike may grow to be about as long in plan view as the thickness of the crust that it traverses. To incorporate uncertainty, maximum dike lengths of 20, 30, and 40 km are used with weights of 0.2, 0.6, and 0.2, respectively. Zone C is defined as the area within a 40-km radius of the proposed repository.

SPATIAL MODELS

The method used to describe the spatial distribution of events is one of "zonation," whereby areas are identified that are assessed to have different likelihoods or probabilities of future volcanic occurrence. Zones are defined based principally on the presence (or absence) of Quaternary volcanoes and secondarily on structural setting. Spatial variation of probabilities *within* such areas (e.g., spatial smoothing methods) are not included because it is judged that we do not have sufficient information to be able to conclude that there is a difference from one part of a "zone" to another.

The region of interest, called Zone C, is a circular area within a 40-km radius from the repository site. Within Zone C, the region is divided into several subzones. Subzone A, the Crater Flat-Lathrop Wells area, is the subzone containing the highest rate of volcanism within the overall region of interest. Subzone B extends to the northwest and southeast of Subzone A. Subzones A and B together are approximately coincident with the Crater Flat volcanic zone of Crowe and Perry (1989). The region to the west of Subzone B that is within the Walker Lane Belt is called

Subzone Cwl. and a counterpart eastern area that is not within the Walker Lane is called Subzone Cn. Subzone D includes Quaternary basalt and lies just outside the 40-km-wide region of interest. All of the Quaternary volcanoes appear to lie on or near the northeast margin of the Walker Lane (Crowe and Perry, 1989).

An alternative to the subzones defined above within the area of interest is to remove the western boundary of the northern part of Subzone B and combine this part with Subzone Cwl. This alternative acknowledges uncertainty in the location of the eastern boundary of the Walker Lane. The model with the northern part of Subzone B and Subzone Cwl considered separately is assigned a weight of 0.80, and the model where these areas are combined is assigned a weight of 0.20.

EVENT COUNTS

I restrict the period of interest to the past one million years, and the rationale for this restriction is twofold. First, looking backward in time two orders of magnitude longer than we are asked to look forward in time is judged sufficient to capture the types and frequency of volcanism expected to be characteristic of the region of interest. Second, looking backward in time even further (say, to 3 or 4 my) would not substantially change the "background" frequency of events. Moreover, locations of these older events are so distant from the proposed repository site that the younger and closer events within the 1 my time window dominate the analysis. Event counts are summarized on Table WD-1.

Lathrop Wells

The Lathrop Wells cone and surrounding volcanic deposits are interpreted to most likely represent 1 event, but may represent 2 events. There are considerable uncertainties in the age estimates such that all of the various mapped units could have been deposited during a single event about 100,000 years ago. Geochemical differences between mapped units are not (alone) definitive indicators of separate events at Lathrop Wells. Uncertainties exist regarding whether some of the separately mapped scoria deposits are primary or secondary. In the 2-event scenario, chronostratigraphic unit I of Crowe et al. (1995) would be considered a separate event from units II-IV.

The 1-event interpretation is assigned a weight of 0.90, and the 2-event interpretation 0.10.

Sleeping Butte Area

The maximum and most likely number of events in this area is 2; the minimum number is 1. The interpretation of 1 event is based on similar isotopic ages (R.J. Fleck, unpublished data presented

at the Sleeping Butte field trip) and a close spatial relationship that would allow Little Black Peak and Hidden Cone to be connected by a dike. However, if Little Black Peak and Hidden Cone were related to a single event, part of a connecting dike should be visible in the exposed bedrock between the two cones.

The event counts and their relative weights for the Sleeping Butte area are: 1 (0.05), 2 (0.95).

1.0 Ma Crater Flat

The ~1.0 Ma basalts in Crater Flat (excluding Lathrop Wells) are interpreted to represent a minimum of 1 event and a maximum of 5 events. In the 1-event scenario, all of the cones are assessed to be related to a single event, fed perhaps by an en echelon set of dikes. The 2-event scenario is based on combining Black, Red, and Makani cones into a single event because of their apparent linear (dike-connected?) relationship, and separating Little Cones into a separate event because it has somewhat different chemistry. In the 3-event scenario, Black and Red cones are considered a single event because of their close spacing, similar chemistry, and isotopic age dates, with Makani and Little Cones each considered a separate event. In the 4-event scenario, the two Little Cones are considered a single event, and they are treated as separate in the 5-event scenario. The rationale for these event counts derives mainly from observations I made during the PVHA Crater Flat field trip, together with published isotopic ages and rock chemistry data.

The event counts and their relative weights assigned for northern Crater Flat are: 1 (0.07), 2 (0.14), 3 (0.26), 4 (0.34), and 5 (0.19).

Amargosa Valley

It is likely that all of the "bullseye" aeromagnetic anomalies in the Amargosa Valley (southern part of Subzone B) are caused by buried volcanic rocks (Langenheim et al., 1993). The presence of both positive and negative anomalies within the area suggests at least two different ages of buried volcanics. Considering the substantial degree of exposure of the 1 Ma lavas in Crater Flat, the burial of all of the anomaly sources in Amargosa Valley by alluvium suggests ages greater than 1 Ma for these magnetic sources. Only one of the anomalies, B, has been drilled. Basalt was encountered beneath 180 m of Quaternary alluvium, and has yielded an isotopic age of about 3.8-4.3 Ma (Crowe et al., 1995). Excluding anomaly B, each of the other anomalies is allowed a probability of 1 in 100 of being less than 1 Ma.

The event counts and their relative weights for the Amargosa Valley area are: 0 (0.95), 1 (0.03), 2 (0.01), 3 (0.005), 4 (0.003), and 5 (0.002).

RATES OF OCCURRENCE

Using the event counts discussed above, rates of occurrence of volcanism are established for use in the PVHA (Table WD-2). The rates for each of the subzones in the analysis are calculated for a 1 Ma period. The bases for the rates are the following. For Subzone A, the counts for northern Crater Flat and Lathrop Wells are summed. For Subzone B, the counts for the Amargosa Valley area are used. For Subzone Cn, there are no known post-1 Ma events identified and the area is outside of the Walker Lane; thus, the rate should be very low. Two alternatives are used: 0 events/1 Ma (0.99) and 1 event/1 Ma (0.01). For Subzone Cwl, there are also no known post-1 Ma events, but the zone lies within the Walker Lane. It is judged that this area should have a rate that is ten times that of Cn (i.e., there is a 10 times higher probability of one event in Subzone Cwl, relative to Subzone Cn). The rationale for this judgement is that existing Quaternary volcanoes in the area are all within the Walker Lane, and that Cwl is in the Walker Lane whereas Cn is not. Within Subzone D, the counts assessed for the Sleeping Butte area are used.

Undetected Events

Extensive field investigations and geophysical studies have been conducted in the region to identify volcanic features that might exist at depths of importance to the repository (less than about 500 m) (Langenheim et al., 1993; Oliver et al., 1990; Bath and Jahren, 1985; Hoffman and Mooney, 1983). To have escaped detection, they must be very small or, if buried by depositional processes, older than 1 Ma. For this analysis, it is assessed that there is some possibility for one event to have escaped detection within the subzone of most interest (Subzone A), but this possibility is very remote.

The following assessment is made: 0 events/1 Ma (0.99), 1 event/ 1 Ma (0.01).

TEMPORAL MODEL

A homogeneous Poisson model is used to describe the temporal behavior of events. This model is believed to be most relevant because of the relatively short time period (the past 1 my) assessed and the lack of any well-defined temporal trends in the existing data base.

EVENT GEOMETRIES

In assessing the size of the region of interest, an assessment was made of the maximum length of a feeder dike system in the upper crust, which was set at 20 to 40 km. This dike length is

interpreted to be appropriate for depths below about 5 km but inappropriate for describing the maximum length of dikes and dike sets shallow enough to impact the repository. For these depths, the preferred length is between 5 and 7 km. This length is based on the possibility that Black, Red, and the Little Cones in Crater Flat are located on a single dike. Dike lengths may range from a minimum of near zero (point intersection) to a maximum of 20 to 40 km in the upper 0.5 km of the crust. The technical basis for shorter dike lengths is the data set compiled by M. Sheridan (presentation at PVHA Workshop 3) for several monogenetic basaltic cone fields, which suggests an average dike length of about 2.5 km. A continuous distribution is adopted having 85% of the probability density between 1 and 7 km and 98% between 1 and the maximum length. Above 7 km the density should fall off toward the maximum value. The maximum extends to values of 20 km, 30 km, or 40 km with weights of 0.2, 0.6, and 0.2, respectively, as discussed above.

Note: At the request of Dr. Duffield, a smooth interpolation function was fit to his discrete cumulative density estimates for dike length. The resulting cumulative distributions and density functions are shown on Figure WD-3.

The preferred dike orientation is N10E. This trend is based on the current orientations of maximum and minimum horizontal stress as deduced from such evidence as first-motion solutions to earthquakes and directions of fluid breakouts in pressurized bore holes. Also, Quaternary normal faults on and near Yucca Mountain trend roughly north (Scott, 1990). Uncertainty in dike orientation is assigned ± 20 degrees, or N10W to N30E, with a 90% probability that the orientation of a future dike will fall within these bounds.

Expected width for a future basaltic dike is about 1 meter. For lack of information to the contrary, in assessing the geometry of an event (dike emplacement) relative to a point location for the event (volcanic cone), the most likely location for the point is assigned to the center of the dike, with a decreasing probability that it would be at either end of the dike. The probability distribution has a triangular shape.

HYDROMAGMATIC ACTIVITY

For rising magma to produce hydromagmatic steam explosions, magma and aquifer water must be able to effectively mix, and the groundwater table must be quite shallow, probably less than about 250 m. Thus, unless there is a substantial rise in the level of groundwater in the Yucca

Mountain area, hydromagmatism is unlikely. The possibility of such an event is judged to be about 1 in 1,000.

TYPE OF ERUPTION

The expected future volcanic events in the region are the injection of basaltic dikes, development of cinder cones, and formation of small lava flows (similar to volcanic products in Crater Flat). A return to silicic volcanism during the next 10,000 years is judged to be extremely unlikely. Cycles of silicic volcanism, such as that represented by Timber Mountain Caldera and associated outflow sheets, tend to occur over hundreds of thousands to about a million years. The thermal pulse that gave rise to Pliocene silicic volcanism in the region has decayed, and there is no evidence that a new silicic magma body is forming.

Wendell A. Duffield
4-10-96

REFERENCES

- Bath, G.D., and Jahren, C.E., 1985, Investigation of an aeromagnetic anomaly on the west side of Yucca Mountain, Nye County, Nevada: U.S. Geological Survey Open-File Report 85-459.
- Crowe, B.M., and Perry, F.V., 1989, Volcanic probability calculations for the Yucca Mountain site: Estimation of volcanic rates: Proceedings, Nuclear Waste Isolation in the unsaturated zone, Focus '89, American Nuclear Society, p. 326-334.
- Crowe, B.M., Perry, F.V., Geissman, J., McFadden, L., Wells, S., Murrell, M., Poths, J., Valentine, G.A., Bowker, L., and Finnegan, K., 1995. Status of volcanism studies for the Yucca Mountain site characterization projects: Los Alamos National Laboratory Report LA-12908-MS, March 1995.
- Delaney, P.T., and Gartner, A.E., 1995, Physical processes of shallow mafic dike emplacement near the San Rafael Swell, Utah: U.S. Geological Survey Open-File Report 95-491, 47 p.
- Hoffman, L.R., and Mooney, W.D., 1983, A seismic study of Yucca Mountain and vicinity, southern Nevada: data report and preliminary results: U.S. Geological Survey Open-File Report 83-588, 50 p.
- Lachenbruch, A.H., and Sass, J.H., 1978, Models of an extending lithosphere and heat flow in the Basin and Range Province, *in* R.B. Smith and G.P. Eaton (eds.), Cenozoic tectonics and regional geophysics of the Western Cordillera: Geological Society of America Memoir 152, p. 209-250.
- Langenheim, V.E., Kirchoff-Stein, K.S., and Oliver, H.W., 1993, Geophysical investigations of buried volcanic centers near Yucca Mountain, southwest Nevada: Proceedings, Fourth International Conference, High-Level Radioactive Waste Management, Las Vegas, Nevada, v. 2, p. 1840-1846.
- Luedke, R.G., and Smith, R.L., 1981, Map showing distribution, composition, and age of late Cenozoic volcanic centers in California and Nevada: U.S. Geological Survey Miscellaneous Investigations Series Map I-1091-C.
- Oliver, H.W., Hardin, E.L., and Nelson, P.H., 1990, Status of data, major results, and plans for geophysical activities, Yucca Mountain project: prepared for the U.S. Department of Energy by the U.S. Geological Survey and S.A.I.C. (YMP 90-38).
- Scott, R.B., 1990, Tectonic setting of Yucca Mountain, southwest Nevada, *in* Wernicke, B.P. (ed.), Basin and Range extensional tectonics near the latitude of Las Vegas, Nevada: Geological Society of America Memoir 176, p. 251-282.

Stewart, J.H., 1992. Walker Lane Belt, Nevada and California - An overview, *in* S.D. Craig (ed.), Structure, Tectonics, and Mineralization of the Walker Lane: Reno, Nevada, Geological Society of Nevada, Proceedings Volume, Walker Lane Symposium, p. 1-16.

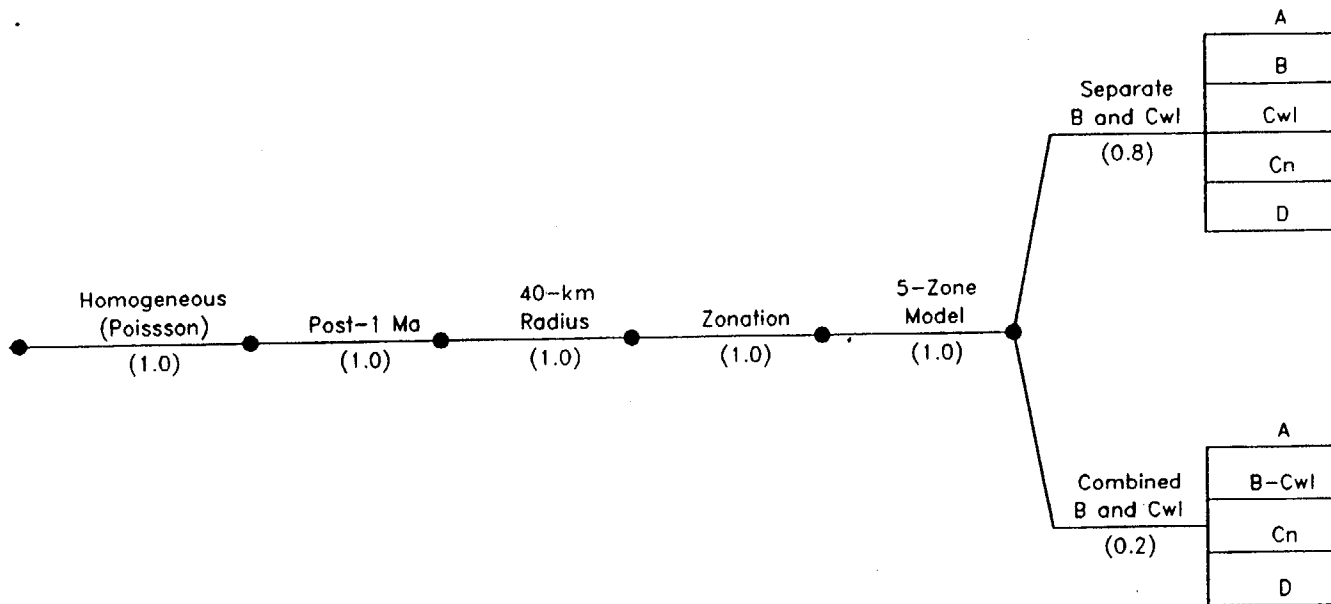
**TABLE WD-1
 WENDELL A. DUFFIELD - EVENT COUNTS**

LOCATION	COUNTS (CONES)	WEIGHT	NOTES
Lathrop Wells	1 I-IV	(0.90)	BC: Black Cone C-G: Aeromagnetic anomalies of V. Langenheim, USGS HC: Hidden Cone LBP: Little Black Peak LC: Little Cones 2LC: 2 separate Little Cones M: Makani Cone RC: Red Cone I-IV: Chronostratigraphic units of Crowe et al. (1995)
	2 I, II-IV	(0.10)	
Sleeping Butte	1 (LBP+HC)	(0.05)	
	2 (LBP, HC)	(0.95)	
1.0 Ma Crater Flat	1 (all)	(0.07)	
	2 (LC, RC+BC, M)	(0.14)	
	3 (LC, RC+BC, M)	(0.26)	
	4 (LC, RC, BC, M)	(0.34)	
	5 (2LC, RC, BC, M)	(0.19)	
Armagosa Valley	0	(0.95)	
	1 (D)	(0.03)	
	2 (C,D)	(0.01)	
	3 (C,D,E)	(0.005)	
	4 (C,D,E,F)	(0.003)	
	5 (C,D,E,F,G)	(0.002)	

**TABLE WD-2
 WENDELL A. DUFFIELD - RATES OF OCCURRENCE**

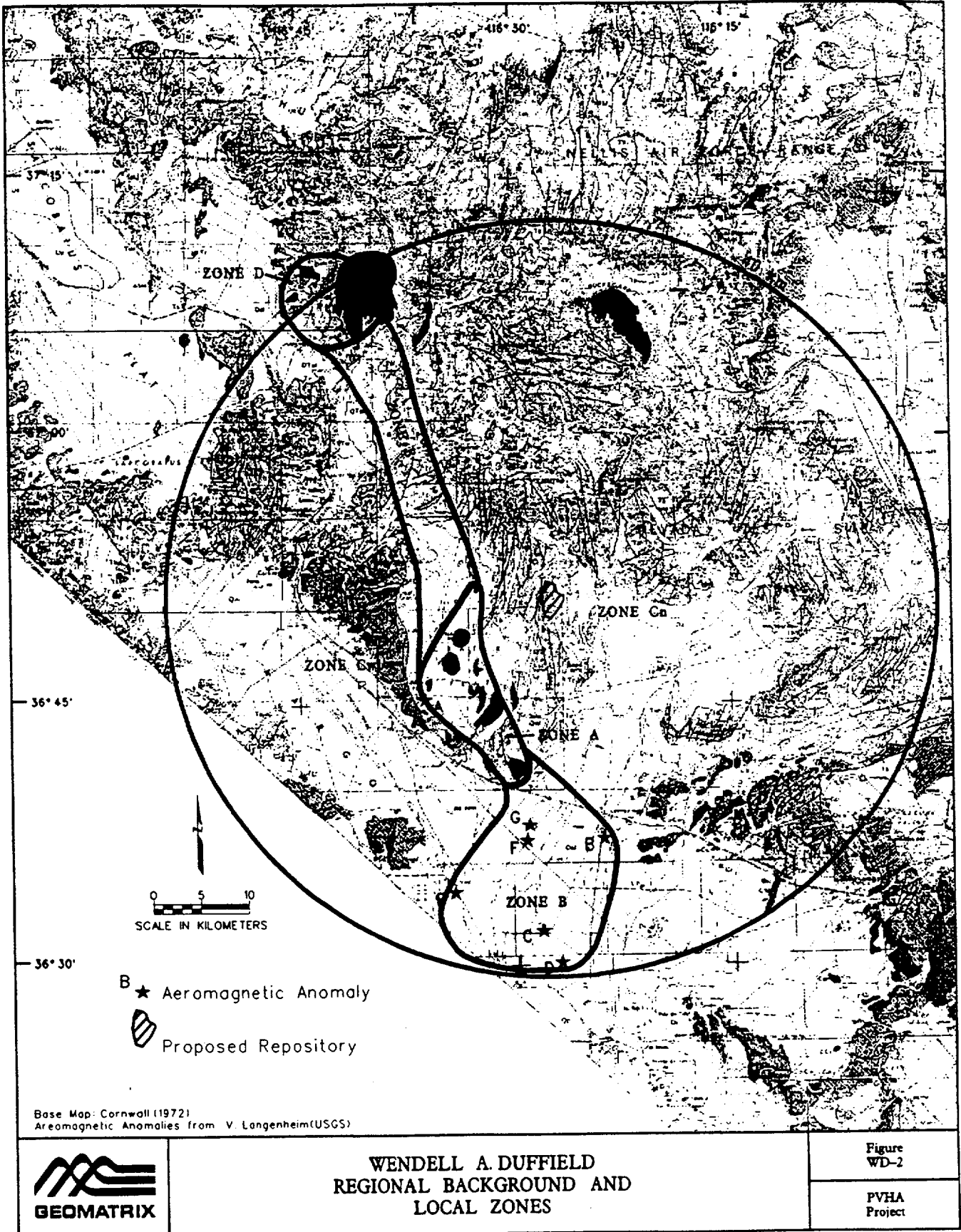
TIME PERIOD	COUNT METHOD FOR SUBZONES	NOTES
Post 1 Ma (1.0)	Subzone A: (NCF+LW) Subzone B: (AV) Subzone Cn: 1 event/1 Ma (0.01) 0 events/1 Ma (0.99) Subzone Cwl: 10 x Cn rate Subzone D: (SB)	AV: Amargosa Valley LW: Lathrop Wells NCF: Northern (1.0 Ma) Crater Flat SB: Sleeping Butte

Temporal Models	Time Period	Region Of Interest	Spatial Models	Zonation Model	Zone Definition	Sources
-----------------	-------------	--------------------	----------------	----------------	-----------------	---------



- A: Subzone A
- B: Subzone B
- D: Subzone D
- Cwl: Subzone C within Walker Lane Belt
- Cn: Subzone C outside Walker Lane Belt
- B-Cwl: Subzone B and subzone Cwl combined

Figure WD-1 PVHA model logic tree developed by Wendell A. Duffield.



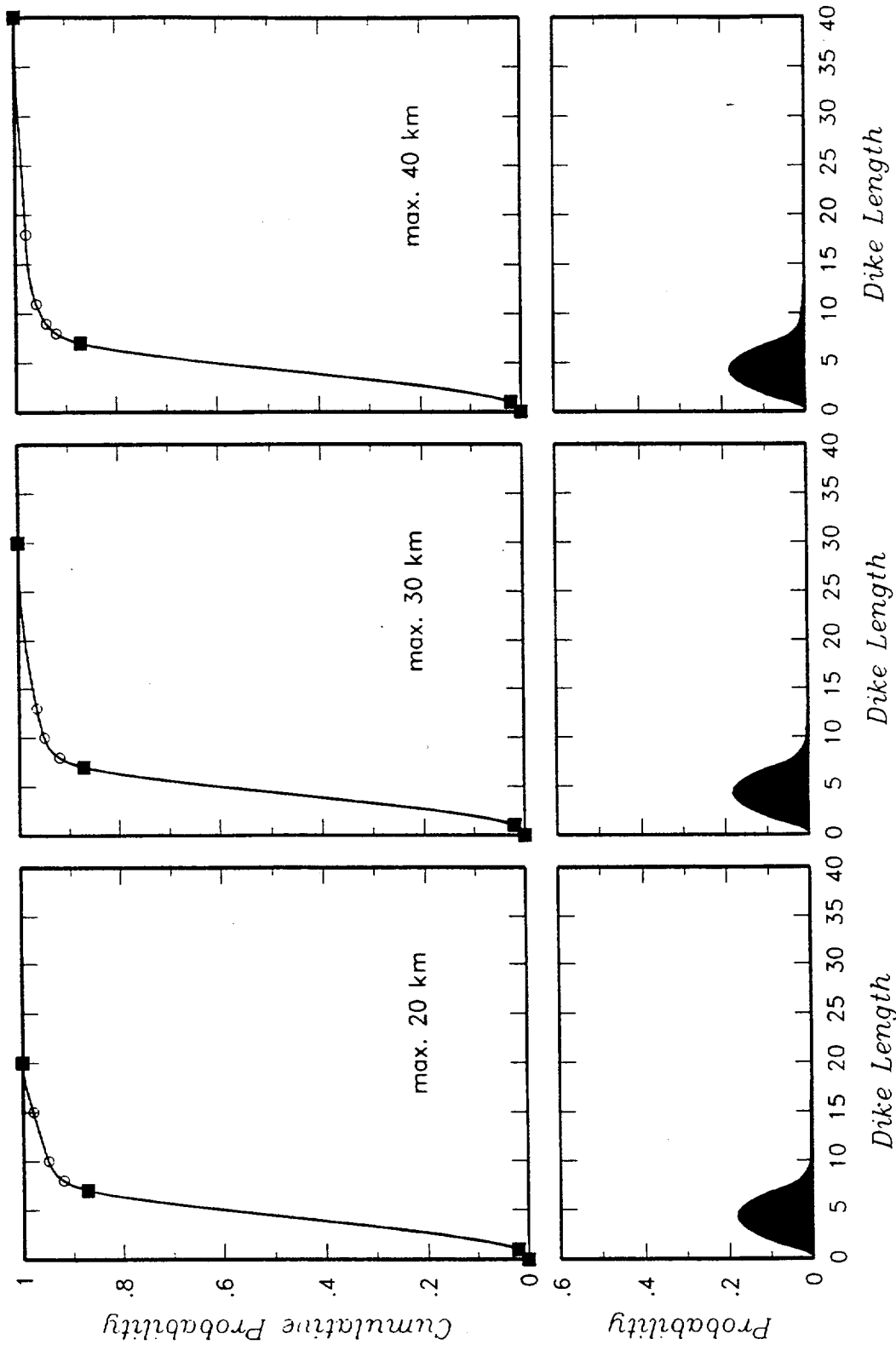


Figure WD-3 Dike length distribution developed by Wendell A. Duffield.

RICHARD V. FISHER
ELICITATION INTERVIEW FOR PVHA PROJECT

VOLCANIC/TECTONIC SETTING

Voluminous silicic volcanism occurred in the Yucca Mountain Region (YMR, defined as the region within a 100-km radius of Yucca Mountain) as part of an extensive pulse of mid-Cenozoic volcanism within the southwestern United States. Yucca Mountain is in the south-central part of a major Cenozoic volcanic field that covered 11,000 square kilometers. In the YMR, silicic volcanism was most active between 15 to 11 Ma, and silicic volcanism ceased at about 8.5 Ma with eruptions of the Black Mountain caldera complex. Significant cessation of subduction coincided with the change from silicic to low-volume basaltic cinder cone and lava flow fields. The tectonic regime is not subduction-driven at the present time. Basaltic volcanism in the YMR is caused by regional extension (Crowe et al., 1995).

Crater Flat is an extensional basin within which basaltic volcanism has taken place over the last 4 my (from 3.7 Ma to less than 1 Ma) (Crowe et al., 1995). Yucca Mountain lies to the east, adjacent to Crater Flat. Crater Flat therefore plays a significant role in probability hazard assessments of the proposed repository, which is discussed more fully under Spatial Models, below. The volcanic events within Crater Flat and the Amargosa Valley are assumed to lie within a volcanic field that I term for this analysis the Crater Flat field (CFF). The recent volcanism in the Sleeping Butte field (SBF) is also considered for the hazard assessment.

EVENT DEFINITION

A volcanic event is any incident that occurs during the propagation of magma upward through the crust and onto the earth's surface, such as earthquakes, gas emission, lava flows, volcanic cone production, etc. Pragmatically, a volcanic event can only be recorded (counted) by noting the deposits or the effects of the event. If only gases are expelled, a past volcanic event is difficult to determine. Volcanic cones, domes, dikes, lava flows, and volcanic ash or other tephra layers result from volcanism and can be called volcanic events.

Temporal Aspects

In low-volume basaltic eruptions, an "event" is the release of energy due to the ascent of magma, commonly as a dike, along which cinder cones or lava flows may develop. More than one cone or eruptive feature is likely to form from a dike, but if it can be inferred that the cones or other eruptive features came from the same dike, they are counted as one event. Low-volume basaltic processes are commonly short-lived, generally less than 100 years, because heat dissipation of small volumes is rapid and the magma cools quickly.

Spatial Aspects

Small-volume basaltic events are commonly generated along dikes, such as at the Lunar Crater Volcanic Field. The distance of an event is relatively short, usually less than 3 to 5 km, with an extreme of 20 km, along which more than one lava flow or cinder cone may develop (Scott and Trask, 1971). Therefore, I consider lava flows or cones that are constructed, say, 25 or 30 km apart at essentially the same time to be separate events.

Geochemical Affinity

Within a volcanic field, the deposits usually display a general isotopic affinity that is related to sharing the same magma source. However, distinguishing between individual events based on geochemical differences within a field is difficult and is not used in this analysis. For example, two cones 3 km apart having essentially the same age, but having differences in their geochemistry, would not be distinguished as separate events based solely upon geochemical signature because differences could be caused by local subsurface contamination.

Note: The elements of the PVHA model are summarized in the form of a logic tree in Figure RF-1.

REGION OF INTEREST

Two large regions of interest are identified that serve as background zones to the assessment of volcanic hazard. The first is the area enclosed within a 100-km radius of the site (Figure RF-2). The second is an "eastern zone" that includes several young volcanic fields in the eastern region of late-Cenozoic volcanic centers shown on the Luedke and Smith (1981) map (Figure RF-3). The purpose for selecting the background region is to provide a regional background rate of occurrence of volcanoes in a tectonic province of significance to the site. Because the 100-km radius area includes a large region with no Quaternary volcanic centers other than the Crater Flat field, it is less preferred and is assigned a weight of 0.2. The eastern

zone is more representative of the regional rate of volcanism related to the proposed repository site and Crater Flat because the young basaltic volcanic fields (Luedke and Smith, 1981) contain Quaternary age volcanoes (2 Ma or less). The eastern zone is assigned a weight of 0.8.

SPATIAL MODELS

Three alternative spatial models are identified to assess the future occurrence of volcanoes in the YMR (summarized in Figure RF-1). The first approach, termed a field shape approach, follows the method suggested by M. Sheridan (presentation at PVHA Workshop 3), in which the geometry of a volcanic field is assumed to follow a bivariate Gaussian distribution. In using this approach, it is assumed that the boundaries of the CFF and SBF (Figure RF-4) represent between the 90th and 98th percentile of the Gaussian distribution. The percentiles and their relative weights are: 90% (0.8), 95% (0.1), and 98% (0.1). These weights reflect the high uncertainty in the location of the field boundaries.

The second approach is spatial smoothing of the observed events, following the general approach outlined by Connor and Hill (1995). An Epanechnikov smoothing kernel is used. It is assumed that the boundaries to the CFF and SBF contain 90%, 95%, or 98% of the probability density with weights of 0.8, 0.1, and 0.1, respectively. Again, these weights reflect the high uncertainty in the location of the field boundaries. The third approach is the zonation approach, whereby events are assumed to have a uniform probability distribution within either the CFF and SBF or the background zone.

The field shape approach is preferred (weight of 0.7) because it takes advantage of observations made at other basaltic fields in the southwestern U.S., and for reasons described in the section below. The spatial smoothing approach is given a lesser weight (0.2) because there are so few events within the CFF and, therefore, it may provide a weak basis for assessing distribution of future events. The zonation approach is given least weight (0.1) because volcanic fields do not show a uniform spatial distribution of volcanoes.

Reasons for Favoring the Field Shape Approach

The volcanic events within Crater Flat and the Amargosa Valley are defined here to lie within the CFF. The CFF differs from the CFVZ of Crowe and Perry (1989) because the Sleeping Butte and Thirsty Mesa centers are excluded. They are excluded from the CFF because there is a distinct spatial gap between volcanoes within the two areas that has persisted for over 5 my. The northwest trend parallels the trend of the Walker Lane (Crowe et al., 1995), but I judge

the Walker Lane structure to have little significance with respect to local volcanism because it is not an extensional structure. Buckboard Mesa is believed to be related to the moat zone of the Timber Mountain caldera and is not related to the Crater Flat volcanics; hence, it is not included in the CFF. The CFF has an elliptical shape, as is expected for a basaltic volcanic field, based upon reasons given below. The rate of occurrence of volcanic events within the CFF is assessed based on activity over the past 1-2 my, even though the location of the CFF includes older events such as those in the 3.7 Ma area of Crater Flat and Amargosa Valley. Only the past 2 my are used to assess the rate of occurrence of volcanic events because events in the Quaternary are more relevant to modern and future events.

Underlying assumptions pertaining to cone density within small-volume basaltic volcanic fields and shapes of the fields are given as follows. Extension of the lithosphere creates local magma batches at various levels beneath the surface, presumably by decompression melting. The magma source lies beneath the resulting volcanic fields. Small magma batches ascend from the source region to the surface. Each rising magma batch follows a path governed by random physical and possibly chemical inhomogeneities toward the surface. These magma batches therefore intersect the surface at different places above the source region, but the place of intersection cannot be predicted. As a consequence, the rise of many separate batches from the same source can be circumscribed by a "cone of ascent" rather than a vertical pipe. This is indicated by the shape of cinder cone fields. The depth and size of the initial magma batch governs the size of the cinder cone field. Therefore, the area of a cinder cone field cannot exceed the limits of the "cone of ascent" of the magma. The deeper the source, the greater the diameter of the cone of ascent when it intersects the earth's surface.

The general field shape outline (usually elliptical) and the location of the field are directly related to the source region and the stress field within the lower ductile crust, but fractures with a different orientation in the upper brittle part of the crust can localize the final magma ascent. Although Quaternary basaltic volcanoes may not follow shallow structural features, there is occasionally a spatial correlation between basalt centers and deep-seated structural features such as strike-slip faults and ring fracture zones of calderas. Structures in the brittle crust are inferred to be passive features that promote the passage of basaltic magma.

Because the exact mechanism for the formation of magma batches is not known, other than a relationship to regional extension, the reason for localization of a field is not known. It is, therefore, not possible to accurately predict where new fields will occur. Basaltic volcanic fields consist of a few to hundreds of cones. The lifetime of a field is commonly about 5 my.

Studies of fields with large numbers of cones display an elliptical shape and appear to display a Gaussian falloff of the number of cones toward the margins of the field (M. Sheridan presentations at PVHA Workshops 3 and 4). This is consistent with the idea that cone fields lie within a cone of ascent with the magma source below the center of a field. Fields with low numbers of events, such as those in the YMR, may not have sufficient numbers of events to infer a Gaussian falloff, but it is used in the model herein because a Gaussian falloff is justified for fields with hundreds of cones (M. Sheridan presentations at PVHA Workshops 3 and 4).

Small-volume volcanic eruptions come from small-volume magma batches. The smaller the volume, the faster the magma batch will freeze. Therefore, each field of basaltic cones comes from a succession of short-lived magma batches. It is not known whether ascending magma batches break away from a larger, longer-lived magma chamber, or recur as small chambers throughout the history of a basalt field. Recurrence of basaltic volcanism within the same field does not exceed 5 my (M. Sheridan presentation at PVHA Workshop 3). Once a field shuts off, it appears not to start up again.

Although it is highly likely that future volcanic events will fall within existing fields and not outside them (that is, the probability of forming a new field is generally very low), the location of cones within a field is random. There does not appear to be a time-series of eruptions within a particular field. This is consistent with the hypothesis given above for the random paths followed by successive magma batches. The recurrence of an eruption at essentially the same place, as in the case of a polygenetic volcano, would be due to a random hit at the same place.

The alignment of vents within a field may have a different orientation from the general outline of the field itself because the vents may be influenced by shallow structures such as existing faults that are not oriented in the same direction as the basalt field. An example might be the cones in northern Crater Flat, which appear to be aligned in a northeast direction at an angle to the general northwest alignment of the inferred CFF (Faulds et al., 1994).

Boundary of Crater Flat Field

The boundary of the CFF is assumed to represent the 90th to 98th percentile of the Gaussian distribution. This assumption is consistent with the model of magma that rises within a cone of ascent circumscribing the highest density of volcanic events within a field. Volcanic events may occur outside the estimated CFF boundary because of the random paths of magma ascent. Thus, there is a small probability that volcanic activity could occur near the proposed repository. Such near-repository activity would most likely occur along dikes.

EVENT COUNTS

Event counts are assessed for two time periods: the past 1 my and the past 2 my. The counts are identical for the two time periods with the exception of those events in the northern Death Valley area. The number of events, their uncertainties, and the basis for the assessments are given below. Event counts are summarized in Table RF-1.

Lathrop Wells

The minimum and most likely number of events at Lathrop Wells is 1, and the maximum is 4 events. The single-event option is preferred based on the morphology of the cone and the author's observation that there are no unequivocal analog polygenetic cones recognized elsewhere in the world. The single-event alternative is also consistent with the event definition, whereby the age estimates overlap and there is close spatial proximity; geochemical differences do not enter into separating out individual events. I observed chronostratigraphic unit IV several years ago, and at that time I interpreted the associated volcanic units to be primary deposits that were not reworked. Given the significance of this interpretation, however, I would like to re-examine the deposits. Because that locality has now been removed by quarrying, and no other localities containing similar deposits have been identified, it is impossible to verify my original interpretation.

In the 2-event alternative, chronostratigraphic unit I and combined units II and III are separate events. This is based upon age determinations that indicate unit I is a distinctive unit, and the age estimates for units II and III overlap; unit IV is not considered a separate event. The 3-event alternative is similar to the 2-event alternative, except that unit IV is considered to be a separate event. In the 4-event alternative, units I, II, III, and IV are each considered separate events.

The following event counts and their relative weights are assigned for the Lathrop Wells center: 1 (0.6), 2 (0.3), 3 (0.05), and 4 (0.05).

Sleeping Butte

The minimum and most likely number of events at Sleeping Butte is 1: the maximum is 3 events. A single event is preferred because a NE-trending dike connects Black Cone and Hidden Cone. The NE orientation is consistent with local faults and the regional stress regime. Black Cone and Hidden Cone each represent a separate event in the 2-event choice. The 3-event alternative is based upon paleomagnetic data presented by D. Champion (PVHA Sleeping Butte field trip) that suggest there were 2 events at Hidden Cone.

The event counts and their relative weights for the Sleeping Butte area are the following: 1 (0.7), 2 (0.25), 3 (0.05).

1.0 Ma Crater Flat

The ~1 Ma basalts of northern Crater Flat most likely represent 1 event, although a maximum of 4 events could have occurred. For the single-event option, eruptions formed cones along an en echelon set of dikes during a 100-year or shorter time frame; the overlapping age determinations and the linear arrangement of the 4 cones provide strong evidence for the single-event option. The 12-km length and the slight curvature to the chain of cones argue against all of the cones resulting from a single dike. More likely, a dike set formed as a set of "fingers" that converge at depths of a few to several kilometers below the surface. The option with 2 events would involve combining adjacent cones (for example, Makani and Black cones as 1 event, Red and Little cones as another event). The 3-event option would involve Red and Black cones as a single event, with Makani Cone and Little Cones each defining additional events. The 4-event option, where each of the 4 cones is related to a single event, is the maximum number for the area (the Little Cones are interpreted to have been erupted during a single event due to their small size and close proximity). If there were evidence of separate dikes, or more accurate age data for the individual cones, 4 events would be more likely than 2 or 3 events because the spatial separation of the cones is close to the maximum separation allowed within this definition of event.

The following event counts and their relative weights are assigned for northern Crater Flat: 1 (0.8), 2 (0.05), 3 (0.05), and 4 (0.1).

Northern Death Valley

Two Quaternary events are identified in the Death Valley area: the 1.7 Ma basalt of Shoreline Butte and the <0.7 Ma basalt of Cinder Hill (also called Split Cone) (B. Crowe informal PVHA memo). In the post-1 Ma period, 1 event is counted; in the post-2 Ma period, 2 events are counted.

Ubehebe Craters

A minimum of 1 and a maximum of 5 post-1 Ma events have occurred in this area; the most likely number is 2. All of the interpretations come from consideration of the data reported in Crowe and Fisher (1973) and my personal observations. All of the features mapped could represent pulses of eruptions during a single eruptive event. Two events can be counted if the

Strombolian eruptions within Ubehebe crater occurred as 1 event followed by the phreatic events. This is the favored alternative. A 4-event alternative would entail the eruption of Ubehebe crater, two clusters, and a Strombolian event. A 5-event alternative would assume that the Little Hebe eruption was a separate event.

The event counts and their relative weights for the Ubehebe Craters area are: 1 (0.3), 2 (0.6), 4 (0.05), and 5 (0.05).

Lunar Crater

The Quaternary Lunar Crater field is an elongate ellipse, about 25 km long, containing 82 vent counts and 28 clusters based upon the work of Crowe et al. (1992). Most of the cinder cones and lava flows are aligned in an en echelon pattern. This suggests that many vents were formed contemporaneously by an en echelon system of dikes that are presently unexposed. It is probable that several vents were simultaneously fed by activity along each assumed dike.

The major clustering pattern suggests the following event counts and their relative weights: 1 (0.05), 2 (0.3), 3 (0.6), and 28 (0.05).

Cima Field

The Cima field has a roughly circular shape, suggesting the presence of multiple events.

The event counts and their relative weights for the Cima field are: 1 (0.01), 7 (0.5), 22 (0.35), and 29 (0.14).

RATES OF OCCURRENCE

The rates of occurrence of volcanic events are calculated from the event counts averaged over two periods: the past 1 my and the past 2 my. The post-1 Ma time period is given higher weight (0.8) because the author believes that the best indicator of the rate of future small-volume basaltic volcanism is the more recent volcanic activity. The 2 Ma period is given lesser weight (0.2), but is included because this includes all of the Quaternary period.

Because the time periods over which the rates are calculated are relatively short compared to the life of a volcanic field, it is judged that the rates should be treated as homogeneous over these periods.

Undetected Events

In addition to events identified and interpreted at the surface, there is the potential for undetected subsurface events that might exist at depths of less than 300 m beneath the present-day topographic surface and not be represented at the surface. Most of the topographic surface of the CFF within which volcanism has occurred is at an elevation below the repository. Therefore, undetected events in CFF would be about 300 m or more below the repository.

I speculate that there are 10 times as many dikes at depths of 2.5 to 5 km than are at the surface. This would mean that the ratio of the number of dikes at depth to the number at the surface is 10:1 at 2.5 to 5 km depth and is 1:1 at the surface. Then, by extrapolating arithmetically the relationship between the ratio and depth to a depth of 300 m, a ratio of 1.5 to 2.0 is determined. As a first estimate, I suggest that the number of events at the surface within a volcanic field could be multiplied by 1.5 to 2.0 to obtain the total number of events that could be present at a depth of 300 m. A logarithmic extrapolation results in ratios of 1.15 and 1.32. I believe that the arithmetic and logarithmic extrapolations should be given equal weight (0.5).

EVENT GEOMETRIES

Individual dike lengths range from 0.5 to 5 km, although an event may consist of a set of dikes longer than 5 km. An event is most likely to be associated with a single dike having a length that is less than 5 km near the surface. En echelon sets of dikes have maximum lengths that are based on the dimension of the volcanic field in the orientation parallel to the direction of regional maximum horizontal compressive stress. In the YMR, this dimension is about 20 km for the CFF along a strike of N30E (Figure RF-5). The following cumulative distribution is assessed for the length of an event:

0.5 km	0.0
1 km	(0.5)
5 km	(0.8)
10 km	(0.97)
20-25 km	(1.0)

Equal weight is given to the maximum lengths of 20 and 25 km.

Note: At the request of Dr. Fisher, the cumulative density was assumed to be linear between the discrete points given. The resulting cumulative distributions and density functions are shown on Figure RF-5.

Dikes should be oriented parallel to the direction of regional maximum horizontal compression, N30E (G. Thompson presentation at PVHA Workshop 2), with an uncertainty of plus or minus 20 degrees representing the 95% confidence interval. Dikes are more likely to be centered on an event than to extend unilaterally. Therefore, a triangular distribution is used to define the event location.

HYDROMAGMATIC ACTIVITY

A large hydromagmatic explosion is very unlikely and has an estimated probability of occurrence of about 1 in 1,000. This type of event would require a significant amount of water and permeable rocks in the subsurface below a depth of about 0.5 km. Hydromagmatic activity generally occurs at depths of about 100 m, and more rarely at a depth of 200 m because of pressures that subdue the ability of steam explosions to occur. There is a higher probability that a hydromagmatic event would occur in a valley where abundant water could be located within alluvium. The groundwater table is about 620 m beneath Yucca Mountain and about 320 m beneath the proposed repository.

TYPE OF ERUPTION

Basaltic eruptions characterized as Strombolian with lava flows and dikes of small volume have occurred in the YMR during the past 1 my, so a continuation of this pattern is most likely. Phreatoplinian eruptions are rare in basaltic fields and are considered unlikely. Although some water was involved in eruptions at Lathrop Wells, it had little effect upon the geometry of the cinder cone.

Silicic volcanism died out in the YMR about 8.5 Ma, and the probability of large-volume silicic volcanism is insignificant within the YMR.

*Approved and signed
Richard Fisher
April 18, 1996*

REFERENCES

- Champion, D.E., 1991, Volcanic episodes near Yucca Mountain as determined by paleomagnetic studies at Lathrop Wells, Crater Flat, and Sleeping Butte, Nevada: Proceedings, Second International Conference, High-Level Radioactive Waste Management, Las Vegas, Nevada, May, v. 1, p. 61-67.
- Connor, C.B., and Hill, B.E., 1995, Three nonhomogenous Poisson models for the probability of basaltic volcanism: application to the Yucca Mountain region, Nevada, USA: Journal of Geophysical Research, v. 100, no. B6, p. 10,107-10,125.
- Crowe, B.M., and Fisher, R.V., 1973, Sedimentary structures in base-surge deposits with special reference to cross-bedding, Ubehebe Craters, Death Valley, California: Geological Society of America Bulletin, v. 84, p. 663-682.
- Crowe, B.M., and Perry, F.V., 1989, Volcanic probability calculations for the Yucca Mountain site; estimation of volcanic rates: Proceedings, Nuclear Waste Isolation in the Unsaturated Zone, Focus '89, American Nuclear Society, p. 326-334.
- Crowe, B., Perry, F., Geissman, J., McFadden, L., Wells, S., Murrel, M., Poths, J., Valentine, G.A., Bowker, L., and Finnegan, K., 1995, Status of volcanism studies for the Yucca Mountain site characterization project: Los Alamos National Laboratory Report LA-12908-MS, March 1995.
- Crowe, B.M., Picard, M., Valentine, G., and Perry, F.V., 1992, Recurrence models of volcanic events; applications to volcanic risk assessment: Proceedings, Third International Conference, High Level Radioactive Waste Management, Las Vegas, Nevada, April 12-16, v. 2, p. 2344-2355.
- Faulds, J.E., Bell, J.W., Feuerbach, D.L., and Ramelli, A.R., 1994, Geologic map of the Crater Flat area, Nevada: Nevada Bureau of Mines and Geology, Map 101.
- Ludke, R.G., and Smith, R.L., 1981, Map showing distribution, composition, and age of volcanic centers in California and Nevada: U.S. Geological Survey Miscellaneous Investigations Series, Map I-1091-C.
- Scott, S.H. and Trask, N.J., 1971, Geology of the Lunar Crater volcanic field, Nye County, Nevada: U.S. Geological Survey Professional Paper 559-I, 36 p.

TABLE RF-1
RICHARD V. FISHER - EVENT COUNTS

LOCATION	COUNTS (CONES)	WEIGHT	NOTES
Lathrop Wells	1 I-IV	(0.6)	BC: Black Cone HC: Hidden Cone 2HC: 2 events at Hidden Cone LBP: Little Black Peak LC: Little Cone M: Makani Cone RC: Red Cone SB: Shoreline Butte SC: Split Cone I-IV: Chronostratigraphic units of Crowe et al. (1995)
	2 I, II+III	(0.3)	
	3 I, II, III	(0.05)	
	4 I, II, III, IV	(0.05)	
Sleeping Butte	1 (LBP+HC)	(0.7)	
	2 (LBP, HC)	(0.25)	
	3 (LBP, 2HC)	(0.05)	
1.0 Ma Crater Flat	1 (all)	(0.8)	
	2 (LC+RC, BC+M)	(0.05)	
	3 (LC, RC+BC, M)	(0.05)	
	4 (LC, RC, BC, M)	(0.1)	
N. Death Valley (1 MA)	1 (SC)	(1.0)	
N. Death Valley (2 Ma)	2 (SC, SB)	(1.0)	
Lunar Crater	1	(0.05)	
	2	(0.30)	
	3	(0.60)	
	28	(0.05)	
Cima	1	(0.1)	
	7	(0.05)	
	22	(0.35)	
	29	(0.14)	

TABLE RF-2
RICHARD V. FISHER - RATES OF OCCURRENCE

TIME PERIOD	COUNT METHOD FOR ZONES	NOTES
Post 1 Ma (0.8)	CFF: (NCF+ LW) SBF: (SB) BK100: (DV1, UH) BKEZ: (DV1, UH, LC, C)	CFF: Crater Flat Field BK100: 100 km radius Background Zone BKEZ: Eastern Background Zone NCF: Northern Crater Flat LW: Lathrop Wells SB: Sleeping Butte
Post 2 Ma (0.2)	CFF: (NCF+ LW) SBF: (SB) BK100: (DV2, UH) BKEZ: (DV2, UH, LC, C)	SBF: Sleeping Butte Field DV1: Death Valley (1 Ma) DV2: Death Valley (2 Ma) UH: Ubehebe LC: Lunar Crater C: Cima

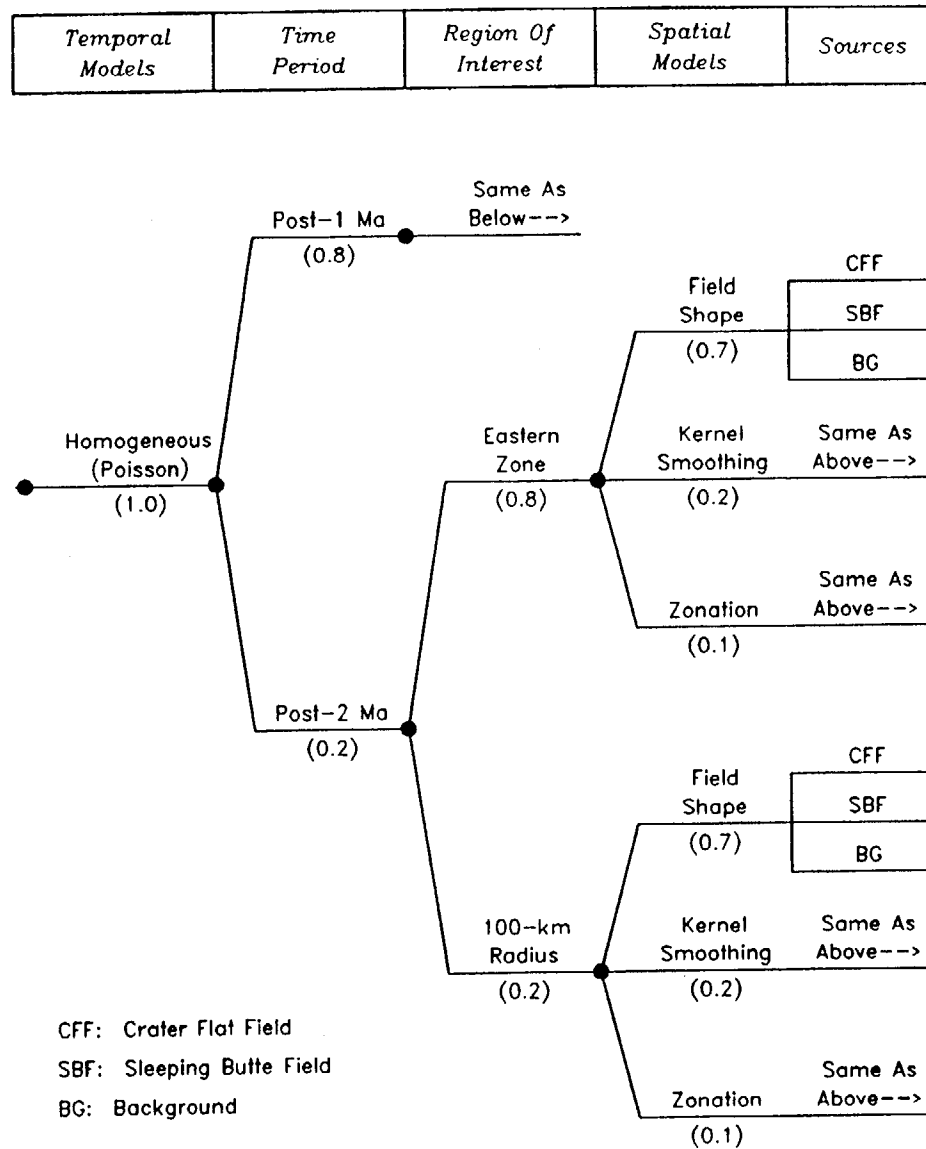
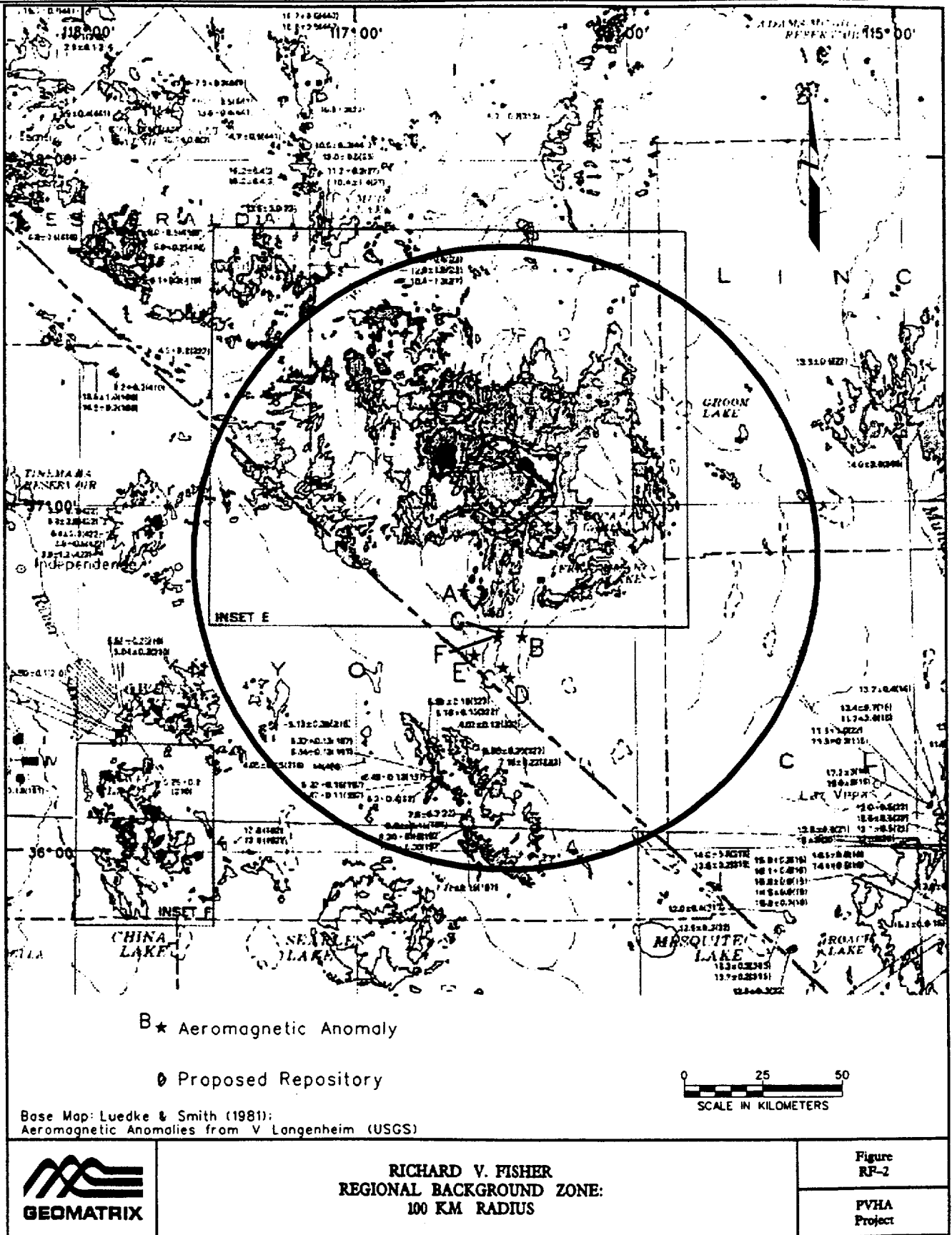
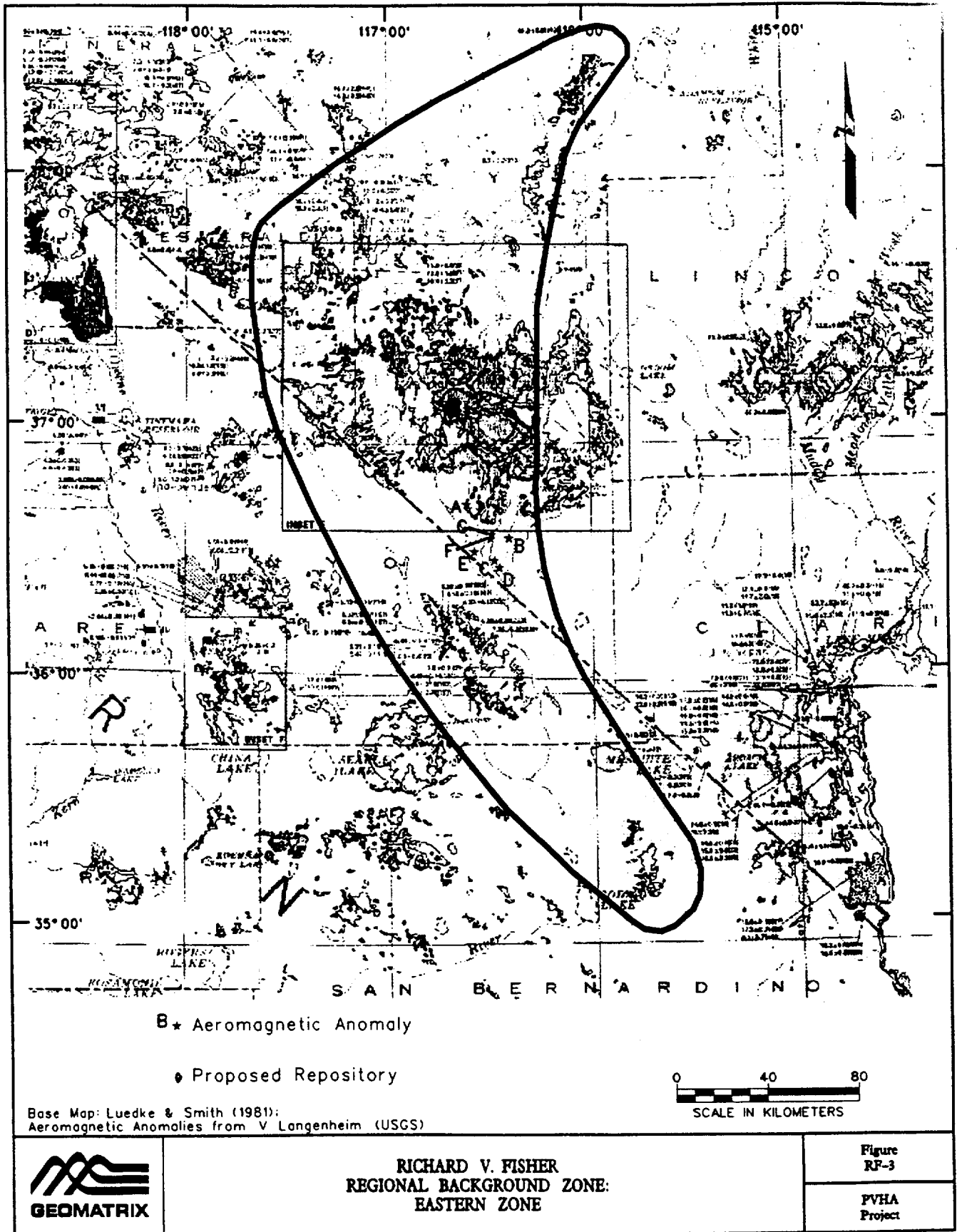


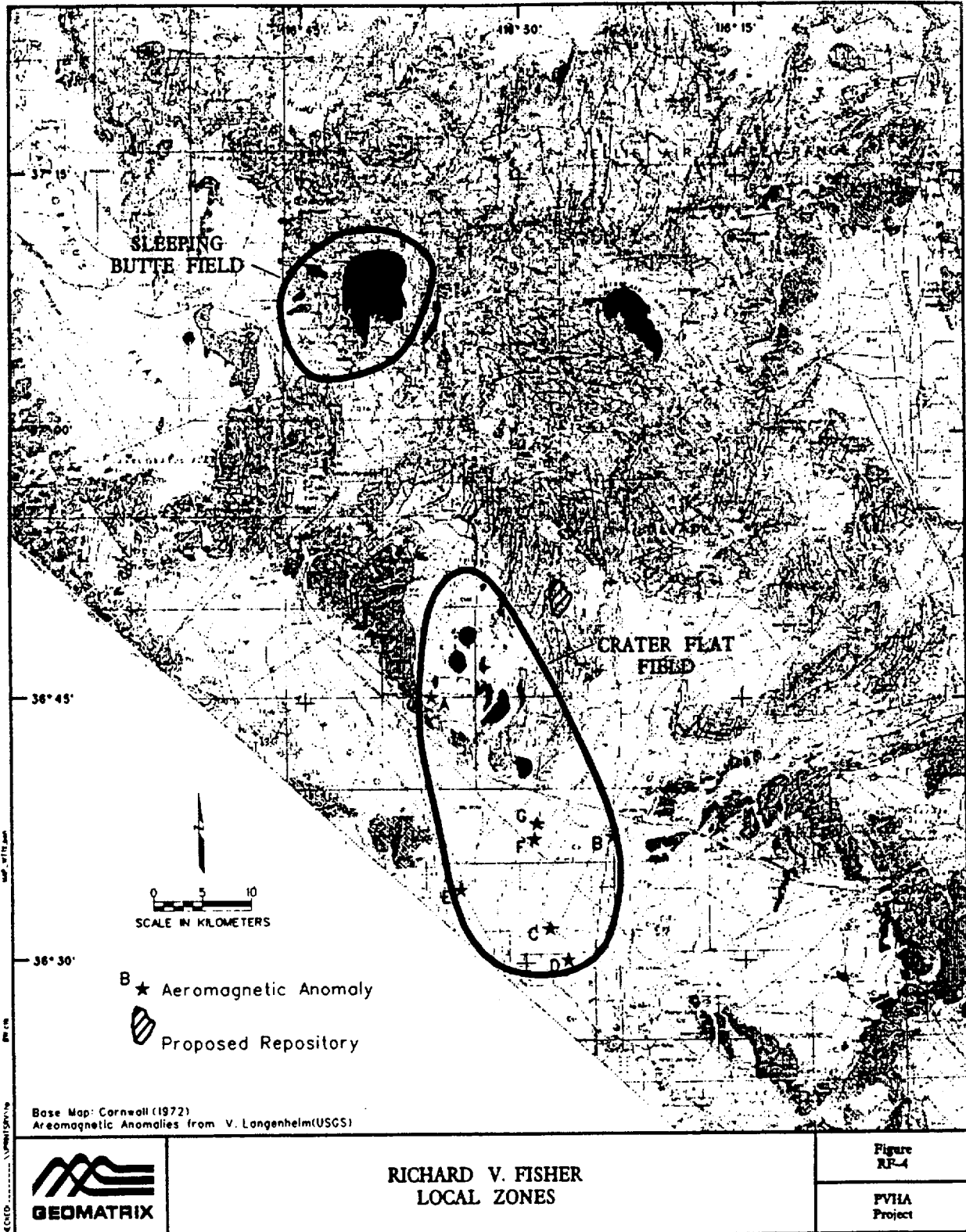
Figure RF-1 PVHA model logic tree developed by Richard V. Fisher.



H:\p\y\yucca\qgn\pvha\ludsmith\rf_02.dgn Rev. 03-28-96



H:\proj\yucca\dgn\pvha\ludsmith\rl_03.dgn Rev. 04-01-96



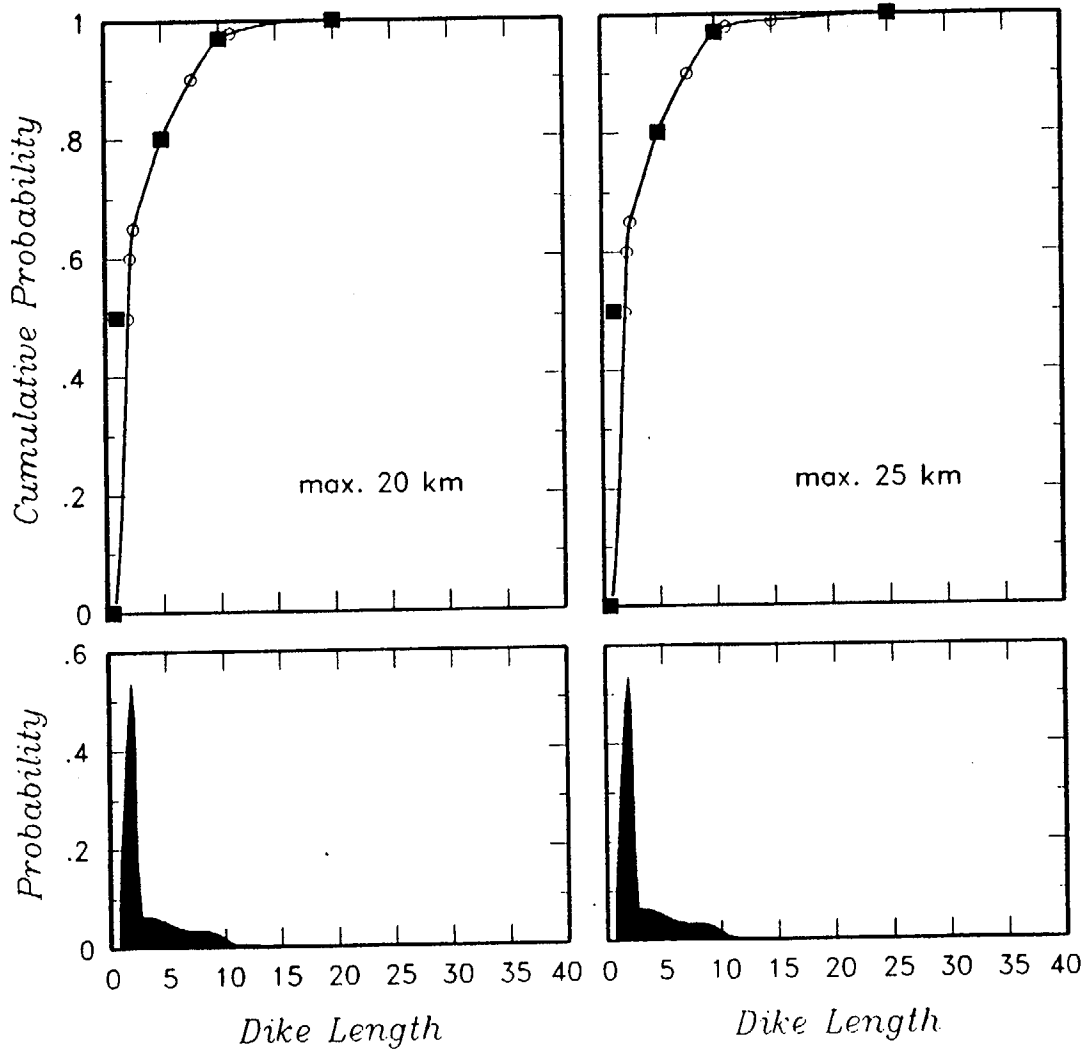


Figure RF-5 Dike length distribution developed by Richard V. Fisher.

WILLIAM R. HACKETT
ELICITATION INTERVIEW FOR PVHA PROJECT

VOLCANIC/TECTONIC SETTING

The Yucca Mountain region (YMR) is the area within a radius of about 100 km centered on the proposed repository site. The YMR lies within the southern Great Basin, on the boundary between the Basin and Range Province, where regional extension is accommodated by a combination of normal faulting and dike intrusion, and the Walker Lane belt, which is characterized by strike-slip movement. The presence of diffuse partial melt at upper-mantle depths beneath the YMR, as may be inferred from geophysical data, does not help to quantify a probabilistic volcanic hazard analysis (PVHA) because this observation may generally apply across the Basin and Range Province. Of greater importance to the PVHA is geologic and geophysical evidence for patterns of past volcanism in the YMR, including vent locations and the nature of volcano clustering, the chronology of volcanism, and the extent to which ascending magma is influenced by the YMR stress field or upper-crustal geologic features.

In the YMR, a key distinction exists between the earlier Miocene, caldera-related eruptions, which were characterized by explosive silicic volcanism, as opposed to post-caldera basaltic volcanism younger than about 10 Ma. Locations of post-caldera basaltic volcanoes have been influenced by regional extension and the development of north-trending, fault-bounded structural depressions. This contrasts with the more localized calderas and other volcanic structures that developed during the earlier period of silicic volcanism.

The probability of a return to silicic volcanism is extremely low. More than 10 my have elapsed since the last silicic volcanism, and this hiatus is substantially longer than the less-than-five-million-year lifetime of typical silicic-caldera volcanic systems worldwide. Large-scale ascent of basaltic magma into the crust would probably be necessary to induce crustal melting and future silicic volcanism. Such a change to silicic volcanism in the YMR is not geologically imminent for several reasons. The small volumes of basalt erupted during the past 10 my suggest a correspondingly small supply of basaltic magma into the crust. In addition, there is no contemporary geophysical evidence, such as anomalous heat flow or hydrothermal activity, to suggest the presence of silicic magma at depth. During the past 8-10 my, silicic volcanism has migrated outside the YMR, to the western margin of the Great Basin.

The Amargosa Valley Isotopic Province (AVIP; G. Yogodzinski presentation at PVHA Workshop 3) encompasses the YMR and is an area in which basaltic volcanoes younger than about 10 Ma have distinctive neodymium-isotopic compositions, suggesting generation of magma from a common source of old lithospheric mantle. The similarity of the isotopic composition of basaltic magma erupted within the AVIP, as distinguished from the surrounding region, allows us to focus our investigation from the entire southern Great Basin to a more local region with common magma properties and with greater significance to the PVHA.

Volcanic fields elsewhere in the Great Basin also offer insights on volcanic processes and event magnitude, but are relatively unimportant for evaluating event frequency in the YMR. As an example, the writer has extensive knowledge of Snake River Plain volcanism. This region is a good analog for understanding basaltic volcanism, dike intrusion, and associated structural disruption, but is not a close analog in terms of volcano clustering, event frequency (recurrence rate), or age of basaltic volcanism in the YMR.

The most probable sites of future volcanism in the YMR should be those areas where young volcanoes have erupted in the past. Thus, the spatial and temporal distribution of past volcanoes in the YMR is the basis for quantifying the probability of future volcanic disruption at the proposed repository.

EVENT DEFINITION

Temporal Aspects

An event is defined as a cogenetic set of intrusives and extrusives that are products of a single magma batch. An event occurs within the geologically brief time it takes to inject magma into the crust and to solidify—decades to hundreds of years. Lithostratigraphic data and isotope geochronology are the principal tools available to determine the age and frequency of volcanism, and usually there is considerable uncertainty.

Spatial Aspects

The spatial dimensions of an event are best constrained by the length of a basaltic dike that has ascended to a kilometer or less beneath the earth's surface. This length is taken to be approximately 2 km, but multiple dikes may have an aggregate length exceeding 10 km, and the maximum length of a dike is estimated to be on the order of 30-40 km (see discussion of Event Geometry below).

Geochemical Affinity

Because the intrusives and extrusives associated with an event are cogenetic, this implies that they result from a single magma batch. However, recent geochemical data from the YMR and other regions suggest that individual magma batches may not be compositionally uniform. Geochemical data are therefore best interpreted in light of lithostratigraphic and geochronologic data, using an integrated approach.

Note: The elements of the PVHA model are summarized in the form of a logic tree in Figure WH-1.

REGION OF INTEREST

The region of interest is an area of detailed analysis that has been chosen to include volcanic centers that are significant to the PVHA in light of the temporal and physical aspects of volcanism in the YMR. The region of interest also defines a background zone of regional volcanism.

The region of interest includes Yucca Mountain, together with major portions of the adjacent structural blocks. Its area is approximately that of a circle with a 40-km radius about the repository site, and 40 km is also about equal to the maximum basaltic-dike length used in this assessment (Figure WH-2).

The region of interest includes the area of most recent volcanism (AMRV; Smith et al., 1990), but expanded to the north and east to include the volcanic centers at Pahute Mesa, Paiute Ridge, and Nye Canyon. The region of interest is thus the northern part of the AVIP. The southern AVIP is not included because of its distance from the repository and because of the predominantly pre-Quaternary age of volcanism (Luedke and Smith, 1984).

As discussed below, the region of interest is called the "10 Ma zone" because it encloses events with ages less than approximately 10 Ma. Volcanic centers younger than about 10 Ma have the greatest significance to the PVHA because this is the period of post-caldera basaltic volcanism that has continued into the Quaternary and is therefore most likely to represent future volcanism. In addition, the writer believes that the 10-11 Ma basalt within the Solitario Canyon fault must be included in the PVHA due to its proximity to the repository site. Internal consistency therefore requires that all other basalts younger than about 10 Ma also must be considered within the region of interest.

SPATIAL MODELS

Homogeneous Source Zones

Two basic approaches are taken to assess the future spatial distribution of volcanic events. The first approach is a "zonation" of the region into several source zones representing different time periods that may have different rates. It is assumed that the probabilistic distribution of events within each zone is uniform in space. Three alternative representations of homogeneous source zones in the region of interest are made. In the first, the region of interest (defined above) is identified and called the 10 Ma zone because it encloses post-10 Ma centers (Figure WH-2). In this zonation, there is no subdivision of the 10 Ma zone. In the second homogeneous source zone, a region is identified—called the 5 Ma zone—that encloses the post-5 Ma centers and is identical to the AMRV of Smith et al. (1990) (Figure WH-3). The 10 Ma zone is also included as a background zone. In the third homogeneous source zone, a smaller region is identified—termed the 1 Ma zone—that encloses the post-1 Ma volcanics in Crater Flat, Lathrop Wells, and Sleeping Butte (Figure WH-4). The 1 Ma zone also follows the northwesterly trend of the Walker Lane. Again, in this zonation the 10 Ma zone serves as the background zone.

Thus, the three alternative source zones are linked to the ages of the volcanic centers in the region of interest. The relative weights assigned to the zones reflect the degree to which the time periods provide useful information about the future spatial distribution of volcanism. The weights assigned are:

1 Ma zone	(0.6)
5 Ma zone	(0.3)
10 Ma zone	(0.1)

The post-1 Ma time period is most important because of its recent geologic age and the proximity of young volcanic centers to the proposed repository. The post-5 Ma time period is also significant because it includes most of the post-caldera basalts of the YMR, and because it is not too old to reflect geologically recent changes in the tectonic regime. The post-10 Ma time period, while it provides a background zone for the other more local zones, probably captures events that are too old to be representative of contemporary or future processes.

Spatial Smoothing

The fact that volcanoes are clustered in the region of interest (Connor and Hill, 1995) is a strong indication that future volcanism will occur in the vicinity of past volcanoes. A second approach therefore assesses the spatial probability of volcanism by using a kernel method that treats volcanism as a point process within a defined spatial and temporal bandwidth. Connor and Hill (1995) use an Epanechnikov kernel as the smoothing operator, but this gives zero probability of

a new volcano forming beyond the smoothing distance "h" from all mapped volcanoes. To allow a finite probability of a new volcano beyond the selected smoothing distances "h" (discussed below), an equivalent Gaussian kernel is used here instead, with the further implication that the Gaussian smoothing distances "h" will be a factor of 2.5 times smaller than equivalent Epanechnikov "h" values (Silverman, 1986).

To assist reviewers in comparing with the results of Connor and Hill (1995), if an Epanechnikov kernel were used here as the smoothing operator, the three smoothing distances and corresponding weights would be: 8 km (0.5), 16 km (0.4), and 24 km (0.1). These distances span the range of possible vent clusters that are observed in the region of interest. The equivalent Gaussian smoothing distances used here are 3.2 km (0.5), 6.4 km (0.4), and 9.6 km (0.1).

The relative weights given to the two approaches for modeling the spatial occurrence of volcanism are: zonation approach (0.4) and spatial smoothing approach (0.6). The spatial smoothing approach is preferred because it takes full advantage of observed volcano locations in the YMR. The fact that volcanoes are clustered in the region of interest is a strong indication that future volcanism will occur in the vicinity of past volcanoes. The selected smoothing distances and weights are chosen to reflect the scales of volcano clustering in the region of interest, specifically based on Figure 2 of Connor and Hill (1995). Greatest weight is assigned to the 8-km smoothing distance because this is the scale at which the Crater Flat and other Quaternary volcanoes of the region of interest are spatially clustered. Greater smoothing distances of 16 and 24 km also are included in the analysis to capture the distances at which volcano clusters begin to group in the YMR. The spatial smoothing approach produces a nonuniform spatial probability distribution with "soft" boundaries. It differs from the homogeneous source zone approach, which assumes a homogenous distribution of past and future events within its source zones, each of which has a "hard" boundary.

EVENT COUNTS

Based on the definition of volcanic "events" given earlier, the number of events—and their uncertainties—are assessed for each of the centers in the region of interest. The number of events is assessed for the past 1, 5, and 10 my, which is the basis for identifying the three different source zones. For the post-1 Ma period, event counts are made for northern Crater Flat, Lathrop Wells, and Sleeping Butte. For the post-5 Ma period, these counts are supplemented with counts from the 3.7 Ma vents of Crater Flat, Amargosa Valley, Buckboard Mesa, and Thirsty Mesa. For the post-10 Ma period, additional counts are made at Rocket Wash, Pahute Mesa, Paiute Ridge, Nye Canyon, Yucca Flat, and Solitario Canyon. Event counts are summarized on Table WH-1.

In all cases, the potential for undetected events is evaluated at each site and is included in the maximum estimate of counts at each location. At young volcanic centers, older events may be undetected as a result of coverage by the younger deposits. At older (Pliocene and Miocene) volcanic centers, events may be undetected as a result of removal by erosion or coverage by surficial deposits. Another type of undetected event is dike intrusion without an accompanying volcanic eruption. The geologic record of volcanism in the region of interest is considered to be a close approximation to the dike-intrusion record. Basaltic magma that has ascended to less than 1 km of the surface will have a high probability of erupting because magma pressure and volatile expansion will generally overcome the low tensile strength of fractured, near-surface country rocks. However, there exists *a priori* a finite probability that some dikes might not erupt. Undetected events are added to the event counts in specific areas.

Lathrop Wells

One to 5 events (including 1 undetected event) are interpreted, with 3 events and 1 event having the highest probabilities. The 1-event interpretation requires a monogenetic cone, consistent with the paleomagnetic data of Champion (1991). The preferred scenario of 3 events is based on geomorphic data cited by S. Wells and L. McFadden (presentations at PVHA Lathrop Wells field trip). Available age dates have major uncertainties, and the best evidence for multiple events is provided by the geomorphic and soils data. The 4-event scenario would include all 4 chronostratigraphic units of Crowe et al. (1995), and the 5-event scenario includes an undetected event.

The following event counts and their relative weights are assigned for the Lathrop Wells center: 1 (0.4), 2 (0.1), 3 (0.4), 4 (0.05), and 5 (0.05).

Sleeping Butte

One to 3 events are interpreted in the Sleeping Butte area, with 2 events most likely. In the 1-event interpretation, Little Black Peak and Hidden Cone are assumed to represent a single event; in the 2-event interpretation, they are assumed to be separate events. The 3-event interpretation allows for 2 events at Hidden Cone, which was suggested by preliminary geomorphic and paleomagnetic data discussed on the PVHA field trip. Three events also allows for the possibility of an undetected event.

The event counts and their relative weights for the Sleeping Butte area are: 1 (0.4), 2 (0.5), and 3 (0.1).

1.0 Ma Crater Flat

One to 6 events (including 1 undetected event) are assessed, with 3 events most likely. In the interpretation that is best supported by the data, Red and Black cones are combined to form 1 event (based on their similar geochemistry), with the additional 2 events represented by Makani Cone and Little Cones. The 1-event interpretation is not given much weight because of the long dimensions for the event (12 km, which would imply a dike set or very long dike), and the different geochemistry of Little Cones from Red Cone and Black Cone. In the 2-event interpretation, the Little Cones represent 1 event (based on their different geochemistry) and Makani, Red, and Black cones are considered 1 event. In the 4- and 5-event interpretations, the 2 Little Cones are considered either 1 event or 2 events, respectively. The 6-event interpretation includes an undetected event.

The following event counts and their relative weights are assigned for northern Crater Flat: 1 (0.1), 2 (0.3), 3 (0.4), 4 (0.1), 5 (0.05), and 6 (0.05).

Buckboard Mesa

The Buckboard Mesa geologic observations (Crowe et al., 1995) indicate a fissure system and 2 vents. The preferred interpretation is that these features represent a single event, but they could have resulted from 2 events.

The number of events and their associated weights are: 1 (0.8), and 2 (0.2).

3.7 Ma Crater Flat

Geologic field observations (Crowe et al., 1995; author's independent observations) of the 3.7 Ma basalts of Crater Flat allow 1 to 8 events (including 2 hidden), with 3 the preferred interpretation. Numerous dikes and scoriaceous outcrops are located in the area, and the centers are eroded, faulted, and dissected, leading to uncertainties in the number of events. Geologic data in Crowe et al. (1995, p. 3-71) provide evidence for 6 events; an additional 2 undetected events may be present. The highest weight is placed on 3 events based on the distribution of vent areas.

The event counts and their relative weights for the 3.7 Ma area are: 1 (0.05), 2 (0.1), 3 (0.3), 4 (0.2), 5 (0.2), 6 (0.1), 7 (0.025), and 8 (0.025).

Amargosa Valley

The aeromagnetic anomalies in Amargosa Valley (V. Langenheim presentation at PVHA Workshop 1) represent a minimum of one event and a maximum of 7, with a most likely number of 3. A direct assessment of the probability that each anomaly represents a volcanic event is:

anomaly A=0.1, B=1.0, C=0.8, D=0.8, E=0.2, F=0.2, and G=0.2. This assessment takes into account the available geologic data (e.g., anomaly B has been drilled and age-dated, anomaly D has been drilled but not dated; the depth of anomalies B, C, and D is known or inferred to be about 200 m below a sequence of Quaternary alluvial deposits).

From this assessment, the following cumulative distribution of the number of events is assessed at: 1 (1.0), 2 (0.8), 3 (0.64), 4 (0.13), 5 (0.03), 6 (0.005), and 7 (0.0005).

Thirsty Mesa

One to 3 events are interpreted, with a preferred estimate of 1 event. The geologic relationships (Crowe et al., 1995) suggest that this is a monogenetic shield volcano that resulted from numerous outpourings over decades, but all are genetically related.

The event counts and their relative weights for the Thirsty Mesa area are: 1 (0.7), 2 (0.2), and 3 (0.1).

Nye Canyon

Geologic field descriptions of the available exposures (Crowe et al., 1995) suggest a minimum of 1 event and a maximum of 6 events (including an undetected event). The preferred interpretation of 4 events is based on the observation that the unit consists of four separate volcanic centers.

The event counts and their relative weights for the Nye Canyon area are: 1 (0.05), 2 (0.1), 3 (0.2), 4 (0.5), 5 (0.1), and 6 (0.05).

Rocket Wash

The Rocket Wash exposure, although highly eroded, appears to have a single vent area (Crowe et al., 1995) and is interpreted to have formed from a single event. The possibility of an undetected event is also allowed in the 2-event scenario.

The event counts and their relative weights for the Rocket Wash are: 1 (0.8), and 2 (0.2).

Yucca Flat

Basalt was identified in a drillhole (Crowe et al., 1995), and the preferred interpretation is that it represents a single lava flow. The preferred count is therefore 1, and, allowing for an undetected event, 2 events are considered.

The event counts and their relative weights for the Yucca Flat area are: 1 (0.9), and 2 (0.1).

Paiute Ridge

The geologic relationships at Paiute Ridge (Crowe et al., 1995) allow interpretations ranging from a minimum of 1 event to a maximum of 6 events (including an undetected event). The preferred count of 2 events, is based on strong paleomagnetic evidence for basalts exposed along Paiute Ridge to be cogenetic (1 event), with the basaltic dike of Scarp Canyon representing a second event.

The event counts and their relative weights for the Paiute Ridge area are: 1 (0.05), 2 (0.4), 3 (0.3), 4 (0.1), 5 (0.1), and 6 (0.05).

Pahute Mesa

Geologic field descriptions from the Pahute Mesa area (Crowe et al., 1995) allow interpretations ranging from a minimum of 1 event to a maximum of 4 events. The preferred count is 2 because of the petrographic contrast of the central group of units, versus two other petrographically similar units to the east and west. If all 3 groups are separate events, the count is 3; the 4-event scenario allows for an undetected event.

The event counts and their relative weights for the Pahute Mesa area are: 1 (0.1), 2 (0.6), 3 (0.2), and 4 (0.1).

Solitario Canyon

A basaltic dike apparently intruded and was subsequently brecciated along the Solitario Canyon fault (Crowe et al., 1995; author's independent observations). Although geochronologic data suggest this basalt may have an age of 11 Ma, it is included with the other post-10 Ma volcanoes because of its proximity to the proposed repository.

The event count for the Solitario Canyon fault area is 1.

RATES OF OCCURRENCE

Using the event counts discussed above, the rates of occurrence are established for use in the PVHA. These rates are calculated over various time periods and for particular source zones (see summary in Table WH-2).

Three alternative time periods are considered for estimating the future rate of occurrence of volcanic events:

Post-1 Ma (0.6)
Post-5 Ma (0.3)
Post-10 Ma (0.1)

Each time period is, in turn, related to particular zones (shown in Figure WH-2 and discussed previously under Spatial Models).

For the post-1 Ma time period, the rate for the 1 Ma zone is derived from the counts at northern Crater Flat, Lathrop Wells, and Sleeping Butte. The background zone rate comes from an equally weighted average of the counts from the entire post-10 Ma period, the period from 10 Ma to 1 Ma, and the period from 10 Ma to 5 Ma.

For the post-5 Ma period, the rate for the 5 Ma zone is derived from the counts at northern Crater Flat, Lathrop Wells, Sleeping Butte, the 3.7 Ma area of Crater Flat, Thirsty Mesa, Buckboard Mesa, and Amargosa Valley. The rate for the background zone is derived in the same way as for the post-1 Ma period.

For the post-10 Ma period, the rate for the 10 Ma zone is derived from the counts at all of the areas used for the post-5 Ma period, plus Rocket Wash, Pahute Mesa, Paiute Ridge, Nye Canyon, Yucca Flat, and Solitario Canyon. The 10 Ma zone is identical to the background zone for this time period.

Undetected Events

Undetected events are included in the event counts at each individual location in the estimate of the maximum number of events.

TEMPORAL MODELS

A homogenous Poisson model is used because the available data satisfy this model, and such a model has the important attribute of simplicity.

The different time frames used in establishing each homogenous source zone (10-, 5-, and 1-Ma zones) have been adopted and weighted in an effort to capture uncertainty about the time period that best represents temporally homogenous (and representative) magmatic events and what these events might imply for the future. The post-10 Ma period captures postcaldera volcanism in the region of interest; permits incorporation of the 10-11 Ma Solitario Canyon basalt near the repository; provides a background zone for the other, more localized zones; and is assigned the lowest weight because the long time frame is believed to be least representative of future

volcanism. The post-5 Ma period does not mark a change of volcanic pattern within the region of interest, but is selected to provide an intermediate time frame for calculating a Pliocene-and-younger volcanic rate; it is given an intermediate weight. The post-1 Ma volcanoes occur in the Crater Flat volcanic field near the proposed repository, and this time period is therefore heavily weighted. Any time-dependent differences in volcanic rates are believed to be captured in the analysis by adopting these three time periods and assigning relative weights to them.

EVENT GEOMETRY AND MAGNITUDE

When an event is defined by two or more features (e.g., cones), the center of mass of the features considering their volumes is used as the point location of the event. These points have been assessed for several centers by the author.

Event dimensions are constrained by the length of a dike or a set of dikes related to a single magmatic event. The following distribution of event lengths is used:

<1 km	(0.2)
1-2 km	(0.3)
2-5 km	(0.3)
5-10 km	(0.1)
10-15 km	(0.05)
>15 km	(0.05)

Dike (event) length is an important parameter in this PVHA because the distribution of dike lengths strongly influences the probability of magma to intrude beyond its volcanic-source zones. The small magma volumes erupted at individual basaltic centers and the low magma-generation rate in the region of interest (Crowe et al., 1995) suggest that feeder dikes are small, and the observed outcrop lengths of exposed dikes and aligned vents in the region of interest indicate that dike lengths are most commonly less than 5 km. The 12-km length of the 1 Ma Crater Flat cones, if fed by a single dike, gives a maximum observed length for an event in the region of interest, but dikes can intrude farther than the aligned vents they produce. A maximum length for dikes in the region of interest is difficult to establish with certainty, but might be on the order of twice the observed maximum length. A value of 30 ± 10 km is adopted here; such a dike would be capable of intruding several structural blocks in the YMR, but might erupt only in topographically low, alluvial valleys. The weights assessed for the maximum dike lengths are 20 km (0.3), 30 km (0.4), and 40 km (0.3), reflecting the large uncertainty and no strong preference for any of the three values. Events are more likely to be centered on the dikes, and a triangular distribution is used to model event location.

Note: At the request of Dr. Hackett, a smooth interpolation function was fit to his discrete cumulative density estimates for dike length. The resulting cumulative distributions and density functions are shown on Figure WH-5.

Dike orientation is an important parameter in this PVHA because potential intersection of the proposed repository by a dike is dependent on dike trajectory as well as length. Abundant empirical, theoretical, and numerical treatments of the dike-intrusion process have shown that dike orientation is strongly controlled by a regional stress field (Parsons and Thompson, 1991). Dikes intrude parallel to sigma-2 and perpendicular to sigma-3. Stock et al. (1985) provide the only published measurements of the in situ stress state at Yucca Mountain. At depths of 1 to 1.3 km, their measurements indicate that sigma-2 is approximately N25E. The orientation of future dikes in the region of interest is therefore taken as N25E±30 degrees, where N25E is the median value of a Gaussian distribution with a two-sigma range of 60 degrees. Twenty degrees of the 30-degree total uncertainty is due to uncertainty in the measurement of in situ stress, and the remaining 10 degrees is due to uncertainty in the dike following a path perpendicular to sigma-3.

The average width of a dike is on the order of 1 m, with a range of 0.5 to 2 m, based on outcrop observations in the YMR and analog regions. The zone of magma-induced faulting and fissuring above a dike is expected to be less than 0.5 km in width (Mastin and Pollard, 1988). The point location for an event is taken to be the center of a dike trace; i.e., dikes are as likely to propagate southwest as northeast. Other geologic controls may operate, such as the easier propagation of dikes through low-density, low-strength alluvium (beneath Crater Flat), relative to welded tuffs and carbonate rocks (comprising Yucca Mountain). This factor was considered, but deemed insignificant, specifically as a discrete boundary condition that would inhibit northeastward dike propagation beyond the eastern boundary of the Quaternary Crater Flat volcanic field. The thickness of alluvium beneath Crater Flat is generally less than a few hundred meters, whereas dikes are fanlike bodies that penetrate several kilometers to tens of kilometers of the crust. Thin alluvial deposits of eastern Crater Flat are therefore considered incapable of significantly influencing the propagation of dikes in the shallow subsurface. That is, the major bedrock units (welded tuffs) through which shallow dikes must propagate are the dominant geologic materials beneath Crater Flat as well as Yucca Mountain. No special condition is warranted to inhibit northeastward dike propagation from future Crater Flat volcanoes toward the proposed repository.

Because the proposed repository is several hundred meters higher in elevation than Crater Flat, buoyancy considerations would argue that future basaltic dikes from Crater Flat might not intersect the repository. However, it should be noted that the zone of magma-induced normal

faulting, tensile fissuring, and gas emission will extend upward from the dike top, and may intersect the repository.

Event "magnitude" is indicated by the area of structural disruption, or the zone of tensile disruption of rocks above an ascending dike. Cogenetic volcanic materials are also most likely to be emplaced within this zone. For this analysis, the most likely dimensions of a future magmatic event are a shallow dike length of 2 km and a zone of structural disruption of about 0.5 km, resulting in a 1 km² area of disruption, with or without accompanying volcanism.

HYDROMAGMATIC ACTIVITY

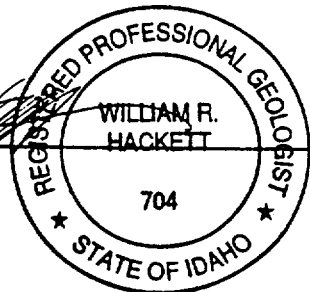
In order to have a significant hydromagmatic explosion, the water table needs to be within about 100 m of the surface for steam pressure to overcome the lithostatic pressure, and porous rocks must be present to allow flux of external water to the magma-water interface (Fisher and Schmincke, 1984). This type of explosion is rarely seen in the YMR and is therefore considered to be extremely unlikely in the site area, given the groundwater conditions.

There is some evidence of small-volume hydrovolcanism at two localities: Lathrop Wells and Nye Canyon (Crowe et al., 1995). Given 2 examples out of about 30 total events, the probability of this type of hydrovolcanism is 2 in 30, or 0.067.

TYPES OF ERUPTION

The types of volcanic features that could occur in the region of interest in the future, based on the record of volcanism during the past 10 my, are monogenetic basaltic features (Crowe et al., 1995): (1) a group of cogenetic scoria cones and small-volume lava flows (<0.1 km³) from a common dike-fed fissure eruption (e.g., Buckboard Mesa); (2) a smaller, single scoria cone and small-volume lava flow that covers only a few km² (e.g., Red Cone and Black Cone); (3) a hydrovolcanic tuff cone or mixed Strombolian/hydrovolcanic tuff cone (explosive volcanism is not a characteristic of the region of interest; however, there is some evidence of hydrovolcanism at Nye Canyon and Lathrop Wells); and (4) a small shield volcano formed by many small-volume lava flows (e.g., Thirsty Mesa). The probability that a future volcanic event will be one of these monogenetic types is: group of scoria cones and lava flows (0.60, or 18 of about 30 total events in the region of interest), single scoria cone (0.30, or 9 of 30 events), hydrovolcanic tuff cone (0.067, or 2 of 30 events), and small shield (0.033, or 1 of 30 events).

A polygenetic tephra cone with a small lava flow, similar to the polygenetic model proposed by Crowe et al. (1995) for the Lathrop Wells volcano, has a probability of less than or equal to 0.033 (less than or equal to 1 in 30 total events). Another type of volcanic event that could occur is a silicic Plinian eruption. This would require a large volume of a type of magma that has been unavailable within the region of interest during about the past 8-10 my. Miocene silicic calderas to the north of the repository show no geologic or geophysical evidence (such as ongoing hydrothermal activity) to suggest that they may be reactivated to produce future silicic Plinian eruptions. Given that there have been no silicic eruptions in the region of interest during the past 8 my, the probability of a return to silicic volcanism is about 1 in 8 million, or 1.2×10^{-7} per year. Silicic volcanism has not only ceased in the region of interest during the past 8-10 my, but has also migrated beyond the region of interest to the western edge of the southern Great Basin (e.g., the Quaternary silicic volcanism of the Coso field, Long Valley caldera, and Mono-Inyo craters). This regional spatial-temporal pattern suggests that the probability estimate of a return to silicic volcanism in the region of interest can be decreased by several orders of magnitude, perhaps to less than 10^{-9} per year.

April 9, 1996

REFERENCES

- Champion, D.E., 1991, Volcanic episodes near Yucca Mountain as determined by paleomagnetic studies at Lathrop Wells, Crater Flat, and Sleeping Butte, Nevada: Proceedings, High-Level Radioactive Waste Management, American Nuclear Society, v. 1, p. 61-67.
- Connor, C.B., and Hill, B.E., 1995, Three nonhomogeneous Poisson models for the probability of basaltic volcanism: application to the Yucca Mountain region, Nevada, USA: Journal of Geophysical Research, v. 100, no. B6, p. 10,107-10,125.
- Crowe, B.M., Perry, F.V., Geissman, J., McFadden, L., Wells, S., Murrell, M., Poths, J., Valentine, G.A., Bowker, L., and Finnegan, K., 1995, Status of volcanism studies for the Yucca Mountain site characterization projects: Los Alamos National Laboratory Report LA-12908-MS, March 1995.
- Fisher, R.V., and Schmincke, H.U., 1984, Pyroclastic rocks: Springer-Verlag, Berlin, 472 p.
- Luedke, R.G., and Smith, R.L., 1984, Map showing distribution, composition and age of late Cenozoic volcanic centers in the western conterminous United States: U.S. Geological Survey Miscellaneous Investigation Series Map I-1523.
- Mastin, L.G., and Pollard, D.D., 1988, Surface deformation and shallow dike intrusion process at Inyo Craters, California: Journal of Geophysics Research, v. 93, p. 13,221-13,235.
- Parsons, T., and Thompson, G.A., 1991, The role of overpressure in suppressing earthquakes and topography: worldwide examples: Science, v. 253, p. 1399-1402.
- Silverman, B.W., 1986, Density estimation for statistics and data analysis: Chapman & Hall, London, 175 p.
- Smith, E.I., Feuerbach, D.L., Nauman, T.R., and Faulds, J.E., 1990, The area of most recent volcanism near Yucca Mountain, Nevada: implications for volcanic risk assessment: Proceedings, High-Level Radioactive Waste Management, v. 1, p. 81-90.
- Stock, J.M., Healy, J.H., Hickman, S.H., and Zoback, M.D., 1985, Hydraulic fracturing stress measurements at Yucca Mountain, Nevada, and relationships to regional stress field: Journal of Geophysical Research, v. 90, no. B10, p. 8691-8706.

**TABLE WH-1
 WILLIAM R. HACKETT - EVENT COUNTS**

LOCATION	COUNTS (CONES)	WEIGHT	NOTES
Lathrop Wells	1	(0.4)	AM: Aeromagnetic anomalies of V. Langenheim, USGS BC: Black Cone HC: Hidden Cone 2HC: 2 events at Hidden Cone LBP: Little Black Peak LC: Little Cone 2LC: 2 separate Little Cones M: Makani Cone RC: Red Cone u: undetected events
	2	(0.1)	
	3	(0.4)	
	4	(0.05)	
	5 (u)	(0.05)	
Sleeping Butte	1 (LBP+HC)	(0.4)	
	2 (LBP, HC)	(0.5)	
	3 (LBP, 2HC)	(0.1)	
1.0 Ma Crater Flat	1 (all)	(0.1)	
	2 (LC, RC+BC+M)	(0.3)	
	3 (LC, RC+BC, M)	(0.4)	
	4 (LC, RC, BC, M)	(0.1)	
	5 (2LC, RC, BC, M)	(0.05)	
	6 (u, 2LC, RC, BC, M)	(0.05)	
Buckboard Mesa	1	(0.8)	
	2	(0.2)	
3.7 Ma Crater Flat	1	(0.05)	
	2	(0.1)	
	3	(0.3)	
	4	(0.2)	
	5	(0.2)	
	6	(0.1)	
	7 (u)	(0.025)	
	8 (2u)	(0.025)	
Amargosa Valley	1 (B)	(0.0184)	
	2 (B+C) or (B+D)	0.0817 (0.0816)	
	3 (B+C+D) or (B+C+G) or (B+D+E)	(0.2949) (0.0660) (0.0660)	
	4 (B+C+D+E) or (B+C+D+G)	(0.1473) (0.1473)	
	5 (B+C+D+B+G)	(0.0853)	
	6 (B+C+D+B+F+G)	(0.0110)	
	7 (A-G)	(0.0005)	
Thirsty Mesa	1	(0.7)	
	2 (u)	(0.2)	
	3 (2u)	(0.1)	
Rocket Wash	1	(0.8)	
	2 (u)	(0.2)	

TABLE WH-1 (Cont'd)
WILLIAM R. HACKETT - EVENT COUNTS

LOCATION	COUNTS (CONES)	WEIGHT	NOTES
Pahute Mesa	1	(0.1)	
	2	(0.6)	
	3	(0.2)	
	4 (u)	(0.1)	
Paiute Ridge	1	(0.05)	
	2	(0.4)	
	3	(0.3)	
	4	(0.1)	
	5	(0.1)	
	6 (u)	(0.05)	
Nye Canyon	1	(0.05)	
	2	(0.1)	
	3	(0.2)	
	4	(0.5)	
	5	(0.1)	
	6 (u)	(0.05)	
Yucca Flat	1	(0.9)	
	2 (u)	(0.1)	
Solitario Canyon	1	(1.0)	

**TABLE WH-2
 WILLIAM R. HACKETT - RATES OF OCCURRENCE**

TIME PERIOD	COUNT METHOD FOR ZONES	NOTES
Post 1 Ma (0.6)	- 1 Ma Zone: (NCF+LW+SB) - Background (10 Ma Zone): Post 10 Ma rate (0.33) (3.7+TM+BM+RW+PR+PM+NC+YF+SC) 10 - 1 Ma rate (0.33) (3.7+TM+BM+RW+PR+PM+NC+YF+SC) 10 - 5 Ma rate (0.33) (RW+PR+PM+NC+YF+SC)	AV: Amargosa Valley BM: Buckboard Mesa LW: Lathrop Wells NC: Nye Canyon NCF: Northern Crater Flat PM: Pahute Mesa PR: Paiute Ridge RW: Rocket Wash SB: Sleeping Butte SC: Solitario Canyon TM: Thirsty Mesa YF: Yucca Flat 3.7: 3.7 Ma Crater Flat
Post 5 Ma (0.3)	- 5 Ma Zone: (NCF+LW+SB+TM+BM+AV) - Background (10 Ma Zone): Post 10 Ma rate (0.33) (PR+PM+NC+YF+ 3.7) 10 - 1 Ma rate (0.33) (PR+PM+NC+YF+3.7) 10 - 5 Ma rate (0.33) (PR+PM+NC+YF)	
Post 10 Ma (0.1)	- 10 Ma Zone: (NCF+LW+SB+TM+BM+AV +RW+PM+PR+NC+YF+SC+ 3.7)	

Temporal Models	Time Period	Region Of Interest	Spatial Models	Sources
-----------------	-------------	--------------------	----------------	---------

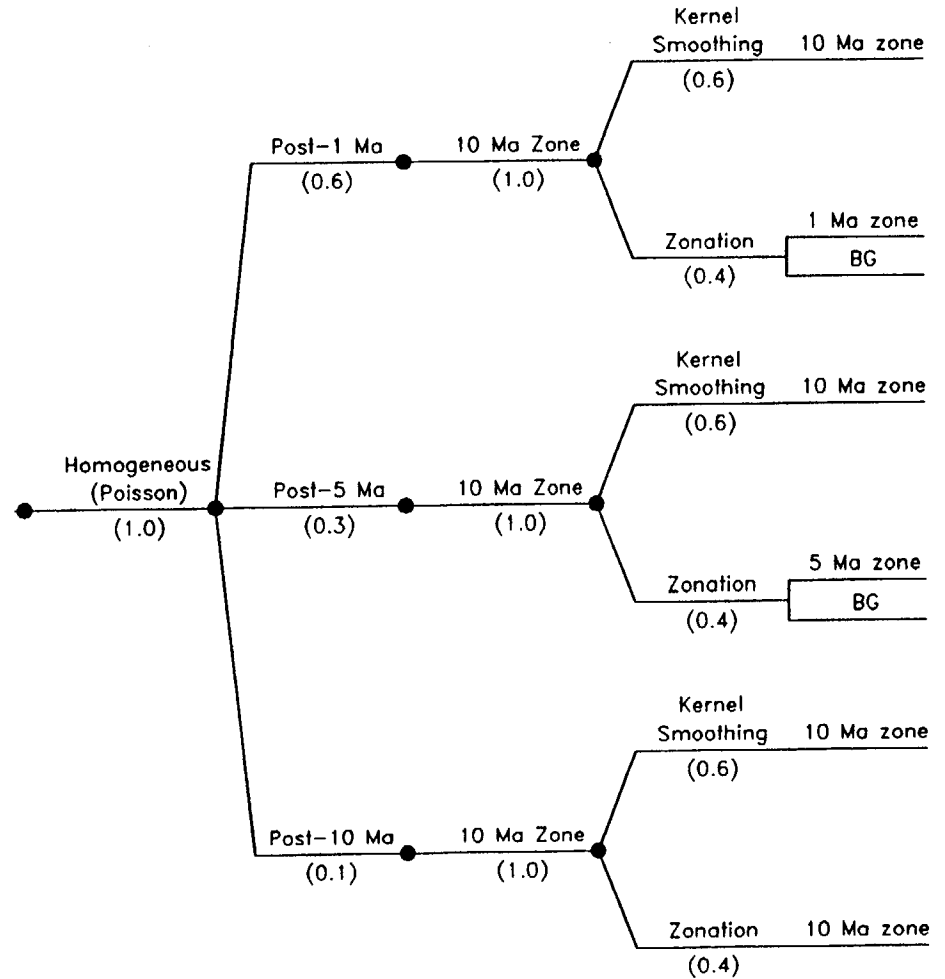
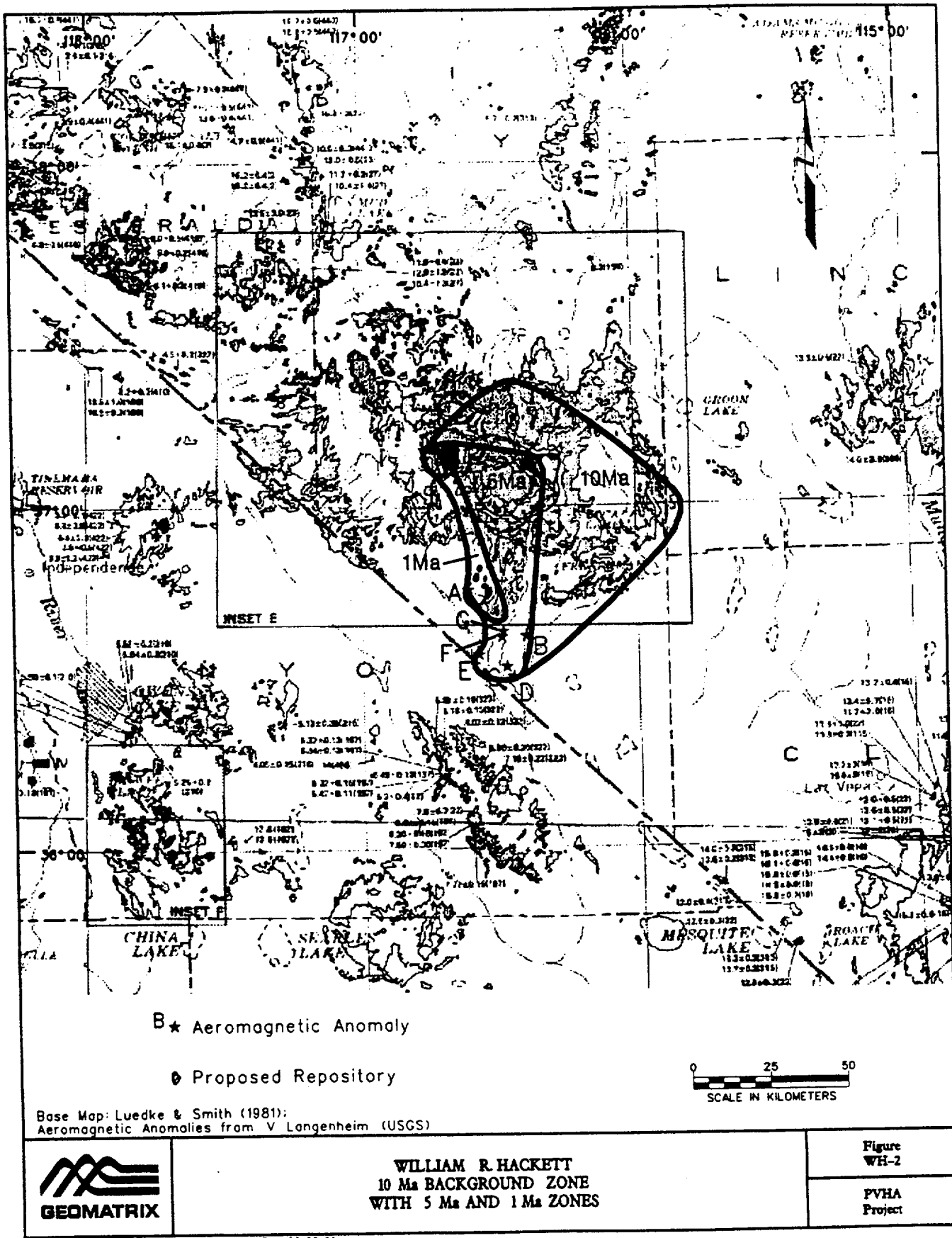
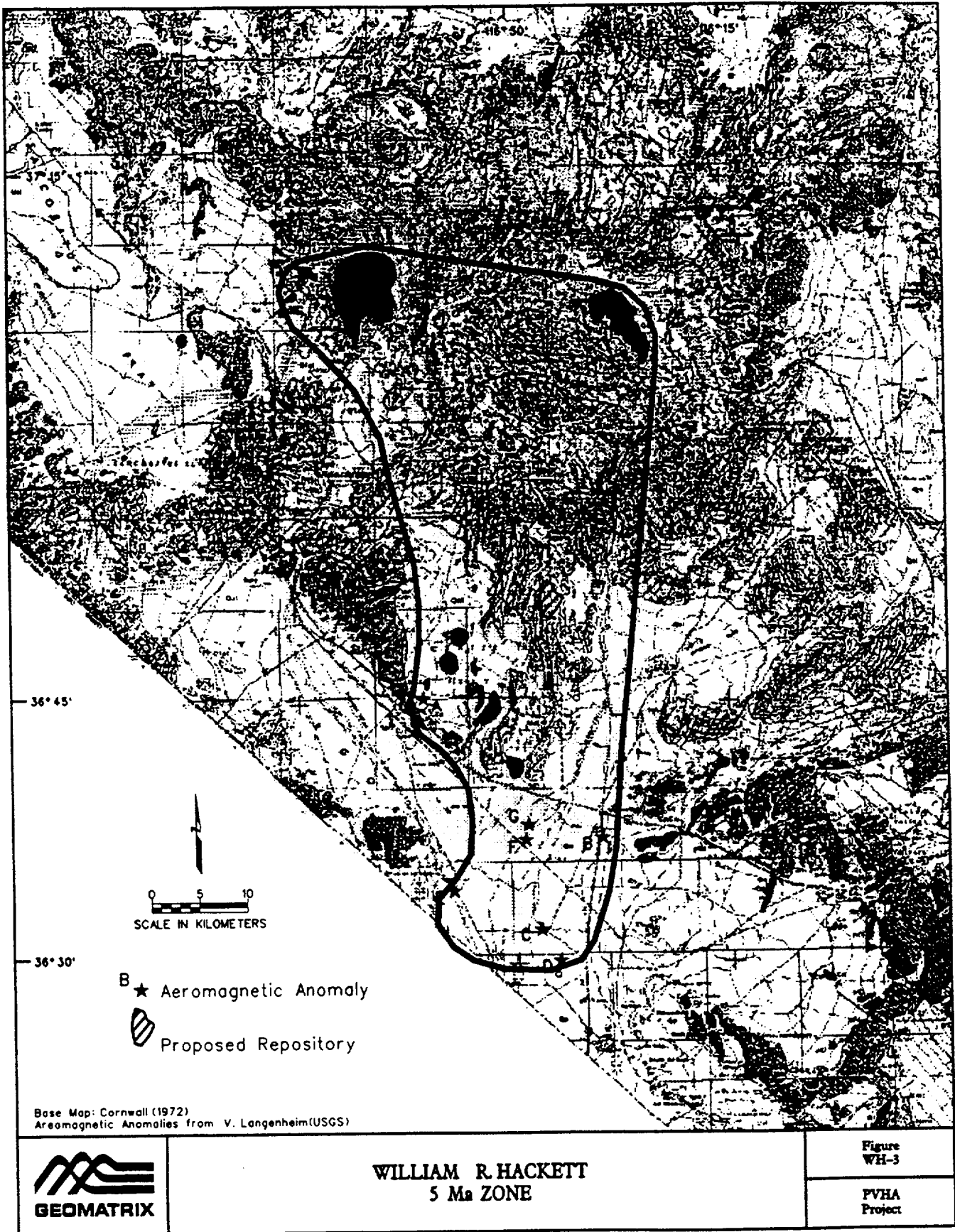
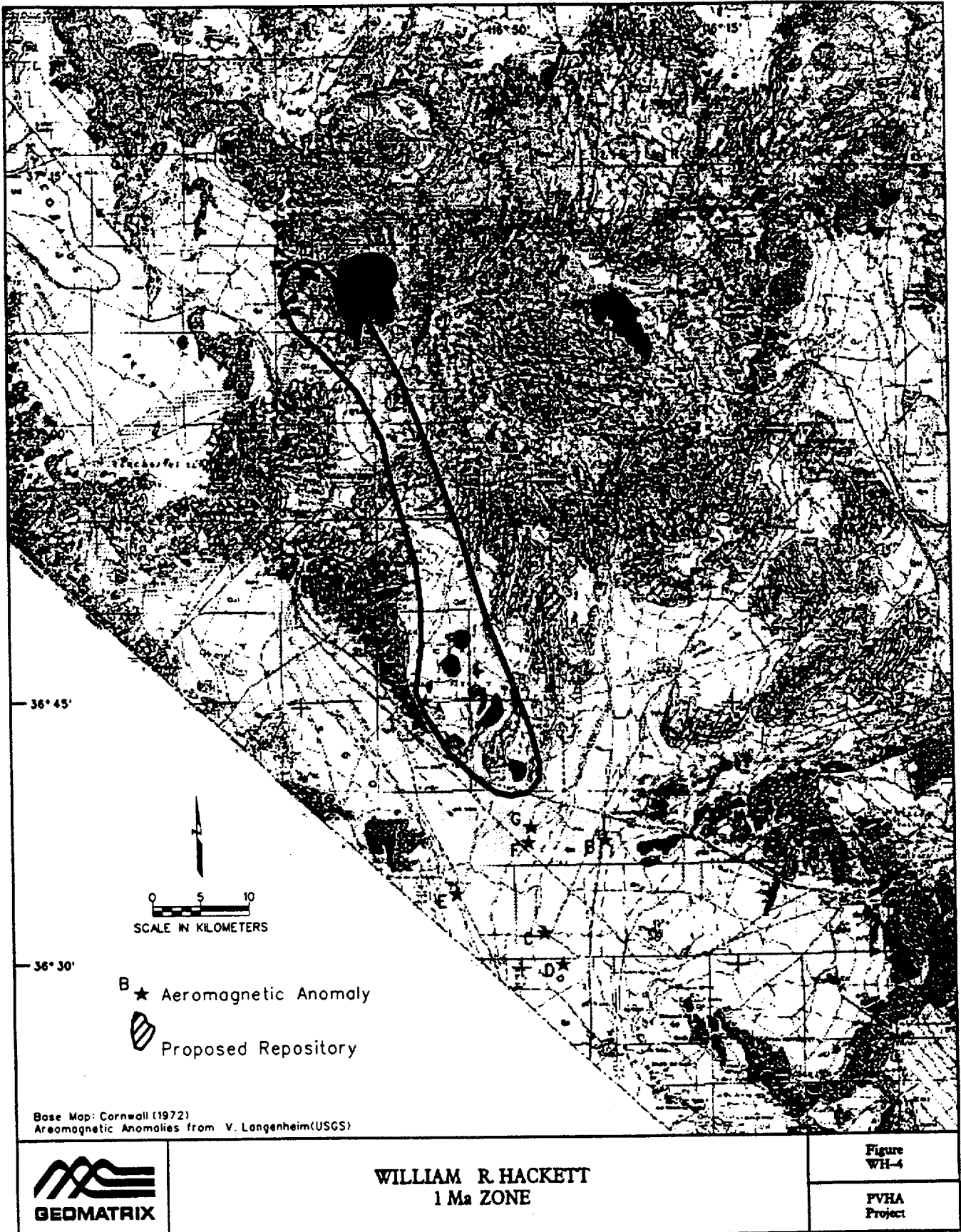


Figure WH-1 PVHA model logic tree developed by William R. Hackett.







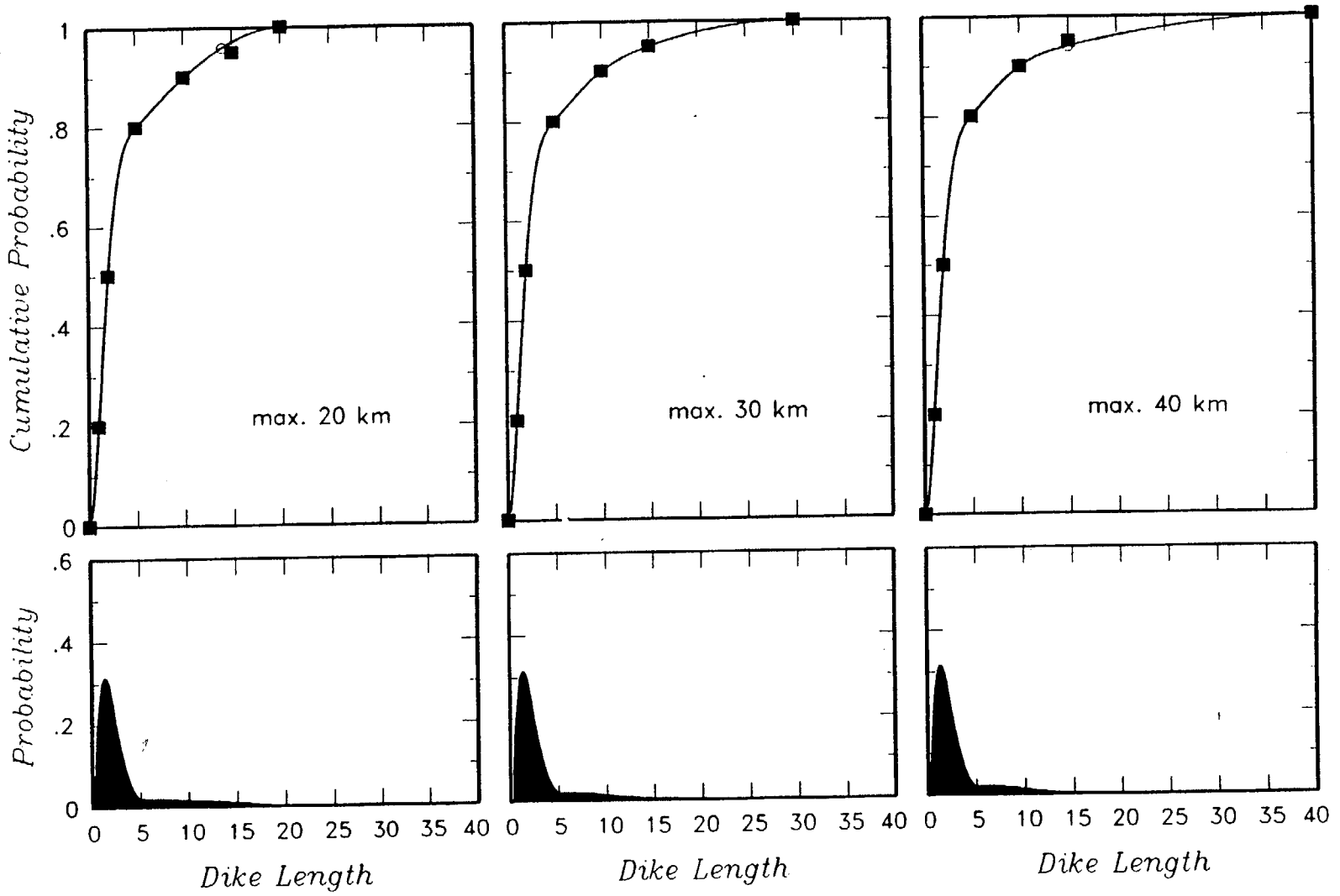


Figure WH-5 Dike length distribution developed by William R. Hackett.

MEL A. KUNTZ
ELICITATION INTERVIEW FOR PVHA PROJECT

VOLCANIC/TECTONIC SETTING

Regional Perspective and Factors Related to Magma Production

The term Yucca Mountain region (YMR) is used herein in a general sense to refer to the area within a radius of 100 km from the proposed high-level nuclear waste repository at Yucca Mountain. The YMR lies near the boundary of the Basin and Range Province, characterized by east-west extension, and the Sierra Nevada belt, characterized mostly by north-south translational movement. The Walker Lane structural belt is the accommodation zone between these provinces, and the YMR lies near the northeastern border of the Walker Lane, but within the Basin and Range Province. Rates of extension were high in the YMR region prior to 10 Ma, but in the post-10 Ma period, extension rates have decreased significantly. Large-volume rhyolitic volcanism has continued over the past several million years in areas of maximum extension at the periphery of the Basin and Range, such as at Long Valley, the Coso Range, and Yellowstone, where a mantle plume may also play a role. In these areas, high rates of extension in the lithosphere may lead to decompression melting in the upper asthenosphere, resulting in large volumes of basaltic magma that produce extensive lithospheric melting and production of large volumes of rhyolitic magma, resulting in classic bimodal volcanism. There has been a change in the style of volcanism in the YMR concurrent with the change in extension rate. Large-volume caldera eruptions, characteristic of the earlier, rapid-extension period, have ceased and have been replaced by small-volume basaltic eruptions over the past 10 my that are widely dispersed in both time and space ¹(Typical sources: Crowe et al., 1995; presentations by B. Crowe, J. Stewart, and G. Thompson at PVHA Workshop 3).

The geothermal gradient in the YMR, when projected to the Moho, suggests that the upper asthenosphere is close to its incipient melting temperature (G. Thompson presentation at PVHA Workshop 4). Mechanisms suggested for tipping the balance in favor of localized melting to produce basaltic magma include injection of hot mantle (a plume); lowering of confining pressure,

1

An immense amount of data and ideas were reviewed for this study, and judgments made for this elicitation were formulated from these sources. Specific references are given whenever possible, otherwise general references for ideas that have been formulated from many sources are given at the end of the paragraph where that type of idea is presented.

perhaps causing decompression melting; or lowering the melting point of the melting region by adding water (R. Carlson presentation at PVHA Workshop 4). Whether these mechanisms are related to regional tectonics or are essentially haphazard is not known. The low volumes of recent basaltic eruptions and the lack of recent rhyolitic volcanism may be due largely to the fact that both the upper asthenosphere and the entire lithosphere in the YMR region have been drained of their low-temperature, partial-melting fractions by previous melting events, resulting in an asthenosphere and a lithosphere that are essentially non-fertile with respect to future melting events. Geophysical data suggest that there is no extensive basaltic magma body beneath the YMR, which implies that basaltic magma production is local and episodic in much of the interior of the Basin and Range (Crowe et al., 1995).

The isotopic studies of G. Yogodzinski (presentation at PVHA Workshop 3) show that basalts in the YMR are part of a regional geochemical province termed the Amargosa Valley Isotopic Province (AVIP), which is the surface expression of a unique mantle region that has been isolated from convecting mantle for about 1 billion years and has not been affected by Basin and Range extension (R. Carlson presentation at PVHA Workshop 4). The significance of the AVIP for my elicitation is that it helps to define the region of interest or background zone for the purpose of evaluating the volcanic hazard for the repository site. As pointed out by G. Walker (presentation at PVHA Workshop 4), the relatively narrow, roughly north-south-oriented distribution of basaltic volcanic vents within the AVIP may represent the plan shape of the zone of mantle melting, which may be roughly akin to a N-S-oriented dike at depth.

Local Perspective and Factors Related to Magma Delivery to the Surface

The relationships between magma generation and magma delivery to the surface involve a complex set of conditions including, but not confined to, extension rate, magma volume, magma supply rate, deep and shallow structural control of dikes by regional stress orientations, presence or absence of favorably oriented near-surface structures, and the integrated density contrast over the entire column of lithosphere and upper asthenosphere above the site of magma generation and below the potential site of eruption. The interrelationships between these processes are poorly understood. A general feeling emerged among some, if not most, members of the expert panel that magma delivery to the surface in the YMR is probably controlled at depth by a roughly north-south-oriented structure, perhaps a deep transverse (?) fault. On the other hand, the orientation of this structure may simply reflect the north-south orientation of the melting anomaly represented by the AVIP, and deep structural control may be lacking or not very influential. It seems clear that near-surface structures affect the orientation of feeder dikes and cinder cones in the Crater Flat volcanic field (CFVF). For example, the alignment of cones in northern Crater Flat appears to be

related to a northeast-trending structure. The ring-fracture zone of the Timber Mountain caldera probably provided conduits to the surface that localized eruptions and ponded basalt flows for the Thirsty Mesa and Buckboard Mesa basalts. In summary, magma may have followed N-S or NNW-SSE-oriented structures at depth, but was largely controlled by NE-trending structures that are parallel to the regional direction of maximum horizontal compressional stress or by local, caldera-related structures in the near surface. (Typical sources: Crowe et al., 1995; presentations by J. Stewart, G. Thompson, G. Walker, J. Faulds, and C. Fridrich at PVHA workshops and field trips).

In several presentations to the expert panel at PVHA workshops, G. Thompson stressed that regional extension in the YMR can be expressed in two ways; normal faulting and/or dike injection. It appears that normal faulting has been the major (only?) process within the Yucca Mountain block in the past 5 my and that faulting and dike injection (volcanism) have both operated within the Crater Flat region within the same time period. Unfortunately, models that adequately explain why one process dominated the other in the two respective areas are not available. If such an explanation were available, it might help to explain why there appears to be such a sharp boundary at the eastern edge of the CFVF, just west of the proposed repository site. It is clear to the author that the eastern boundary of the CFVF is sharp in terms of distribution of volcanic vents; basaltic eruptions have not occurred beyond this boundary eastward into Yucca Mountain in Pleistocene and Pliocene time. Recent field studies of the Yucca Mountain-Crater Flat area by C. Fridrich (in press), and newly acquired seismic reflection data for the same area interpreted for the expert panel by G. Thompson (presentation at PVHA Workshop 4) indicate that the boundary is not a significant structural break such as a major fault. Rather, "the faults that cut Yucca Mountain and that have facilitated extension are minor, and the magnitude of extension is small to moderate; no major bounding faults that define the mountain structurally are known to exist; therefore, Yucca Mountain is not a discrete tectonic block, or at least has not functioned as one in post-Paleocene time" (O'Leary and Weissenberg, in press). Fridrich (in press) states that "Yucca Mountain is an arcuate, multiple-fault-block ridge that wraps around the north, east, and south flanks of the Crater Flat alluvial basin. This ridge and the flat that it nearly encloses are structurally inseparable; together, they constitute a single domain in terms of their structural style and tectonic history, and they are distinct in these features from adjacent areas." Thus, factors that govern the eastern boundary of the CFVF appear not to be of a structural nature, and they remain largely unexplained and unknown at this time. Uncertainty about the character of the boundary is reflected in and incorporated in my hazard analysis models. (Typical sources: Fridrich, in press; O'Leary and Weissenberg, in press; Ferrill et al., 1995; and presentations by G. Thompson, C. Fridrich, and G. Walker at PVHA workshops and field trips.)

A factor that may be important in localizing volcanism within Crater Flat, but not in Yucca Mountain, involves subtle differences in the integrated density contrast over the entire column of lithosphere and upper asthenosphere above a site of magma generation and below a potential site of eruption and its effect on magma-driving pressures. This factor may be related to the general observation (there are obvious exceptions) that volcanic vents in the YMR generally occur in low topographic areas (e.g., Crater Flat, Amargosa Valley) and that high topographic areas (e.g., Yucca Mountain, Bare Mountain) have fewer or no vents. An explanation for this relationship may lie in the fact that an extra few hundred meters of low-density rocks in the higher topographic areas may provide a density barrier to emplacement of basalt dikes. I suggested that subtle density differences in the upper crust affected magma-driving pressures and produced areas of no eruptions in an otherwise widespread region of volcanic vents in the eastern Snake River Plain, Idaho (Kuntz, 1992). There are insufficient density data available for the Crater Flat-Yucca Mountain region to make basic calculations to evaluate this factor as it relates to volcanic hazard for the repository site. However, this factor may be important in localizing basaltic vents in Crater Flat with respect to Yucca Mountain.

EVENT DEFINITION

Temporal Aspects

A *volcanic event* in the context of the basaltic volcanism expected in the YMR is defined as a set of eruptive and noneruptive fissures and associated cones and flows that form during a single dike episode. An event may consist of a dike set, such as an echelon dikes, and multiple separate vents. Based on my knowledge of the timing of volcanism in Hawaii and the eastern Snake River Plain, I view a volcanic event as occurring within a few months to no more than a few years or, possibly, a few tens of years. The crystallization time of an ascending dike in the crust is the principal control on the time frame; dikes a few meters thick and 1 to 10 km long cannot remain fluid for long periods (months or years) in the middle to shallow crust in the YMR.

Spatial Aspects

A volcanic event may have different features (e.g., eruptive fissures, cones, flows) because of the range of processes that operate. These features are generally close to one another (typically 1-10 km) and generally aligned, which helps group the features into a single event. Typically, the maximum distance between eruptive features in a single event is a few kilometers, with maximum distances of perhaps 15 km (the 12-km end-to-end distance of vents in northern Crater Flat is close to the largest distance imaginable). Once an event has occurred, it is not expected that another

event would recur in the same exact location, because stress has been released and the dike system has cooled and sealed.

Geochemical Affinity

The significance of geochemical differences in distinguishing between events is unclear. The Lathrop Wells cone is the best-studied cone in the world from a geochemical perspective. It is not known whether the subtle geochemical differences associated with this cone are significant because there are no similar studies elsewhere that can be used to determine the chemical variability or "noise" level in single eruptive episodes. A geochemical perspective is needed from multiple geochemical analyses in analog areas, particularly historical examples, where it is known with certainty that the deposits occurred within a single event. Because of these uncertainties, I do not use geochemical affinities or differences to define volcanic events.

Note: The elements of the PVHA model are summarized in the form of a logic tree in Figure MK-1.

REGION OF INTEREST

As stated by R.V. Fisher (presentation at PVHA Workshop 4), choosing a region of interest or background zone provides a regional assessment of occurrence rate of basaltic volcanoes in a tectonic province that is of immediate significance for the repository site. The principal factors that I used to identify the region of interest are age of volcanic deposits and the isotopic composition of the flows. The age range chosen (Quaternary and Pliocene, 0-5 Ma) encompasses tectonic and structural regimes that governed the basaltic volcanism in the YMR; those factors are not likely to change in the next 10,000 to 100,000 years, the time-frame for the hazard analysis. The second factor is defined by the AVIP, which contains Quaternary and Pliocene volcanic fields near the repository and provides information regarding the magma source region and recurrence rates.

The AVIP region extends from the Buckboard Mesa-Sleeping Butte on the north, through the volcanoes that constitute the Crater Flat field, and south to include the Amargosa Valley aeromagnetic anomalies. I exclude the Death Valley region from my background zone because of large uncertainties in data relating to the age and number of volcanic events in that region. Additional factors favoring exclusion are that much of the basaltic volcanism of the southern Death Valley region is older than 5 Ma and Death Valley is affected by a tectonic regime that is

different than the regime affecting the YMR. (Sources: G. Yogodzinski presentation at PVHA Workshop 3, and B. Crowe informal PVHA memo)

The background zone is subdivided into 5 zones assessed to have different recurrence rates for future volcanism (Figure MK-2). Zone A is coincident with the background zone. The boundaries of Zone A were selected to include Bare Mountain on the west, Thirsty Mountain and Buckboard Mesa on the north, and the Amargosa Valley aeromagnetic anomalies on the south. The boundaries essentially follow those given by G. Yogodzinski for the northern two-thirds of the AVIP. Zones B and C are coincident with the northern and southern sections, respectively, of the Crater Flat volcanic zone (CFVZ) identified by Crowe and Perry (1989). Zone D contains a block of relatively deep basement rock brought up along and to the west of the Bare Mountain fault. Zone E contains the Yucca Mountain structural block, and Zone F contains the Timber Mountain caldera.

SPATIAL MODELS

Four alternative models are used to assess the future locations of volcanic activity in the YMR:

- (1) **Uniform Zone:** In this model, the future distribution of volcanic events is assumed to have a uniform probability of occurrence anywhere within Zone A. The model consists of post-5 Ma volcanoes that have a geochemical affinity suggestive of the same asthenospheric source (i.e., within AVIP).
- (2) **Zonation:** In this model, volcanism within Zone A is not randomly distributed; rather, the volcanism is confined to certain areas within the zone. I believe there are geologically reasonable explanations for the clustering of some of the post-5 Ma vents within the background zone and for the lack of vents within other parts of the background zone, as described above in the section on local perspective and factors related to magma delivery to the surface. For that reason, I subdivide the background zone into subzones B to F that have different vent distributions and, therefore, different likelihoods for future eruptions. Within each zone, there is an assumed uniform probability of occurrence. Zone C has the highest frequency of young volcanoes in the area of interest, and Zone B has the next highest frequency. Zone D does not contain evidence of Quaternary faulting nor post-Miocene volcanism. Zone E contains the Yucca Mountain structural block, which is highly faulted but contains no young volcanic features. The boundary between Zone C and Zone E separates 2 areas with very distinct differences in the rate of volcanic occurrence. Low-density rhyolite outflow facies on the edge of the Timber Mountain caldera within Zone E may have

created a density barrier to post-11.5 my basaltic eruptions. Zone F includes the Timber Mountain caldera and the 2.8 Ma Buckboard Mesa basalts.

- (3) **Spatial Smoothing:** Observed locations of volcanic events in Zone C (the Crater Flat-Amargosa Valley area) are smoothed using a smoothing operator, following the general approach suggested by Connor and Hill (1995). The smoothing kernel is Gaussian in order to avoid the sharp edges of the Epanechnikov kernel and the associated sharp truncations in the probability surface. Smoothing is done only for those events within Zone C because there are no observed events within adjacent zones, and the events in the northern and southern parts of the background zone do not contribute to the hazard at the site. In order to reflect my uncertainty in the nature and location of the boundary between subzones C and E (which contains the proposed repository site), I assumed that the boundary contains, alternatively, 90 or 95 percent of the probability density, with the remaining probability allowed to occur in the regions outside of Zone C. The weightings for these two options are 0.6 and 0.4, respectively. This reflects my judgment that future volcanic events have a high likelihood of occurring within Zone C and not in adjacent regions.
- (4) **Field Shape:** Following the method of Sheridan (1992), the observed locations of volcanic events within Zone C are assumed to represent realizations of a parametric shape for a volcanic field. A bivariate Gaussian shape is assumed and the distribution of observed vents is used to define the orientation of axes, aspect ratio, and absolute dimensions.

The relative weights assigned to the four alternative spatial models are: uniform zone (0.2), zonation (0.35), spatial smoothing (0.3), and field shape (0.15).

An important aspect in dealing with the four alternative spatial models is that they should reflect my uncertainty in the nature and location of the boundary between subzones C and E. My uncertainty regarding the boundary is dealt with in two ways. First, I have given higher weights to those models that better account for a diffuse boundary (uniform background model, spatial smoothing, and field shape) and lower weight to the subzone model that emphasizes hard boundaries. Second, within the subzone model, I have chosen to make the western boundary hard to reflect the fact that I believe the Bare Mountain fault is a sharp limit to the distribution of vents in the Crater Flat volcanic field, i.e., I believe that vents will not occur to the west of that boundary and dikes located within the field will not extend beyond that boundary. The eastern edge of the Crater Flat source zone, however, is not considered to be an absolute boundary to the events occurring within the zone. The rate density decays linearly from the rate within the zone to the background rate over a distance L . The value of L ranges from 0 (an absolute boundary) to 5 km.

There are very few geologic indicators that one can use to select L. I have chosen to base L on the eastern edge of the Crater Flat basin as determined by seismic and gravity evidence (V. Langenheim presentation at PVHA Workshop 1; G. Thompson presentation at PVHA Workshop 4). The eastern edge of the basin lies about 5 km east of the eastern topographic (hard) boundary of Crater Flat, thus the maximum value of L is 5 km. I judge that L values of 0 and 5 are equally likely.

EVENT COUNTS

Based on the definition of a volcanic event given above, the number of events and their uncertainties are assessed for each of the centers in the YMR. Sources of information used for these assessments included many presentations made at PVHA workshops and field trips (particularly those by B. Crowe, S. Minor, R. Fleck, and D. Champion) as well as my own interpretations of map and field data. Event counts are summarized in Table MK-1.

Lathrop Wells

The Lathrop Wells center represents 1 to 4 events, with 1 event most likely. The volcanic units are in close spatial proximity and, given the considerable uncertainty in dates, all could be related to a single event that occurred over a few years at about 125 ka. The scatter in available age dates is a function of the various analytical techniques, and if a perfect technique were developed, units Q1, Q2, and Q3 (after Crowe et al., 1995) could yield the same age. More weight is given to the paleomagnetic data of D. Champion and J. Geissman (presentations at PVHA Workshop 3) than to the other techniques, and the paleomagnetic data do not suggest more than 2 events. In the 2-event interpretation, based mainly on paleomagnetic data, units Q1 and Q2 are combined to represent 1 event and Q3 represents a separate event. In the 3-event interpretation, Q1, Q2, and Q3 are considered to be separate events. There is no evidence of an ash blanket associated with Q4, and this unit is considered unlikely to represent a separate eruptive event; Q4 is considered a separate event only in the 4-event scenario.

The following event counts and their relative weights are assigned for the Lathrop Wells center: 1 (0.95), 2 (0.03), 3 (0.019), and 4 (0.001).

Sleeping Butte

The geologic relationships in the Sleeping Butte area suggest 1 to 3 events, with 2 events most likely. Hidden Cone (HC) and Little Black Peak (LBP) have similar ages, but paleomagnetic data suggest they represent 2 separate events with a close spatial relationship. A possible separate

event is postulated for an older flow associated with Hidden Cone (OHC). This postulated basalt forms an arm that extends to the NW from the main cone and has been dated by R. Fleck at 0.37 ± 0.042 Ma (handout with sample locality 913-8B, PVHA Sleeping Butte field trip). Four scenarios are considered, as follows: 1 event—LBP and HC are 1 event; 2 events—LBP and HC are 1 event and OHC is 1 event (interpretation 2a) or OHC is not an event and LBP and HC form separate events (interpretation 2b); 3 events—OHC, HC, and LBP each form separate events.

The event counts and their relative weights for the Sleeping Butte area are: 1 (0.6), 2 (0.3), and 3 (0.1).

1.0 Ma Crater Flat

The 1.0 Ma basalts represent 1 to 4 events. One event is judged most likely on the basis of the available dates, including paleomagnetic data, the close spatial relationship of the cones, and the cones' orientation. In this interpretation, the cones would likely be related to a dike set, rather than a single dike, because the 12-km length is probably too long to be a single dike. Red and Black cones represent a single event in the 3-event interpretation, and Red, Black, and Little Cones are considered 1 event (based on their spatial relationship) in the 2-event interpretation. The maximum number of events is 4, because the 2 cones exposed at Little Cones are considered to be related to the same event.

The following event counts and their relative weights are assigned for northern Crater Flat: 1 (0.6), 2 (0.3), 3 (0.05), and 4 (0.05).

Buckboard Mesa

The basalts of Buckboard Mesa are interpreted to be associated with a single eruptive event. There is a single vent feature, and the basalts appear to be ponded in the moat zone of the caldera complex. The location of the deposits is likely related to the ring fracture zone, where a significant amount of collapse has occurred, thus providing ready access of basaltic magmas to the surface and a depression for ponding of flows.

Event counts and probabilities are as follows: 1 (0.95), 2 (0.05).

3.7 Ma Crater Flat

The 3.7 Ma basalts represent 1 to 6 events, with 1 event most likely. The single-event interpretation is preferred because of the proximity of the vent areas (within 4-5 km), similarities in age estimates, and similarities in flow types (i.e., low-density, fissure eruptions). Larger

numbers of events are considered possible based on considering each of the vent features interpreted by Crowe et al. (1995) to be either individual events or in various combinations.

The following event counts and their relative weights are assigned for the 3.7 Ma area of Crater Flat: 1 (0.75), 2 (0.05), 3 (0.15), 4 (0.02), 5 (0.02), and 6 (0.01).

Amargosa Valley

The designation of aeromagnetic anomalies A to G is that given by V. Langenheim (presentation at PVHA Workshop 1). Anomaly A is not easily distinguishable from the large anomaly associated with the Timber Mountain caldera complex and is not considered further here. Anomaly B has been drilled and dated; its age is 3.8-4.3 Ma and it is covered by 105 m of Quaternary alluvial deposits. Anomaly D has been drilled for a water well and lies at a depth of 183 m. Unlike anomaly B, which has reversed magnetic polarization, D has normal magnetic polarization. Anomaly C has reverse magnetic polarization and is modeled to occur at a depth of about 200 m, but has not been drilled. Based on depth of Quaternary burial where known and interpreted, available dates, and magnetic polarities, it is judged that all of the anomalies are relatively close in age and span the age range of 3 Ma to 4.3 Ma. This time period includes an older period of reversed magnetic polarity, a period of normal polarity, and a younger period of reversed magnetic polarity. In interpreting numbers of events, uncertainties in these age estimates are considered.

One to 6 events are considered based on interpretation of aeromagnetic anomalies; the 3-event interpretation is judged most likely (see Table MK-1 for the various combinations). Anomalies B, C, and D are the most likely anomalies to represent buried basalt centers, and most of the weight is given to interpretations that include them as separate events. The minimum of 1 event is based on anomaly D being older than 5 Ma and anomaly C not representing a buried basalt body. The 2-event interpretation is based on anomalies B and D representing separate events; the 3-event interpretation includes anomaly C as an event.

The following event counts and their relative weights are assigned to the Amargosa Valley area: 1 (0.02), 2 (0.1), 3 (0.6), 4 (0.15), 5 (0.1), and 6 (0.03).

Thirsty Mesa

The 4.8 Ma lava and scoria deposits comprising Thirsty Mesa appear to have occurred during a single eruptive event (some field data provided via pers. comm. with S. Minor, USGS).

The event counts and their weights are as follows: 1 (0.95), 2 (0.04) and 3 (0.01).

Rocket Wash

At Rocket Wash, a single event is interpreted with an approximate age of 8 Ma.

Solitario Canyon

A basalt dike identified in the Solitario Canyon fault represents the only known post-caldera volcanic event to have affected the Yucca Mountain block. An age of approximately 11 Ma has been reported for this dike (PVHA Background Report 3). The limited exposures suggest a single event.

RATES OF OCCURRENCE

Using the event counts discussed above, the rates of occurrence of future volcanic events are established for use in the PVHA. These rates are calculated over various time periods and for particular source zones (see summary in Table MK-2).

Three alternative time periods are considered for estimating the future rate of occurrence of volcanic events. These alternatives, and the volcanic event counts included, are as follows:

Post-2 Ma	Northern Crater Flat, Sleeping Butte, Lathrop Wells
Post-5 Ma	Post-2 Ma events plus Buckboard Mesa, 3.7 Ma Crater Flat, Amargosa Valley, Thirsty Mesa
Post-11 Ma	Post-5 Ma events plus Rocket Wash and Solitario Canyon

The weights for the alternative time periods are: Post-2 Ma (0.5), Post-5 Ma (0.45), and Post-11 Ma (0.05).

The post-2 Ma period is given the highest weight because it is a period during which tectonic processes and rates of extension similar to those expected in the future have been operative. Due to the low rates of activity and low number of volcanic events in the YMR, however, the post-2 Ma period may not include enough events to provide a realistic picture of rates. Thus, in order to increase the number of events to evaluate rates, the post-5 Ma period is given a relatively high weighting. The post-11 Ma period is least preferred because it spans a period that includes the immediate post-caldera tectonic activity, as well as the more recent tectonic regime defined by lower rates of extension. This period is included as part of the analysis because it includes the dike in the Solitario Canyon area of the Yucca Mountain block, which is the only identified basaltic volcanic event known to have affected the Yucca Mountain block.

Estimated Rates

The primary basis for estimating the rates of occurrence within Zones A through F is the event counts over the three alternative time periods. Some of the zones, however, contain no events so their rates have been estimated relative to those zones containing events. Zone A is the large regional zone and contains sufficient numbers of events to estimate rates. Zone C has the highest rates, followed by Zone B to the north. Zone F has the next highest rate, as represented by the event at Buckboard Mesa. The rate in Zone E should be very low, as indicated by a lack of events over the past 5 my and only one interpreted event (Solitario Canyon) in the past 11 my. Zone D should have the lowest rate, as no events have been recognized in the past 11 my. Further support for the relative differences between Zones B and C and Zones D, E, and F lies in the observation that B and C lie in structural basins and D, E, and F lie in uplifted structural blocks. The geologic record indicates that basaltic eruptions are more likely to occur in valleys than uplifted structural blocks.

The estimated rates for the various zones and time periods are shown in Table MK-2. In most cases these are related to the counts at locations within the zones. For example, for the post-5 Ma time period, the rate within Zone C is assessed based on the sum of the counts at northern Crater Flat, the 3.7 Ma area of Crater Flat, Lathrop Wells, and Amargosa Valley. For all time periods, the rates within Zones D and E are assessed, first, relative to each other and, second, relative to zones containing events. These assessments are consistent with the relative rates discussed previously. Note that these estimates have considerable uncertainty, which is included in the logic tree.

Undetected Events

In addition to those events identified and interpreted at the surface, there is the potential for undetected, or subsurface, events that might exist at depths below 300 m (depth of the proposed repository) but not be represented at the surface. In general, dikes ascending through the crust that extend to as shallow as 300 m would be expected to vent at the surface. At deep crustal levels, magma pressure drives the ascent of the dike. But at shallow depths (upper 1-2 km) gas exsolution is also an additional driving factor and probably ensures an eruption at the surface. If such shallow subsurface dikes exist in the YMR, they would likely have been identified, although they may not be detectable in all cases.

The following factors should be multiplied by the rates for all time periods to account for undetected events: 1.0 (0.25), 1.1 (0.5), 1.5 (0.2), and 2.0 (0.05).

TEMPORAL MODELS

Two temporal models are considered: a homogeneous model (see Connor and Hill, 1995) that assumes that the rate of occurrence of volcanic events is uniform through time; and a nonhomogeneous model that accounts for a waxing or waning of occurrence rates through time (e.g., the model described by Ho et al., 1991). These alternative models are assigned weights as follows: homogeneous (0.8) and nonhomogeneous (0.2).

For both models, start times of 2, 5, and 11 Ma (and their associated weights of 0.5, 0.45, and 0.05, respectively) are used. Because there may be too few events within any given source zone to exercise the nonhomogeneous model, the ratio of the rates using the homogeneous and nonhomogeneous models should be determined for Zone A (for the three start times), and the same ratios should be used for Zones B to F.

EVENT GEOMETRIES

When an event is defined by two or more features (e.g., cones), the mid-point of the features should be used as the point location of the event.

The length of a future individual dike would likely be 1 to 3 km; however, the length of a dike set could be more than 12 km on the basis of the 12-km dike or dike set that is postulated to link the 1 Ma eruptive centers in Crater Flat. The *cumulative* distribution of individual dike lengths and dike-set lengths has the following form:

1 km	(0.1)
3 km	(0.5)
8 km	(0.75)
10 km	(0.90)
10-18 km	(1.0)

The above specifies the distribution for dike (or dike-set) lengths in an individual eruptive episode. The value of 10 km represents a limiting dike-set length. This value is the preferred estimate for the maximum dike-set length because studies of well-exposed dike swarms emplaced at depths of about 2 km or less in Utah have shown that dike-set lengths do not exceed 10 km (Delaney and Gartner, 1995), and this value is only slightly less than the 12-km dike or dike set postulated to link the 1 Ma eruptive centers in Crater Flat. The value however is uncertain and is assessed to range from 10 to 18 km with weights of 10 (0.4), 12 (0.3) 15 (0.2) and 18 km (0.1).

Note: At the request of Dr. Kuntz, a smooth interpolation function was fit to his discrete cumulative density estimates for dike length. The resulting cumulative distributions and density functions are shown on Figure MK-3.

Dike orientations for future events are judged to have two possible orientations. The main orientation would have a central tendency at N30°E, parallel to the maximum horizontal compressional stress direction for the region, based on earthquake focal mechanisms and borehole breakouts. There is a 90% probability that the orientation lies between north-south and N60°E (i.e., N30E ±30). Based on the inferred orientation for feeder dikes at the Lathrop Wells volcanic center and for inferred dikes at several cones in the 1 Ma volcanic centers in northern Crater Flat, a second possible dike orientation is N15°W±15°. There is a 90% probability that the dike orientation lies within this range for the second orientation. The relative frequencies for the two dike orientations are as follows: N30°E (0.7), N15°W (0.3). Expected dike widths are 1 to 2 m.

In assessing the geometry of events relative to a point location for the event, the most likely location for the point is the center of the dike, with a decreasing probability that it would be at either end of the dike. The probability distribution has a semicircular shape.

HYDROMAGMATIC ACTIVITY

The likelihood of a significant, hydromagmatic explosion in the YMR is very small. There is very little evidence for hydromagmatic eruptions at the volcanic centers in the region. The evidence for basal surge deposits at Lathrop Wells is equivocal. In the repository site area, the groundwater table is about 2000 ft below the land surface. In the eastern Snake River Plain, less than 5% of volcanic vents show evidence for hydromagmatic activity. About half of the maar volcanoes in the Snake River Plain were erupted through water-bearing alluvial sediments (e.g., Menan Buttes) and the remainder were erupted through at least 600 feet of overlying basalt flows. At the proposed repository site, the water table is at a depth of about 2,000 feet below the land surface and the water table is about 600 feet below the land surface in Crater Flat. Based on the comparison between the eastern Snake River Plain and the YMR, I suggest that 2 to 4 out of every 100 volcanic events in the YMR could be expected to be associated with significant hydromagmatic activity.

TYPE OF ERUPTION

The expected type of eruption in the YMR over at least the next 10,000 years is basaltic fissure eruptions forming cinder cones. Some eruptions will approach Strombolian activity with associated significant deposits of ash. Lava flows will be thick and extend less than a few kilometers, volumes

will be low, and ash blankets could extend as far as 12 to 15 km away from the vent. Zones of deformation will likely form above an ascending dike, as described by Hackett and Smith (1994) for the eastern Snake River Plain. The chances for silicic volcanism are negligible because there is no evidence for such in the YMR in the past 11 my.

Mel A. Kuntz
5/22/96

REFERENCES

- Connor, C.B., and Hill, B.E., 1995, Three nonhomogeneous Poisson models for the probability of basaltic volcanism: application to the Yucca Mountain region, Nevada, USA: *Journal of Geophysical Research*, v. 100, no. B6, p. 10,107-10,125.
- Crowe, B.M., and Perry, F.V., 1989, Volcanic probability calculations for the Yucca Mountain site: estimation of volcanic rates: *Proceedings, Nuclear Waste Isolation in the Unstaturated Zone, Focus '89, American Nuclear Society*, p. 326-334.
- Crowe, B.M., Perry, F.V., Geissman, J., McFadden, L., Wells, S., Murrell, M., Poths, J., Valentine, G.A., Bowker, L., and Finnegan, K., 1995, Status of volcanism studies for the Yucca Mountain site characterization projects: *Los Alamos National Laboratory Report LA-12908-MS, March 1995*.
- Delaney, P.T., and Gartner, A.E., 1995, Physical processes of shallow mafic dike emplacement near the San Rafael Swell, Utah: *U.S. Geological Survey Open-File Report 95-491*, 47 p.
- Ferrill, D.A., Stirewalt, G.L., Henderson, D.B., Stamatakos, J.A., Morris, A.P., Wernicke, B.P., and Spivey, K.H., 1995, Faulting in the Yucca Mountain region: critical review and analyses of tectonic data from the central Basin and Range: prepared for the Nuclear Regulatory Commission by the Center for Nuclear Waste Regulatory Analyses, San Antonio, Texas.
- Fridrich, C.J., 1995 (in press), Characterization of detachment faults in the Yucca Mountain region, *in* Simonds, et al. (eds.): *Final report on detachment faulting*, U.S. Geological Survey Administrative Report.
- Hackett, W.R., and Smith, R.P., 1994, Volcanic hazards of the Idaho National Engineering Laboratory and adjacent areas: prepared for the U.S. Department of Energy, Idaho National Engineering Laboratory Report INEL-94/0276, December 1994.
- Ho, C.H., Smith, E.I., Feuerbach, D.L., and Naumann, T.R., 1991, Eruptive probability calculation for the Yucca Mountain site, USA: Statistical estimation of recurrence rates: *Bulletin of Volcanology*, v. 54, p. 50-56.
- Kuntz, M. A., 1992, A model-based perspective of basaltic volcanism, eastern Snake River Plain, Idaho, *in* Link, P.K., Kuntz, M.A., and Platt, L.B., (eds.), *Regional geology of eastern Idaho and western Wyoming: Geological Society of America Memoir 179*, p.289-304.
- O'Leary, D.W., and Weisenberg, C.W., 1995 (in press), Current evaluation of tectonic models for the Yucca Mountain region: U.S. Geological Survey Administrative Report. (Final report due in 1996).

Sheridan, M.F., 1992, A Monte Carlo technique to estimate the probability of volcanic dikes:
Proceedings, High-Level Radioactive Waste Management, v. 2, p. 2033-2038.

TABLE MK-1
MEL A. KUNTZ - EVENT COUNTS

LOCATION	COUNTS (CONES)	WEIGHT	NOTES
Lathrop Wells	1 (Q1-4)	(0.95)	BC: Black Cone B-G: Aeromagnetic anomalies of V. Langenheim, USGS HC: Hidden Cone 2HC: 2 events at Hidden Cone LBP: Little Black Peak LC: Little Cones M: Makani Cone Q1-4: Quaternary map units of Crowe et al. (1995) RC: Red Cone
	2 (Q1+2, 3)	(0.03)	
	3 (Q1, 2, 3)	(0.019)	
	4 (Q1, 2, 3, 4)	(0.001)	
Sleeping Butte	1 (LBP+HC)	(0.6)	
	2 (LBP, HC)	(0.3)	
	3 (LBP, 2HC)	(0.1)	
1.0 Ma Crater Flat	1 (all)	(0.6)	
	2 (LC+RC+BC, M)	(0.3)	
	3 (RC+BC, LC, M)	(0.05)	
	4 (RC, BC, LC, M)	(0.05)	
Buckboard Mesa	1	(0.95)	
	2	(0.05)	
3.7 Ma Crater Flat	1	(0.75)	
	2	(0.05)	
	3	(0.15)	
	4	(0.02)	
	5	(0.02)	
	6	(0.01)	
Amargosa Valley	1 (B)	(0.02)	
	2 (B, D)	(0.1)	
	3 (B, C, D)	(0.6)	
	4 (B, C, D, E) or (B, C, D, F+G)	(0.075) (0.075)	
	5 (B, C, D, F, G) or (B, C, D, E, F) or (B, C, D, E, G)	(0.033) (0.034) (0.033)	
	6 (B, C, D, E, F, G)	(0.03)	
Thirsty Mesa	1	(0.95)	
	2	(0.04)	
	3	(0.01)	
Rocket Wash	1 event	(1.0)	
Solitario Canyon	1	(1.0)	

TABLE MK-2
MEL A. KUNTZ - RATES OF OCCURRENCE

TIME PERIOD	COUNT METHOD FOR ZONES	NOTES
Post 2 Ma (0.5)	A: (NCF+LW+SB)	AV: Amargosa Valley BM: Buckboard Mesa LW: Lathrop Wells NCF: Northern (1.0 Ma) Crater Flat RW: Rocket Wash SB: Sleeping Butte SC: Solitario Canyon TM: Thirsty Mesa 3.7: 3.7 Ma Crater Flat
	B: (SB)	
	C: (NCF+LW)	
	D: 1.0 of E (0.1) 0.5 of E (0.5) 0.1 of E (0.4)	
	E: 1.0 of F (0.01) 0.5 of F (0.25) 0.1 of F (0.55) 0.01 of F (0.19)	
	F: 1/3 of B (0.7) 1/6 of C (0.3)	
Post 5 Ma (0.45)	A: (NCF+3.7+LW+TM+SB+AV+BM)	
	B: (TM+SB)	
	C: (NCF+3.7+LW+AV)	
	D: 1.0 of E (0.1) 0.1 of E (0.5) 0.1 of E (0.2)	
	E: 0.5 of F (0.25) 0.1 of F (0.55) 0.01 of F (0.19)	
	F: (BM)	
Post 11 Ma (0.05)	A: (NCF+3.7+LW+TM+SB+AV+BM+RW+SC)	
	B: (TM+SB+RW)	
	C: (NCF+3.7+LW+AV)	
	D: 1.0 of E (0.1) 0.1 of E (0.5) 0.1 of E (0.2)	
	E: (SC)	
	F: (BM)	

Temporal Models	Time Period	Region Of Interest	Spatial Models	Sources
-----------------	-------------	--------------------	----------------	---------

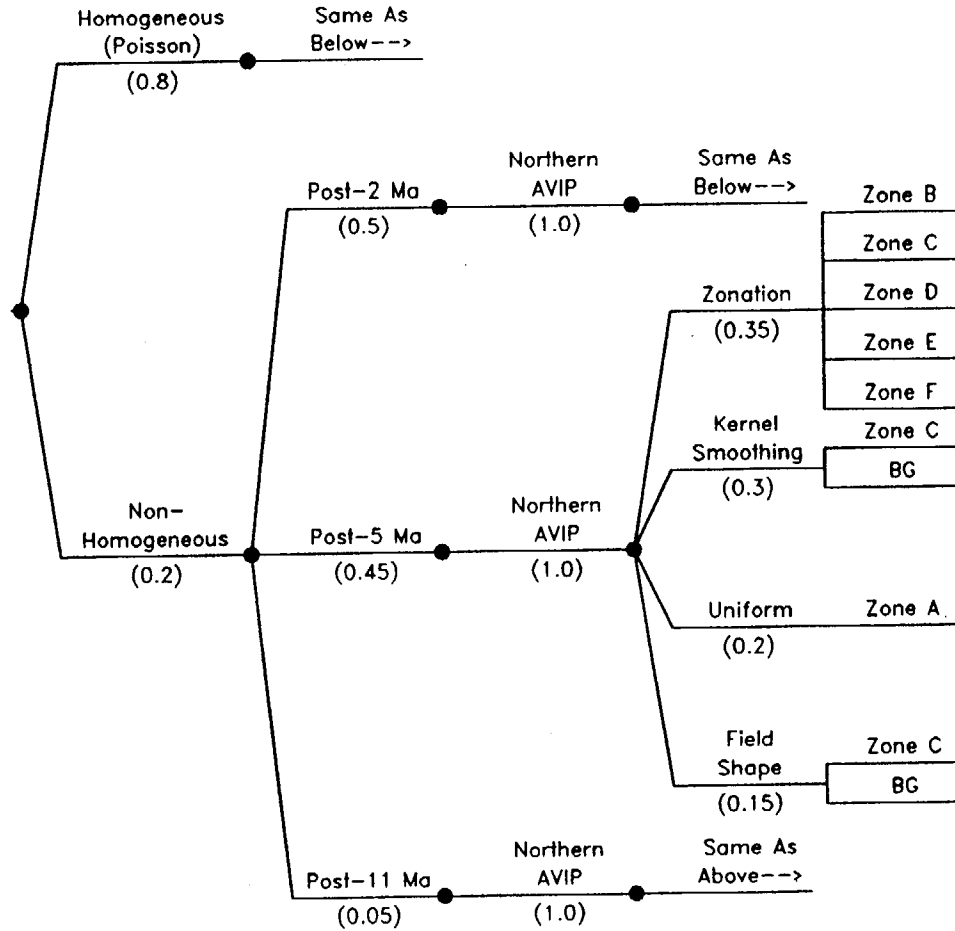
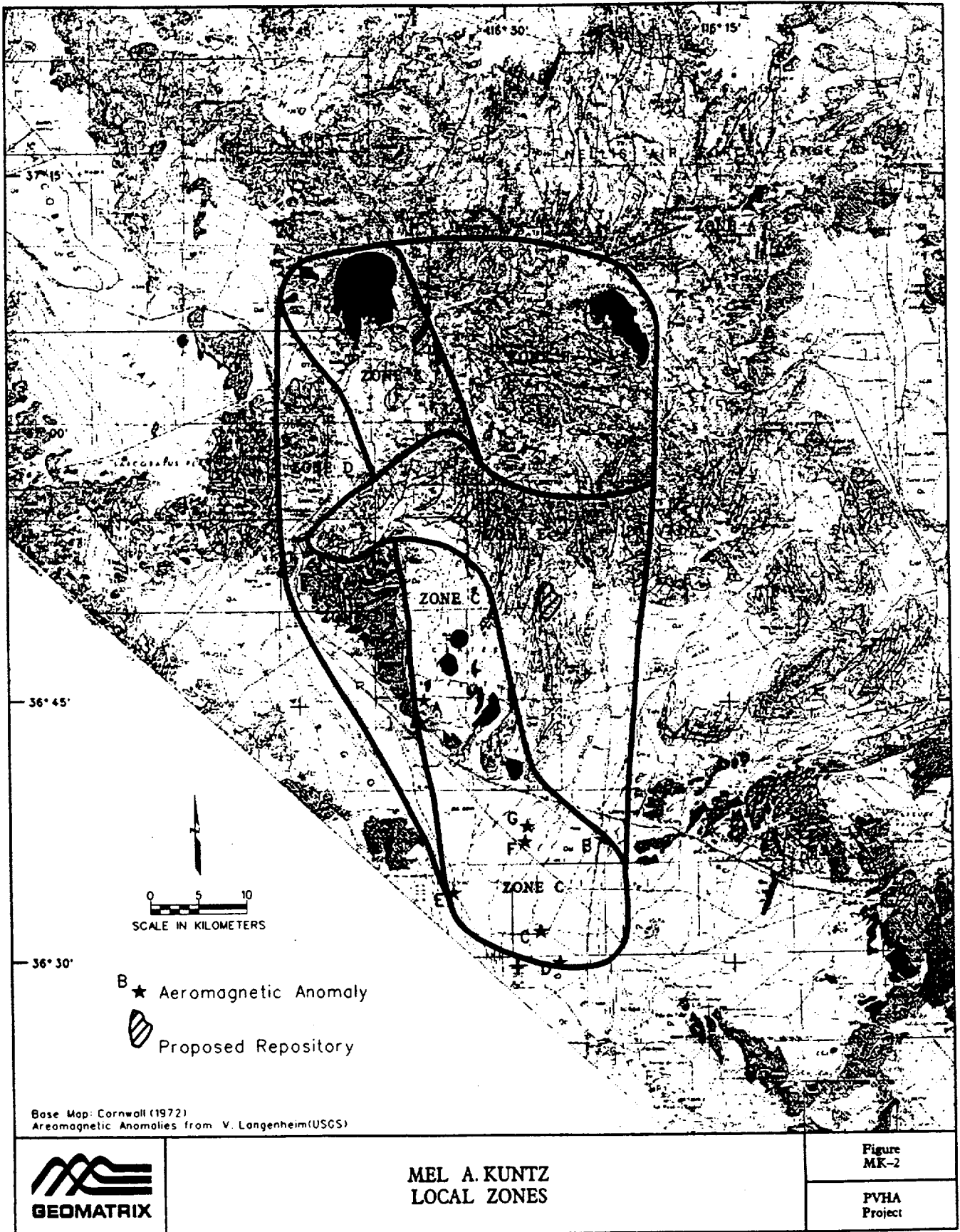


Figure MK-1 PVHA model logic tree developed by Mel A. Kuntz.



MEL A. KUNTZ
LOCAL ZONES

Figure
MK-2

PVHA
Project

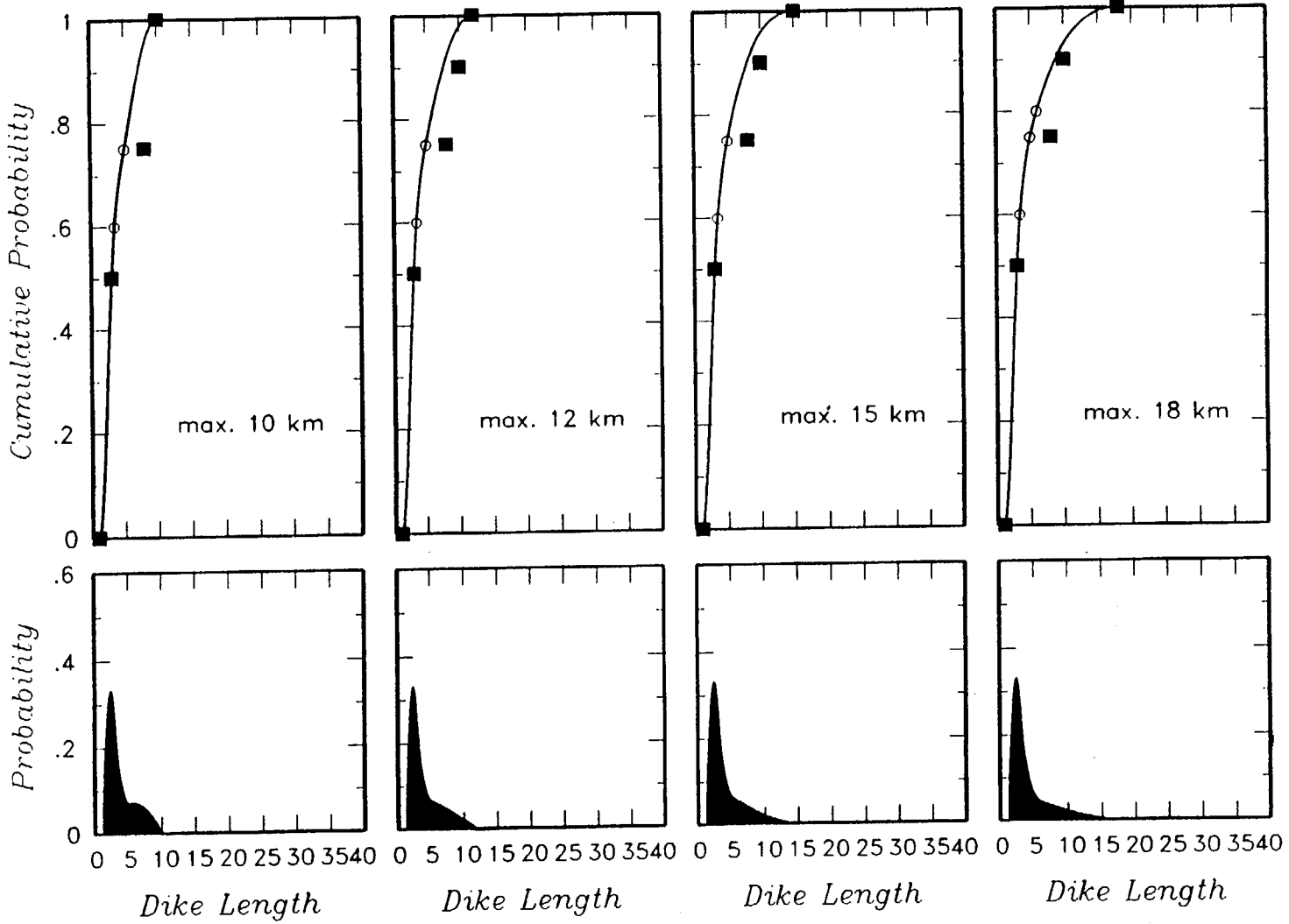


Figure MK-3 Dike length distribution developed by Mel A. Kuntz.

ALEXANDER R. McBIRNEY
ELICITATION INTERVIEW FOR PVHA PROJECT

VOLCANIC/TECTONIC SETTING

The distribution of volcanism in space and time is governed by a combination of conditions in the mantle and overlying lithosphere. Deep-seated controls govern the long-term, regional patterns, whereas shallow structures influence local, short-term behavior. Most melting anomalies in the mantle are manifested in magmatism that takes advantage of structural pathways through the crust. The main spatial controls are structural features of the lithosphere; mantle conditions are reflected only in the broad, regional distribution of volcanism.

The Amargosa Valley Isotopic Province (AVIP) proposed by G. Yogodzinski (presentation at PVHA Workshop 3) is probably the surface expression of a melting anomaly in the mantle, but the resulting volcanism has an uneven spatial distribution within the broad outline of the province. Some areas, such as the Walker Lane, are totally devoid of volcanism; whereas others, such as the Death Valley region, have a dense cluster of eruptive centers. It does not seem to matter what is occurring in the mantle; if there are no favorable channelways to the surface, the magma is obstructed at depth and fails to reach the surface. Where the pattern of strain is favorable, particularly in terms of the orientation of faults with respect to regional stresses, the distribution of vents is mainly a function of conditions within each individual structural block.

The fault system around Yucca Mountain dates back at least to the Miocene (Ferrill et al., 1995). Owing to the large number of existing faults that can accommodate regional stresses, formation of new faults is less likely than reactivation of older ones. The interaction of stresses in the region is very complex, and the strain in individual structural zones cannot be measured accurately (thus, areas cannot be ranked quantitatively in terms of the ability of magma to open new vents). Nevertheless, the AVIP can be divided into a number of types of structural settings that can be ranked in a relative sense according to the likely frequency of eruptions (see section below on Spatial Models). The ranking is based on the general distribution of volcanism in the Basin and Range Province as a whole and is purely qualitative.

The record of volcanism for the past 10 my in the central Basin and Range region suggests that there has been a long-term decline in the rate of both volcanism and faulting and that this will continue to decrease over the next 10,000 years. The data are not sufficient, however, to make

precise estimates of the rate of decline, and in view of the large short-term variations and episodic nature of activity, it is reasonable to assume that the rates will be essentially the same as they have been for the past 10,000 years.

EVENT DEFINITION

Temporal Aspects

A volcanic event, as defined for this PVHA, is an identifiable period that is limited by the time required for magma to rise to shallow levels of the crust and cool. It is normally of the order of a few tens of years (Williams and McBirney, 1979). Examples of such events are those of the young Nicaraguan volcano, Cerro Negro, where discrete eruptive events are separated by a few tens of years (Mooser et al., 1958). In other places where there is a longer history of activity, it is found that, although the frequency of eruptions may vary, the average production rate of magma over several cycles is relatively constant. This indicates that each event represents the release of magma that has accumulated during the preceding repose interval. The timing of eruptions is governed by a combination of tectonic strain rates and structural conditions in the volcano.

The long-term distribution of volcanism is governed by large-scale mantle conditions that tend to be episodic on a scale of a few million years. On a shorter time-scale, the timing of eruptions is probably related to the regional strain rate. Although magma may be produced at a more-or-less constant rate in the mantle, the strain conditions in the lithosphere govern the frequency with which magma is able to reach the surface. This is why the volumes of erupted magma tend to be larger after long periods of repose.

Spatial Aspects

The spatial dimensions of a volcanic event are generally those that are typical of a single basaltic dike (about 5 km long). However, a single event may consist of a fissure system that is as long as 15 km.

Geochemical Affinity

Eruptive products associated with an event are expected to have similar compositions, but little importance is given to geochemical affinities in defining events, because crustal contamination can lead to large variations, even during a single eruption. This was observed, for example, during the nine-year eruption of Paricutin volcano (McBirney et al., 1987).

Note: The elements of the PVHA model are summarized in the form of a logic tree in Figure AM-1.

REGION OF INTEREST

The region of interest is the area defined as the AVIP (described above). The Pliocene-and-younger volcanoes in this area have a regionally distinctive isotopic composition, which probably is inherited from a common mantle source. The most recent volcanic events in the AVIP have a wide areal distribution. The southern part of the AVIP is not included in this analysis for two reasons: (1) the presence of large active faults in this area may indicate differences in the spatial and temporal controls of volcanism; and (2) there has been a significant decline in the rate of volcanism from the Pliocene to the Quaternary, indicating that this activity has migrated to the north.

In the spatial models for the PVHA, the region of interest is subdivided into sub-regions according to their relative potentials for future volcanism. The criteria that are believed to be important for assessing future volcanism are geologic structure, the presence of young volcanic centers, and the age, and composition of the volcanic rocks. Of these criteria, geologic structures are the primary means by which the region has been subdivided for the probability analysis (Scott, 1990; Simonds et al., 1995).

The volcanism of Crater Flat and its relation to Yucca Mountain can be characterized in the general context of the regional tectonic conditions. All recent structural, neotectonic, and geophysical studies agree that the area is a pull-apart basin bounded on the west by the east-dipping Bare Mountain fault and on the east by two or more west-dipping faults (Ferrill et al., 1995; Fridrich, 1995). Although the surface trace of the Bare Mountain fault coincides with the western edge of the alluvial basin, the eastern boundary is more difficult to define. Some recent studies have placed it east of Yucca Mountain (Ferrill et al., 1995; Fridrich, 1995), but the concentration of volcanism in Crater Flat clearly indicates that, so far as volcanism is concerned, the elevated and depressed blocks must be treated independently.

Faults, even where well defined, do not coincide exactly with the boundaries of volcanic domains. The dips of the fault planes decrease downward until they are nearly horizontal (Ferrill et al., 1995; Fridrich, 1995). They must extend beneath at least some of the volcanic centers. This is best seen from the 1995 deep reflection seismic profile across the valley (G. Thompson

interpretation of T. Brocher work in presentation at PVHA Workshop 4) that shows that the feeder for Red Cone must have intersected the Bare Mountain fault. This must be true of the other cones as well. Thus, the structural control of the vents must lie at a deeper level, and the boundary of the Crater Flat domain is related only indirectly to the surface traces of faults.

This conclusion finds support in the observations that (a) the alluvial valley is the region of maximum extension and (b) the orientation of the dike system beneath the cones corresponds to a right-lateral component of offset seen in some of the faults. The north-northeast orientation of the line of cones is very close to the direction of maximum compressive stress and would be consistent with coupled right-lateral movement on the boundary faults. Opinions seem to differ regarding the amount of strike-slip motion that has occurred on these faults (Ferrill et al., 1995; Fridrich, 1995). Even though no motion of this kind has been found either in the seismic record or in exposures of the fault traces (Ferrill et al., 1995; Fridrich, 1995), this does not rule out a strike-slip component of earlier earthquakes. The proximity to the Walker Lane would make right-lateral displacement likely at depth, even if it is not seen at the surface.

If the main trend of the line of cones reflects stresses deeper in the lithosphere, the smaller dikes cutting individual cones are oriented normal to the inferred extension on the boundary faults. Thus, the major alignment is probably controlled by the regional stress field, while the subsidiary dikes reflect conditions in the shallow crust.

Although the Lathrop Wells center is included in the Crater Flat domain, it differs in several ways from the cones of Crater Flat. It is located within an area where several transcurrent faults appear to be converging (e.g., near the mapped southern limits of the Bare Mountain, Solitario Canyon, Stagecoach Road, and other faults). The history of repeated eruptions at Lathrop Wells may reflect periodic offset on one or more of these faults.

SPATIAL MODELS

Two approaches are used to define the future distribution of volcanism in the Yucca Mountain region (YMR, defined as the region within a 50-km radius of Yucca Mountain). The first, termed a "zonation" approach, divides the region into five different types of structural settings (Figure AM-2). These are listed in order of decreasing potential for future volcanism.

1. The most favorable condition is that of pull-apart basins, where eruptions occur along dilational fractures in fault-bounded valleys. If the stress regime is purely tensional, the fissures and dikes are parallel to the long axis of the valley, but if there is a strike-slip component, they may be at an oblique angle.
2. Intersections of strike-slip faults are favorable zones for volcanism, because the lateral offset where two faults cross tends to produce local fractures that can serve as channelways for rising magma.
3. The large calderas in this part of the Basin and Range province date from an earlier tectonic regime, and their magmatism is either terminated or in the final stages of decline. Eruptions associated with these features are located mainly along ring fractures, but a few may occur on radial fractures on the flanks. The magmas have compositions that are distinct from those of eruptions related to the AVIP.
4. Fault-bounded blocks of uplifted basement rock normally have fewer volcanoes and dikes than areas of lower elevation (Connor and Hill, 1995). There are, of course, exceptions to this generalization, but it is a pattern observed throughout the world (Connor and Hill, 1995). Because the boundary faults tend to isolate the interiors of such blocks from the regional strain, dilational fractures are less likely. In addition, the topographic elevation adds an additional vertical distance the magma must rise, and long dikes can find outlets at lower levels.
5. Large transcurrent fault systems have few volcanoes along their main trace. Eruptions are limited to areas of offsets or the ends of propagating branches of the main system.

The second spatial model, termed a "smoothing" approach, uses the spatial distribution of observed events to assess the probability of future events. The approach is essentially that given in Connor and Hill (1995). A Gaussian smoothing kernel is used, rather than the Epanechnikov kernel used by Connor and Hill, in order to allow for a longer tail on the probability distribution. To arrive at the same mean probabilities as Connor and Hill using the Gaussian kernel, the smoothing distances of Connor and Hill are decreased by a factor of 2.5. The resulting values of h are used: 6, 9, and 12 km. The three values are given equal weight because there is no strong preference for one over the other.

The relative weights assigned to the two alternative spatial models are: zonation approach (0.9), smoothing approach (0.1). The zonation approach is preferred because it has a stronger geologic basis that takes into account different structural provinces, faults, and their ages.

EVENT COUNTS

In accordance with the definition of volcanic "event" given earlier, the number of events and their uncertainties are assessed for each of the centers in the YMR. The event counts are assessed for the post 1-Ma period and for the post-5 Ma period. Event counts are summarized on Table AM-1.

Lathrop Wells

One to 4 events are represented at Lathrop Wells and the 3-event possibility is the most likely. A minimum of 1 event is based on chemical compositions for the identified chronostratigraphic units not being significantly different, the overlapping age determinations and homogeneous appearance of the cone being consistent with a monogenetic interpretation. Different lines of evidence, including stratigraphic, geomorphic, and soils data, suggest there have been 2 or more events: chronostratigraphic units Q1 and Q2 (Crowe et al., 1995) are more likely to be separate events than Q3 and Q4. Q3 is the most extensive unit, blanketing Q1 and Q2, and age dates for Q3 are significantly younger, supporting the separation from Q1 and Q2. The evidence for Q4 is considered relatively weak, as geochemical differences could reflect shallow crustal processes and the thermoluminescence dates are not reliable.

The following event counts and their relative weights are assigned for the Lathrop Wells center: 1 (0.3), 2 (0.2), 3 (0.4), and 4 (0.1).

Sleeping Butte

One to 3 events are represented at Sleeping Butte. Two events are most likely because Hidden Cone and Little Black Peak appear to have distinct ages. Alternatively, they could be part of the same event. Some geomorphic and possibly paleomagnetic data provide suggestive evidence for 2 events at Hidden Cone, giving some possibility to 3 events.

The event counts and their relative weights for the Sleeping Butte area are: 1 (0.05), 2 (0.8), and 3 (0.15).

1.0 Ma Crater Flat

The 1 Ma basalts of northern Crater Flat represent 1 to 5 events. One event is most likely because age determinations for the various cones overlap, and the cones appear to be located along a single fissure system. Two events are represented if Makani Cone is a separate event from the three cones to the south. Three events assumes that Black Cone and Red Cone form a single event, and the Makani and Little Cones are each separate events. Four events assumes Makani, Black, Red and Little Cones are all separate events. Five events assumes that each cone is a separate event and that there are two events at Little Cone.

The following event counts and their relative weights are assigned for northern Crater Flat: 1 (0.9), 2 (0.05), 3 (0.025), 4 (0.015), and 5 (0.01).

Buckboard Mesa

Zero to 2 events are represented at Buckboard Mesa. Zero events is most likely because the calc-alkaline basalts at Thirsty Mesa are unlike the other basalts in the AVIP. The difference in composition cannot be explained by contamination from the continental crust. However, the AVIP is defined to include them, so some weight is given to 1 or 2 events.

The following event counts and their relative weights are assigned for the Buckboard Mesa area: 0 (0.8), 1 (0.1), and 2 (0.1).

3.7 Ma Crater Flat

One to 6 events are represented at the 3.7 Ma area of Crater Flat. Two events is the most likely possibility, because the field relations suggest two en echelon fissure systems, but a single fissure system is possible. Three or more events are suggested by the detailed geologic relationships given by Crowe et al. (1995). Available geochronological data (Crowe et.al, 1995) suggest a single event but cannot preclude multiple events.

The following event counts and their relative weights are assigned for the 3.7 Ma area of Crater Flat: 1 (0.75), 2 (0.05), 3 (0.05), 4 (0.05), 5 (0.05), 6 (0.05).

Amargosa Valley

Two to 8 events may be represented by the aeromagnetic anomalies in Amargosa Valley. Five events are most likely, because of the high confidence given to the five anomalies with strong

dipole signatures (anomalies A, B, C, D, and E on the aeromagnetic map presented by V. Langenheim at PVHA Workshop 1). The minimum of 2 events is based on the basalts encountered in wells (anomalies B and D on the V. Langenheim aeromagnetic map); anomalies F and G most likely represent 1 event, but they could represent 0 or 2 events with equal likelihood; 6 events are obtained by combining anomalies F and G for 1 event and adding that event to the preferred interpretation of 5 events for anomalies A, B, C, D, and E.

The following event counts and their relative weights are assigned to the Amargosa Valley area: 2 (0.02), 3 (0.03), 4 (0.05), 5 (0.2), 6 (0.5), 7 (0.15), and 8 (0.05).

Thirsty Mesa

One or 2 events might be represented at Thirsty Mesa. The surface geology does not indicate that any interval of weathering or erosion separated the eruptions from this center. Because evidence for an earlier event could be concealed by the extensive products of the last eruption, allowance should be made for this possibility.

The following event counts and their relative weights are assigned for the Thirsty Mesa area: 1 (0.9), and 2 (0.1).

RATES OF OCCURRENCE

Using the event counts discussed above, the rates of occurrence are established for use in the PVHA. These rates are calculated over two time periods and for source zone types 1-5 (see summary in Table AM-2). The rates (number of events per square kilometer) are calculated by summing the counts for the centers within each zone, divided by the sum of the areas of zones of a particular type. For example, the post-1 Ma rate for the Zone 1 regions is derived from the sum of the counts at northern Crater Flat and Sleeping Butte, divided by the area of the Zone 1 regions.

Two alternative time periods are considered for estimating the future rate of occurrence of volcanic events:

Post-1 Ma (0.1)

Post-5 Ma (0.9)

The post-5 Ma period is given highest weight because it is a period during which similar tectonic processes have been operative. The post-1 Ma period is given relatively low weight because it excludes too many events that are believed to be significant to the potential for future volcanism (e.g., Crater Flat and Amargosa Valley).

Undetected Events

In addition to those events identified and interpreted at the surface, there is the potential for undetected events, the effects of which might be buried at depths of less than 300 m (depth of the repository) but not be represented at the surface. These events, which include both cones that were subsequently covered by younger materials and shallow dikes that did not erupt, should be added to the rates considered from surface observations.

For rates assessed for the post-1 Ma period, it is not necessary to consider additional undetected events, because there is a negligible chance of additional events within the 1 my time frame, given the extensive geologic and geophysical investigations that have been conducted within the area of interest.

For the post-5 Ma period, there is a finite possibility that there were events in addition to those recorded by their observed products. It is estimated that there may be an additional 10% of the observed counts (i.e., the observed post-5 Ma counts should be multiplied by 1.1 to arrive at the total counts).

TEMPORAL MODELS

One temporal model is considered appropriate: a homogeneous model that assumes the rate of occurrence of volcanic events is uniform through time. This is because the starting times of 1 Ma and 5 Ma are recent enough for the rate of volcanism to be considered homogeneous. If a longer time period were used (e.g., 10 Ma), a temporal model describing the waning of volcanic activity would be required.

EVENT GEOMETRIES

The dimensions of volcanic events are expected to be essentially the dimensions of basaltic dikes. Long dikes require large volumes of magma. In the YMR the volumes of eruptions are small, and

dike dimensions are also expected to be small. The expected length of a dike is about 5 km; the minimum length is 3 km and the maximum length is 15 km. The maximum length would likely include a fissure system of multiple dikes, rather than a single dike. The lengths of dikes and their relative weights are the following: 3 km (0.3), 5 km (0.6), and 15 to 20 km (0.1). Equal weights are given to maximum values of 15 and 20 km.

Note: At the request of Dr. McBirney, a smooth interpolation function was fit to his discrete cumulative density estimates for dike length. The resulting cumulative distribution and density functions are shown on Figure AM-3.

The orientation of dikes is expected to be N30E, with an uncertainty of ± 45 degrees (representing 80% of the probability). This orientation is consistent with the NW orientation of the least horizontal compressive stress deduced from earthquake focal mechanisms and the orientation of normal faults.

Topographic relief has an effect on the ability of dikes to intrude shallow levels of the crust. Because magma is a liquid that flows from high to low elevations, long dikes are less likely to approach the surface of elevated blocks than valley floors. This is why volcanic cones and fissures are much less common on horsts than in grabens. Thus, even if a dike extends from Crater Flat into Yucca Mountain, the probability that it will rise to the level of the repository below the crest of the mountain is very low.

Given the center of an event, the probability distribution for the location of the event relative to the center is assumed to be trapezoidal, with 75% of the density between 0.2 and 0.8 of the dike length.

HYDROMAGMATIC ACTIVITY

Because the proposed repository site lies within the Yucca Mountain block, the potential for significant (large-volume) hydromagmatic activity is very low. It is estimated that 1 out of every 100 volcanic eruptions in the YMR will be associated with significant hydromagmatic activity.

TYPE OF ERUPTION

The expected type of eruption in the YMR is a small-volume basaltic eruption. Although there is no consistent pattern, many mature volcanic fields have had rhyolitic volcanism as well. The probability that the region will evolve into a period of rhyolitic volcanism is estimated to be 0.1 in 10,000 years. Given such a change, the probability of a significant rhyolitic volcanic event is 0.25. Therefore, the probability of a significant rhyolitic volcanic event is $(0.1 \times 0.25) = 0.025$.

A R McJannet
29 April 1996

REFERENCES

- Connor, C.B., and Hill, B.E., 1995, Three nonhomogeneous Poisson models for the probability of basaltic volcanism: Application to the Yucca Mountain region, Nevada, USA: *Journal of Geophysical Research*, v. 100, no. B6, p. 10,107-10,125.
- Crowe, B.M., Perry, F.V., Geissman, J., McFadden, L., Wells, S., Murrell, M., Poths, J., Valentine, G.A., Bowker, L., and Finnegan, K., 1995, Status of volcanism studies for the Yucca Mountain site characterization projects: Los Alamos National Laboratory Report LA-12908-MS, March.
- Ferrill, D.A., Stirewalt, G.L., Henderson, D.B., Stamatakos, J.A., Morris, A.P., Wernicke, B.P., and Spivey, K.H., 1995, Faulting in the Yucca Mountain region: Critical review and analyses of tectonic data from the central Basin and Range (CNWRA 95-017): prepared by the Center for Nuclear Waste Regulatory Analyses, San Antonio, Texas, for the Nuclear Regulatory Commission, August.
- Fridrich, C.J., 1995, Characterization of detachment faults in the Yucca Mountain region, *in* Simonds et al. (eds.), Final report on detachment faulting: U.S. Geological Survey Administrative Report.
- McBirney, A.R., 1959, Factors governing emplacement of volcanic necks: *American Journal of Science*, v. 257, p. 431-448.
- McBirney, A.R., Taylor, H.P., and Armstrong, R.L., 1987, Paricutin re-examined: a classic example of crustal assimilation in calc-alkaline magmas: *Contributions to Mineral Petrology*, v. 95, p. 4-20.
- Mooser, F., Meyer-Abich, H., and McBirney, A.R., 1958, Catalogue of the active volcanoes of the world - Part VI: Central America: International Association of Volcanologists, 146 p.
- Scott, R.B., 1990, Tectonic setting of Yucca Mountain, southwest Nevada, *in* B.P. Wernicke (ed.), Basin and Range extensional tectonics near the latitude of Las Vegas, Nevada: Boulder, Colorado, Geological Society of America Memoir 176, p. 251-282.
- Simonds, W.F., Whitney, J.W., Fox, K.F., Ramelli, A., Yount, J.C., Carr, M.D., Menges, C.M., and Dickerson, R., 1995, Map of fault activity in the Yucca Mountain area, Nye County, Nevada: U.S. Geological Survey Miscellaneous Investigations Series Map I-2520, scale 1:24,000.
- Williams, H., and McBirney, A.R., 1979, *Volcanology*: Freeman & Cooper, 397 p.

**TABLE AM-1
 ALEXANDER R. McBIRNEY - EVENT COUNTS**

LOCATION	COUNTS (CONES)	WEIGHT	NOTES
Lathrop Wells	1 (all) 2 (Q1, 2) 3 (Q1, 2, 3) 4 (Q1, 2, 3, 4)	(0.3) (0.2) (0.4) (0.1)	BC: Black Cone HC: Hidden Cone 2HC: 2 events at Hidden Cone LBP: Little Black Peak LC: Little Cones 2LC: 2 events at Little Cones M: Makani Cone Q1-4: Chronostratigraphic units of Crowe et al. (1995) RC: Red Cone
Sleeping Butte	1 (HC+LBP) 2 (HC, LBP) 3 (2HC, LBP)	(0.05) (0.8) (0.15)	
1.0 Ma Crater Flat	1 (all) 2 (LC+RC+BC, M) 3 (LC, RC+BC, M) 4 (LC, RC, BC, M) 5 (2LC, RC, BC, M)	(0.9) (0.05) (0.025) (0.015) (0.01)	
Buckboard Mesa	0 1 2	(0.8) (0.1) (0.1)	
3.7 Ma Crater Flat	1 2 3 4 5 6	(0.75) (0.05) (0.05) (0.05) (0.05) (0.05)	
Amargosa Valley	2 3 4 5 6 7 8	(0.02) (0.03) (0.05) (0.2) (0.5) (0.15) (0.05)	
Thirsty Mesa	1 2	(0.9) (0.1)	

**TABLE AM-2
ALEXANDER R. McBIRNEY - RATES OF OCCURRENCE**

TIME PERIOD	COUNT METHOD FOR ZONES	NOTES
<p>Post 1 Ma</p> <p>(0.1)</p>	<p>Zone 1: (NCF+SB) Zone 2: (LW) Zone 3: Use Post-5 Ma rate Zone 4: Use Post-5 Ma rate Zone 5: Use Post-5 Ma rate</p>	<p>NCF: Northern (1.0 Ma) Crater Flat SB: Sleeping Butte LW: Lathrop Wells 3.7: 3.7 Ma Crater Flat TM: Thirsty Mesa AV: Amargosa Valley BM: Buckboard Mesa</p>
<p>Post 5 Ma</p> <p>(0.9)</p>	<p>Zone 1: (NCF+SB+3.7+TM) Zone 2: (LW+AV) Zone 3: (BM) Zone 4: (BM) Zone 5: 0.5 x rate of Zone 3</p>	

Temporal Models	Time Period	Region Of Interest	Spatial Models	Sources
-----------------	-------------	--------------------	----------------	---------

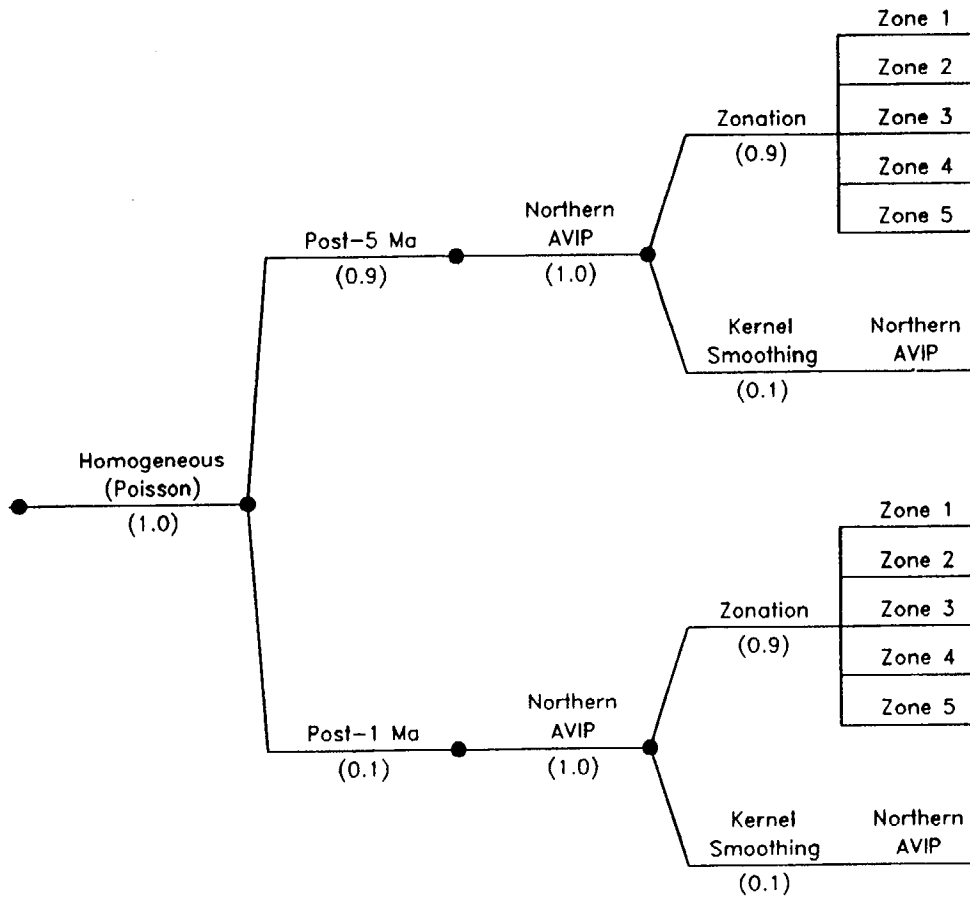
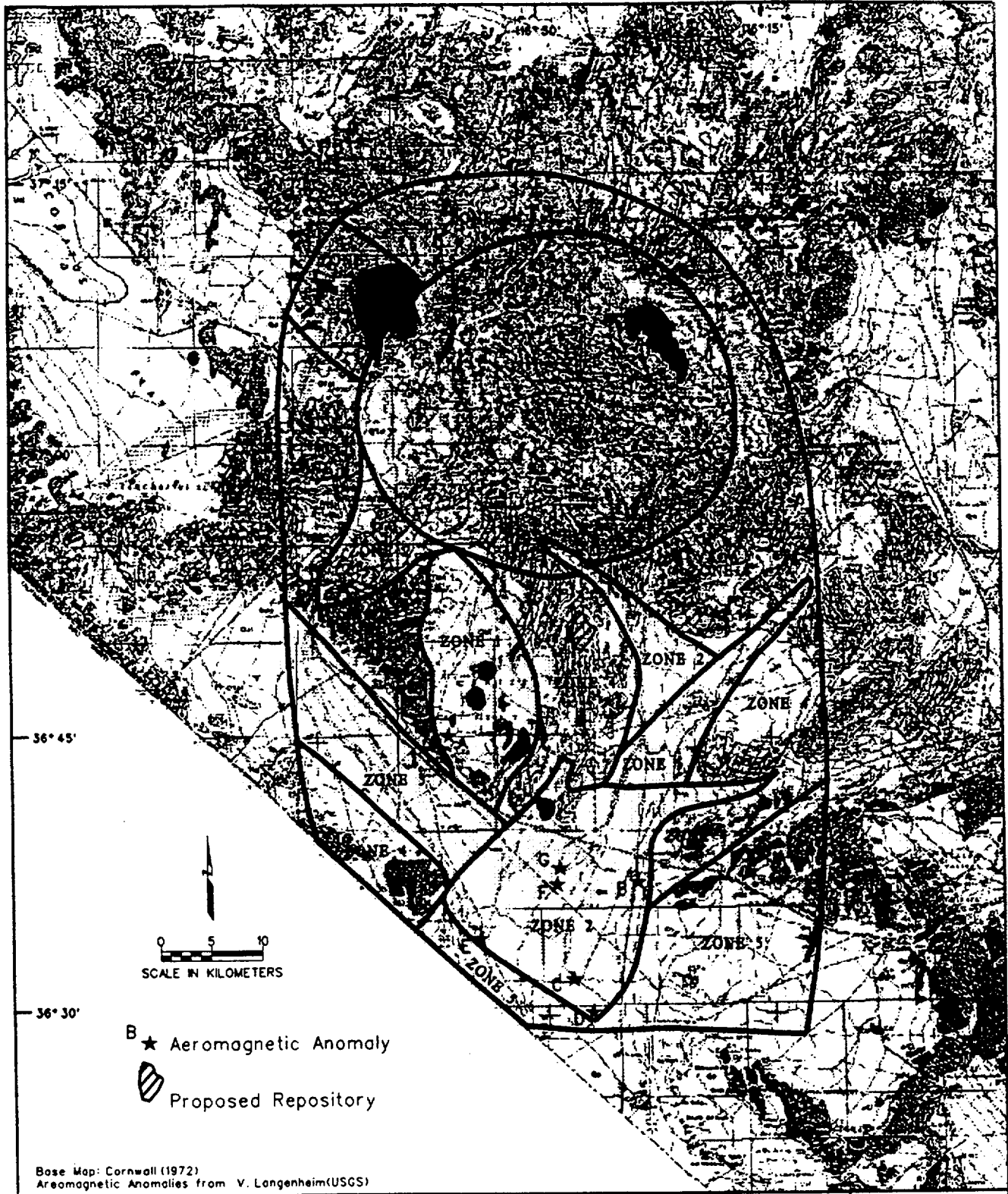


Figure AM-1 PVHA model logic tree developed by Alexander R. McBirney.



Base Map: Cornwall (1972)
Aeromagnetic Anomalies from V. Langenheim(USGS)



ALEXANDER R. McBIRNEY
LOCAL ZONES

Figure
AM-2

FVHA
Project

m:\proj\yucca\gpr\p\hrc\cornwall\ram_02.dgn Rev. 03-28-98

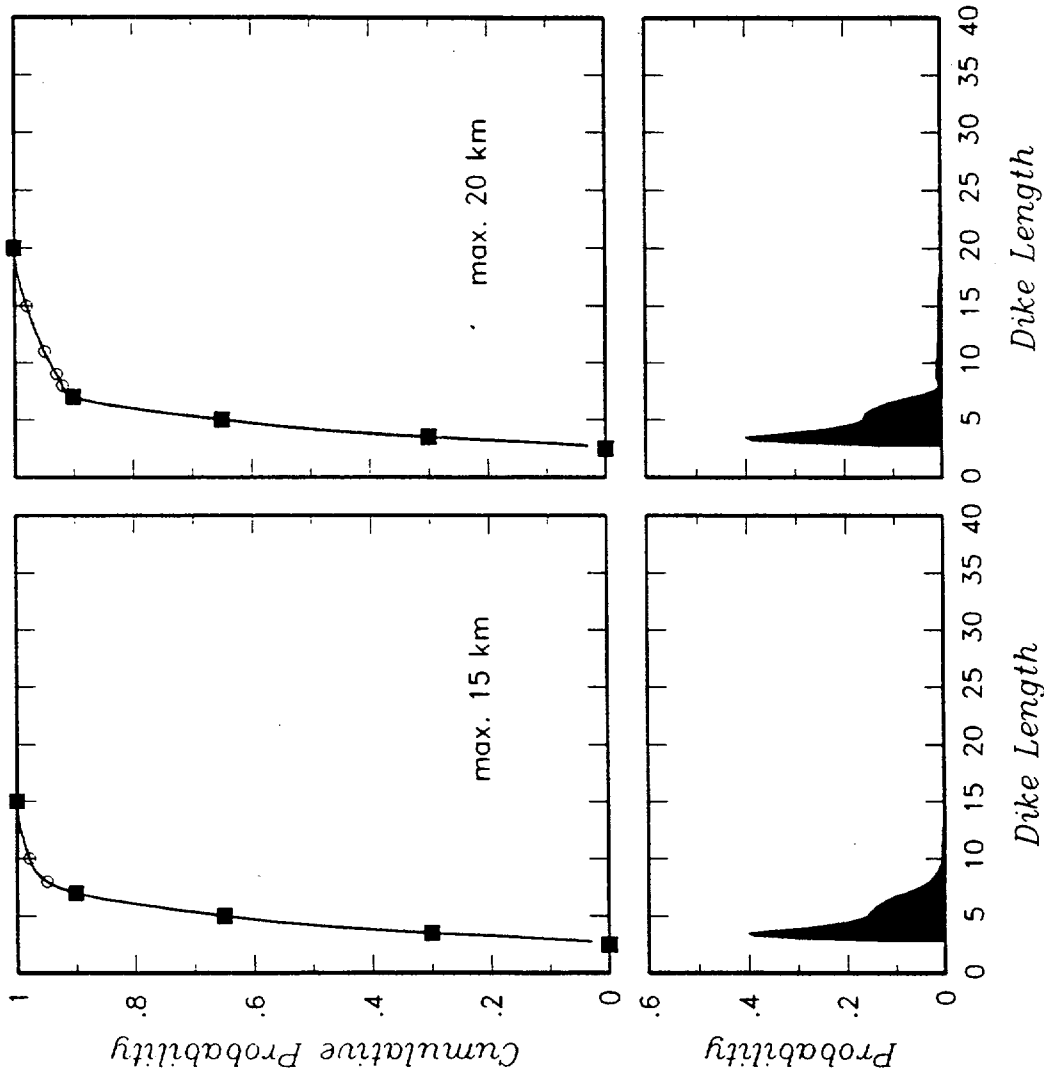


Figure AM-3 Dike length distribution developed by Alexander R. McBimney.

MICHAEL F. SHERIDAN
ELICITATION INTERVIEW FOR PVHA PROJECT

VOLCANIC/TECTONIC SETTING

Over the past 15 my, basaltic volcanism in the Basin and Range of the western U.S. has been episodic within defined fields; new fields have appeared randomly over a broad regional area during this time. Conditions for persistent basaltic volcanism were created by: (1) subduction of either the East Pacific Rise or new basaltic crust generated near the rise beneath the North American plate, which caused an abnormally high thermal regime within the lithosphere; (2) cessation of widespread subduction related rhyolitic volcanism, which produced ash-flow sheets and calderas; and (3) gradual separation of triple points along the western margin of North America, behind which an extensional tectonic regime allowed the rise to the surface of dominantly basaltic magmas. As the two triple points diverged along the western margin of the North American plate, subduction related effects died as extensional features developed (Atwater, 1970). The cessation of subduction related to plate impingement began about 20 Ma and the conditions for dominantly basaltic volcanism reached the Yucca Mountain area about 10 Ma. Extensional tectonism associated with basaltic volcanism continues to the present at this location (Christiansen and Lipman, 1972; Luedke and Smith, 1981). Because it is not clear whether volcanism has been waxing or waning in the vicinity of Yucca Mountain in the past 5 my, the more recent geologic record is considered to be the best indicator of what can be expected in the future.

Due to the strong clustering of mapped volcanoes, future volcanic eruptions in the western U.S. will most likely occur again within the boundaries of established fields. In particular, those fields with the highest recurrence rates are the most probable sites for future volcanism. Volcanic events outside known fields represent the initiation of a new field; an event much less likely than an another eruption within a field. Older calderas in the Basin and Range province could be responsible for localizing small basaltic fields or volcanic centers, provided that their silicic magmas have solidified (Smith and Bailey, 1968; Smith, 1979). This is due to the penetration of these structures through the crust, causing attendant fracturing and weakening of surrounding rocks. Basaltic fields such as Sleeping Butte, Thirsty Mesa, and Buckboard Mesa near the Timber Mountain caldera could be examples of such a mechanism, although this has yet to be proven in the region.

The basic process leading to volcanism involves generation of a melt from a source zone within the asthenosphere or lower lithosphere and migration of the magma to the surface where it erupts. At present there is not much spatial or temporal predictive power to magma generation models (i.e., they are not useful in predicting where and when future volcanoes will occur in the Basin and Range). The typical lifetime of late Cenozoic volcanic fields in the southern Basin and Range province is 1 to 15 my (Nealey and Sheridan, 1989), suggesting that source zones may be active for at least this duration. The reason repeated activity occurs within fields rather than being widely dispersed is not well understood. Volcano clusters may correspond to the distribution of melt source zones or they may be the location of leaky places in the system where magma can escape more easily.

The state of stress in the lithosphere is very important in assessing the near-surface locations of volcanism because the migration of basaltic magma to the surface is favored by extension (Delaney et al., 1986). Near-surface faults do not play a major role in the location of volcanic fields, but faults may have some influence on the locations of vents and cones. In general, the number of cones decreases with distance from faults. However, the use of faults in developing a spatial model of volcanism is not sufficiently understood to be warranted in a model of volcanic forecasting.

EVENT DEFINITION

Temporal Aspects

An event is equivalent to an "eruption cycle," or an "eruptive episode," in which active periods of eruptions occur between quiescent phases. An active period typically includes short pauses and may extend from several years to thousands of years. The spatial arrangement is the most important characteristic to consider in identifying events. The uncertainty associated with dating young basaltic volcanic rocks, such as those in the region of interest, is about 100,000 yr. Because of the large uncertainties of age-dates (Crowe et al., 1995), a long-duration and large-sized event was used for this analysis. Therefore, the time-frame for an event is assessed to be 100,000 yr.

Spatial Aspects

The spatial relationships among eruptive features are the most important criteria for identifying events in the region of interest because of the lower precision of geochronologic data. A single event may produce 0 to 5 or more cones. For example, the Paricutin eruption of 1943-52 produced several cones and exhibited many different phases (Foshag and Gonzalez, 1956). For my model, the cones must be associated with a single linear dike or a dike system with more complex geometry. If eruptions of similar ages (i.e., $\pm 100,000$ yr or less) cannot be linked by a single linear

dike or dike system, then they are considered to be separate events. Dikes feeding individual cones have the most frequent dimension of about 1.0 to 2.5 km (Delaney et al., 1986; Sheridan, 1992), and dike systems feeding multiple cones may be as long as 15 km in the broad region of the western Great Basin. Longer dikes have been described in areas of rifting such as the eastern Snake River Plain and Iceland (Sigurdsson, 1987).

Geochemical Affinity

The role of chemical affinity in defining an event is complex. Greatly different magmas may erupt during the same event due to magma mixing or other processes. Such magmas may have different phenocryst suites, isotopic ratios, trace element patterns, and bulk major element chemistry. Thus, I do not believe that geochemistry is useful for distinguishing events in the region of interest, especially at Lathrop Wells. I do believe, however, that isotopes and trace elements can be useful in identifying broad source regions. Hence, I like the model of G. Yogodzinski (presentation at PVHA Workshop 3; Yogodzinski and Smith, 1995) that defines the Amargosa Valley Isotopic Province (AVIP) as the source region for all the young basalts in the region of interest. This concept is useful to confirm some bounds set on the region of interest. I favor his interpretation that the AVIP is an area underlain by cooler Proterozoic lithosphere that is the source for basaltic magmas responsible for the weak volcanism of this area.

Note: The elements of the PVHA model are summarized in the form of a logic tree in Figure MS-1.

REGION OF INTEREST

A key determinant in the decision regarding a relevant region of interest for the PVHA is the concept of volcanic fields (Schwartz et al., 1991). A field contains volcanic features that are spatially, temporally, and genetically related (i.e., formed by magma that is generated by melting in the lower lithosphere or upper asthenosphere and that migrates to the surface in a focused area). The length of basaltic fields in the western Great Basin and southern Basin and Range (Luedke and Smith, 1981; Lynch, 1989; Nealy and Sheridan, 1989) is on the order of 15-50 km. Basaltic volcanic fields in this area may be active for a duration of 1 my up to 15 my with an average life of 5 my (Christiansen and Lipman, 1968; Luedke and Smith, 1981; Lynch, 1989). Individual active phases may have time scales that last a few years to a few hundred years. Longer-period time scales are preferred to define events for the purpose of this analysis because of the large time span considered for the PVHA (10,000 yr) and the limitation of current radiometric dating techniques ($\pm 100,000$ yr). The location of renewed volcanic activity at the surface is unlikely to

be at the exact location of a previous eruption (i.e., at the same cone), but it has a high probability of occurring within the defined boundaries of a field.

Considering the concept of volcanic fields as fundamental to descriptions of future locations of volcanoes (Sheridan, 1992), two alternative areas are evaluated (Figure MS-2): (1) volcanic fields in a regional area within a 200-km radius of Yucca Mountain, identified on the Luedke and Smith (1981) map and used to calculate the rate of birth of new volcanic fields; and (2) volcanic fields, events, and individual cones identified and counted in a local area within a radius of about 40 km of Yucca Mountain, here termed the "region of interest," used for event recurrence rate calculations. All of the region of interest lies within the AVIP, the suspected source region for all of the young basalts that it encompasses. Both the 200-km-radius region and the 40-km-radius region of interest are used to calculate probability in my model.

SPATIAL MODELS

Two alternative spatial models are used to assess the future locations of volcanic activity in the region of interest: (1) the volcanic field approach and (2) the volcanic zone approach. The field approach takes into consideration the general characteristics of other basaltic fields in the Basin and Range. The shape and distribution of volcanic features within a field are important in this model. The volcanic zone approach assumes a random distribution of volcanic events in time and space within the designated zone.

Based on studies of a large number of basaltic volcanic fields in the southwestern U.S., typical fields have an elliptical shape, with length-to-width aspect ratios of about 2:1, and the events within fields are assumed to follow a bivariate Gaussian distribution (Sheridan, 1992). In this analysis, the best fit of events to a bivariate Gaussian distribution is used to define the event probabilities of the single field closest to the site. This area, called the Crater Flat field, is defined by the distribution and uncertainties of surface and subsurface events younger than 5 Ma in Crater Flat and the Amargosa Desert. The large spatial separation of Sleeping Butte, Thirsty Mesa, and Buckboard Mesa from the Crater Flat field, and the complete absence of basaltic centers between them over the past 10 my, strongly argues for their being separate fields. Gaussian distributions centered on these distant fields have such low probabilities that they were not considered to be significant related to the proposed repository site.

In applying the field shape approach, events are represented as points, either centered on individual cones or the midpoint of clusters defined by multiple aligned cones. Because event points in the Crater Flat field are assumed to represent realizations of a bivariate Gaussian

distribution, they are used directly to define the center, length, width, and orientation of this field by a mathematical best fit algorithm. The data set is too small to justify using non-homogeneous models in time and space such as those suggested by Ho (1991) and Connor and Hill (1993). These models are very sensitive to starting times and event definitions. The aspect ratio of fields is restricted to a maximum of 5 based on observations of existing, well-defined fields.

In the volcanic zone approach, or zonation model, the spatial probability distribution of future volcanic events is assumed to be uniform across a zone. The zone used for this analysis is the inner 40-km-radius area, and the rate is defined by event counts within the zone. Post-10 Ma volcanic rocks are used in this analysis only to help define the rate of birth of new fields in the region. The post-5 Ma events exclusively are used in defining rates of occurrence within the smaller 40-km region of interest.

Weights assigned to the field approach and zonation approach are 0.75 and 0.25, respectively. The field approach is given higher weight than the zonation approach because it is judged to have a stronger technical basis for assessing the future location of volcanism, one that takes into account observations of centers in the region of interest as well as the behavior of fields in analogue regions.

FIELD AND EVENT COUNTS

For both the field approach and the zonation approach, the number of events occurring over a particular time period must be specified. In addition, for the field approach, the number of fields must be counted.

EVENT COUNTS

Based on the definition of volcanic events given above, the number of events and their uncertainties are assessed for each of the centers in the inner 40-km-radius zone (Table MS-1). The event counts were made for the post-5 Ma time interval. This time interval, used in many publications on regional volcanism (e.g., Luedke and Smith, 1981), is sufficiently long to provide accurate rate data. It is the most appropriate time interval for evaluating rates because: (1) data for post-5 Ma events are more complete than for older events; (2) scoria cones and other eruptive features that are used to define events are preserved for up to about 5 my before their complete removal by erosion, thus event counts for older periods are difficult to make; and (3) counts made for a more recent period would include too few events to provide a meaningful estimate of the rate. The counts given here are based on interpretations of eruptive features at the surface reported in

publications and noted by my personal field observations. Also considered are subsurface events that might exist at shallow depths but not at the surface (see following section "Undetected Events").

Lathrop Wells

The Lathrop Wells cone represents 1 cone and 1 event. The geologic history of the Lathrop Wells cone is complex, and we could still be within the active period of the "event" (see Rates of Occurrence, below). By my definition, Lathrop Wells would be only a single, albeit complex, event. The large ambiguity in the numerous radiometric and other dates and the geomorphic youth of this feature justify considering it to be a single event. The possible extremes of radiometric dates and the geomorphic complexity (Wells et al., 1990) make the continuing life of Lathrop Wells as a 2-event scenario a weak possibility.

The following event counts and their relative weights are assigned for the Lathrop Wells center: 1 (0.9), and 2 (0.1).

Sleeping Butte

Little Black Peak and Hidden Cone are most likely a single event connected by a NE-trending dike because of the closeness in their ages. With a lower probability, the cones could represent 2 events.

The event counts and their relative weights for Sleeping Butte are: 1 (0.67) and 2 (0.33).

1.0 Ma Crater Flat

The 1 Ma basalts of the surface cones in northern Crater Flat could represent from 1 to 3 events, with the most likely being 1 event. These features include Makani Cone, Black Cone, Red Cone, and two Little Cones. It is judged unlikely that all of these cones are separate events. The favored scenario is that all of the cones are related to a single dike or dike system having a northeast trend. The alignment of the surface cones and the consistent radiometric dating are the bases for the surface cones being a single event. Aeromagnetic anomaly A of V. Langenheim (presentation at PVHA Workshop 1), which is buried beneath the alluvium near the alignment of the 1 Ma chain, has a probable age of about 3.8 Ma and represents a unique event that is included with my analysis of the other buried events in the Amargosa Desert.

The probability of more than 3 events is assigned zero weight because of the large age difference required by my definition of an event (an age range or uncertainty of $\pm 400,000$ years would be

required). Two events assumes that Makani Cone was formed by a separate event, and 3 events assumes the two Little Cones formed as separate events.

The following event counts and their relative weights are assigned for northern Crater Flat: 1 (0.7), 2 (0.2) and 3 (0.1).

Buckboard Mesa

The geologic relationships at Buckboard Mesa suggest that it represents 1 event. Venting occurred at a single scoria cone and a fissure that extends to the SW (Lutton, 1968). However, there is uncertainty about the number of events at Buckboard Mesa. Because of the large volume of lava (1 km³) and lack of detailed mapping or dating (Crowe et al., 1995), additional vents could be present. Because there is no direct basis for evaluation of uncertainty magnitude, as many as 6 events have been considered. The maximum number would assume an average event volume of lava of 0.13 km³ and a possible cumulative age range uncertainty of ± 0.6 my. Each multiple event possibility was given an equal probability (0.05) because there is no justification for weighting them differently.

The following event counts and their relative weights are assigned to the Buckboard Mesa area: 1 (0.75), 2 (0.05), 3 (0.05), 4 (0.05), 5 (0.05), and 6 (0.05).

3.7 Ma Crater Flat

The 3.7 Ma basalts exposed at the surface of Crater Flat could represent from 1 to 6 events, with the 2 event scenario preferred. The basis for assuming a 2 event sequence is the location and geometry of two well-defined dikes trending N-S through this outcrop area. Radiometric dating cannot distinguish between events, and the only theoretical basis for assuming multiple events is the separation of the two large dike segments. Also, the suspected vents along the dikes seem to be well aligned in the N-S direction. More than 4 events are unlikely considering the age limitation of my definition (1.0 my of uncertainty is needed for 5 events). The higher probability assigned for 3 events is based on the possibility of a third dike system.

The following event counts and their relative weights are assigned for the 3.7 Ma area of Crater Flat: 1 (0.1), 2 (0.6), 3 (0.2) and 4 (0.1).

Amargosa Valley

The 7 aeromagnetic anomalies within Amargosa Valley and Crater Flat (V. Langenheim presentation at PVHA Workshop 1; Langenheim et al., 1993) might represent as few as 5 and as many as 7 events, with a preferred interpretation of 6 events. Anomalies B and D both have been

drilled and confirmed to be basalt covered by about 100-200 m of Quaternary alluvium. Anomaly B is basalt dated at 3.84 Ma. Modeling of anomaly C suggests that it is also a basaltic cone buried about 200 m below the surface, consistent with a pre-Quaternary age.

Determination of the number and location of events in this area takes into account the location and potential orientation, as well as the magnetic polarity of the anomalies. Events A, D, and E are considered unique events in all scenarios due to their wide geographic spacing. Anomaly E is a separate event from anomalies F and G due to probable differences in polarity. In the 5-event scenario, anomalies F/G and B/C are assumed to be 2 separate events related to northeast-trending dikes. In the 6-event scenario anomalies B and C are considered to be separate events because of their geographic separation. The 7-event scenario considers all anomalies to represent separate events due to the high uncertainty in ages. The 6-event scenario is preferred because it assumes NE dike trends similar to the trend observed in the alignment of cones in northern Crater Flat. *(Note: Anomalies F and G on the unpublished aeromagnetic map presented by V. Langenheim at PVHA Workshop 1 correspond to anomaly A in the Langenheim et al. (1993) reference.)*

The following event counts and their relative weights are assigned to the Amargosa Valley area: 5 (0.25), 6 (0.5), and 7 (0.25).

Thirsty Mesa

The number of events at Thirsty Mesa could range from 1 to 4 events, based on the large volume of lava and the possibility of undetected events. Thirsty Mesa most likely represents 1 event, with low probabilities assigned to 2 to 4 events.

The event counts and their relative weights for Thirsty Mesa are: 1 (0.9), 2 (0.033), 3 (0.033) and 4 (0.033).

Field Counts

The field approach to the spatial distribution of volcanism requires that the rate of occurrence of volcanoes outside of the local fields (i.e., Crater Flat, Buckboard Mesa, and Sleeping Butte fields) be defined by the rate of formation of a new field. This rate is calculated by counting the number of fields that have formed between 0 and 5 Ma and between 5 and 10 Ma in the region of interest (both the 200-km-radius and the 40-km-radius regions). The locations and ages of fields are interpreted from the information given on the Luedke and Smith (1981) map. Within the 200-km-radius area, 30 fields are identified as younger than 10 Ma, and 16 fields are younger than 5 Ma. Within the 40-km-radius region of interest, 5 fields are younger than 10 Ma, and 2 fields are younger than 5 Ma (Crater Flat and Buckboard Mesa).

RATES OF OCCURRENCE

Event Rates

The rate of occurrence of volcanic events within fields is calculated from the counts over the post-5 Ma period in centers located within the 40-km-radius region of interest (the Crater Flat field, the Sleeping Butte/Thirsty Mesa field, and the Buckboard Mesa fields) (see summary on Table MS-2). Due to the youthfulness of the Lathrop Wells center, there is a possibility that we are still within the active period of an "event" and this is accounted for in assessing the rate. Approximately 125,000 yr have elapsed since the last eruption at Lathrop Wells. Given the definition of an event (i.e., can occur over 100,000 yr), it is judged that there is a 0.25 probability that we are still within the event giving rise to the most recent eruption at Lathrop Wells. There is a 0.75 probability that the event has ended and, in this case, the Lathrop Wells cone is simply counted as another event in the post-5 Ma time period.

In the case where the event is assumed to still be occurring, the following rate is derived. It is assumed that the full length of an event is 200,000 yr ($\pm 100,000$ yr). At the end of the 200,000 yr period, the probability of another eruption within this event will be zero. If 125,000 yr have elapsed, the probability of an event in the next 75,000 yr is simply $1/75,000$. It is assumed that this represents an equivalent annual rate, given that we are still within the most recent event.

Rate of New Field Birth

The rates of formation of volcanic fields are assessed for two regions: a 200-km-radius circle from the site (given a weight of 0.75) and the inner 40-km-radius zone (given a weight of 0.25). The event counts are for two time periods: post-10 Ma and post-5 Ma. The post-10 Ma time period is given higher weight (0.75) because it is judged that the regional tectonic setting within the regions of interest has been relatively constant over this time period; the maps appear to be complete for volcanics of this age; and a larger, perhaps more significant, number of events is identified than for the post-5 Ma time period, thus providing a more stable rate estimate.

Undetected Events

This PVHA is focused on assessing the probability of intersection of the proposed repository (at a depth of approximately 300 m below the surface) with a volcanic event. The events discussed above are related to surface observations. It is also possible that some events may occur in the shallow subsurface but not be present at the surface. The aeromagnetic anomalies in the Amargosa Desert and Crater Flat are assumed to be scoria cones. These represent surface events that were buried but have been identified, hence they are not undetected events. The major type of undetected event in the northern Crater Flat area would be subsurface dikes which could be

present within about 1 km of the valley floor and which may have a geometry that is difficult to recognize by current geophysical techniques (vertical thin sheet).

The technical justification for these features is related to the presentation of G. Thompson (at PVHA Workshop 2) on crustal extension that follows the model of Bursik and Sieh (1989): in a zone of extension the horizontal strain can be accommodated by either intrusion of dikes parallel to the plane of maximum extension or by normal faulting with both horizontal and vertical components of displacement. According to Bursik (1993), density plays a major role that inhibits the vertical extent of lava in dikes. Magma within the dikes would have a tendency to move down-hill and break to the surface at some point lower than its maximum elevation. Eruptions on Hawaii are good examples of this hypothesis.

The present Yucca Mountain block apparently has had no dikes emplaced during the past 5 my, and its tectonic response has been uplift as a more-or-less rigid block bounded by normal faults. The deep structure of the adjacent Crater Flat basin is not clear, and several models were presented at the PVHA workshops (e.g., G. Thompson presentation at Workshop 4). The model I favor is a pull-apart basin with a horizontal strain accommodated by dike intrusion. Using this model, the subsurface dike system of the 1.0 Ma cones is a manifestation of one or more deeper dike systems. This would also apply to the 3.7 Ma volcanic features in Crater Flat and the young cones of Lathrop Wells.

To estimate undetected events, using my definition of an event as having $\pm 100,000$ year life span, there could be as many as 25 events in the 5 Ma under consideration. This number, minus the number of recognized events, yields the number of undetected dikes in the subsurface. For the Crater Flat field, in which there are 15 recognized events, this simplifies to about 10 undetected events ± 5 at the 90% confidence level. The computed rates, based on observations, should then be multiplied by factors of 1.33 $[(15+5)/15]$, 1.67 $[15+10]/15]$, or 2.0 $[(15+5)/15]$ with weights of: 0.185, 0.63, and 0.185, respectively.

TEMPORAL MODELS

The temporal distribution of the occurrence of field formation and of volcanic events is assumed to be homogeneous. Non-homogeneous models, such as the Weibull model, are not considered to be appropriate because of the low numbers of events and because such models are highly sensitive to the "start times" that are assumed. By examining the data for field formation during both the post-10 Ma and post-5 Ma periods, and the post-5 Ma period for events within volcanic fields, the assumption of a homogeneous process seems to be reasonable.

EVENT GEOMETRIES

The geometry of events is a function of the type of event being considered. Cone-type events (defined by a single cone) will have dike lengths that are typical of those measured in the San Rafael Swell by Delaney and Gartner (1995) [mean of 1.03 +1.74 - 0.65, log normal] and the field observations made in several basalt fields reported by Sheridan (1992) [2.5 km \pm 0.8 km, Gaussian]. For "lumped" events (defined as more than one cone or eruptive feature on a dike system), the distribution of event lengths is taken from the actual dimensions of volcanic features mapped in the region of interest. The mean length is 5 km and the lognormal variance ranges about +7 km to -3 km for the 90th and 10th percentiles. There is a \pm 25% uncertainty on the mean and on the standard deviation. These are models with weights of 0.185, 0.63, and 0.185. The event location on the dike will have a preference for the middle point and can be modeled by a triangular distribution.

Note: The resulting cumulative distributions and density functions for dike length are shown on Figure MS-3.

The interpretation of the orientation is also a function of the event type. For cone-type events, the dike orientation is parallel to the maximum horizontal compression direction (Pollard, 1987). This direction is N30E defined from earthquake focal mechanisms, in-situ stress measurements, and strain accumulation (Savage et al., in press). One standard deviation uncertainty is estimated to be \pm 20 degrees. In the case of "lumped" events, the orientation comes from the mean direction of observed surface features and is based on assumptions of Delaney et al. (1986). This methodology also gives a direction of N30E with a standard deviation of \pm 15 degrees.

HYDROMAGMATIC ACTIVITY

Hydrovolcanic explosions require a specific range of hydrologic and volcanic conditions (Sheridan and Wohletz, 1981; 1983). One of the best means of estimating the probability of hydrovolcanic events is to count the number of tuff rings and tuff cones relative to the scoria cones in volcanic fields (Wohletz and Sheridan, 1982). The number of tuff cones and scoria cones in Plio-Pleistocene volcanic fields in Arizona is tabulated by Lynch (1989). Low numbers of tuff cones and tuff rings (maars) also occur in the Lunar Crater and Cima volcanic fields. There are none in the 40-km-radius region of interest near Yucca Mountain. Given a dike injection in the vicinity of the site, the probability of a significant hydromagmatic explosion with a large volume of ejected materials (defined as more than 10^6 m³) is estimated at 0.01 - 0.02, or 1-2 maar or tuff cone for every 100 scoria cones. This estimate is based on the ratio of cone counts from scoria eruptions

versus those related to hydromagmatic processes within analogue regions in the southern Basin and Range.

TYPES OF ERUPTION

The most likely type of eruption expected in the future would be a small scoria cone and associated lava flows. In this type of event, roughly equal amounts of scoria (explosive products) and lava (effusive products) would total about 0.1 km^3 (order of magnitude) of magma. Another, but less probable, type of event would be the formation of a basaltic lava shield composed mostly of thin flows. Such volcanoes would have a volume of about 1.0 km^3 , but the probability of this type of event would be about 1/10 that of the small scoria cone. A third possibility would be a hydromagmatic explosion, with the formation of a crater and tuff ring with only about 0.01 km^3 of juvenile magma but about 0.1 km^3 of surrounding accidental material. The conditional probability of such explosions given a volcanic event would be about 0.01. A final possibility would be the eruption of more evolved magma to form an explosive ash-flow deposit of large volume. The conditional probability of such an event in the region of interest is estimated to be about 10^{-4} compared with that of a scoria cone and lava event.

Michael J Sheppard

5/16/96

REFERENCES

- Atwater, T., 1970, Implications of plate tectonics for the Cenozoic tectonic evolution of western North America: Geological Society of America Bulletin, v. 81, p. 3513-3536.
- Bursik, M., 1993, Subplinian eruption mechanisms inferred from volatile and clast dispersal data: Journal of Volcanology and Geothermal Research, v. 57, p. 57-70.
- Bursik, M., and Sieh, K., 1989, Range front volcanism in the Mono Basin, eastern California: Journal of Geophysical Research, v. 94, p. 15,587-15,609.
- Christiansen, R.L. and Lipman, P.W., 1972, Cenozoic volcanism and plate tectonic evolution of the western United States, II, late Cenozoic: Philosophical Transactions Royal Society London Series A, v. 271, p. 249-284.
- Connor, C.B., and Hill, B.E., 1993, Estimating the probability of volcanic disruption of the candidate Yucca Mountain repository using spatially and temporally non-homogeneous Poisson models: Proceedings, Site Characterization and Model Validation Focus '93 Symposium Volume, American Nuclear Society, La Grange Park, Illinois, p. 174-181.
- Crowe, B., Perry, F., Geissman, J., McFadden, L., Wells, S., Murrell, M., Poths, J., Valentine, G.A., Bowker, L., and Finnegan, K., 1995, Status of volcanism studies for the Yucca Mountain Site Characterization Project: Los Alamos National Laboratories Report LA-12908-MS, March 1995.
- Delaney, P.T., and Gartner, A.E., 1995, Physical processes of shallow mafic dike emplacement near the San Rafael Swell, Utah: U.S. Geological Survey Open-File Report 95-491, 47 p.
- Delaney, P.T., Pollard, D.D., Ziony, J.I., and McKee, E.H., 1986, Field relations between dikes and joints: Emplacement processes and paleostress analysis: Journal of Geophysical Research, v. 91, p. 4920-4938.
- Foshag, W.F., and Gonzalez, J., 1956, Birth and development of Paricutin Volcano, Mexico: U.S. Geological Survey Bulletin 965-D, 489 p.
- Ho, C.H., 1991, Time trend analysis of basaltic volcanism for the Yucca Mountain Site. Journal of Volcanology and Geothermal Research, v. 46, p 61-72.
- Langenheim, V.E., Kirchoff-Stein, K.S., and Oliver, H.W., 1993, Geophysical investigations of buried volcanic centers near Yucca Mountain, southwest Nevada: Proceedings, High Level Radioactive Waste Management Conference, Las Vegas, Nevada, American Nuclear Society, La Grange Park, Illinois, p. 1840-1846.

- Luedke, R.G., and Smith, R.L., 1981, Map showing distribution, composition, and age of late Cenozoic volcanic centers in California and Nevada: U.S. Geological Survey Miscellaneous Investigation Series Map I-1090-C.
- Lutton, R.J., 1968, Internal structure of the Buckboard Mesa basalt: *Bulletin of Volcanology*, p. 579-593
- Lynch, D.J., 1989, Neogene volcanism in Arizona: the recognizable volcanoes, *in* Jenny, J.P., and Reynolds, S.J. (eds), *Arizona Geological Society Digest*, v. 17, p. 681-700.
- Nealey, L.D., and Sheridan, M.F., 1989, Post-Laramide volcanic rocks of Arizona and northern Sonora, Mexico and their inclusions, *in* Jenny, J.P. and Reynolds, S.J. (eds), *Arizona Geological Society Digest*, v. 17, p. 609-647.
- Pollard D.D., 1987, Elementary fracture mechanics applied to the structural interpretation of dykes, *in* Halls, H.C. and Fahrig, W.F. (eds), *Mafic Dyke Swarms: Geological Association of Canada Special Paper 34*, p. 5-24.
- Savage, J.C., Lisowski, M., Scarc, J.L., and Gross, W.K., in press, Strain accumulation across the central Nevada seismic zone, 1973-1994: *Journal of Geophysical Research*.
- Schwartz, F.W., McGuire, R.K., Bullen, D.B., Cook, N., Coppersmith, K.J., Kemeny, J., Long, A., Pearson, F.J. Jr., Sheridan, M.F., and Youngs, R.R., 1991, Demonstration of a decision analysis methodology for assessing the performance of the Yucca Mountain site in southern Nevada: *Waste Management*, v. 11, p. 287-306.
- Sheridan, M.F., 1992, A Monte Carlo technique to estimate the probability of volcanic dikes: *Proceedings, High Level Radioactive Waste Management Conference, Las Vegas, Nevada, American Nuclear Society, La Grange Park, Illinois*, v. 2, p. 1840-1846.
- Sheridan, M.F., and Wohletz, K.H., 1981, Hydrovolcanic explosions, the systematics of water-tephra equilibrations: *Science*, v. 212, p. 1387-1389.
- Sheridan, M.F., and Wohletz, K.H., 1983, Explosive hydrovolcanism: basic considerations and review, *in* Sheridan, M.F., and Barberi, F. (eds), *Explosive Volcanism: Journal of Volcanology Geothermal Research*, v. 17, p. 1-29.
- Sigurdsson, H., 1987, Dyke injection in Iceland: A review, *in* Halls, H.C., and Fahrig, W.F. (eds.), *Mafic Dyke Swarms: Geological Association of Canada Special Paper 34*, p. 55-64.
- Smith, R.L., 1979, Ash-flow magmatism, *in* Chapin, C.E. and Elston, W.E. (eds), *Ash Flow Tuffs: Geological Society of America Special Paper 180*, p. 5-27.

Smith, R.L., and Bailey, R.A., 1968, Resurgent Cauldrons, *in* Coats, R.R., et al. (eds), *Studies in Volcanology*: Geological Society of America Memoir 116, p. 153-210.

Wells S.G., McFadden, L.D., Renault, C.E., and Crowe, B.M., 1990, Geomorphic assessment of late Quaternary volcanism in the Yucca Mountain area, southern Nevada: implications for the proposed high-level radioactive waste repository: *Geology*, v. 19, p 549-553.

Wohletz, K.H., and Sheridan M.F., 1982, Evolution of tuff cones and tuff rings: *American Journal of Science*, v. 283, p. 385-413.

Yogodzinski, G.M., and Smith, E.I., 1995, Isotopic domains and the area of interest for volcanic hazard assessment in the Yucca Mountain area: Abstract, *Eos, Transactions, American Geophysical Union*, 1995 Fall Meeting, p. F669.

**TABLE MS-1
 MICHAEL F. SHERIDAN - EVENT COUNTS**

EVENT COUNTS			
LOCATION	COUNTS (CONES)	WEIGHT	NOTES
Lathrop Wells	1	(0.9)	
	2	(0.1)	
Sleeping Butte	1	(0.67)	
	2	(0.33)	
1.0 Ma Crater Flat	1	(0.7)	
	2	(0.2)	
	3	(0.1)	
Buckboard Mesa	1	(0.75)	
	2	(0.05)	
	3	(0.05)	
	4	(0.05)	
	5	(0.05)	
	6	(0.05)	
3.7 Ma Crater Flat	1	(0.1)	
	2	(0.6)	
	3	(0.2)	
	4	(0.1)	
Amargosa Valley	5	(0.25)	
	6	(0.5)	
	7	(0.25)	
Thirsty Mesa	1	(0.9)	
	2	(0.033)	
	3	(0.034)	
	4	(0.033)	

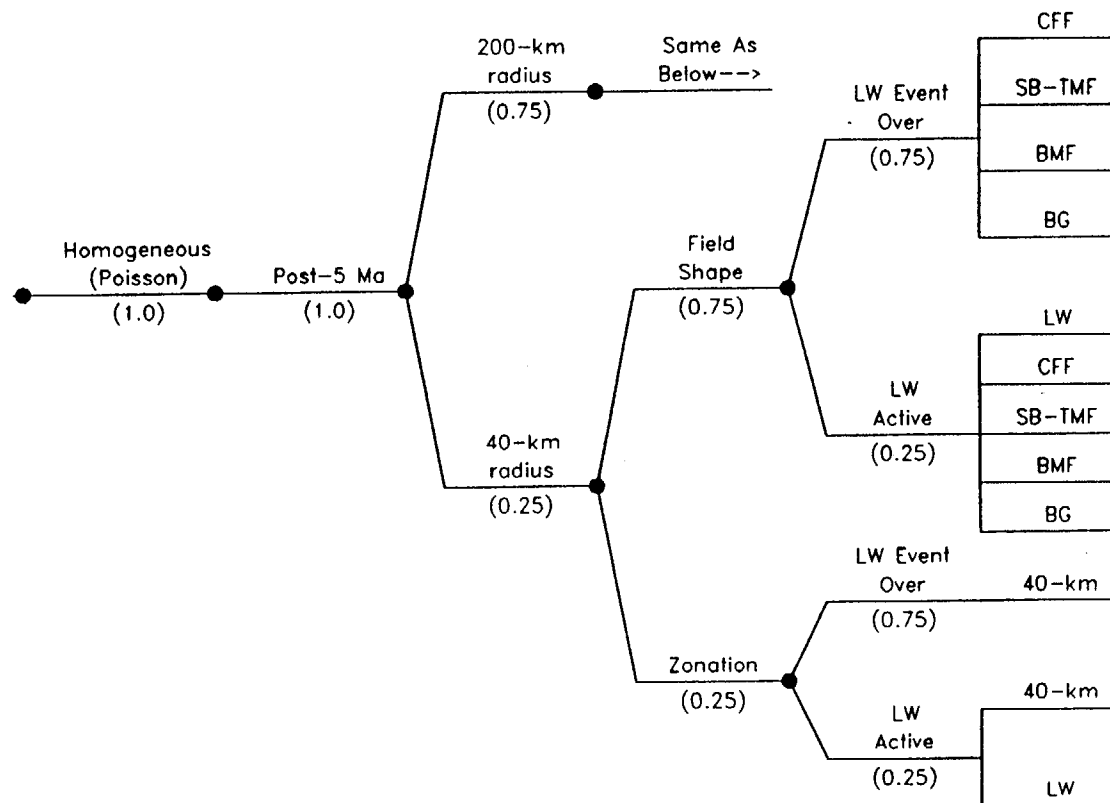
FIELD COUNTS

REGION	TIME PERIOD	COUNTS	WEIGHT
Within 200 km	Post 10 Ma	30	(1.0)
	Post 5 Ma	16	(1.0)
Within 40 km	Post 10 Ma	5	(1.0)
	Post 5 Ma	2	(1.0)

TABLE MS-2
MICHAEL F. SHERIDAN - RATES OF OCCURRENCE

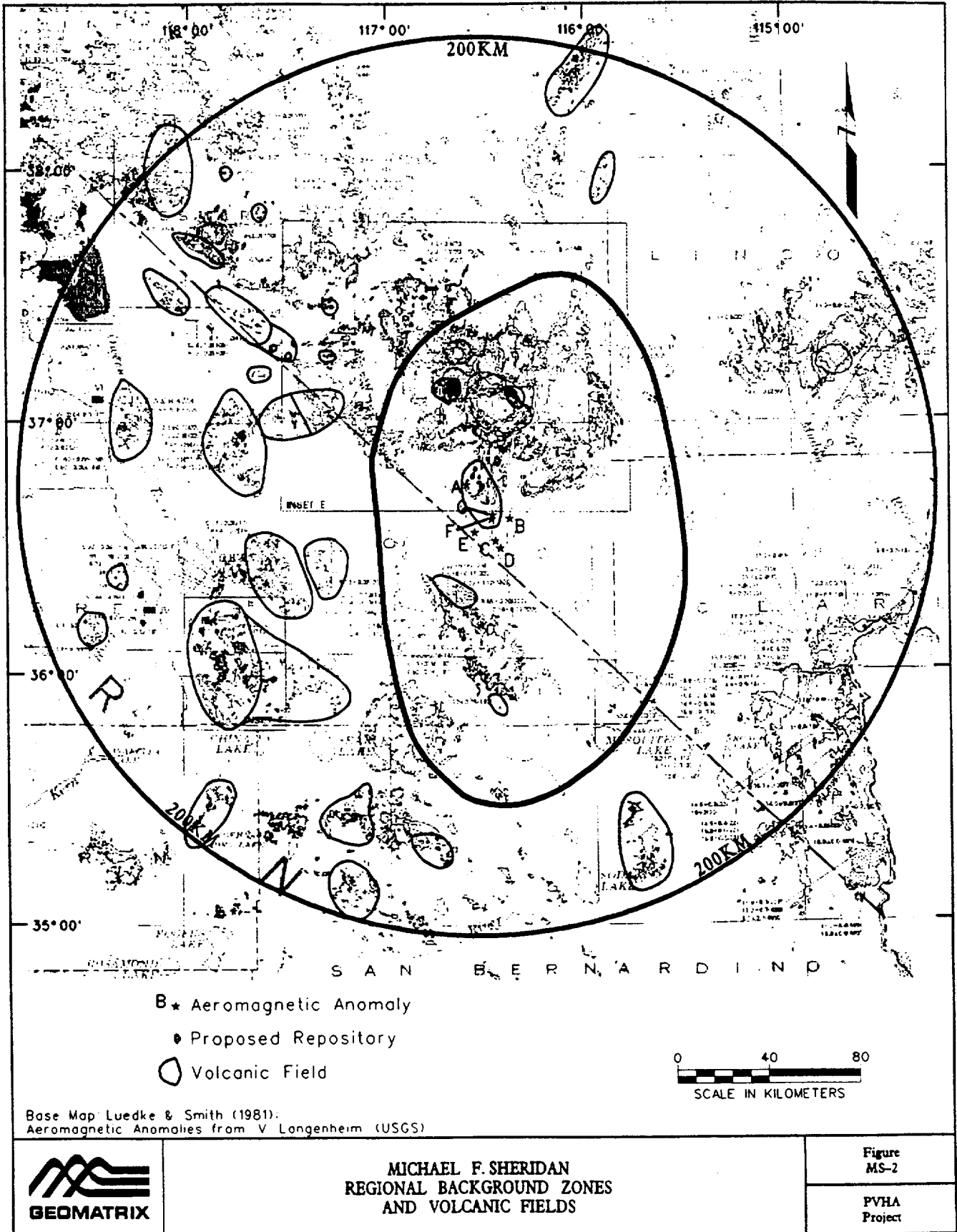
TIME PERIOD	COUNT METHOD FOR FIELDS	NOTES
5 MA (1.0)	CFF: (LW+3.7+NCF, AV) SBTMF: (SB+TM) BMF: (BM) 200 km: 10 Ma (0.75) 5 Ma (0.25) 40 km: 10 km (0.75) 5 Ma (0.25)	CFF: Crater Flat Field SBTMF: Sleeping Butte/Thirsty Mesa Field BMF: Buckboard Mesa Field NCF: Northern (1.0 Ma) Crater Flat 3.7: 3.7 Ma Crater Flat LW: Lathrop Wells TM: Thirsty Mesa SB: Sleeping Butte AV: Amargosa Valley BM: Buckboard Mesa 200 km: 200 km Radius 40 km: 40 km Radius

Temporal Models	Time Period	Region Of Interest	Spatial Model	Zonation Model	Sources
-----------------	-------------	--------------------	---------------	----------------	---------



CFF: Crater Flat Field
 SB-TMF: Sleeping Butte-Thirsty Mesa Field
 BMF: Buckboard Mesa Field
 LW: Lathrop Wells
 BG: Background

Figure MS-1 PVHA model logic tree developed by Michael F. Sheridan.



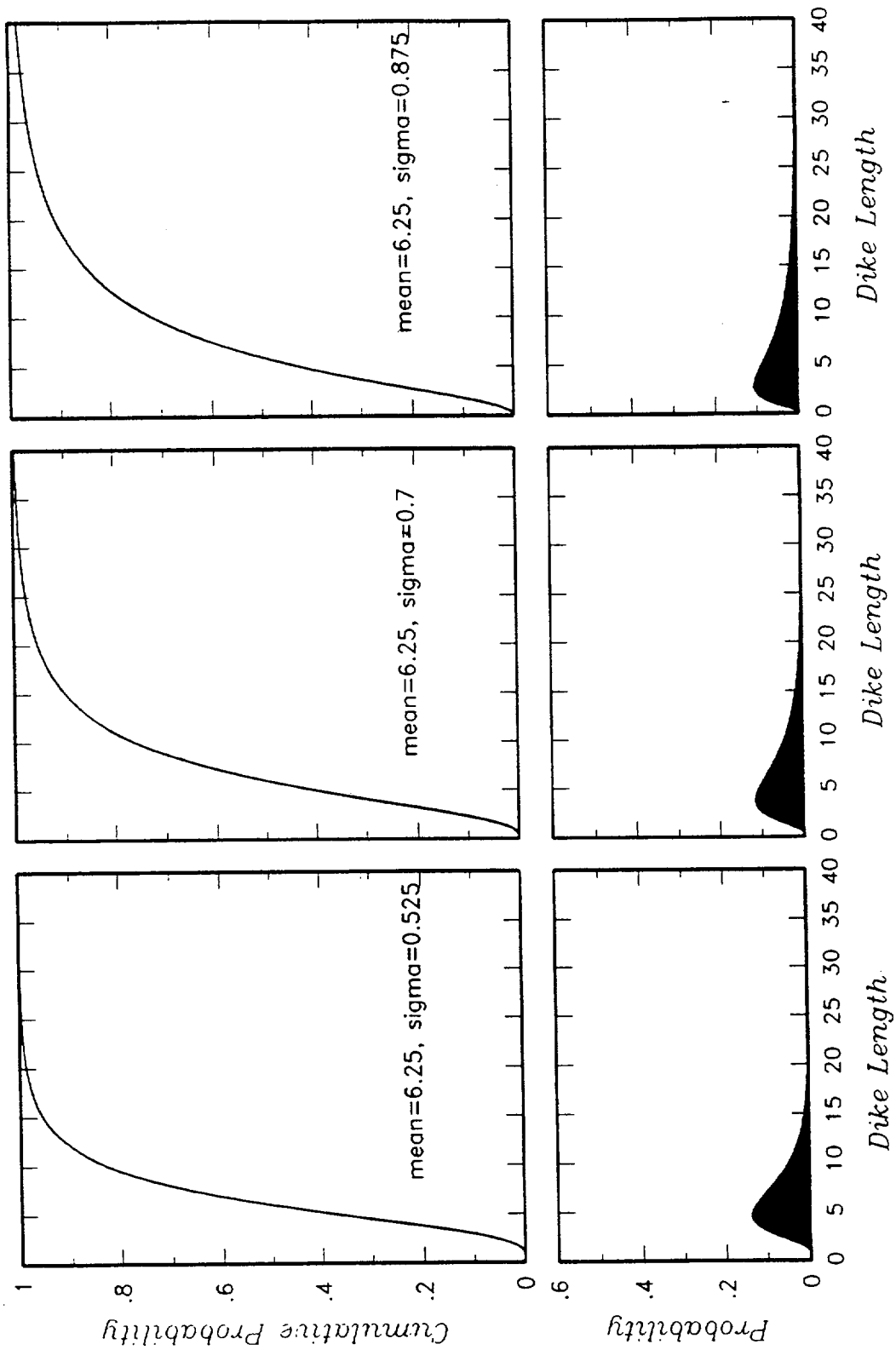


Figure MS-3 Dike length distribution developed by Michael F. Sheridan.

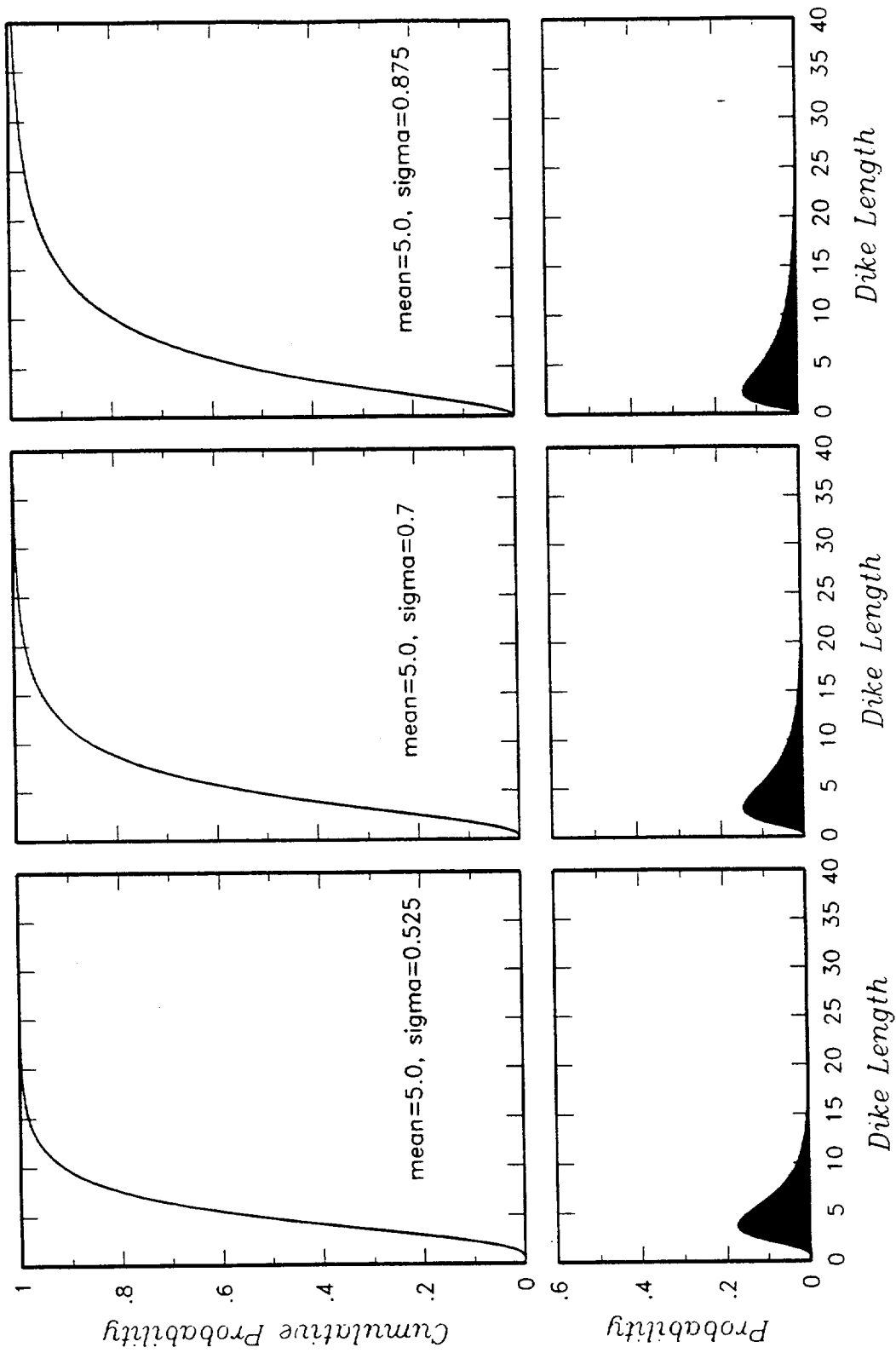


Figure MS-3 (Cont'd) Dike length distribution developed by Michael F. Sheridan.

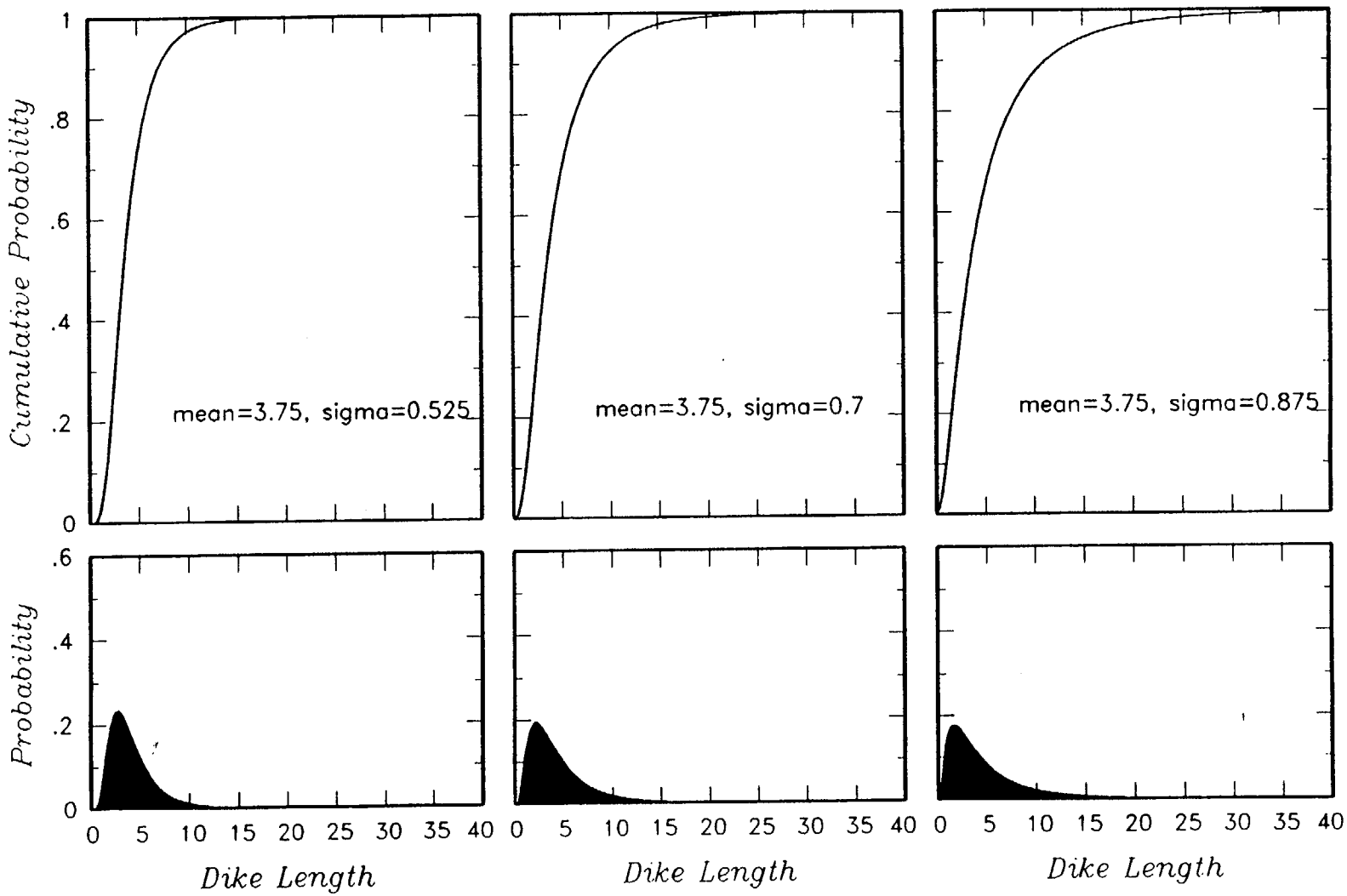


Figure MS-3 (Cont'd) Dike length distribution developed by Michael F. Sheridan.

GEORGE A. THOMPSON
ELICITATION INTERVIEW FOR PVHA PROJECT

VOLCANIC/TECTONIC SETTING

The Yucca Mountain region (YMR, defined as the region within a radius of about 50 km centered on Yucca Mountain) is located on the boundary between the Basin and Range province, characterized by extension, and the Walker Lane belt, characterized by oblique-normal and strike-slip movement. Most of the tectonism within the Basin and Range province appears to be nearly pure extension, expressed as either normal faulting or dike emplacement (strike-slip is locally important). The local picture in the region of interest (Bare Mountain, Crater Flat, Yucca Mountain) is consistent with the broad picture in this part of the Basin and Range: the cone alignment in northern Crater Flat is parallel to the maximum compressional stress direction of about NNE, and the Lathrop Wells cone lies at the southern end of Quaternary faults.

Dike emplacement and normal faulting both are mechanisms for accommodating regional extension. In places where magma supply is high, volcanism will occur; where supply is low, faulting will occur. In the same way that coseismic fault displacement relieves accumulated stress, dikes are emplaced quickly and extensional stresses are relieved. The Paiute Ridge area northeast of Yucca Mountain (Byers and Barnes, 1967; Crowe et al., 1995) provides insights into the interplay between normal faults and dikes. This area contains a complex graben, where about 0.5 km of erosion has exposed dikes and volcanic features. Some dikes are replaced by normal faults along strike, verifying that dike emplacement and faulting are both accomplishing net extension. The interspacing and dip of faults can provide information on the depth to the dikes.

A key part of the interpretation of the Basin and Range tectonics is the close temporal relationship between normal faulting and dike emplacement (Parsons and Thompson, 1991). Because both normal faults and dikes are relieving extensional stress, those areas with evidence of young faulting will often be associated with volcanism. For example, the Lathrop Wells cone erupted about 100,000 years ago just south of a series of faults that display evidence of multiple displacements in late Quaternary time (Frizzel and Shulters, 1990). In contrast, the faults within Bare Mountain do not show evidence of late Cenozoic displacement, and the most recent dikes are about 14 Ma (Monsen et al., 1992).

The southern end of Yucca Mountain has been rotated in a clockwise direction, based on paleomagnetic data (O'Neill et al., 1992). The left-lateral component of shear exhibited on the regional faults is consistent with a "book shelf type of deformation" imposed by the right-lateral regional shear of the Walker Lane. However, the extensional component of strain on these faults is the most important for accommodating regional extension.

Areas where active extension is occurring, as indicated by recent faulting and dike emplacement, are the most favorable sites for future volcanism. Inherently, extensional features tend to be concentrated in basins because normal faults that formed the basins generally dip inward and converge downward beneath the basins. During the past 2 my, fault rupture has occurred on several faults in the vicinity of Yucca Mountain, including the Solitario Canyon and Bow Ridge faults. The preferred orientation of dikes is roughly parallel with the trends of active fault systems. It is unlikely that future volcanism will occur within structural blocks that have not been faulted in the late Cenozoic. The proposed repository site in the Yucca Mountain block has revealed no evidence of late Cenozoic faulting, and is much less likely to be disrupted than faulted areas to the south. The Lathrop Wells area is the most likely site for future volcanism, as the area contains a temporal association between recent faulting and volcanism. Specifically, faults responding to the regional stress system could be underlain by dikes that have erupted at Lathrop Wells. In contrast, the Bare Mountain block exhibits no internal evidence of late Cenozoic activity other than tilting and is considered to have a low potential for future volcanism. The Bare Mountain fault is roughly parallel to the 14 Ma dikes in the area.

EVENT DEFINITION

Temporal Aspects

A volcanic event occurs within the time required to solidify a feeder dike, roughly on the order of a few years (it is acknowledged that rapid continuous flow with accompanying heat input may prevent solidification). In some cases where multiple dikes are emplaced as part of a dike set and where multiple cones are formed, the time may be as long as several hundred years. The short time period is due to the lack of crustal storage and the short time it takes to freeze a basaltic dike. It is acknowledged that available age dating methods do not allow sufficient resolution to differentiate between two events separated by less than several thousand years. This uncertainty is accounted for in estimating the number of events at any given volcanic center.

Spatial Aspects

Generally, an event has dimensions associated with the length of a dike, which is about 1 to 5 km. In some cases, a dike set may be as long as 10 to 15 km. The cones in northern Crater Flat may be related to a single event and, if so, would represent an event with a length of 12 km. Most likely, such an event would be the result of a set of dikes, and not a single dike. Longer event lengths would require significantly larger volumes than observed or expected in the YMR.

Geochemical Affinity

The geochemistry of volcanic deposits can provide useful information on the magma source (e.g., depth) and residence time in the crust. However, geochemistry is not judged to be particularly useful in identifying individual events.

Note: The elements of the PVHA model are summarized in the form of a logic tree in Figure GT-1.

REGION OF INTEREST

The region of interest is the area defined as the Amargosa Valley Isotopic Province (AVIP) by G. Yogodzinski (presentation at PVHA Workshop 3). This area includes young faults, and the isotopic data may distinguish between crustal and mantle sources. The isotopic data suggest a common magma source for the AVIP that is distinct from surrounding regions.

An alternative region of interest is that defined by a 200-km radius from Yucca Mountain, as characterized by M. Sheridan (presentation at PVHA Workshop 4). The alternative zone includes several volcanic fields that are distinct from those in the YMR. As discussed below, the number of fields in the 200-km region is used to define the rate of occurrence of volcanism within this region.

The 200-km radius captures basalt vent clusters or fields within the age range of 0-5 Ma, which tend to be spaced roughly 50-100 km apart (Luedke and Smith, 1981); this is also the scale of lithosphere dimensions. From a geophysical perspective the spacing may reflect withdrawal of heat and magma from widespread incipient melt in the Basin and Range mantle; that is, a critical volume of melt needs to be gathered from an extended area in order for it to rise into and through the crust. The probability of eruptions between fields may be much diminished because of depletion of magma and heat.

The regions of interest defined by the AVIP and by the 200-km radius serve as "background" zones in the PVHA. The relative weight given to the background alternatives are: AVIP (0.7), radius approach (0.3). The AVIP approach is preferred because it takes into account the geologic characteristics of the volcanic fields in the region.

A "local region of interest" is also defined, as discussed below in the context of source zones.

SPATIAL MODELS

The spatial model that is used is a zonation of the region into zones that have different rates of occurrence of volcanic events. The basis for these zones comes from a consideration of age of tectonism and the style (i.e., volcanism versus faulting).

The background zones are described above in the section on the region of interest. These zones are regional in extent and serve to provide a regional rate of occurrence of volcanism in the part of the Basin and Range province of significance to the site.

Within the background zone, three local zones are assessed. The first is a Local Domain zone (Figure GT-2), which encloses an area south of the Timber Mountain caldera complex and east of the Bare Mountain uplifted block, and encloses the uplifted Yucca Mountain block and the Amargosa Valley. It is not judged to be appropriate for the Local Domain zone to include the Sleeping Butte region to the northwest because of the large spatial separation with Crater Flat. This separation has persisted for at least the past 8 my, suggesting that the two areas are separate volcanic fields.

Within the Local Domain are the "Volcanic Domain" zone, which includes the Quaternary volcanoes of Crater Flat and Lathrop Wells, as well as the Pliocene events in the Amargosa Valley, and the "Quaternary Faulting Domain," which includes the Quaternary faults in the YMR. These two local zones are interpreted to represent two different mechanisms for accomplishing extension: extension by dike emplacement and by normal faulting. The two domains overlap in the region of the 3.7 Ma volcanics, suggesting that Quaternary faulting replaced volcanism as the primary mechanism for extension in this region. The boundaries of the two sources differ, depending on the time period being considered. When the 1 Ma time period is considered, faulting is the controlling process in the area of overlap, and the source zones are the Quaternary Faulting Domain and that portion of the Volcanic Domain lying outside the Quaternary Faulting

Domain. When the 4 Ma time period is considered, volcanic processes are dominant in the area of overlap, and the source zones are the Volcanic Domain and the area of the Quaternary Faulting Domain outside the Volcanic Domain. The eastern edge of the Volcanic Domain may represent a hard boundary, or the rate density will decay linearly over a distance of 5 km. The relative weights assigned to these two models are: hard boundary (0.67) and transition zone (0.33).

EVENT COUNTS

Based on the definition of volcanic "events" given earlier, the number of events and their uncertainties are assessed for each of the centers in the region (Table GT-1). The number of events is assessed for the past 4 my, which is judged to be the time period of most relevance to estimates of future hazard. In addition, the event counts are assessed for the past 1 my.

Lathrop Wells

The relationships at Lathrop Wells suggest from 1 to 4 events (Crowe et al., 1995); one event is preferred simply because most of the volume is attributed to one event and age dates do not unequivocally separate the events. Spatially, all of the deposits occurred at essentially the same place; therefore, differences in timing are the most important aspects in defining separate events (recall that geochemical differences are not relied on for identifying events). The radiometric age estimates are very uncertain, but stratigraphic and soils evidence are suggestive of satellite eruptions that may have been well separated in time.

The following event counts and their relative weights are assigned for the Lathrop Wells center: 1 (0.75), 2 (0.08), 3 (0.08), and 4 (0.08).

1.0 Ma Crater Flat

The 1 Ma basalts of northern Crater Flat may represent 1 to 5 events, with 4 events most likely. Stress changes could have resulted in pulses of small-volume eruptions that formed cones propagating towards the NE. Possible connecting dikes, if only a meter or so in width, will be difficult to identify in the subsurface because magnetic surveys can resolve them only to a depth of a few meters in the presence of background noise (basalt flows and float in the area).

In the 2-event scenario, the Makani Cone is considered a separate event (based on distance) from the combined event represented by the Black, Red, and Little Cones to the south. For the 3-event scenario, Red and Black cones are combined and Makani and Little Cones each represent separate

events. For the 4-event scenario, Makani, Red, Black and Little Cones each represent separate events; for 5 events, Little Cone represents 2 events.

The following event counts and their relative weights are assigned for northern Crater Flat: 1 (0.2), 2 (0.15), 3 (0.1), 4 (0.5), and 5 (0.05).

3.7 Ma Crater Flat

The 3.7 Ma basalts are most likely to represent 1 or 2 events that have subsequently been disaggregated by local faulting, erosion, and alluvial deposition (Crowe et al., 1995). The center seems to be more voluminous than other centers in the region. The dike feeders appear to have an orientation of N-S to NNE. There is no strong evidence for more than 1 event; however, up to 6 events could be represented, as described by Crowe et al. (1995, p. 7-31).

The following event counts and their relative weights are assigned for the 3.7 Ma area of Crater Flat: 1 (0.4), 2 (0.5), 3 (0.04), 4 (0.03), 5 (0.02), and 6 (0.01).

Amargosa Valley

Five to 7 events might be represented in Amargosa Valley based on interpretation of aeromagnetic anomalies (V. Langenheim presentation at PVHA Workshop 1). The most likely scenario of 5 events is based on the interpretation that anomalies A, B, C, D, and E (on the aeromagnetic map presented by V. Langenheim at PVHA Workshop 1) are cones, as indicated by their strong, bipolar aeromagnetic signatures. Interpretation of the origin of anomalies F and G is more uncertain.

The following event counts and their relative weights are assigned to the Amargosa Valley area: 5 (0.9), and 7 (0.1).

RATES OF OCCURRENCE

Using the event counts discussed above, the rates of occurrence are established for use in the PVHA. These rates are calculated over various time periods and for particular source zones (see summary in Table GT-2).

For the Volcanic Domain zone and the Quaternary Faulting Domain zone, rates are calculated over two time periods: the past 1 my and the past 4 my. Higher weight is given to the past 4 my (0.7)

than 1 my (0.3) because this includes a period of significant volcanism at 3.7 Ma. However, the past 1 my is probably more significant to the period of Quaternary faulting.

In assessing rates for the post-4 Ma time period, the counts for the regional background zones are assumed to be those estimated by Crowe et al. (1995) for AVIP and by Sheridan for the 200-km radius circle (M. Sheridan presentation at PVHA Workshop 4). The Local Domain outside of the Quaternary Faulting and Volcanic domains is assumed to have a rate comparable to the background zones. The Volcanic Domain rates are based on counts for the 1 Ma area of Crater Flat, the 3.7 Ma area, Lathrop Wells, and Amargosa Valley. For the post-1 Ma period, the Quaternary Faulting Domain includes the area of the 3.7 Ma basalts of Crater Flat, but, because they are older, does not include additional event counts. The rate for the Quaternary Faulting Domain is based on the relative likelihood of undetected events in the two domains discussed below. That is, the rate in the Quaternary Faulting Domain is 0.1 times the rate of the Volcanic Domain.

Undetected Events

In addition to those events identified and interpreted at the surface, there is the potential for undetected, or subsurface, events that might exist at depths of less than 300 m (depth of the proposed repository) but not be represented at the surface.

In the YMR, the surface distribution of dikes may not be a good indicator of dike distribution at depths of about 1 km; dikes could extend to within a few hundred meters of the ground surface but not be exposed at the surface. The spacing of dikes (exposed or within about 1 km of the surface) may be equivalent to the 1-km spacing of faults in the YMR. Dike conduits may not be vertical (Parsons and Thompson, 1991). In addition to dikes, sills may be present in the area, but formation of sills is most likely when the magma supply exceeds the amount of regional extension that is accommodating dike emplacement. This is unlikely to be the case in the YMR, where magma volumes are low.

The number of undetected events is judged to be different in the Volcanic Domain and the Quaternary Faulting Domain. In the Volcanic Domain, no extensional features (e.g., faults) that could indicate the presence of undetected or buried dikes have been observed in the Crater Flat area, suggesting that the level of resolution is too low to identify these features (Frizzel and Shulters, 1990; T. Brocher, pers. comm., 1995). It is estimated that there is approximately equal probability that the number of undetected events in the domain ranges from zero to equal to the

number of observed events (0.5 and 0.5 probabilities, respectively). Recent seismic reflection results show continuous, unbroken basalt of 3.7 Ma under western Crater Flat, indicating no Quaternary fault activity (T. Brocher, pers. comm., 1995).

In the Quaternary Faulting Domain, the number of undetected events is expected to be far less than the Volcanic Domain. This is supported by the small number of events observed within this domain over the past 10 my, despite the fact that this region has been uplifted and eroded (the 11 Ma dike in Solitario Canyon may represent such an event). The author has been a reviewer of the T. Brocher manuscript describing the analysis of the 1995 deep reflection seismic line across Crater Flat. Within the resolution of the reflection data (a few meters) the 3.7 Ma basalt reflection is unbroken and thus precludes Quaternary fault offsets in that part of Crater Flat. The reflection data generally support the earlier gravity and refraction seismic modeling of the subsurface structure of Crater Flat by Langenheim et al. (1991) but add considerably to the resolution and to the depth variation of the basement surface. The ages of several faults are constrained to be pre-Quaternary. It is estimated that the ratio of undetected events in the Quaternary Faulting Domain relative to the Volcanic Domain is 1:10.

TEMPORAL MODELS

Two start times are assessed for the Volcanic Domain and the Quaternary Faulting Domain zones: 1 Ma and 4 Ma, with probabilities of (0.3) and (0.7), respectively. A homogeneous temporal Poisson model is assumed because this model adequately fits the data.

EVENT GEOMETRIES

Event lengths and widths should be consistent with the dike data reported by Delaney and Gartner (1995): 1 to 5 km long and 1.1 m wide. The dike length data were compiled by Delaney and Gartner for mafic dikes and are considered to be good analogs to the YMR (relative to the very long lengths of dike swarms present in the northern Nevada Rift, Canadian shield areas, etc.). Because the magma volumes in the YMR are expected to be small volumes, volcanic events are expected to be essentially single basaltic dikes. However, it is also possible, but improbable, that some events will be represented by multiple dikes forming a dike set. The maximum length of such a dike set is 10 to 12 km, such as that possibly represented by the volcanoes in northern Crater Flat. Ninety percent of the probability density lies between an event length of 1 to 5 km; a low probability tail exists out to lengths of 10 to 12 km. Equal weights (0.5 and 0.5) are given

to maximum lengths of 10 and 12 km. Events are assumed to be more likely to occur near the center of dikes, and a triangular distribution is used to model event geometries.

Note: At the request of Dr. Thompson, a smooth interpolation function was fit to his discrete cumulative density estimates for dike length. The resulting cumulative distributions and density functions are shown on Figure GT-3.

Dike orientations are consistent with the maximum horizontal stress orientations inferred from earthquake focal mechanisms and in-situ stress measurements (e.g., Stock and Healey, 1988). A N30°E direction is preferred, plus or minus 15 degrees (95% interval).

HYDROMAGMATIC ACTIVITY

A shallow water table and the proper overburden of rock is necessary to generate a significant hydromagmatic explosion. Where such conditions are favorable, about 1 in 1,000 eruptions will show significant hydromagmatic activity. Given the conditions of a low water table at the site, the chances are 1 in 1,000,000.

TYPE OF ERUPTION

The most likely style of future volcanism is the type that has occurred in the past 4 Ma in the region. The termination of silicic volcanism is clearly linked to the change in the subducting plate margin, and therefore, is very unlikely to reoccur. The evidence suggests that the recent volcanism is related to magmas coming from the mantle, and there is no evidence for crustal melts that would give rise to rhyolitic domes.

George C. Thompson 4-15-96

REFERENCES

- Byers, F.M., Jr., and Barnes, H., 1967, Geologic map of the Paiute Ridge quadrangle: U.S. Geological Survey Map GQ-577.
- Crowe, B.M., Perry, F.V., Geissman, J., McFadden, L., Wells, S., Murrell, M., Poths, J., Valentine, G.A., Bowker, L., and Finnegan, K., 1995, Status of volcanism studies for the Yucca Mountain site characterization projects: Los Alamos National Laboratory Report LA-12101-MS, March 1995.
- Delaney, P.T., and Gartner, A.E., 1995, Physical processes of shallow mafic dike emplacement near the San Rafael Swell, Utah: U.S. Geological Survey Open-File Report 95-491, 47 p.
- Frizzel, V.A., Jr., and Shulters, J., 1990, Geologic map of the Nevada Test Site, southern Nevada: U.S. Geological Survey Miscellaneous Investigations Series Map I-2046.
- Langenheim, V.E., Carlé, S.F., Ponce, D.A., and Phillips, J.D., 1991, Revision of an aeromagnetic survey of the Lathrop Wells area, Nevada: U.S. Geological Survey Open-File Report 91-46.
- Luedke, R.G., and Smith, R.L., 1981, Map showing distribution, composition, and age of late Cenozoic volcanic centers in California and Nevada: U.S. Geological Survey Miscellaneous Investigations Series Map I-1091-C.
- Monsen, S.A., Carr, M.D., Reheis, M.C., and Orkild, P.P., 1992, Geologic map of Bare Mountain, Nye County, Nevada: U.S. Geological Survey Miscellaneous Investigations Series Map I-2201.
- O'Neill, J.M., Whitney, J.W., and Hudson, M.R., 1992, Photogeologic and kinematic analysis of lineaments at Yucca Mountain, Nevada: Implications for strike-slip faulting and oroclinal bending: U.S. Geological Survey Open-File Report 91-623, 24 p.
- Parsons, T., and Thompson, G.A., 1991, The role of magma overpressure in suppressing earthquakes and topography: worldwide examples: *Science*, v. 253, p. 1399-1402.
- Stock, J.M., and Healy, J.H., 1988, Stress field at Yucca Mountain, Nevada, *in*, Carr, M.D., and Yount, J.C., eds., Geologic and hydrologic investigations of a potential nuclear waste disposal site at Yucca Mountain, southern Nevada: U.S. Geological Survey Bulletin 1790, p. 87-93.

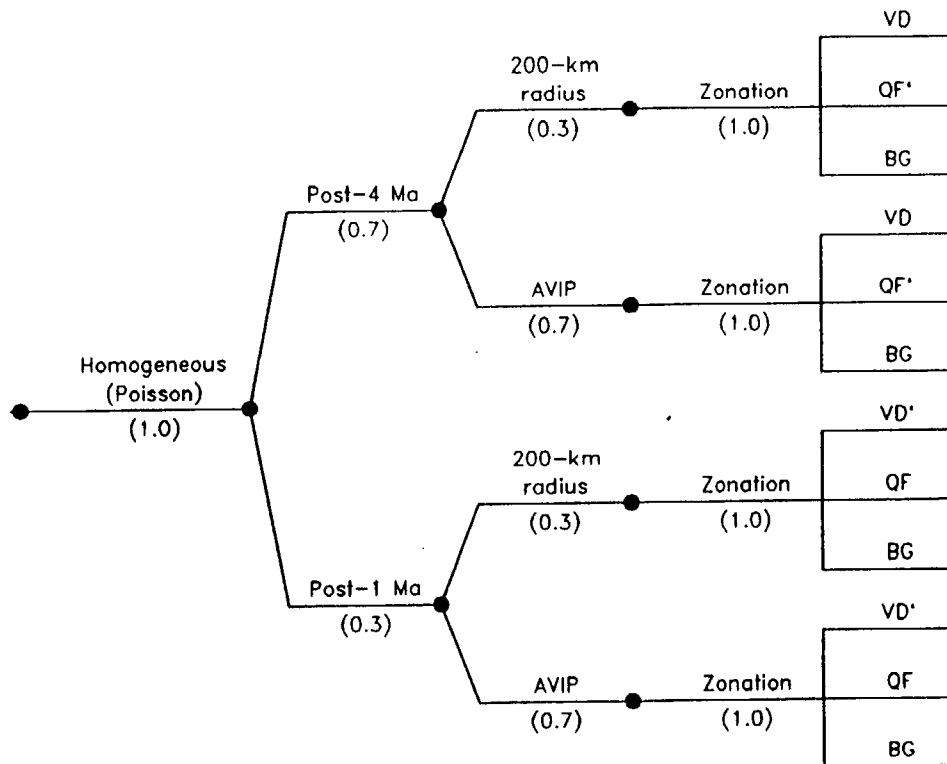
**TABLE GT-1
 GEORGE A. THOMPSON - EVENT COUNTS**

LOCATION	COUNTS (CONES)	WEIGHT	NOTES
Lathrop Wells	1	(0.75)	BC: Black Cone LC: Little Cones 2LC: 2 separate Little Cones M: Makani Cone RC: Red Cone SB: Shoreline Butte SC: Split Cone
	2	(0.09)	
	3	(0.08)	
	4	(0.08)	
Sleeping Butte	1	(0.35)	
	2	(0.65)	
1.0 Ma Crater Flat	1 (all)	(0.2)	
	2 (LC+RC+BC, M)	(0.15)	
	3 (LC, RC+BC, M)	(0.1)	
	4 (LC, RC, BC, M)	(0.5)	
	5 (2LC, RC, BC, M)	(0.05)	
Buckboard Mesa	1	(0.7)	
	2	(0.3)	
3.7 Ma Crater Flat	1	(0.4)	
	2	(0.5)	
	3	(0.04)	
	4	(0.03)	
	5	(0.02)	
	6	(0.01)	
Amargosa Valley	5	(0.9)	
	7	(0.1)	
Background 200 km radius	16 in 5 Ma	(1.0)	
Background AVIP (1 Ma)	1 in 1 Ma (SC)	(1.0)	
Background AVIP (4 Ma)	2 (SC+SB)	(0.35)	
	3 (SC+2SB)	(0.35)	
	4 (SC+3SB)	(0.30)	

**TABLE GT-2
 GEORGE A. THOMPSON - RATES OF OCCURRENCE**

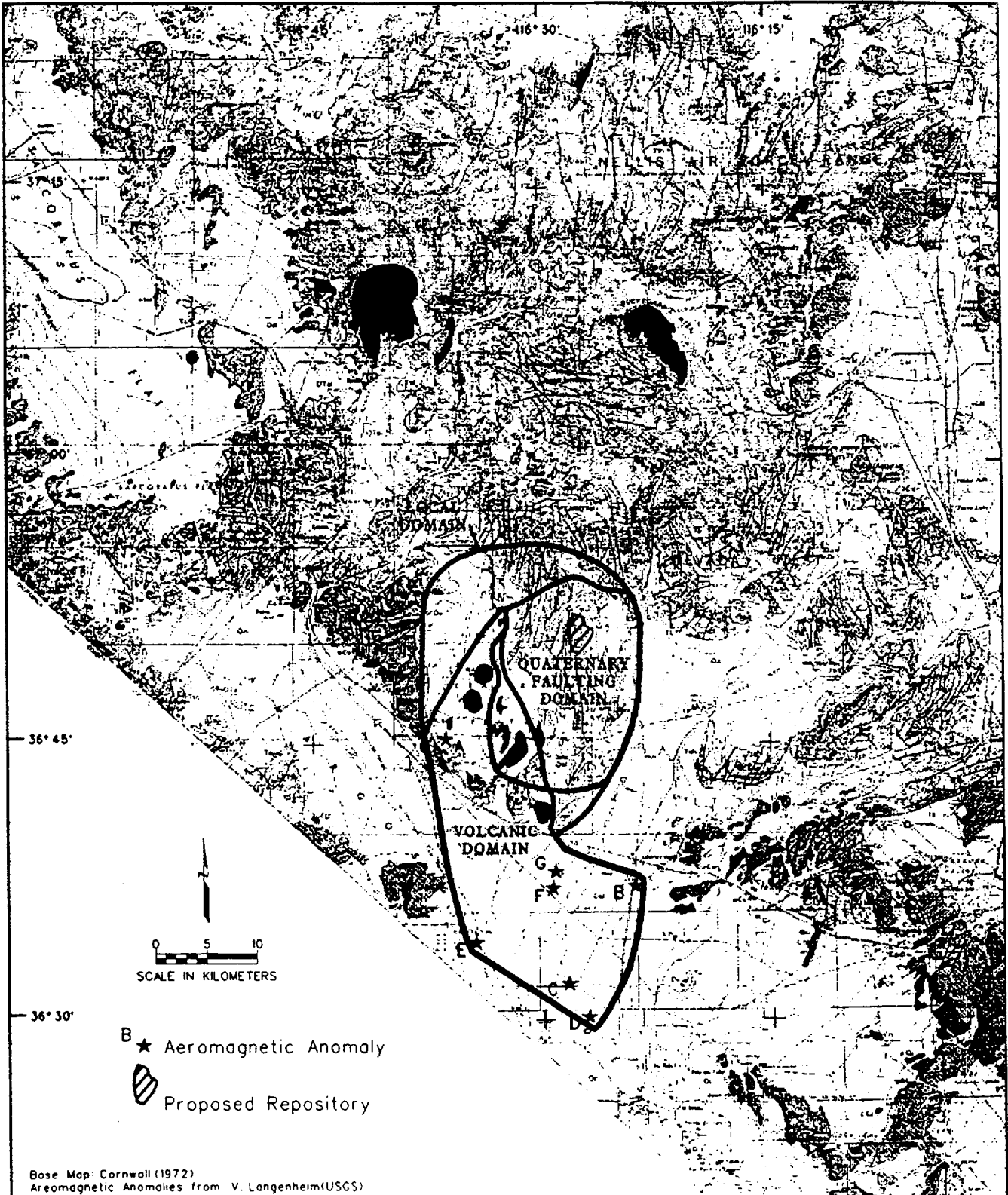
TIME PERIOD	COUNT METHOD FOR ZONES	NOTES
Post 1 Ma (0.3)	VD: (LW+NCF) QFD: 1/10 VD B200 km: (200 k) BAVIP: (SB+DV1)	AV: Amargosa Valley BAVIP: Background, Amargosa Valley Isotopic Province B200 km: Background, 200 km Radius BM: Buckboard Mesa DV1: Death Valley 1 Ma DV4: Death Valley 4 Ma LW: Lathrop Wells NAVIP: Northern Amargosa Valley Isotopic Province of Yogodzinski (1995)
Post 4 Ma (0.7)	VD: (LW+NCF+3.7+AV) QFD: 1/10 VD B200 km: (200 k) NAVIP: (SB+BM+DV4)	NCF: Northern (1.0 Ma) Crater Flat QFD: Quaternary Faulting Domain SB: Sleeping Butte VD: Volcanic Domain 3.7: 3.7 Ma Crater Flat 200 km: 200 km Radius Field Counts

Temporal Models	Time Period	Region Of Interest	Spatial Models	Sources
-----------------	-------------	--------------------	----------------	---------



VD: Volcanic Domain
 QF: Quaternary Faulting Domain
 VD': Volcanic Domain Outside of Quaternary Faulting Domain
 QF': Quaternary Faulting Domain Outside of Volcanic Domain
 BG: Background

Figure GT-1 PVHA model logic tree developed by George A. Thompson.



Base Map: Cornwall (1972)
Aeromagnetic Anomalies from V. Langenheim (USGS)

	GEORGE A. THOMPSON LOCAL ZONES	Figure GT-2
		PVHA Project

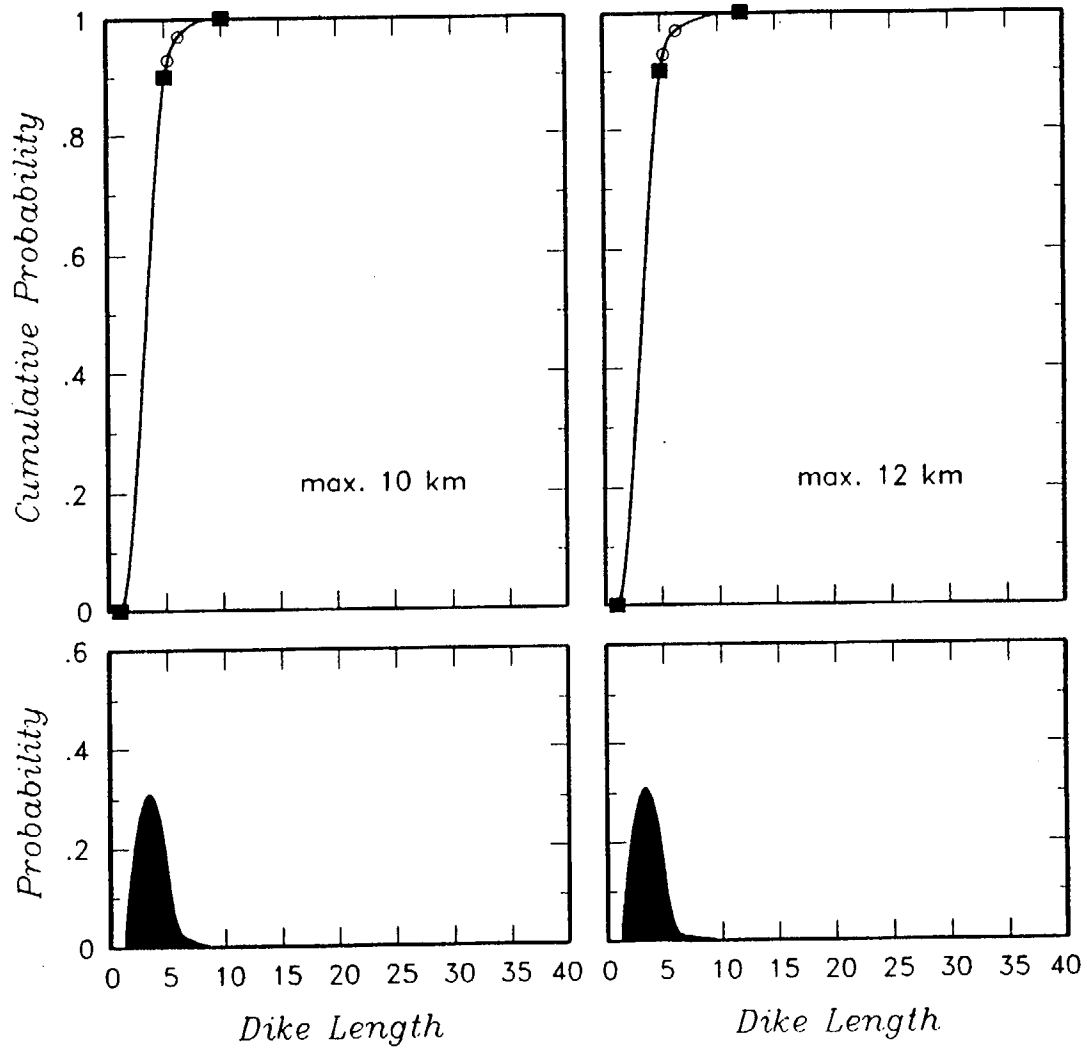


Figure GT-3 Dike length distribution developed by George A. Thompson.

GEORGE P.L. WALKER
ELICITATION INTERVIEW FOR PVHA PROJECT

VOLCANIC/TECTONIC SETTING

The presence of volcanoes in the region of interest (discussed below) indicates that a melting anomaly is present in the underlying mantle. Melting anomalies are characteristic of the Basin and Range province. These anomalies can occur from a section of mantle that is hotter than usual, or from an unusually shallow section of mantle in which melt is generated by the lowering of external pressure or from the presence of water in the mantle. Melting anomalies are accompanied locally by volcanism. The Basin and Range province has been subject to large-scale extension, with volcanism a direct result. In addition, a kind of mantle plume likely underlies the region (mantle plumes have dimensions of about 1000 to 2000 km), and scores of melting anomalies can be associated with a single plume.

The Crater Flat area is a volcanic field, but is not well defined relative to many other fields in the world. Structural control is indicated by the alignment of Makani, Red, Black, and Little Cones, but it is difficult to assess the extent to which orientation is a function of structure or the shape of the melting anomaly. Melting anomalies have a minimum size, comparable to the local thickness of the lithosphere (probably a few tens of kilometers in the region of interest). Within a melting anomaly there may be local areas, or "nodes," where there are higher magma generation rates and a higher potential for future volcanism. The NNE-trending Death Valley-Pancake Range (DV-PR) volcanic belt proposed by Smith et al. (1990) could trace the form of a melting anomaly, or it may be a tectonic line of some type (e.g., a major deep-seated fault). This belt, which extends from Death Valley to Lunar Crater, has been operative for the past 12 my, and appears to have a few "nodes," or fields, of more active volcanism due, most likely, to higher magma generation rates. There is no need to fill in the "gaps" between nodes of a melting anomaly through time. A ~10 my time frame is a typical lifetime for a melting anomaly, although they may also last much longer, such as the Hawaiian hotspot anomaly that has been active for at least 80 my.

The volcanism in the Crater Flat area is of monogenetic type. At the scale of the ascent of basaltic dikes, the recurrence of an eruption at the same location is purely random. Once a dike has cooled, there is no advantage for a new dike to follow the same path as the earlier dike, but there is some probability that it will coincide with it randomly. In general, however, the occurrence of

polygenetic volcanism is due to an advantage in the ascent of magma at the same location and utilizing the same conduit (or pathway). The physical model for polygenetic volcanism should attempt to explain this advantage (G. Walker presentation at PVHA Workshop 4, summary notes).

EVENT DEFINITION

Temporal Aspects

A volcanic event is equivalent to a volcanic eruption, consisting of the ascent of magma, and one or more episodes of surface eruption, followed by crystallization of the basaltic dike. Observation of this process elsewhere suggests that it lasts, at most, ten to a few tens of years. Among historical eruptions in monogenetic fields and flood basalts, that of Heimaey (Iceland) lasted about one month, and those of Laki (Iceland, 1783) and Capelinhos (Faial, Azores, 1957-58) about one year. Eruptions that lasted several years include Lanzarote (Canary Islands, 1730-36), Paricutin (Mexico, 1943-52), and El Jorullo (Mexico, 1759-74). At Krafla (Iceland) in 1978-84, a series of short rifting and eruptive episodes punctuated the general period of strong ground deformation that lasted from 1978 to 1984, and can be regarded collectively as a single magmatic event. There also are a few basaltic volcanoes (e.g., Stromboli and Etna) that show persistent activity spread over centuries; such volcanoes are rare.

Spatial Aspects

Dikes in monogenetic fields are typically less than 3 km long. Looking at modern fields, one can find alignments of cones that extend for 3 km or more. It is not clear whether these alignments are related to one dike or to a set of dikes. Areas of flood-basalt volcanism, such as Iceland and the eastern Snake River Plain, where 30-km-long dikes occur, are not good analogs to the Yucca Mountain area because of their much higher magma generation and eruption rates. There are, however, monogenetic volcanic fields where dikes exceed 3 km. Perhaps the best example is Lanzarote (Canary Islands), where a crater row 14 km long formed in the eruption of 1730-36. It is conceivable, but unlikely, that an event in the region of interest might extend over dimensions as large as this.

Geochemical Affinity

The geochemical and mineralogical affinity among volcanic deposits are clearly very important in identifying volcanic events.

Note: The elements of the PVHA model are summarized in the form of a logic tree in Figure GW-1.

REGION OF INTEREST

The region of interest is the area defined as the DV-PR volcanic belt by Smith et al. (1990). This belt, which extends from Death Valley to Lunar Crater, has shown persistent activity over the past 12 my and contains nodes of activity, such as Crater Flat and Lunar Crater, where volcanism has been more concentrated and is likely to continue to be active.

Within the DV-PR belt, a node of volcanism identified as the Crater Flat volcanic zone (CFVZ) (defined by Crowe and Perry, 1989) is particularly significant for this hazard analysis (Figures GW-2 and GW-3). Over the past 4.6 my, no significant changes in the volume or position of eruptions in the CFVZ have occurred and all eruptions have occurred within the zone. Over this time period, there is no strong evidence to indicate whether the volcanic system in the region is waning or waxing.

SPATIAL MODELS

Three alternative models are used to assess the future locations of volcanic activity in the Yucca Mountain area. These models and their weights are as follows:

Zonation	(0.1)
Field Shape	(0.4)
Spatial Smoothing	(0.5)

In the zonation approach, two zones are identified that are interpreted to have different rates of occurrence. These zones are the CFVZ, which is extended to include the Amargosa Valley aeromagnetic anomalies, and the background zone that is drawn to represent the "node" within the DV-PR volcanic belt (Figure GW-2).

The "field shape" approach is that developed by Sheridan (1992). In this model, the volcanic field defined by centers having ages less than 4.6 Ma follows a bivariate Gaussian distribution. It is assumed that the centers in the CFVZ are realizations of this distribution.

The spatial smoothing approach is generally that presented in Connor and Hill (1995), whereby the observed locations of volcanoes are smoothed with an Epanechnikov smoothing operator to assess the probability of future events. An important constraint on the approach is that 90% of the

probability density is assumed to occur within the CFVZ. This reflects the fact that the locus of volcanic activity over the past 5 my has been primarily within the CFVZ.

EVENT COUNTS

Based on the definition of volcanic "events" given earlier, the number of events and their uncertainties are assessed for each of the centers in the CFVZ (Table GW-1). The number of events is assessed for the past 5 my, which is judged to be the time period of most relevance to estimates of future hazard.

Lathrop Wells

Multiple events may have occurred at Lathrop Wells, but 1 event is most likely. The scoria blanket observed around the cone to the SE, S, SW, W, and NW appears to be continuous and provides evidence of only one eruption (the steep cone slopes are unstable and the sequence is difficult to decipher, so these observations were made beyond the base of the cone). Paleomagnetic data are consistent with a single event; other age-dating methods have large uncertainties because the rocks are so young. Geochemical differences between stratigraphic units are small and not considered to be strong evidence for multiple events, as the geochemical "noise" level in cinder cones is not yet sufficiently well established to assess the significance of small chemical variations. Scoria mounds on the E side of the cone are believed to be sections of collapsed cone rafted on lava, and not evidence of separate vents. At both the north and south ends of the principal cone, however, there is evidence of primary vents associated with in situ cones; these features define a 1.5-km NNW-trending fissure through the principal cone. Fitting of scoria mounds to linear fissures conceivably could represent 2 or 3 events additional to the main one.

The following event counts and their relative weights are assigned for the Lathrop Wells center: 1 (0.9), 2 (0.07), 3 (0.02), and 4 (0.01).

Sleeping Butte

Hidden Cone and Little Black Peak could represent 1 event with their 3-km spacing, or they could be separate events. To the south at the 3.7 Ma area of Crater Flat and at Lathrop Wells, the fissures have a NS strike. If this is the dominant fissure or dike trend in the region, Hidden Cone and Little Black Peak would most likely be separate events. Alternatively, but less likely, they could be connected by a NE-trending dike.

The event counts and their relative weights for the Sleeping Butte area: 1 (0.4), and 2 (0.6).

1.0 Ma Crater Flat

One, 3, or 4 events are represented at northern Crater Flat, where 4 cones dated at 1.0 Ma occur near a straight line trending NNE. This lineation could be the surface expression of a dike, but what appear to be eruptive fissures at Red Cone and Lathrop Wells have a more nearly NNW trend. A dike following a convenient fracture may make side steps, forming an en echelon pattern, but these steps are usually on the order of a few meters apart. The 1.5-km distance between Red and Black cones seems too large to be associated with a side-stepping dike. Red and Black cones could be 1 or 2 events, but are most likely to be separate events. Either interpretation can be made from the similar K-Ar age dates, or the variable geochemistry. The presence of amphibole at Black Cone and not at Red Cone weakly supports the interpretation of separate events. If there was evidence of a dike connecting Red and Black cone, it would strengthen the single-event interpretation. Little Cones is located 3 km from Red Cone, and it is possible that a single dike connects the two features. The small, secondary cone at Little Cones, which is considered to be part of the event that formed the larger cone, is located along the trend of this possible dike. Makani Cone is most likely a separate event because of the distance that separates it from Black Cone. If all of the cones are considered to be part of the same event, they could be related to "tension-gashes" in a NNW-trending strike-slip system.

These scenarios are considered: 1 event involving all four cones; 3 events consisting of Little Cones, Red and Black cones together, and Makani Cone; and four events (assumes Little Cones is 1 event).

The following event counts and their relative weights are assigned for northern Crater Flat: 1 (0.1), 3 (0.35), and 4 (0.55).

Buckboard Mesa

Several of the features appear to be consistent with a single event. There is a main cinder cone, the geochemical analyses show a reasonably tight clustering of values, and the volume is not implausibly large for a single eruption. This area was not field checked by the author, so he has not formed an independent position.

The following event counts and their relative weights are based primarily on the Crowe et al. (1995) assessment for Buckboard Mesa: 1 (0.75), and 2 (0.25).

3.7 Ma Crater Flat

At least two dikes can be observed in the northern part of the 3.7 Ma area and, because more than one dike is not usually associated with a single event, multiple events are likely represented. In the southern part of the area, the larger volumes suggest several events; however, the author has not made a field visit.

Based on the limited information available, the following event counts and their relative weights for the 3.7 Ma area are: 2 (0.5), 3 (0.25), 4 (0.20), 5 (0.05).

Amargosa Valley

Two to 6 events may be present in the Amargosa Valley based on interpretation of the aeromagnetic anomalies; 3 events are most likely. The minimum of 2 events is based on the basalts encountered in wells (anomalies B and D on the aeromagnetic map presented by V. Langenheim at PVHA Workshop 1); the 3-event scenario includes anomaly C, which has a strong dipolar signature. Anomalies E, F, and G are small and less likely to represent events, as they could be ancient features related to the rugged relief on the top of basement rock. It is difficult to evaluate if anomalies F and G represent 1 or 2 events. In addition to anomalies B, C, D, and E, the 5-event scenario includes anomalies F and G as a single event, and the 6 event scenario includes them as 2 separate events. Anomaly A, at the southern end of the 1.0 Ma Crater Flat basalts, is not considered to represent a separate event because it may be part of the larger anomaly related to the Tertiary volcanics.

The following event counts and their relative weights are assigned to the Amargosa Valley area: 2 (0.3), 3 (0.4), 5 (0.15), and 6 (0.15).

Thirsty Mesa

This area was visited but not field checked carefully by the author, so he has not formed an independent position and will follow the interpretations of Crowe et al. (1995). It is noted that the volumes at Thirsty Mesa are not implausibly large to have been associated with a single event.

The following event counts and their relative weights are based primarily on the Crowe et al. (1995) assessment for Thirsty Mesa: 1 (0.85), 2 (0.09), and 3 (0.06).

RATES OF OCCURRENCE

Using the event counts discussed above, the rates of occurrence are calculated for use in the PVHA. These rates are calculated for the post-4.6 Ma time period and for each of the 2 source zones (see summary in Table GW-2).

The selected time period for the rate estimates is from 4.6 Ma to the present. If more recent time periods are used, there are too few points to provide meaningful rate estimates. If older time periods are used (e.g., 10 Ma) changes in tectonics and volumes of volcanics have occurred that can lead to problems in assessing rates. Over the past 4.6 my there have not been significant changes in volumes, the location of volcanism has persisted within the CFVZ without evidence of migration, and there is no significant evidence for waxing or waning of volcanism from the data available.

The rates within the CFVZ are assessed using the counts within northern (1.0 Ma) Crater Flat, 3.7 Ma area, Lathrop Wells, Thirsty Mesa, Sleeping Butte, and Amargosa Valley. The background zone is the "node" of the DV-PR belt. The rate for the background zone comes from the counts at Buckboard Mesa.

Undetected Events

There is no evidence for undetected or buried events in the CFVZ, but in many other volcanic areas in the world there is ample evidence of these features. What could be referred to as "abortive eruptions" have been observed in many tectonic environments. Earthquake swarms of the type that presage eruptions have been recorded in areas where underground magma movements were suspected on the basis of ground deformation. The geologic record includes features such as sill swarms that provide evidence of large-scale subsurface magma movements. Most large sill swarms were emplaced in non-lithified sediments just above basement rock, an area that is typically coincident with the level of neutral buoyancy (LNB). LNB occurrence in an area is an important control, as is magma viscosity, with more viscous magmas like andesites less likely to reach the surface. In active volcanic areas, abortive eruptions could compose up to 50% of the total number of events. Possible examples include: Krafla in northern Iceland, which experienced major rifting events in 1978-84, but only small lava flows were erupted; Rabaul in Papua New Guinea, which had an intense earthquake swarm peaking in 1983, but no eruption (an eruption did, however, occur in 1995); Long Valley in California, which experienced a seismic crisis in 1982; and recent earthquake swarms off Sao Miguel in the Azores. Kilauea volcano in Hawaii also experiences dike injection events commonly without eruption, the event in the Southwest Rift Zone in August 1981 being a fine example.

To account for the possibility of undetected events in assessing the rates for the PVHA, and considering possible analogues, the following factors should be used to multiply the counts derived from observed/interpreted events:

Cumulative

1 x counts	(0.3)
2 x counts	(0.5)
5 x counts	(1.0)

TEMPORAL MODELS

A homogeneous Poisson temporal model is used to describe the distribution in time of volcanic event occurrence. In terms of a time-series analysis, there is definite evidence for temporal clustering of events. However, given the small numbers of events, we are not able to reject the hypothesis that the rate is uniform over the past 4.6 my. Further, the 4.6 my time period is selected to maximize the number of events that can be used for the analysis, while minimizing the variations in volume and location.

EVENT GEOMETRIES

Dike lengths associated with future events are as long as about 3 km. There is uncertainty in the tail of the dike length distribution (i.e., if the 1.0 Ma basalts in Crater Flat represent 1 event, then dike lengths up to 12 km are allowable). Dike lengths are controlled by the intensity of melting anomalies and associated magma generation rates. The CFVZ is considered to be a low intensity field. On a spectrum of intensity, monogenetic fields such as Crater Flat are on one end, and flood basalt fields, such as in the eastern Snake River Plain, are on the other end. In monogenetic fields that are appropriate analogues for the CFVZ (e.g., El Jorullo in Mexico, active in the 1700s), dikes are no more than about 3 km in length. The cumulative distribution of length is: 2 km (0.5), 3 km (0.9), and 12 km (0.95). For small monogenetic volcanic fields, like those of the Yucca Mountain region, the maximum dike length would be in the range of 15 to 20 km. Both maximum values should be used with equal weight. The dike is likely to be centered on the "event." Therefore, a triangular distribution is used for the event location on the dike.

Note: At the request of Dr. Walker, a smooth interpolation function was fit to his discrete cumulative density estimates for dike length. The resulting cumulative distributions and density functions are shown on Figure GW-4.

Data on dike orientations collected recently in Scotland indicates that dikes follow fractures and other zones of weakness with a wide variety of trends. The magnitude of stress differences may control these orientations. Observations of a N-trending fissure system at Red Cone, N-trending dikes at the 3.7 Ma area, and the NNW-trend of fissures at Red Cone and Lathrop Wells are not

consistent with the regional direction of least horizontal compressional stress, N60W (after Stock and Healey, 1988). They are consistent, however, with the NNE-trend of the DV-PR zone. The tension pattern at the top of the crust may be different from the pattern at depth. In Crater Flat, for example, the deep dikes may trend NE as tension gashes but finger upwards toward the surface and form shallow dikes that trend NNW. Future dike orientations in the YMR are assessed to have a bimodal distribution centered on $N20W \pm 30$ (2σ) and $N40E \pm 30$ (2σ) with equal frequency.

Dike widths can be estimated using a length to width ratio of about 1,000/1. Width to length ratios are dependent on the elastic properties of rock and the rate of cooling. The longer the dike, the greater the width of the dike. Ballooning of dikes near the ground surface may occur from erosion of dike walls through mechanical or thermal effects.

HYDROMAGMATIC ACTIVITY

A wide variety of hydromagmatic eruptions have been observed around the world, including small steam explosions, huge-volume phreato-magmatic eruptions, maar-type eruptions, etc. Hydromagmatic eruptions inland from the coast are most common in areas having a good regional aquifer and shallow water table. The author disagrees with the interpretation that some of the ashes at Lathrop Wells are hydrovolcanic. Therefore, there is not a single example of hydrovolcanism in the entire region, suggesting a very low probability of future occurrence. An assessment is made that the estimate of M. Sheridan (presentation at PVHA Workshop 4) of 1 or 2 hydrovolcanic events per 100 events is reasonable.

TYPE OF ERUPTIONS

Volcanism in the area of interest is consistent with monogenetic field analogues, and future volcanism will most likely erupt small volumes (0.1 to 0.2 km^3) of slightly alkalic basalts. The record of volcanism in the area of interest indicates some mildly explosive volcanism, including Strombolian activity typical of monogenetic field analogues, so this pattern is likely to continue. Lavas will be more viscous than Hawaiian tholeiite, but fairly fluid. There is no evidence for a bimodal composition of lavas; therefore, the probability of rhyolite appearing in the region is small (<0.05).

George P. L. Walker

MAY 9, 1996

REFERENCES

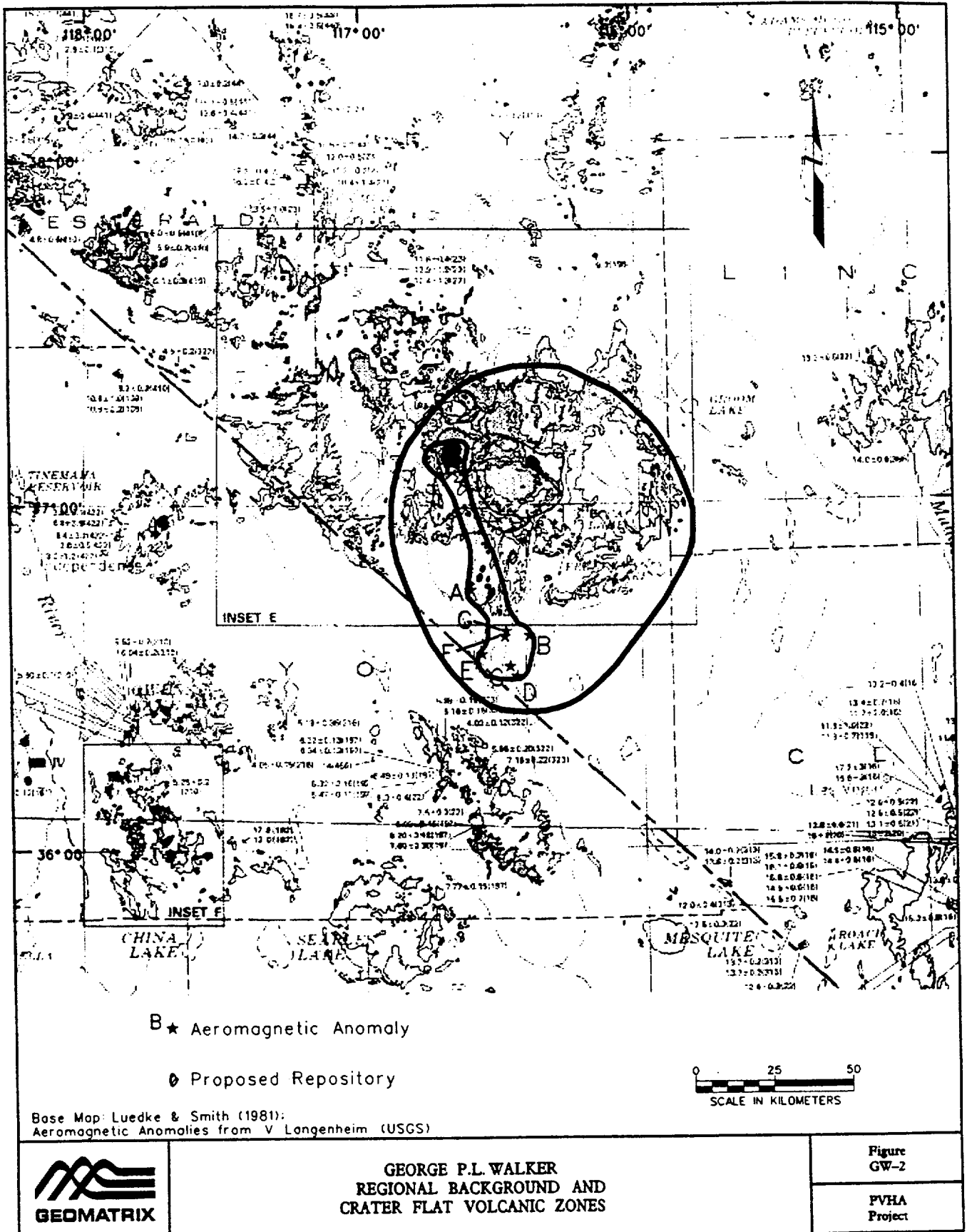
- Connor, C.B., and Hill, B.E., 1995, Three nonhomogeneous Poisson models for the probability of basaltic volcanism: application to the Yucca Mountain region, Nevada, USA: *Journal of Geophysical Research*, v. 100, no. B6, p. 10,107-10,125.
- Crowe, B.M., and Perry, F.V., 1989, Volcanic probability calculations for the Yucca Mountain site: estimation of volcanic rates: *Proceedings, Nuclear Waste Isolation in the Unsaturated Zone, Focus '89, American Nuclear Society*, p. 326-334.
- Crowe, B.M., Perry, F.V., Geissman, J., McFadden, L., Wells, S., Murrell, M., Poths, J., Valentine, G.A., Bowker, L., and Finnegan, K., 1995, Status of volcanism studies for the Yucca Mountain site characterization projects: Los Alamos National Laboratory Report LA-12908-MS, March.
- Sheridan, M.F., 1992, A Monte Carlo technique to estimate the probability of volcanic dikes: *Proceedings, High-Level Radioactive Waste Management*, v. 2, p. 2033-2038.
- Smith, E.I., Feuerbach, D.L., Nauman, T.R., and Faulds, J.E., 1990, The area of most recent volcanism near Yucca Mountain, Nevada: implications for volcanic risk assessment: *Proceedings, High-Level Radioactive Waste Management*, v. 1, p. 81-90.
- Stock, J.M., and Healey, J.H., 1988, Geological and hydrologic investigations of a potential nuclear waste disposal site at Yucca Mountain, southern Nevada, *in* M.D. Carr and J.C. Yount (eds.), *Geologic and Hydrologic Investigations of a Potential Nuclear Waste Disposal Site at Yucca Mountain, Southern Nevada*: U.S. Geological Survey Bulletin 1790, p. 87-93.

**TABLE GW-1
 GEORGE P.L. WALKER - EVENT COUNTS**

LOCATION	COUNTS (CONES)	WEIGHT	NOTES
Lathrop Wells	1	(0.9)	BC: Black Cone LC: Little Cones M: Makani Cone RC: Red Cone
	2	(0.07)	
	3	(0.02)	
	4	(0.01)	
Sleeping Butte	1	(0.4)	
	2	(0.6)	
1.0 Ma Crater Flat	1 (all)	(0.1)	
	3 (LC, RC+BC, M)	(0.35)	
	4 (LC, RC, BC, M)	(0.55)	
Buckboard Mesa	1	(0.75)	
	2	(0.25)	
3.7 Ma Crater Flat	2	(0.5)	
	3	(0.25)	
	4	(0.20)	
	5	(0.05)	
Amargosa Valley	2	(0.3)	
	3	(0.4)	
	5	(0.15)	
	6	(0.15)	
Thirsty Mesa	1	(0.85)	
	2	(0.09)	
	3	(0.06)	

**TABLE GW-2
 GEORGE P.L. WALKER - RATES OF OCCURRENCE**

TIME PERIOD	COUNT METHOD FOR ZONES	NOTES
Post 4.6 Ma (1.0)	- CFVZ zone: NCF, 3.7, LW, TM, SB, AV - Background Node: BM	NCF: Northern (1.0 Ma) Crater Flat 3.7: 3.7 Ma Crater Flat LW: Lathrop Wells TM: Thirsty Mesa SB: Sleeping Butte AV: Amargosa Valley BM: Buckboard Mesa



H:\pva\yucca\gdg\pva\hds\smith\gw-02.dgn, Rev. 01/19/96

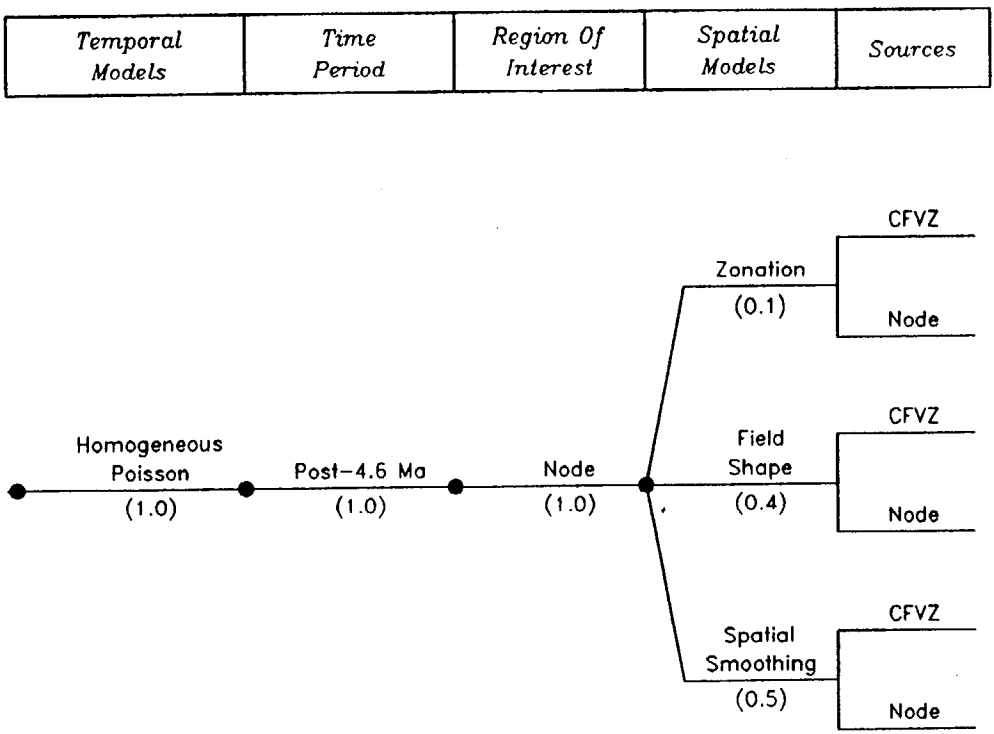
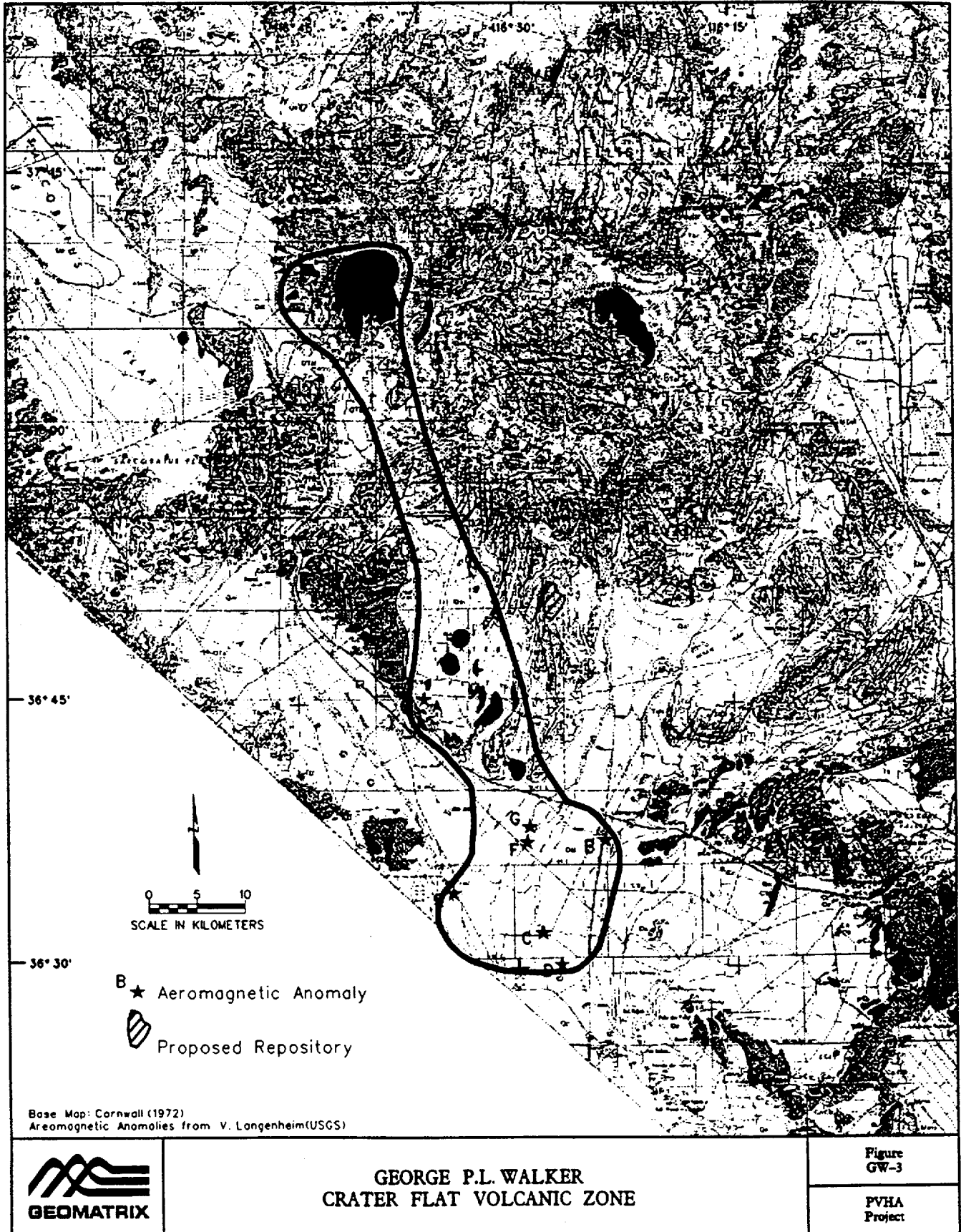


Figure GW-1 PVHA model logic tree developed by George P.L. Walker.



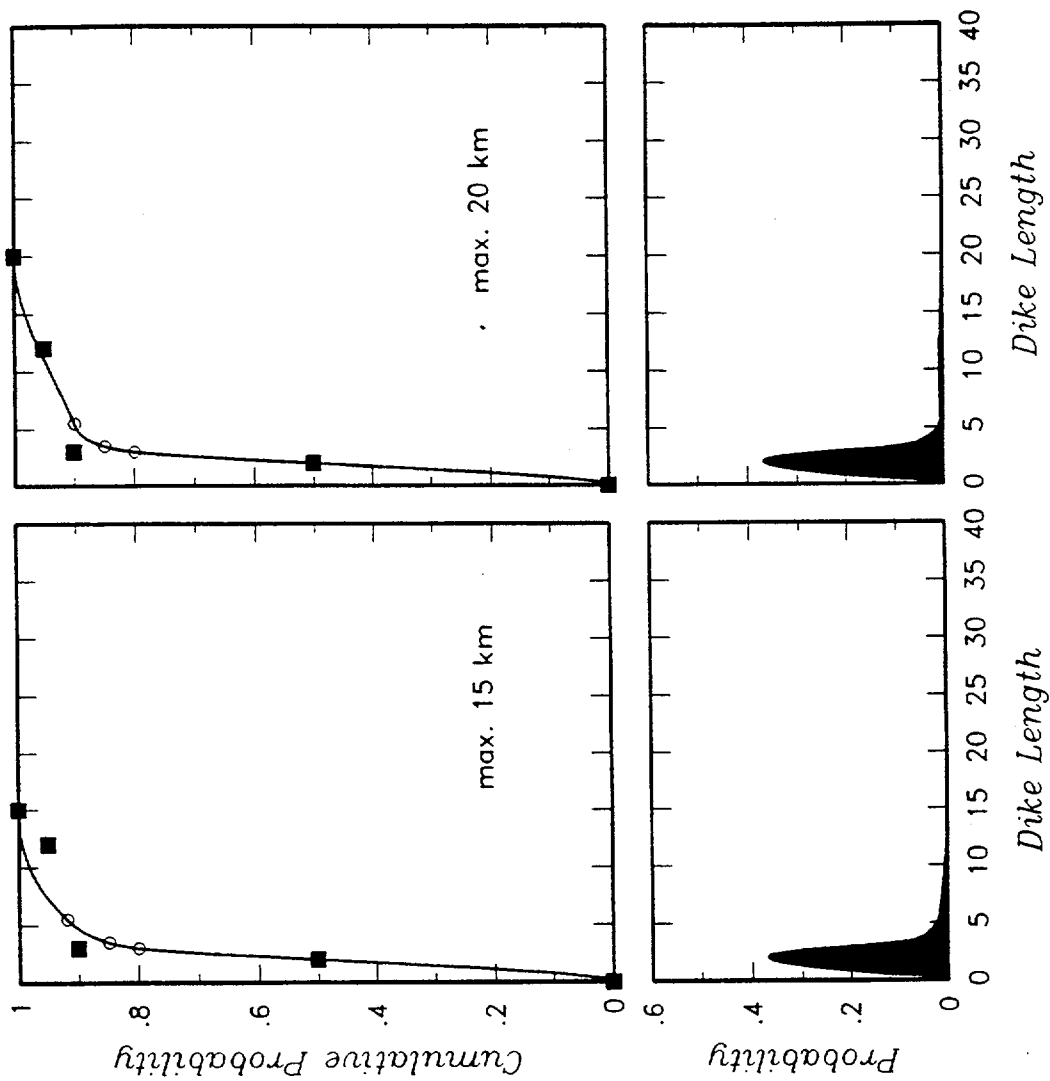


Figure GW-4 Dike length distribution developed by George P.L. Walker.

APPENDIX F

DETAILS OF HAZARD FORMULATION

APPENDIX F DETAILS OF HAZARD FORMULATION

This appendix presents additional details of the mathematical formulations used to compute the volcanic hazard.

TEMPORAL MODELS

Two basic types of temporal models were used to represent the rate of volcanic events, the homogeneous Poisson process and the nonhomogeneous Weibull process.

The homogeneous Poisson process specifies that the probability distribution for the number of events, n , occurring in time period t is given by:

$$P(n) = \frac{(\lambda t)^n e^{-\lambda t}}{n!} \quad (\text{F-1})$$

where λ is the mean rate of occurrence of events. The maximum likelihood estimate for the mean rate, $\hat{\lambda}$, given the observation of N events in time period T is just N/T (e.g. Benjamin and Cornell, 1970). Weichert (1980) developed an approach for defining confidence intervals for the parameter λ . Specifically, the upper, $\lambda_{U(\alpha)}$, and lower, $\lambda_{L(\alpha)}$, points of a $(1-\alpha)100\%$ confidence interval for λ based on N events are given by:

$$\begin{aligned} \lambda_{U(\alpha)} &= \hat{\lambda} \cdot \frac{\chi^2(N+0.5, 1-\alpha/2)}{N} \\ \lambda_{L(\alpha)} &= \hat{\lambda} \cdot \frac{\chi^2(N, \alpha/2)}{N} \end{aligned} \quad (\text{F-2})$$

where $\chi^2(n, \alpha)$ defines the α probability point of the chi² distribution with n degrees of freedom.

The Weibull process is a nonhomogeneous Poisson process in which the rate parameter $\lambda(t)$ changes monotonically with time following a particular functional form: (e.g. Ho, 1991):

$$\lambda(t) = \frac{\beta}{\theta} \left(\frac{t}{\theta} \right)^{\beta-1} \quad \text{for } t \geq 0 \quad (\text{F-3})$$

where t is time measured from t_0 when the process "starts", and β and θ are parameters. Application of this model to evaluating the rate of volcanism is described by Ho (1991, 1992). The data used to estimate the parameters β and θ consist of the number of volcanic events, N , that have occurred during time interval T and the age dates for each event. Defining T_i as the age date of the i^{th} event (e.g., 1 Ma) and defining $T=t_0$ as the age date for the beginning of the process (e.g., 5 Ma), then the maximum likelihood estimates for the parameters of the Weibull process are given by the relationships (Crow, 1974):

$$\beta = \frac{N}{\sum_{i=1}^N \ln(T/t_i)} \quad (\text{F-4})$$

$$\theta = T/N^{1/\beta}$$

where $t_i=T-T_i$ is the time interval from the start of the process to the i^{th} event. Crow (1982) tabulates confidence interval factors for the Weibull process. The homogeneous Poisson and Weibull process 90-percent confidence intervals are compared on Figure F-1 for data sets of 2 to 20 events. The two confidence intervals are similar in width.

SPATIAL MODELS

Linear Gradient for a Homogeneous Zone Boundary The locally homogeneous spatial model assumes that the spatial density of events $f(x,y)$ is uniform within a zone and equal to $1/A$, where A is the area of the zone. Thus the integral of the spatial density over the zone area equals unity

$$\int_Z \int_Z f(x,y) dx dy = \int_Z \int_Z \frac{dx dy}{A} = \frac{A}{A} = 1 \quad (\text{F-5})$$

In this model there is an abrupt step in the spatial density function at the edge of the zone. An alternative is to assume that $f(x,y)$ decreases linearly from $1/A$ at the zone boundary to zero over a distance h . Within the transition zone the spatial density is given by

$$f_T(x,y) = \frac{(h-d)/h}{A} \quad (\text{F-6})$$

where d is the distance from the zone boundary and is confined to the range of 0 to h . However, the effective area of the zone has now expanded by A_T , the area of the transition zone. Thus, the integral of the spatial density over the effective area of the zone, $A+A_T$ will exceed unity, requiring renormalization to produce a proper density function. The renormalization factor is the integral

of $f(x,y)$ over the entire effective region of the zone. For zones in which the transition region lies along one side, the normalization factor is approximately equal to the area within the zone plus one-half of the area within the transition region. Thus the spatial density becomes

$$\begin{aligned} f(x,y) &\cong \frac{1}{A+A_T/2} && \text{for } (x,y) \text{ within } A \\ f(x,y) &\cong \frac{(h-d)/h}{A+A_T/2} && \text{for } (x,y) \text{ within } A_T \end{aligned} \quad (\text{F-7})$$

The method used to compute the volcanic hazard directly calculated the normalization factor by numerically integrating the spatial density over the zone and transition areas and then renormalized the spatial density function to unity.

Gaussian Field Parameters Two approaches were used to define the parameters of a Gaussian field model for the spatial density defined by the relationship

$$f(x,y) = \frac{e^{-[(x-\mu)^T \Sigma^{-1} (x-\mu)]/2}}{2\pi |\Sigma|^{1/2}} \quad (\text{F-8})$$

where x is the location of point (x,y) , μ is the location of the center of the field (mean of x and y for all events) and Σ is the covariance matrix of the x and y locations of observed events in the field. If the field parameters are to be estimated from the n observed events then the maximum likelihood estimators are (Johnson and Wichern, 1992):

$$\begin{aligned} \mu &= \frac{1}{n} \sum_{i=1}^n x_i \\ \Sigma &= \frac{1}{n} \sum_{i=1}^n (x_i - \mu)^T (x_i - \mu) \end{aligned} \quad (\text{F-9})$$

where x_i is the location of the i^{th} event in the field. The five parameters of the field are the mean of the x and y locations, μ_x and μ_y , and the covariances of the x and y locations, σ_x^2 , σ_y^2 , and σ_{xy}^2 . The asymptotic covariance of the estimated field mid point μ is equal to Σ/n . The asymptotic covariance for the parameters of Σ are computed using the relationship given by (Searle, 1971)

$$\text{var}(c_i, c_j) = 2 \left(\text{Trace} \left[\Sigma^{-1} \frac{\partial \Sigma}{\partial c_i} \Sigma^{-1} \frac{\partial \Sigma}{\partial c_j} \right] \right)^{-1} \quad (\text{F-10})$$

where c_x and c_y refer to the three components of the covariance matrix σ_x^2 , σ_y^2 , and σ_{xy} . These estimates were used to establish ranges for the field parameters. The relative likelihood of a particular set of field parameters, μ^j and Σ^j , being the "correct" model that generated the observed set of events was computed by (Johnson and Wichern, 1992):

$$L(\mu^j, \Sigma^j) = \frac{e^{-\sum_{i=1}^n (x_i - \mu^j)^T (\Sigma^j)^{-1} (x_i - \mu^j)}}{(2\pi)^n |\Sigma^j|^{n/2}} \quad (\text{F-11})$$

Three values for each of the five parameters were selected, the maximum likelihood value and \pm one standard error of estimation. Equation (F-11) was then used to compute the likelihood of the 243 possible parameter sets and the resulting values normalized to sum to unity to define a discrete probability distribution for the field parameters.

The alternative approach to specifying a Gaussian field was to define a source zone boundary to correspond to a specified density ellipse of the Gaussian field. The ellipse that encloses 100(1- α) percent of the density of the field satisfies the relationship (Johnson and Wichern, 1992)

$$(x - \mu)^T \Sigma^{-1} (x - \mu) \leq \chi^2(2, \alpha) \quad (\text{F-12})$$

where $\chi^2(2, \alpha)$ defines the upper α probability point of the chi distribution with 2 degrees of freedom. Given a source zone boundary and a specified value of α , Equation (F-12) was used to find the field parameters that minimized the mean square error between $(x - \mu)^T \Sigma^{-1} (x - \mu)$ calculated at points along the zone boundary and the corresponding value for $\chi^2(2, \alpha)$.

Kernel Density Estimation Equations (3-10) and (3-11) of Section 3.1.4 define axisymmetric kernel densities for Epanechnikov and Gaussian kernels, respectively. Silverman (1986) indicates that one can generalize the kernels to have an anisotropic shape. Defining the aspect ratio of the kernel, R^k , to be the ratio of the long axis to the short axis, $R^k \leq 1$, and defining the azimuth of the long axis of the kernel to be ϕ , then the coordinate system of the spatial grid can be rotated through angle ϕ and the kernel density estimates computed by the relationship

$$K^E(d_i') = \frac{2}{\pi |\Sigma_k|^{1/2}} \left[1 - d_i'^T \Sigma_k^{-1} d_i' \right] \quad \text{for } d_i'^T \Sigma_k^{-1} d_i' < 1$$

$$= 0 \quad \text{otherwise} \quad (\text{F-13})$$

for the Epanechnikov kernel and by the relationship

$$K^G(d_i') = \frac{e^{-d_i'^T \Sigma_k^{-1} d_i'}}{2\pi |\Sigma_k|^{1/2}} \quad (\text{F-14})$$

for the Gaussian kernel. The vector d_i' defines the relative coordinates between point (x,y) and event i in the transform rotated coordinate system and Σ_k is a covariance matrix of the kernel in the rotated coordinate system given by

$$\Sigma_k = \begin{bmatrix} h^2 & 0 \\ 0 & (R_k h)^2 \end{bmatrix} \quad (\text{F-15})$$

As discussed in Section 3.1.4, the value of the smoothing parameter h was either specified directly or was specified by defining a zone boundary as the approximate $100(1-\alpha)$ percentile density contour for the local field. A nonlinear optimization routine was then used to find the value of h that minimized the difference between the zone boundary and the specified density contour computed using kernel density estimation. The process is illustrated on Figure F-2.

A source zone is defined containing a number of events. A trial value of h is selected, for example 5 km, and the 95 percent density contour of a kernel density function is computed. This is denoted by the stippled area. The measure of the error is taken to be the area between the computed density contour and the zone boundary. This includes both the stippled area outside of the source zone boundary and the area inside the source zone that is outside of the computed 95 percent density contour, and is shown on Figure F-2 by the area filled with open circles. In the left hand plot of Figure F-2 there is very little area outside of the zone boundary but a large area of mismatch inside the zone. The process is repeated for a second value of h . The middle plot shows the results for h equal to 10 km. Now the zone is nearly filled by the 95 percent density contour, but there is a large area inside of the 95 percent density contour that lies outside of the source zone. Using a minimization algorithm, the value of h that minimizes the area of mismatch is found to be 7.4 km. The result 95 percent density contour is shown in the right hand plot of Figure F-2. These results were obtained using a Gaussian kernel. Repeating the process with an Epanechnikov kernel yields a best fit value of h equal to 18.9 km. This value is approximately 2.5 times the best fit h for the Gaussian kernel, consistent with the discussion by Silverman (1986) about the ratio of smoothing parameters that produce similar results using the two different kernels.

REFERENCES

- Benjamin, J.R., and Cornell, C.A., 1970, *Probability, Statistics, and Decision for Civil Engineers*: McGraw-Hill, New York.
- Crow, L.H., 1974, Reliability analysis of complex repairable systems: *in* Proschan, F., and Serfling, R.J. (eds.), *Reliability and Biometry*: SIAM, Philadelphia, Penn., p. 392-410.
- Crow, L.H., 1982, Confidence interval procedures for the Weibull process with applications for reliability growth: *Technometrics*, v. 24, p. 67-72.
- Ho, C.-H., 1991, Time trend analysis of basaltic volcanism for the Yucca Mountain site: *Journal of Volcanology and Geothermal Research*, v. 46, p. 61-72.
- Ho, C.-H., 1992, Risk assessment for the Yucca Mountain high-level nuclear waste repository site: estimation of volcanic disruption: *Mathematical Geology*, v. 24, no. 4, p. 347-364.
- Johnson, R.A., and Wichern, D.W., 1992, *Applied Multivariate Statistical Analysis*: 3rd Edition, Prentice Hall, New Jersey.
- Searle, S.R., 1971, *Linear Models*: John Wiley and Sons, New York.
- Silverman, B.W., 1986, *Density Estimation for Statistics and Data Analysis*: Monographs on Statistics and Applied Probability 26: Chapman and Hall, New York.
- Weichert, D.H., 1980, Estimation of the earthquake recurrence parameters for unequal observation periods for different magnitudes: *Bulletin of the Seismological Society of America*, v. 70, p. 1337-1346.

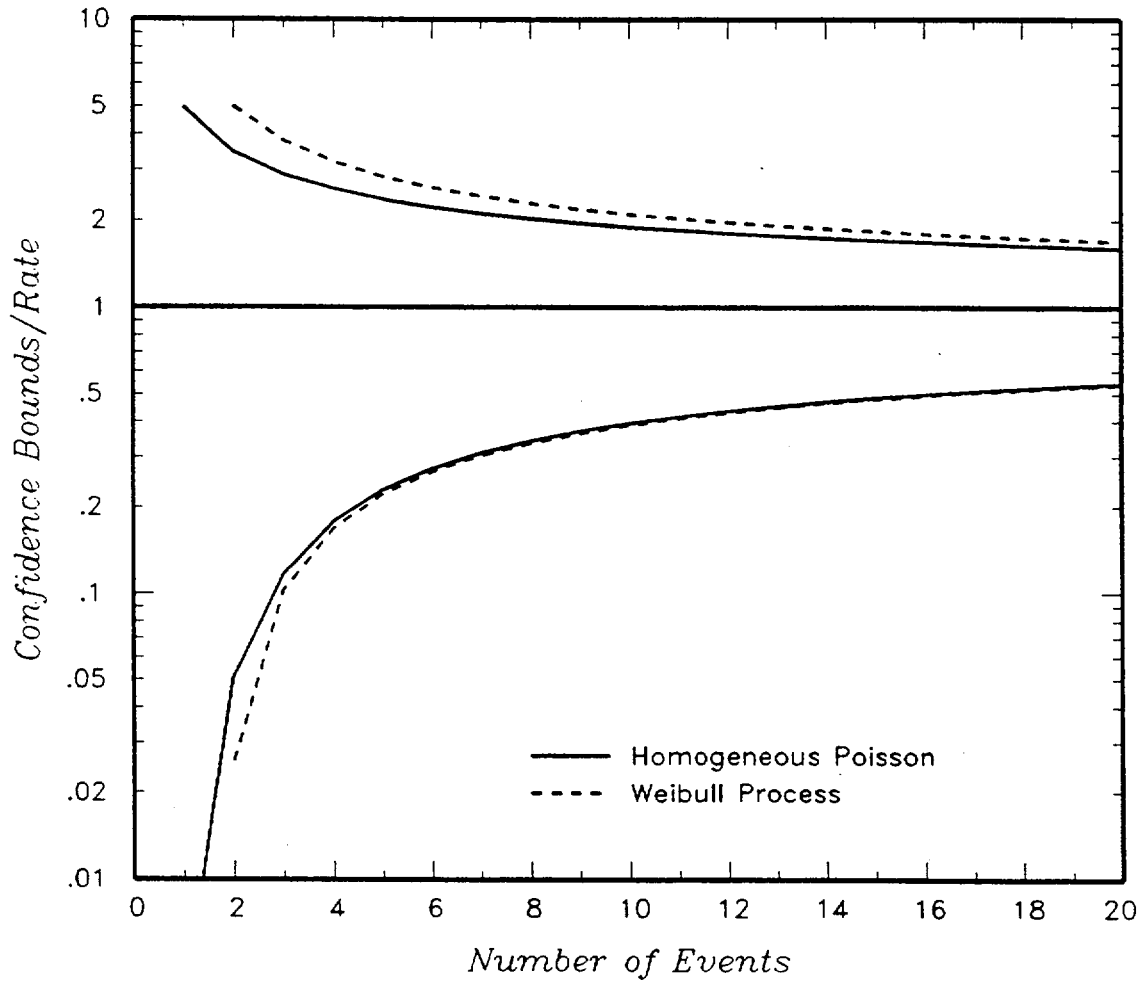


Figure F-1 Ninety-percent confidence intervals for the homogeneous Poisson and Weibull process models as a function of the number of data points.

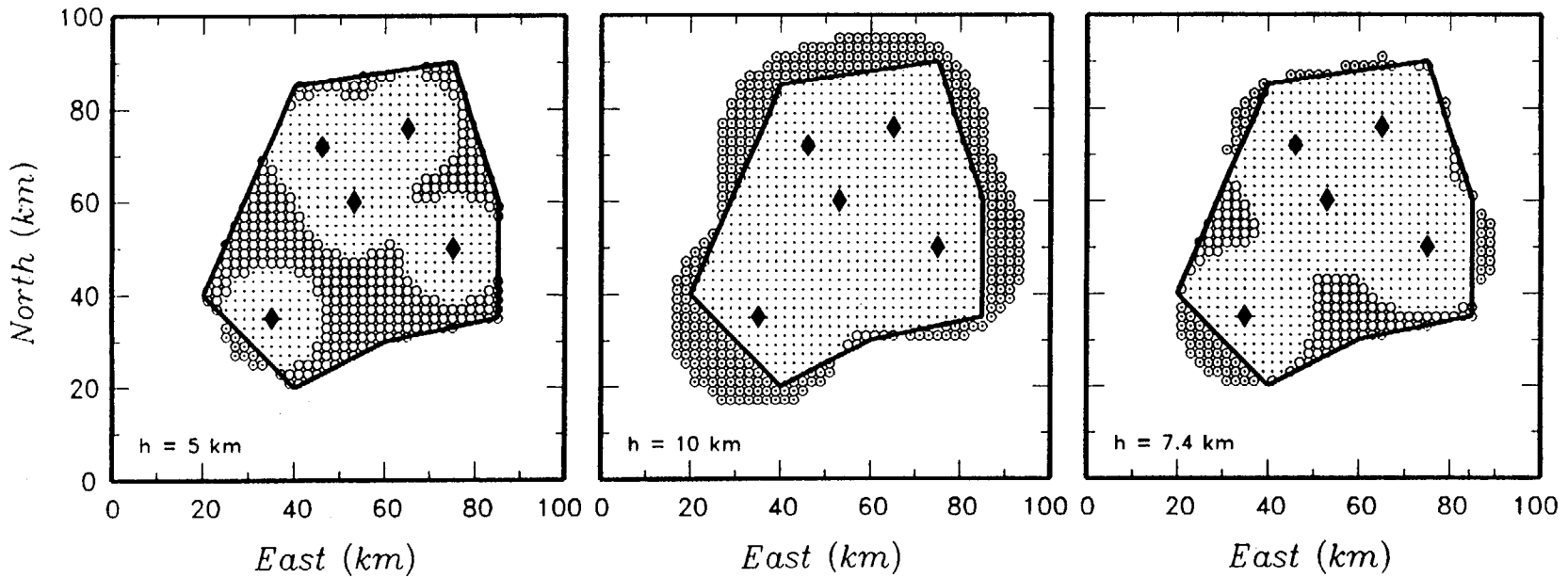


Figure F-2 Illustration of the procedure used to determine the smoothing parameter, h , for the kernel density estimation by minimizing the area of mismatch between a zone boundary and a specified density contour computed from the data. The solid triangles represent the data points and the small dots define the 95-percent density contour computed from the data using the indicated values of h and a Gaussian kernel. The open circles define the area of mismatch (when they are outside of the zone boundary they contain a dot within them).

APPENDIX G
PROBABILISTIC VOLCANIC HAZARD ANALYSIS
CALCULATION ILLUSTRATIONS

APPENDIX G

TABLE OF CONTENTS

	PAGE
G.1 CALCULATION OF THE CONDITIONAL PROBABILITY OF INTERSECTION	2
G.2 CALCULATION OF FREQUENCY OF INTERSECTION	6
G.2.1 Event Rate Calculation	6
G.2.2 Spatial Density Calculation	7
G.2.3 Combined Hazard Calculation	23
G.3 REFERENCE	29

APPENDIX G PROBABILISTIC VOLCANIC HAZARD ANALYSIS EXAMPLE CALCULATION

This appendix presents the approach used for the probabilistic volcanic hazard calculation and illustrates this approach with examples of the type of calculations performed.

The measure of volcanic hazard used in this study was the annual frequency of intersection of the repository, v_j . The basic formulation for calculating v_j is given by equation (3-4) in the main text:

$$v_j(t) = \iint_R \lambda(t) \cdot f(x,y) \cdot P_j(x,y) \, dx \, dy \quad (3-4)$$

where $v_j(t)$ indicates that v is a function of time, with t equal to 0 representing the present. Also, as discussed in Sections 3 and 4 of the main text, the volcanic experts treated $v(t)$ as an uncertain quantity dependent on a number of parameters, designated herein by the vector Θ . The experts specified discrete distributions for the parameters through the use of logic trees, resulting in discrete parameter sets, θ_k , with a specified probability of being the "correct" parameter set, $P(\Theta=\theta_k)$. The frequency of intersection was calculated for each possible parameter set. The results of these calculations formed a discrete distribution for the frequency of intersection. The expected value or mean of this distribution was used as the estimate of the volcanic hazard.

The calculation of $v_j(t|\theta_k)$ was performed by discretizing the region of interest, R , on a grid with spacing Δx and Δy and replacing equation (3-4) by the equivalent summation:

$$v_j(t|\theta_k) = \sum_{i=1}^{N_x} \sum_{j=1}^{N_y} \lambda(t) \cdot f(x_i, y_j) \cdot P_j(x_i, y_k) \cdot \Delta x \cdot \Delta y \quad (G-1)$$

Calculation of equation (G-1) was performed in two steps using the variety of approaches outlined in Section 3.1 and Appendix F. The first step was to calculate the conditional probability of intersection, $P_j(x, y)$, for each point in the gridded site region. Then the rate parameter $\lambda(t)$ and the discrete spatial mass density, $f(x, y)$ were calculated following the approaches specified by the expert, and the resulting values multiplied by the conditional probability of intersection and summed over all points in the grid.

G.1 CALCULATION OF THE CONDITIONAL PROBABILITY OF INTERSECTION

The conditional probability of intersection is calculated using the discrete form of Equation (3-17):

$$P_j(x_i, y_j) = \sum_{l=1}^{N_L} P(L=l) \cdot P[\phi_1(x_i, y_j, l) \leq \phi \leq \phi_2(x_i, y_j, l)] \quad (G-2)$$

where $P(L=l)$ is the discrete probability mass function for the length of an event (represented as a linear dike) extending from the grid point toward the repository and $P[\phi_1(x_i, y_j, l) \leq \phi \leq \phi_2(x_i, y_j, l)]$ is the probability that the dike azimuth lies between ϕ_1 and ϕ_2 (see Figure 3-12). The discrete probability mass function for event length was calculated from a total dike length distribution specified by the expert. The probability distribution for dike azimuth was assumed to be a normal distribution with mean, μ_ϕ , and standard deviation, σ_ϕ , specified by the expert. The distribution for ϕ was assumed to be doubly truncated at $\mu_\phi \pm 90^\circ$.

Figure G-1, part (a) shows an example distribution for total dike length, TL , specified as uniform between 0 and a maximum length of 10 km. The expert then specified a symmetric probability density function for the location of the point event on the dike, Ω (varying from $0 \cdot TL$ to $1 \cdot TL$). Part (b) of Figure G-1 shows an example of a uniform density function for event location, Ω . The probability mass function for event length was then calculated from the expert-specified distributions using a computer program **DCPELD**(v1.0). Two event length distributions were calculated, the preferred distribution assuming a randomly placed dike and a second distribution assuming that the dike is centered on the point event. The probability mass function is a compound distribution [see Benjamin and Cornell (1970) p. 306-307] and is calculated by the formula:

$$P(L=l) = \sum_{\Omega} P(TL=tl) \cdot P(\Omega=\omega | l=tl \cdot \omega) \quad (G-3)$$

Program **DCPELD** works by discretizing the cumulative distribution into intervals specified by $tl \pm \Delta l / 2$ and the event location distribution into intervals of $\omega \pm \Delta \omega / 2$. For the case of the event centered dike, all of the probability mass for Ω is placed on $\omega = 0.5$. The program then forms a discrete distribution for event length with intervals $l \pm \Delta l / 2$. All possible combinations of the discrete values of tl and ω are calculated and the probability $P(Tl=tl) \cdot P(\Omega=\omega)$ is added to the probability mass for the event length interval $l=tl \cdot \omega$. After completing all combinations, the probability mass function for l is summed to form a cumulative mass function.

The following is a listing of example input and output files for program **DCPELD**.

Input File: DCPELD.IN

```

    examp.scd          input discrete cumul. dist. for total dike length
    1 .005 'u'        Δtl=Δl, Δω, type of distribution for Ω ('u' = uniform)
    examp.dld         output file name
    q                 q to quit
    
```

Input File: EXAMP.SCD

```

    Example Dike Length Distribution  10 Max          Label for distribution
    11                                number of mass points
    0.0      0.0                                tl, P(TL≤tl)
    1.0      0.1
    2.0      0.2
    3.0      0.3
    4.0      0.4
    5.0      0.5
    6.0      0.6
    7.0      0.7
    8.0      0.8
    9.0      0.9
    10.0     1.0
    
```

Output File: EXAMP.DLD

```

    Example Dike Length Distribution  10 Max          Label for distribution
    11                                number of mass points
    0.000    0.995000000E-01    0.204448403E+00    l, P(L≤l|event centered dike), P(L≤l|randomly placed dike)
    1.000    0.299499989E+00    0.433895228E+00
    2.000    0.499499977E+00    0.596842047E+00
    3.000    0.699499965E+00    0.718122209E+00
    4.000    0.899499953E+00    0.810235703E+00
    5.000    0.100000000E+01    0.879849198E+00
    6.000    0.100000000E+01    0.931129354E+00
    7.000    0.100000000E+01    0.966933327E+00
    8.000    0.100000000E+01    0.989344436E+00
    9.000    0.100000000E+01    0.999949998E+00
    10.000   0.100000000E+01    0.100000000E+01
    
```

The resulting cumulative mass functions for event length are plotted on part (c) of Figure G-1.

The calculation of $P_f(x, y)$ was performed by computer program CPDI(v1.0). The inputs to this program are the coordinates defining the outline of the proposed repository, the discrete probability distribution for event length, and the dike azimuth distribution parameters μ_ϕ and σ_ϕ . The program calculates three values for $P_f(x, y)$, one assuming point events with a finite radius, one assuming that the dikes are centered on the event, and one assuming that the dikes are randomly placed on the event.

The following is an example calculation using CPDI. Figure G-2 shows an example repository foot print and the points of the calculation grid with $\Delta x = \Delta y = 5$ km. The event cumulative length distributions calculated with using program DCPELD are rediscritized at the same intervals $l \pm \Delta l/2$. At each grid point the following set of calculations are made. For a given value of l the two angles of intersection, ϕ_1 and ϕ_2 (see Figure 3-12), are calculated. The probability mass $P[\phi_1(x, y, l) \leq \phi \leq \phi_2(x, y, l)]$ is calculated by the expression:

$$P(\phi_1 \leq \phi \leq \phi_2) = F_T \left(\frac{\phi_2 - \mu_\phi}{\sigma_\phi} \right) - F_T \left(\frac{\phi_1 - \mu_\phi}{\sigma_\phi} \right) \quad (G-4)$$

where $F_T()$ is the standard normal distribution doubly truncated at $\mu_\phi \pm 90^\circ$. The probability $P(L=l) \cdot P[\phi_l(x, y), l \leq \phi \leq \phi_2(x, y), l]$ is then added to $P_f(x, y)$. The process is repeated for all values of l .

The following is a listing of example input and output files for program CPDI.

Input File: CPDI.IN

n	y or n for binary output
examp.cpi	output file name
Example 10 km Max	output label
examp.rep	repository outline coordinates (km)
0.25 1	size of point events, # header records in event length dist. file
examp.dld	event length distribution file (output of DCPELD listed above)
1 45 30 1.0 0.1	# of azimuth dist., μ_ϕ , σ_ϕ , fraction of population, repeated for multiple means), azimuth discretization increment°
525 575 5 4050 4100 5	start of x grid, end of x grid, Δx , start of y grid, end of y grid, Δy
q	q to stop

Input File: EXAMP.REP

Example Repository	Repository file label
5	# of vertices
547.5 4082.5	x, y coordinates (km) of vertices
547.5 4077.5	
552.5 4077.5	
552.5 4082.5	
547.5 4082.5	

Output File: EXAMP.DLD

Example 10 km Max	Output file label
10 525.00 575.00 5.00 10 4050.00 4100.00 5.00	grid parameters
525.000 4050.000 0.0000000E+00 0.0000000E+00 0.0000000E+00	$x_i, y_j, P_l(x_i, y_j)$ for point event,
525.000 4055.000 0.0000000E+00 0.0000000E+00 0.0000000E+00	event centered dike, and
525.000 4060.000 0.0000000E+00 0.0000000E+00 0.0000000E+00	randomly placed dike
525.000 4065.000 0.0000000E+00 0.0000000E+00 0.0000000E+00	
525.000 4070.000 0.0000000E+00 0.0000000E+00 0.0000000E+00	
525.000 4075.000 0.0000000E+00 0.0000000E+00 0.0000000E+00	
525.000 4080.000 0.0000000E+00 0.0000000E+00 0.0000000E+00	
525.000 4085.000 0.0000000E+00 0.0000000E+00 0.0000000E+00	
525.000 4090.000 0.0000000E+00 0.0000000E+00 0.0000000E+00	
525.000 4095.000 0.0000000E+00 0.0000000E+00 0.0000000E+00	
525.000 4100.000 0.0000000E+00 0.0000000E+00 0.0000000E+00	
530.000 4050.000 0.0000000E+00 0.0000000E+00 0.0000000E+00	
530.000 4055.000 0.0000000E+00 0.0000000E+00 0.0000000E+00	
530.000 4060.000 0.0000000E+00 0.0000000E+00 0.0000000E+00	
530.000 4065.000 0.0000000E+00 0.0000000E+00 0.0000000E+00	
530.000 4070.000 0.0000000E+00 0.0000000E+00 0.0000000E+00	
530.000 4075.000 0.0000000E+00 0.0000000E+00 0.0000000E+00	
530.000 4080.000 0.0000000E+00 0.0000000E+00 0.0000000E+00	
530.000 4085.000 0.0000000E+00 0.0000000E+00 0.0000000E+00	
530.000 4090.000 0.0000000E+00 0.0000000E+00 0.0000000E+00	
530.000 4095.000 0.0000000E+00 0.0000000E+00 0.0000000E+00	
530.000 4100.000 0.0000000E+00 0.0000000E+00 0.0000000E+00	

535.000	4050.000	0.0000000E+00	0.0000000E+00	0.0000000E+00
535.000	4055.000	0.0000000E+00	0.0000000E+00	0.0000000E+00
535.000	4060.000	0.0000000E+00	0.0000000E+00	0.0000000E+00
535.000	4065.000	0.0000000E+00	0.0000000E+00	0.0000000E+00
535.000	4070.000	0.0000000E+00	0.0000000E+00	0.0000000E+00
535.000	4075.000	0.0000000E+00	0.0000000E+00	0.0000000E+00
535.000	4080.000	0.0000000E+00	0.0000000E+00	0.0000000E+00
535.000	4085.000	0.0000000E+00	0.0000000E+00	0.0000000E+00
535.000	4090.000	0.0000000E+00	0.0000000E+00	0.0000000E+00
535.000	4095.000	0.0000000E+00	0.0000000E+00	0.0000000E+00
535.000	4100.000	0.0000000E+00	0.0000000E+00	0.0000000E+00
540.000	4050.000	0.0000000E+00	0.0000000E+00	0.0000000E+00
540.000	4055.000	0.0000000E+00	0.0000000E+00	0.0000000E+00
540.000	4060.000	0.0000000E+00	0.0000000E+00	0.0000000E+00
540.000	4065.000	0.0000000E+00	0.0000000E+00	0.0000000E+00
540.000	4070.000	0.0000000E+00	0.0000000E+00	0.0000000E+00
540.000	4075.000	0.0000000E+00	0.0000000E+00	0.2430110E-02
540.000	4080.000	0.0000000E+00	0.0000000E+00	0.3836453E-02
540.000	4085.000	0.0000000E+00	0.0000000E+00	0.2421387E-03
540.000	4090.000	0.0000000E+00	0.0000000E+00	0.0000000E+00
540.000	4095.000	0.0000000E+00	0.0000000E+00	0.0000000E+00
540.000	4100.000	0.0000000E+00	0.0000000E+00	0.0000000E+00
545.000	4050.000	0.0000000E+00	0.0000000E+00	0.0000000E+00
545.000	4055.000	0.0000000E+00	0.0000000E+00	0.0000000E+00
545.000	4060.000	0.0000000E+00	0.0000000E+00	0.0000000E+00
545.000	4065.000	0.0000000E+00	0.0000000E+00	0.0000000E+00
545.000	4070.000	0.0000000E+00	0.0000000E+00	0.2430110E-02
545.000	4075.000	0.0000000E+00	0.7194468E-01	0.1028100E+00
545.000	4080.000	0.0000000E+00	0.1697034E+00	0.1484004E+00
545.000	4085.000	0.0000000E+00	0.1495051E-02	0.3450712E-02
545.000	4090.000	0.0000000E+00	0.0000000E+00	0.2421387E-03
545.000	4095.000	0.0000000E+00	0.0000000E+00	0.0000000E+00
545.000	4100.000	0.0000000E+00	0.0000000E+00	0.0000000E+00
550.000	4050.000	0.0000000E+00	0.0000000E+00	0.0000000E+00
550.000	4055.000	0.0000000E+00	0.0000000E+00	0.0000000E+00
550.000	4060.000	0.0000000E+00	0.0000000E+00	0.0000000E+00
550.000	4065.000	0.0000000E+00	0.0000000E+00	0.0000000E+00
550.000	4070.000	0.0000000E+00	0.0000000E+00	0.3836453E-02
550.000	4075.000	0.0000000E+00	0.1697034E+00	0.1484004E+00
550.000	4080.000	0.1000000E+01	0.1000000E+01	0.1000000E+01
550.000	4085.000	0.0000000E+00	0.1697034E+00	0.1484004E+00
550.000	4090.000	0.0000000E+00	0.0000000E+00	0.3836453E-02
550.000	4095.000	0.0000000E+00	0.0000000E+00	0.0000000E+00
550.000	4100.000	0.0000000E+00	0.0000000E+00	0.0000000E+00
555.000	4050.000	0.0000000E+00	0.0000000E+00	0.0000000E+00
555.000	4055.000	0.0000000E+00	0.0000000E+00	0.0000000E+00
555.000	4060.000	0.0000000E+00	0.0000000E+00	0.0000000E+00
555.000	4065.000	0.0000000E+00	0.0000000E+00	0.0000000E+00
555.000	4070.000	0.0000000E+00	0.0000000E+00	0.2421387E-03
555.000	4075.000	0.0000000E+00	0.1495051E-02	0.3450712E-02
555.000	4080.000	0.0000000E+00	0.1697034E+00	0.1484004E+00
555.000	4085.000	0.0000000E+00	0.7194468E-01	0.1028100E+00
555.000	4090.000	0.0000000E+00	0.0000000E+00	0.2430110E-02
555.000	4095.000	0.0000000E+00	0.0000000E+00	0.0000000E+00
555.000	4100.000	0.0000000E+00	0.0000000E+00	0.0000000E+00
560.000	4050.000	0.0000000E+00	0.0000000E+00	0.0000000E+00
560.000	4055.000	0.0000000E+00	0.0000000E+00	0.0000000E+00
560.000	4060.000	0.0000000E+00	0.0000000E+00	0.0000000E+00
560.000	4065.000	0.0000000E+00	0.0000000E+00	0.0000000E+00
560.000	4070.000	0.0000000E+00	0.0000000E+00	0.0000000E+00
560.000	4075.000	0.0000000E+00	0.0000000E+00	0.2421387E-03
560.000	4080.000	0.0000000E+00	0.0000000E+00	0.3836453E-02
560.000	4085.000	0.0000000E+00	0.0000000E+00	0.2430110E-02
560.000	4090.000	0.0000000E+00	0.0000000E+00	0.0000000E+00
560.000	4095.000	0.0000000E+00	0.0000000E+00	0.0000000E+00
560.000	4100.000	0.0000000E+00	0.0000000E+00	0.0000000E+00
565.000	4050.000	0.0000000E+00	0.0000000E+00	0.0000000E+00
565.000	4055.000	0.0000000E+00	0.0000000E+00	0.0000000E+00

565.000	4060.000	0.0000000E+00	0.0000000E+00	0.0000000E+00
565.000	4065.000	0.0000000E+00	0.0000000E+00	0.0000000E+00
565.000	4070.000	0.0000000E+00	0.0000000E+00	0.0000000E+00
565.000	4075.000	0.0000000E+00	0.0000000E+00	0.0000000E+00
565.000	4080.000	0.0000000E+00	0.0000000E+00	0.0000000E+00
565.000	4085.000	0.0000000E+00	0.0000000E+00	0.0000000E+00
565.000	4090.000	0.0000000E+00	0.0000000E+00	0.0000000E+00
565.000	4095.000	0.0000000E+00	0.0000000E+00	0.0000000E+00
565.000	4100.000	0.0000000E+00	0.0000000E+00	0.0000000E+00
570.000	4050.000	0.0000000E+00	0.0000000E+00	0.0000000E+00
570.000	4055.000	0.0000000E+00	0.0000000E+00	0.0000000E+00
570.000	4060.000	0.0000000E+00	0.0000000E+00	0.0000000E+00
570.000	4065.000	0.0000000E+00	0.0000000E+00	0.0000000E+00
570.000	4070.000	0.0000000E+00	0.0000000E+00	0.0000000E+00
570.000	4075.000	0.0000000E+00	0.0000000E+00	0.0000000E+00
570.000	4080.000	0.0000000E+00	0.0000000E+00	0.0000000E+00
570.000	4085.000	0.0000000E+00	0.0000000E+00	0.0000000E+00
570.000	4090.000	0.0000000E+00	0.0000000E+00	0.0000000E+00
570.000	4095.000	0.0000000E+00	0.0000000E+00	0.0000000E+00
570.000	4100.000	0.0000000E+00	0.0000000E+00	0.0000000E+00
575.000	4050.000	0.0000000E+00	0.0000000E+00	0.0000000E+00
575.000	4055.000	0.0000000E+00	0.0000000E+00	0.0000000E+00
575.000	4060.000	0.0000000E+00	0.0000000E+00	0.0000000E+00
575.000	4065.000	0.0000000E+00	0.0000000E+00	0.0000000E+00
575.000	4070.000	0.0000000E+00	0.0000000E+00	0.0000000E+00
575.000	4075.000	0.0000000E+00	0.0000000E+00	0.0000000E+00
575.000	4080.000	0.0000000E+00	0.0000000E+00	0.0000000E+00
575.000	4085.000	0.0000000E+00	0.0000000E+00	0.0000000E+00
575.000	4090.000	0.0000000E+00	0.0000000E+00	0.0000000E+00
575.000	4095.000	0.0000000E+00	0.0000000E+00	0.0000000E+00
575.000	4100.000	0.0000000E+00	0.0000000E+00	0.0000000E+00

G.2 CALCULATION OF FREQUENCY OF INTERSECTION

The remaining variables needed for the calculation of the frequency of intersection, $v_i(t|\theta_k)$, are the rate parameter $\lambda(t)$ and the discrete spatial mass density, $f(x,y)$.

G.2.1 Event Rate Calculation

The event rate parameter is calculated using two approaches. If the temporal process is assumed to be homogeneous, then the rate parameter is calculated by the maximum likelihood estimate N/T , where N is the number of volcanic events that have occurred in time T . If the nonhomogeneous Weibull process is assumed to apply, then the rate parameter is calculated using Equation (F-3) with the maximum likelihood estimates of the parameters of Equation (F-3) given by Equation (F-4). Statistical uncertainty in the estimate of the rate parameter was specified by a three-point discrete distribution with the maximum likelihood estimate assigned a probability of 0.63 and the 5th and 95th percentiles of the sampling distribution assigned a probability of 0.185. The 5th and 95th percentiles of the sampling distribution for the homogeneous process are given by Equation (F-2). The 5th and 95th percentiles of the sampling distribution for the Weibull process are tabulated in Crow (1982). Both of these approaches were implemented in the various computer programs used to calculate the spatial density function.

G.2.2 Spatial Density Calculation

Three basic types of spatial models are used to calculate the spatial density function, $f(x,y)$, a source zone within which $f(x,y)$ is assumed to be uniform, a bivariate Gaussian distribution modeling a volcanic field, and a nonparametric kernel density function. Separate computer programs were used to perform each type of spatial density calculation and the summation defined by Equation (G-1). Each of these programs has the same general structure in that they account for the uncertainty in the numbers of volcanic events, the uncertainty in the number of hidden events, and the statistical uncertainty in the rate parameter.

Calculation of Frequency of Intersection for Uniform Volcanic Zone. Figure G-3 shows an example volcanic source zone in which seven events have been identified to have occurred post 5 Ma. These events are separated into a northern center with three events and a southern center with four events. The calculation of the frequency of intersection for a uniform source zone was performed using program **UZVH**(v1.0). The program performs the following operations. First, it reads in the conditional probability of intersection values for the computation grid (the output of program **CPDI**). Then it reads in the source zone boundary(s). The source zones can consist of several disjoint pieces and can include holes. The zones can also have gradual edges with a linear decrease in the spatial density over a specified distance. The approximate zone area within the calculation grid is determined by the number of grid points within the zone boundary multiplying by the grid unit area ($\Delta x \Delta y$). The spatial density, $f(x,y)$, is then set equal to the inverse of the zone area. The program then reads in the discrete distributions for the volcanic event counts at each of the volcanic centers that lie within the source zone. Using nested loops, the program calculates all possible combinations of event counts within the source zone. For each possible event count a three point distribution for the rate parameter is calculated for either a homogeneous or nonhomogeneous process (Section G.2.1 above). The program then performs the summation of Equation (G-1) for each rate parameter, resulting in three possible values for the frequency of intersection, given a specific set of events. If a distribution for hidden event factors is specified, then frequencies of intersection are calculated for each hidden event factor. The program calculates the exact mean hazard and creates a discrete distribution for the frequency of intersection by placing each individual calculated value into discrete intervals equally spaced on a log scale with 100 intervals per log decade.

The following is a listing of example input and output files for program **UZVH** using the example shown of Figure G-3. Two sets of inputs and outputs are presented, one with no uncertainty in the event counts and one with uncertainty in the event counts.

Input File: UZVH.IN

```
uz.in          first individual source zone input file (no uncertainty in event counts)
uzue.in       second individual source zone input file (uncertainty in event counts)
q             q to quit
```

Input File: UZ.IN

```
.\cpdi\examp.cpi
Example Zone 5m years - homogeneous
uz-h
1
Example Zone
1
'examp.z' 1 0 0

1 1 LN
'X'

1 1 NWCF
'nvc.3'
1 1 SECF
'svc.4'
1 1 AG
'X'
1 1 SB
'X'
1 1 TM
'X'
1 1 BM
'X'
t 5000000 1.0 0 1 1.0 1.0

for
```

```
output of program CPDI
Label for first calculation
output file name
number of zones
zone name
number of enclosed zone segments
zone file name, zone factor (-1 means remove piece), western ramp distance,
eastern ramp distance (these allow for a gradual decrease in the
spatial density)
# of event counts at 1st center, probability of each event count
file name with first event count at 1st center (X indicates no
events at this center within this source zone)
# of event counts at 2nd center, probability of each event count
file name with first event count at 2nd center
# of event counts at 3rd center, probability of each event count
file name with first event count at 3rd center
# of event counts at 4th center, probability of each event count
file name with first event count at 4th center
# of event counts at 5th center, probability of each event count
file name with first event count at 5th center
# of event counts at 6th center, probability of each event count
file name with first event count at 6th center
# of event counts at 7th center, probability of each event count
file name with first event count at 7th center
t for homogeneous, time period, rate factor, # of additional centers within
zone, # of hidden event factors, hidden event factor, probability
```

```
Example Zone 5m years - nonhomogeneous
uz-w
1
Example Zone
1
'examp.z' 1 0 0

1 1 LN
'X'

1 1 NWCF
'nvc.3'
1 1 SECF
'svc.4'
1 1 AG
'X'
1 1 SB
'X'
1 1 TM
'X'
1 1 BM
'X'
f 5000000 1.0 0 1 1.0 1.0

within

for
```

```
factor (pairs repeated for each factor)
Label for next calculation
output file name
number of zones
zone name
number of enclosed zone segments
zone file name, zone factor (-1 means remove piece),
western ramp distance, eastern ramp distance (these allow
for a gradual decrease in the spatial density)
# of event counts at 1st center, probability of each event count
file name with first event count at 1st center (X indicates no
events at this center within this source zone)
# of event counts at 2nd center, probability of each event count
file name with first event count at 2nd center
# of event counts at 3rd center, probability of each event count
file name with first event count at 3rd center
# of event counts at 4th center, probability of each event count
file name with first event count at 4th center
# of event counts at 5th center, probability of each event count
file name with first event count at 5th center
# of event counts at 6th center, probability of each event count
file name with first event count at 6th center
# of event counts at 7th center, probability of each event count
file name with first event count at 7th center
f for nonhomogeneous, time period, rate factor, # of additional centers
zone, # of hidden event factors, hidden event factor, probability
factor (pairs repeated for each factor)
```

Input File: EXAMP.Z

```
Example Zone          Zone Label
18                   # of zone boundary vertices
532.5 4062.5         x, y of zone boundary vertex
532.5 4067.5
```

532.5 4072.5
532.5 4077.5
532.5 4082.5
532.5 4087.5
535.0 4087.5
537.5 4085.0
540.0 4082.5
542.5 4080.0
545.0 4077.5
547.5 4075.0
547.5 4070.0
547.5 4062.5
547.5 4062.5
542.5 4062.5
537.5 4062.5
532.5 4062.5

Input File: NVC.3

North Center 3 events
3 0
534.0 4077.0 0.5
535.0 4082.0 1.0
538.0 4080.0 1.5

label for file
of mapped events, # of hidden events
x, y, age (Ma) of first event
x, y, age (Ma) of second event
...

Input File: SVC.3 (same format as NVC.3)

South Center 4 events
4 0
535.0 4067.0 3.0
537.5 4065.0 3.5
542.5 4070.0 4.0
545.0 4068.0 4.5

The program produces three output files for each calculation.

Output File: UZ-H.OUT

Example Zone 5m years - homogeneous
Source SUM1 SUM2 SUM3 mambda mbeta sbeta
Example Zone 0.0000E+00 0.6058E-02 0.9390E-02 0.1509E-05 0.000 0.000

This lists the sum of $f(x,y) \cdot P_i(x,y)$ over the source zone for the three event representations (point event, event-centered dike, and randomly placed dike), the mean value of $\lambda(t=0)$, and the mean and standard error of the β parameter of the Weibull process (if used).

Output File: UZ-H.HAZ

Example Zone 5m years - homogeneous
3
1 0.000000E+00 0.000000E+00 0.000000E+00 0.000000E+00 0.000000E+00 0.000000E+00 0.000000E+00
0.000000E+00 0.000000E+00 0.000000E+00 0.000000E+00 0.000000E+00 0.000000E+00
2 0.9145091E-08 0.2239166E-16 0.000000E+00 0.000000E+00 0.000000E+00 0.000000E+00 0.000000E+00
0.000000E+00 0.000000E+00 0.000000E+00 0.000000E+00 0.000000E+00 0.2239166E-16
3 0.1417393E-07 0.5378866E-16 0.000000E+00 0.000000E+00 0.000000E+00 0.000000E+00 0.000000E+00
0.000000E+00 0.000000E+00 0.000000E+00 0.000000E+00 0.000000E+00 0.5378866E-16

This file contains three main lines of output, one for each type of event representations (1 - point event, 2 - event-centered dike, 3 - randomly placed dike). Each line contains the mean frequency of intersection, the variance in the frequency of intersection, and the breakdown of the variance into the components associated with each type of uncertainty. The last component is the variance in the hazard due to the statistical distribution for the rate parameter.

Output File: UZ-H.DST

Example Zone 5m years - homogeneous

```
3
1
0.0000E+00 0.1000E+01
3
0.2630E-08 0.1850E+00 0.8511E-08 0.6300E+00 0.1778E-07 0.1850E+00
3
0.4074E-08 0.1850E+00 0.1318E-07 0.6300E+00 0.2754E-07 0.1850E+00
```

This file contains three blocks of output. Each block is the discrete distribution for frequency of intersection calculated for all of the alternative parameter values defined in the input file. In this example, there are only three alternatives, corresponding to the three-point distribution for the rate parameter. Only one value (0) is shown for the point event representation because the value of the conditional probability of intersection is zero everywhere within the source zone.

The corresponding output files for the nonhomogeneous case are:

Output File: UZ-W.OUT

Example Zone 5m years - nonhomogeneous

Source	SUM1	SUM2	SUM3	mambda	mbeta	sbeta
Example Zone	0.0000E+00	0.6058E-02	0.9390E-02	0.1656E-05	1.042	0.000

Note that the mean value of $\lambda(t=0)$ is larger than for the homogeneous case because $\beta > 1$.

Output File: UZ-W.HAZ

Example Zone 5m years - nonhomogeneous

```
3
1 0.0000000E+00 0.0000000E+00 0.0000000E+00 0.0000000E+00 0.0000000E+00 0.0000000E+00 0.0000000E+00 0.0000000E+00
0.0000000E+00 0.0000000E+00 0.0000000E+00 0.0000000E+00 0.0000000E+00 0.0000000E+00 0.0000000E+00 0.0000000E+00
2 0.1003296E-07 0.3502814E-16 0.2237134E-23 0.2237134E-23 0.2237134E-23 0.2237134E-23 0.2237134E-23 0.2237134E-23
0.2237134E-23 0.2237134E-23 0.2237134E-23 0.2237134E-23 0.2237134E-23 0.3502814E-16
3 0.1555003E-07 0.8414365E-16 0.3728359E-23 0.3728359E-23 0.3728359E-23 0.3728359E-23 0.3728359E-23 0.3728359E-23
0.3728359E-23 0.3728359E-23 0.3728359E-23 0.3728359E-23 0.3728359E-23 0.8414365E-16
```

Output File: UZ-W.DST

Example Zone 5m years - nonhomogeneous

```
3
1
0.0000E+00 0.1000E+01
3
0.2692E-08 0.1850E+00 0.8913E-08 0.6300E+00 0.2138E-07 0.1850E+00
3
0.4169E-08 0.1850E+00 0.1380E-07 0.6300E+00 0.3311E-07 0.1850E+00
```

The second input file contains an example with uncertainty in the event counts.

Input File: UZUE.IN

. \cpdi\examp.cpi	output of program CPDI
Example Zone 5m years uncertain events -	homogeneous label for first calculation
uzue-h	output file name
1	number of zones
Example Zone	zone name
1	number of enclosed zone segments
'examp.z' 1 0 0	zone file name, zone factor (-1 means remove piece), western ramp distance, eastern ramp distance (these allow

```
1 1 LN                                     for a gradual decrease in the spatial density)
'X'                                       # of event counts at 1st center, probability of each event count
                                         file name with first event count at 1st center (X indicates no
                                         events at this center within this source zone)
2 .3 .7 NWCF                             # of event counts at 2nd center, probability of each event count
'nvc.2'                                  file name with first event count at 2nd center
'nvc.3'                                  file name with second event count at 2nd center
2 .4 .6 SECF                             # of event counts at 3rd center, probability of each event count
'svc.2'                                  file name with first event count at 3rd center
'svc.4'                                  file name with second event count at 3rd center
1 1 AG                                    # of event counts at 4th center, probability of each event count
'X'                                       file name with first event count at 4th center
1 1 SB                                    # of event counts at 5th center, probability of each event count
'X'                                       file name with first event count at 5th center
1 1 TM                                    # of event counts at 6th center, probability of each event count
'X'                                       file name with first event count at 6th center
1 1 BM                                    # of event counts at 7th center, probability of each event count
'X'                                       file name with first event count at 7th center
t 5000000 1.0 0 1 1.0 1.0              t for homogeneous, time period, rate factor, # of additional
                                         centers within zone, # of hidden event factors, hidden
                                         event factor, probability for factor (pairs repeated for
                                         each factor)

Example Zone 5m years uncertain events - nonhomogeneous Label for next calculation
uzue-w output file name
1 number of zones
Example Zone zone name
1 number of enclosed zone segments
'examp.z' 1 0 0 zone file name, zone factor (-1 means remove piece), western ramp distance,
                                         eastern ramp distance (these allow for a gradual decrease in the
                                         spatial density)

1 1 LN                                     # of event counts at 1st center, probability of each event count
'X'                                       file name with first event count at 1st center (X indicates no
                                         events at this center within this source zone)
2 .3 .7 NWCF                             # of event counts at 2nd center, probability of each event count
'nvc.2'                                  file name with first event count at 2nd center
'nvc.3'                                  file name with second event count at 2nd center
2 .4 .6 SECF                             # of event counts at 3rd center, probability of each event count
'svc.2'                                  file name with first event count at 3rd center
'svc.4'                                  file name with second event count at 3rd center
1 1 AG                                    # of event counts at 4th center, probability of each event count
'X'                                       file name with first event count at 4th center
1 1 SB                                    # of event counts at 5th center, probability of each event count
'X'                                       file name with first event count at 5th center
1 1 TM                                    # of event counts at 6th center, probability of each event count
'X'                                       file name with first event count at 6th center
1 1 BM                                    # of event counts at 7th center, probability of each event count
'X'                                       file name with first event count at 7th center
f 5000000 1.0 0 1 1.0 1.0              f for nonhomogeneous, time period, rate factor, # of additional
                                         centers within zone, # of hidden event factors, hidden
                                         event factor, probability for factor (pairs repeated for
                                         each factor)
```

The additional input files not listed above are:

Input File: NVC.2

```
North Center 2 events
2 0
534.0 4077.0 0.5
538.0 4080.0 1.5
```

Input File: SVC.2

```
South Center 2 events
2 0
```

535.0 4067.0 3.0
545.0 4068.0 4.5

The corresponding output files for the homogeneous case are:

Output File: UZUE-H.OUT

Example Zone 5m years uncertain events - homogeneous
Source SUM1 SUM2 SUM3 mambda mbeta sbeta
Example Zone 0.0000E+00 0.6058E-02 0.9390E-02 0.1290E-05 0.000 0.000

Output File: UZUE-H.HAZ

Example Zone 5m years uncertain events - homogeneous
3
1 0.000000E+00 0.000000E+00 0.000000E+00 0.000000E+00 0.000000E+00 0.000000E+00 0.000000E+00 0.000000E+00
0.000000E+00 0.000000E+00 0.000000E+00 0.000000E+00 0.000000E+00 0.000000E+00 0.000000E+00
2 0.781530E-08 0.207433E-16 0.000000E+00 0.000000E+00 0.306835E-18 0.140273E-17 0.000000E+00 0.000000E+00
0.000000E+00 0.000000E+00 0.000000E+00 0.000000E+00 0.000000E+00 0.000000E+00 0.190337E-16
3 0.121128E-07 0.498290E-16 0.000000E+00 0.737079E-18 0.336960E-17 0.370253E-24 0.370253E-24 0.370253E-24
0.370253E-24 0.370253E-24 0.370253E-24 0.370253E-24 0.370253E-24 0.457224E-16

Note that additional components of variance appear. (The extremely small variance components, of the order of 10⁻²⁴ are a result of numerical round off error during single precision arithmetic.)

Output File: UZUE-W.DST

Example Zone 5m years uncertain events -
3
1
0.0000E+00 0.1000E+01
12
0.8710E-09 0.2220E-01 0.1380E-08 0.5180E-01 0.1995E-08 0.3330E-01 0.2630E-08 0.7770E-01 0.4898E-08 0.7560E-01
0.6026E-08 0.1764E+00 0.7244E-08 0.1134E+00 0.8511E-08 0.2646E+00 0.1259E-07 0.2220E-01 0.1445E-07 0.5180E-01
0.1622E-07 0.3330E-01 0.1778E-07 0.7770E-01
12
0.1349E-08 0.2220E-01 0.2138E-08 0.5180E-01 0.3090E-08 0.3330E-01 0.4074E-08 0.7770E-01 0.7586E-08 0.7560E-01
0.9333E-08 0.1764E+00 0.1122E-07 0.1134E+00 0.1318E-07 0.2646E+00 0.1950E-07 0.2220E-01 0.2239E-07 0.5180E-01
0.2512E-07 0.3330E-01 0.2754E-07 0.7770E-01

Note that the distributions now contain 12 values, 4 possible sets of event counts times 3 rates per event count.

The corresponding output files for the nonhomogeneous case are:

Output File: UZUE-W.OUT

Example Zone 5m years uncertain events - nonhomogeneous
Source SUM1 SUM2 SUM3 mambda mbeta sbeta
Example Zone 0.0000E+00 0.6058E-02 0.9390E-02 0.1487E-05 1.093 0.127

Note that there is now uncertainty in β due to the uncertainty in the event counts.

Output File: UZUE-W.HAZ

Example Zone 5m years uncertain events - nonhomogeneous
3
1 0.000000E+00 0.000000E+00 0.000000E+00 0.000000E+00 0.000000E+00 0.000000E+00 0.000000E+00 0.000000E+00
0.000000E+00 0.000000E+00 0.000000E+00 0.000000E+00 0.000000E+00 0.000000E+00
2 0.900807E-08 0.355857E-16 0.504643E-24 0.122762E-17 0.195184E-18 0.164337E-23 0.164337E-23 0.164337E-23
0.164337E-23 0.164337E-23 0.164337E-23 0.164337E-23 0.164337E-23 0.341629E-16
3 0.139615E-07 0.854830E-16 0.000000E+00 0.294899E-17 0.468848E-18 0.155374E-23 0.155374E-23 0.155374E-23
0.155374E-23 0.155374E-23 0.155374E-23 0.155374E-23 0.155374E-23 0.820652E-16

Output File: UZUE-W.DST

Example Zone 5m years uncertain events -

```
3
1
0.0000E+00 0.1000E+01
12
0.8913E-09 0.2220E-01 0.1738E-08 0.5180E-01 0.1778E-08 0.3330E-01 0.2692E-08 0.7770E-01 0.5248E-08 0.7560E-01
0.6761E-08 0.1134E+00 0.7762E-08 0.1764E+00 0.8913E-08 0.2646E+00 0.1698E-07 0.2220E-01 0.1738E-07 0.3330E-01
0.2138E-07 0.7770E-01 0.2188E-07 0.5180E-01
12
0.1380E-08 0.2220E-01 0.2692E-08 0.5180E-01 0.2754E-08 0.3330E-01 0.4169E-08 0.7770E-01 0.8128E-08 0.7560E-01
0.1047E-07 0.1134E+00 0.1202E-07 0.1764E+00 0.1380E-07 0.2646E+00 0.2630E-07 0.2220E-01 0.2692E-07 0.3330E-01
0.3311E-07 0.7770E-01 0.3388E-07 0.5180E-01
```

Calculation of Frequency of Intersection for Bivariate Gaussian Field. The second approach to estimating the spatial density of volcanic events, $f(x,y)$, was to assume that the events within a volcanic field are distributed following a bivariate Gaussian distribution. Two approaches were used to define the parameters of this distribution. The first was to assume that a specified source zone boundary approximates a specified density contour of the field. Equation (F-12) defines the coordinates of a specified density ellipse for a bivariate Gaussian distribution. The computer program FITFIELD(v1.0) was used to find the parameters of the equivalent Gaussian field that minimize the mean square error between $(x-\mu)^T \Sigma^{-1} (x-\mu)$ calculated at points along the zone boundary and the corresponding value for $\chi^2(2,\alpha)$, where $1-\alpha$ is the specified density contour. The minimization is performed using minimization routines given in Press et al. (1992).

Figure G-4 shows an example of fitting a bivariate Gaussian field to the volcanic source zone shown on Figure G-3, assuming that it represents an approximate 95 percent density contour. The input and output files to program FITFIELD are:

Input File: FITFIELD.IN

```
Fit Gaussian Fit to Example Zone ChI2=95%
5.99 20 .01
1 '*'
examp.z
```

```
Label for calculation
 $\chi^2(2,\alpha)$ , max # iterations, stopping tolerance
# headers in zone file, format
zone boundary file (listed above)
```

Output File: FITFIELD.OUT

Fit Gaussian Fit to Example Zone ChI2=95%

INITIAL FLOATING PARAMETERS :

```
-----
C( 1) = 0.5387500000E+03
C( 2) = 0.4073333250E+04
C( 3) = 0.9244791980E+01
C( 4) = 0.2135416980E+02
C( 5) = -0.3211805580E+01
```

starting parameters calculated using zone vertices

Maximum tolerance = 0.9999999780E-02

Direction Set: Powell algorithm

Iteration No.= 1 MSE = 0.366829E+01 first iteration results
C= 0.5387E+03 0.4073E+04 0.1659E+02 0.2943E+02 -0.6677E+01

Iteration No.= 2 MSE = 0.345864E+01
C= 0.5384E+03 0.4072E+04 0.1486E+02 0.3080E+02 -0.6275E+01

Iteration No.= 3 MSE = 0.336030E+01
C= 0.5386E+03 0.4072E+04 0.1411E+02 0.3208E+02 -0.6171E+01

FINAL RESULT :

Iteration Number = 4 MSE = 0.3273E+01 final results
CH12 Mean X Mean Y sigmaX2 sigmaY2 sigmaXY
5.990 538.957 4071.693 12.966 34.955 -5.975

The field parameters are then used to calculate the spatial density associated with the field. The rate term, $\lambda(t=0)$ is calculated in the same way as for the homogeneous source zone using the events within the zone boundary. The annual frequency of intersection is calculated using program **PFGVH**(v1.0). The program performs the following operations. First, it reads in the conditional probability of intersection values for the computation grid (the output of program **CPDI**). Then it reads in the field parameters calculated by program **FITFIELD** and calculates the spatial density, $f(x,y)$, using Equation (3-9). The program then follows the structure of **UZVH**, reading in the discrete distributions for the volcanic event counts at each of the volcanic centers that lie within the source zone and using nested loops to calculate all possible combinations of event counts associated with the field. For each possible event count a three point distribution for the rate parameter is calculated for either a homogeneous or nonhomogeneous process (Section G.2.1 above). The program then performs the summation of Equation (G-1) for each rate parameter, resulting in three possible values for the frequency of intersection, given a specific set of events. If a distribution for hidden event factors is specified, then frequencies of intersection are calculated for each hidden event factor. The program calculates the exact mean hazard and creates a discrete distribution for the frequency of intersection by placing each individual calculated value into discrete intervals equally spaced on a log scale with 100 intervals per log decade.

The following is a listing of example input and output files for program **PFGVH** using the example shown of Figure G-4. The example presents only calculations for the homogeneous temporal model. Results for the nonhomogeneous Weibull process are obtained in exactly the same manner as in the use of program **UZVH**.

Input File: PFGVH.IN

pfg.in first individual source zone input file
q q to quit

Input File: pfg.IN

```
.\cpdi\examp.cpi output file from program CPDI
95% Gaussian field fit to Example Zone - homogeneous field calculation label
pf-h output file name
1 # of fields
Example Zone field label
538.957 4071.693 12.966 34.955 -5.975 field parameters (from program FITFIELD)
1 1 LN remaining parameters are the same as described above for input file
'X' UZ.IN used in program UZVH
1 1 NWCf
'nvc.3'
1 1 SECF
'svc.4'
1 1 AG
'X'
1 1 SB
'X'
1 1 TM
'X'
1 1 BM
'X'
t 5000000 1.0 0 1 1.0 1.0
```

As before, the program produces three output files for each calculation.

Output File: PF-H.OUT

```
95% Gaussian field fit to Example Zone - homogeneous
Source SUM1 SUM2 SUM3 mambda mbeta sbeta
Example Zone 0.1089E-03 0.3334E-02 0.4700E-02 0.1509E-05 0.000 0.000
```

Output File: PF-H.HAZ

```
95% Gaussian field fit to Example Zone - homogeneous
3
1 0.1643792E-09 0.7234425E-20 0.0000000E+00 0.0000000E+00 0.0000000E+00 0.0000000E+00 0.0000000E+00
0.0000000E+00 0.0000000E+00 0.0000000E+00 0.0000000E+00 0.0000000E+00 0.7234425E-20
2 0.5033139E-08 0.6782474E-17 0.0000000E+00 0.0000000E+00 0.0000000E+00 0.0000000E+00 0.0000000E+00
0.0000000E+00 0.0000000E+00 0.0000000E+00 0.0000000E+00 0.0000000E+00 0.6782474E-17
3 0.7094505E-08 0.1347580E-16 0.4018061E-24 0.4018061E-24 0.4018061E-24 0.4018061E-24 0.4018061E-24
0.4018061E-24 0.4018061E-24 0.4018061E-24 0.4018061E-24 0.4018061E-24 0.1347580E-16
```

Output File: PF-H.DST

```
95% Gaussian field fit to Example Zone -
3
3
0.4786E-10 0.1850E+00 0.1549E-09 0.6300E+00 0.3236E-09 0.1850E+00
3
0.1445E-08 0.1850E+00 0.4677E-08 0.6300E+00 0.9772E-08 0.1850E+00
3
0.2042E-08 0.1850E+00 0.6607E-08 0.6300E+00 0.1380E-07 0.1850E+00
```

The second approach calculates the parameters of the bivariate Gaussian distribution directly from the observed volcanic events. Equation (F-9) is used to calculate the maximum likelihood estimates of the field parameters from the observed events in a field. Statistical uncertainty in the field parameters is modeled in the hazard calculation by defining three values for each parameter, the maximum likelihood value and $\pm 1\sigma$ [calculated using Equation (F-10)]. The result is $3^5=243$ possible sets of field parameters. Equation (F-11) is used to calculate the likelihood value for each set of parameters and these likelihoods are normalized to form a joint probability distribution for the field parameters.

This approach to calculating the spatial density and the resulting frequency of intersection is implemented in program **FPFGVH**(v1.0). Figure G-5 shows the example volcanic events from Figure G-3 and the maximum likelihood bivariate Gaussian distribution fit to the seven event locations. The program performs the following operations. First, it reads in the conditional probability of intersection values for the computation grid (the output of program **CPDI**). Then it reads in the discrete distributions for the volcanic event counts at each of the volcanic centers associated with the field. The program then uses nested loops to calculate all possible combinations of event counts associated with the field. For each possible event count a bivariate Gaussian field is fit to the event locations and distributions for the field parameters are calculated. Each set of field parameters is used to calculate the spatial density for future events associated with the field. These spatial densities are combined with the three point distribution for the rate parameter calculated as described above. The program then performs the summation of Equation (G-1) for each rate parameter and field parameter set, resulting in $3^6=729$ possible values for the frequency of intersection, given a specific set of events. Hidden event factors are then included in the same manner as in the calculations described above.

The following is a listing of example input and output files for program **FPFGVH** using the example shown of Figure G-5. The example presents only calculations for the homogeneous temporal model. Results for the nonhomogeneous Weibull process are obtained in exactly the same manner as in the use of program **UZVH**.

Input File: FPFGVH.IN

```
fpf.in          first individual source zone input file
q              q to quit
```

Input File: fpf.IN

```
.\cpdi\examp.cpi          output file from program CPDI
Gaussian Field fitted to events - homogeneous    calculation label
fpf-h                    output file name
1                        number of fields
Example Zone             field label
  538.143 4072.714   14.765   39.918   -9.888 7   default field parameters calculated from a selected
```

set of events, usually the most likely,
and used when the number of events is too
few to estimate the field parameters (<3),
maximum aspect ratio for the field

1 1 LN the remaining parameters are the same as those in the input to the
above programs

'X'
1 1 NWCF
'nvc.3'
1 1 SECF
'svc.4'
1 1 AG
'X'
1 1 SB
'X'
1 1 TM
'X'
1 1 BM
'X'
t 5000000 1.0 0 1 1.0 1.0

As before, the program produces three output files for each calculation.

Output File: FPF-H.OUT

Gaussian Field fitted to events - homogeneous

Source	SUM1	SUM2	SUM3	mambda	mbeta	sbeta	Mean ar	sig ar
Example Zone	0.7040E-03	0.4875E-02	0.6049E-02	0.1509E-05	0.000	0.000	1.955	0.000

Note that the output file lists the statistics of the aspect ratios for the fitted fields (based on the maximum likelihood fits).

Output File: FPF-H.HAZ

Gaussian Field fitted to events - homogeneous

3

1	0.1062704E-08	0.4299878E-17	0.0000000E+00	0.0000000E+00	0.0000000E+00	0.0000000E+00	0.0000000E+00	0.0000000E+00
0.0000000E+00	0.0000000E+00	0.3153261E-17	0.1979248E-25	0.1979248E-25	0.1146616E-17			
2	0.7357951E-08	0.7342884E-16	0.2568802E-22	0.0000000E+00	0.0000000E+00	0.0000000E+00	0.0000000E+00	0.0000000E+00
0.0000000E+00	0.0000000E+00	0.4648722E-16	0.0000000E+00	0.0000000E+00	0.2694160E-16			
3	0.9130597E-08	0.9166999E-16	0.7797159E-22	0.0000000E+00	0.0000000E+00	0.0000000E+00	0.0000000E+00	0.0000000E+00
0.0000000E+00	0.0000000E+00	0.5470306E-16	0.8440318E-24	0.8440318E-24	0.3696686E-16			

Note that the partition of the total variance that is due to the uncertainty in the field parameters is given by the fourth from the end value.

Output File: FPF-H.HAZ

Gaussian Field fitted to events - homoge

3

316

0.0000E+00	0.5465E-01	0.1047E-11	0.5545E-02	0.1072E-11	0.3378E-02	0.1096E-11	0.8543E-02	0.1122E-11	0.7872E-05
0.1148E-11	0.4887E-05	0.1175E-11	0.4747E-02	0.1202E-11	0.5533E-02	0.1230E-11	0.2807E-04	0.1259E-11	0.2618E-03
0.1288E-11	0.8707E-03	0.1318E-11	0.1104E-04	0.1380E-11	0.9698E-03	0.1413E-11	0.4863E-06	0.1445E-11	0.1065E-02
0.1479E-11	0.1881E-04	0.1514E-11	0.7134E-05	0.1549E-11	0.3576E-05	0.1585E-11	0.1918E-02	0.1622E-11	0.2539E-03
0.1660E-11	0.8622E-06	0.1698E-11	0.2445E-02	0.1778E-11	0.4158E-04	0.1820E-11	0.8500E-03	0.1905E-11	0.2131E-04
0.1950E-11	0.1026E-02	0.1995E-11	0.9426E-04	0.2042E-11	0.3758E-04	0.2089E-11	0.1208E-02	0.2188E-11	0.4379E-03
0.2239E-11	0.5633E-03	0.2291E-11	0.1656E-05	0.2399E-11	0.4335E-05	0.2455E-11	0.7548E-03	0.2512E-11	0.5430E-04
0.2570E-11	0.7402E-05	0.2630E-11	0.7526E-04	0.2692E-11	0.6117E-05	0.2754E-11	0.2496E-03	0.2884E-11	0.6257E-05
0.3020E-11	0.2288E-04	0.3090E-11	0.2936E-05	0.3162E-11	0.1944E-04	0.3311E-11	0.1957E-05	0.3631E-11	0.3393E-04
0.3715E-11	0.4863E-06	0.3802E-11	0.2169E-06	0.3981E-11	0.1273E-05	0.4074E-11	0.3502E-02	0.4169E-11	0.3117E-02
0.4266E-11	0.2174E-05	0.4467E-11	0.4114E-02	0.4571E-11	0.1796E-05	0.4677E-11	0.4228E-06	0.4786E-11	0.4718E-02
0.4898E-11	0.3930E-03	0.5495E-11	0.2264E-04	0.5623E-11	0.2863E-04	0.5754E-11	0.7958E-04	0.5888E-11	0.1432E-02
0.6310E-11	0.3245E-03	0.6761E-11	0.3287E-02	0.7244E-11	0.3585E-02	0.7413E-11	0.8481E-03	0.7586E-11	0.1118E-02

0.7762E-11 0.8937E-04 0.7943E-11 0.2862E-04 0.8318E-11 0.1208E-02 0.8913E-11 0.3326E-03 0.9120E-11 0.1053E-03
0.9550E-11 0.1155E-03 0.1000E-10 0.3055E-02 0.1072E-10 0.8406E-05 0.1122E-10 0.9579E-02 0.1148E-10 0.5430E-04
0.1202E-10 0.3244E-02 0.1230E-10 0.2898E-04 0.1288E-10 0.1440E-05 0.1318E-10 0.1221E-01 0.1349E-10 0.1176E-03
0.1413E-10 0.2450E-03 0.1479E-10 0.1250E-03 0.1549E-10 0.8258E-04 0.1622E-10 0.3810E-03 0.1660E-10 0.6958E-03
0.1698E-10 0.4399E-02 0.1738E-10 0.2822E-07 0.1778E-10 0.4702E-03 0.1820E-10 0.5439E-02 0.1862E-10 0.3036E-07
0.1905E-10 0.3393E-04 0.1950E-10 0.1091E-01 0.1995E-10 0.2828E-03 0.2042E-10 0.8666E-04 0.2138E-10 0.1874E-01
0.2188E-10 0.2888E-02 0.2239E-10 0.2862E-02 0.2570E-10 0.6522E-05 0.2630E-10 0.4228E-06 0.2692E-10 0.5895E-02
0.2754E-10 0.3452E-04 0.2951E-10 0.3058E-02 0.3020E-10 0.1169E-01 0.3090E-10 0.6291E-03 0.3162E-10 0.3966E-03
0.3236E-10 0.3208E-02 0.3311E-10 0.5998E-04 0.3388E-10 0.1541E-02 0.3467E-10 0.1257E-02 0.3631E-10 0.1134E-01
0.3715E-10 0.1019E-03 0.3981E-10 0.3531E-02 0.4074E-10 0.8304E-04 0.4169E-10 0.2192E-10 0.4365E-10 0.4419E-02
0.4467E-10 0.3478E-03 0.4571E-10 0.8580E-03 0.4677E-10 0.3218E-02 0.4786E-10 0.6040E-03 0.4898E-10 0.1210E-03
0.5012E-10 0.6018E-03 0.5129E-10 0.2556E-02 0.5248E-10 0.5265E-03 0.5370E-10 0.9609E-07 0.5495E-10 0.1601E-02
0.5623E-10 0.4583E-03 0.5754E-10 0.2092E-01 0.5888E-10 0.1034E-06 0.6310E-10 0.3492E-02 0.6457E-10 0.8631E-03
0.6761E-10 0.2251E-01 0.6918E-10 0.2662E-02 0.7413E-10 0.4460E-03 0.7586E-10 0.3208E-02 0.7943E-10 0.1195E-02
0.8128E-10 0.6566E-02 0.8511E-10 0.8114E-02 0.9120E-10 0.2450E-03 0.9333E-10 0.1052E-01 0.9550E-10 0.1104E-01
0.9772E-10 0.2142E-02 0.1000E-09 0.1276E-02 0.1023E-09 0.1092E-01 0.1047E-09 0.5169E-03 0.1072E-09 0.9965E-02
0.1096E-09 0.8962E-03 0.1122E-09 0.2822E-07 0.1148E-09 0.1889E-02 0.1175E-09 0.1246E-02 0.1202E-09 0.5419E-02
0.1230E-09 0.3036E-07 0.1259E-09 0.1114E-02 0.1288E-09 0.1021E-03 0.1349E-09 0.1129E-02 0.1380E-09 0.2469E-02
0.1413E-09 0.7239E-02 0.1445E-09 0.7420E-03 0.1479E-09 0.1116E-01 0.1514E-09 0.2057E-02 0.1549E-09 0.4121E-03
0.1622E-09 0.1409E-02 0.1698E-09 0.2599E-02 0.1778E-09 0.4194E-02 0.1820E-09 0.1221E-01 0.1862E-09 0.2168E-02
0.1950E-09 0.4254E-05 0.1995E-09 0.6238E-02 0.2042E-09 0.2555E-02 0.2089E-09 0.5085E-02 0.2138E-09 0.4527E-02
0.2188E-09 0.9064E-02 0.2239E-09 0.2941E-02 0.2291E-09 0.1104E-04 0.2344E-09 0.2943E-03 0.2399E-09 0.3024E-02
0.2455E-09 0.5376E-03 0.2512E-09 0.9435E-02 0.2570E-09 0.1164E-02 0.2630E-09 0.2145E-01 0.2692E-09 0.1545E-02
0.2754E-09 0.3952E-02 0.2818E-09 0.2192E-03 0.2884E-09 0.1395E-02 0.3020E-09 0.1549E-01 0.3090E-09 0.1095E-01
0.3162E-09 0.5544E-02 0.3236E-09 0.2277E-03 0.3311E-09 0.4536E-03 0.3388E-09 0.1602E-01 0.3467E-09 0.2400E-02
0.3715E-09 0.4244E-02 0.3802E-09 0.7432E-02 0.3890E-09 0.8646E-03 0.4074E-09 0.1770E-02 0.4169E-09 0.3007E-02
0.4266E-09 0.1007E-02 0.4365E-09 0.1653E-02 0.4467E-09 0.1206E-01 0.4571E-09 0.2937E-02 0.4677E-09 0.3248E-02
0.5012E-09 0.3422E-02 0.5248E-09 0.3748E-03 0.5370E-09 0.2441E-02 0.5495E-09 0.1537E-01 0.5623E-09 0.3036E-03
0.5754E-09 0.1345E-02 0.5888E-09 0.4369E-02 0.6026E-09 0.5674E-02 0.6310E-09 0.4845E-03 0.6457E-09 0.1015E-01
0.6761E-09 0.1889E-01 0.7079E-09 0.2022E-02 0.7244E-09 0.8066E-02 0.7413E-09 0.1206E-02 0.7586E-09 0.1413E-02
0.7762E-09 0.6577E-02 0.7943E-09 0.1859E-01 0.8128E-09 0.1257E-02 0.8318E-09 0.2035E-02 0.8511E-09 0.3828E-02
0.8710E-09 0.1711E-02 0.8913E-09 0.1132E-01 0.9120E-09 0.2965E-03 0.9333E-09 0.5320E-02 0.9550E-09 0.3180E-02
0.9772E-09 0.1269E-01 0.1000E-08 0.2653E-02 0.1023E-08 0.8750E-02 0.1047E-08 0.1205E-02 0.1072E-08 0.1133E-02
0.1096E-08 0.2319E-02 0.1148E-08 0.2593E-02 0.1175E-08 0.1186E-02 0.1202E-08 0.2325E-02 0.1230E-08 0.9763E-02
0.1259E-08 0.2290E-02 0.1288E-08 0.1227E-02 0.1318E-08 0.1684E-01 0.1349E-08 0.1835E-02 0.1413E-08 0.4229E-02
0.1445E-08 0.6615E-02 0.1514E-08 0.1420E-02 0.1622E-08 0.1185E-01 0.1660E-08 0.1480E-02 0.1698E-08 0.9335E-02
0.1738E-08 0.9171E-03 0.1778E-08 0.1034E-02 0.1820E-08 0.1489E-02 0.1862E-08 0.1018E-01 0.1905E-08 0.2469E-02
0.1950E-08 0.8866E-03 0.1995E-08 0.5086E-03 0.2042E-08 0.4243E-02 0.2089E-08 0.1149E-02 0.2138E-08 0.1964E-02
0.2188E-08 0.1264E-01 0.2291E-08 0.3148E-02 0.2344E-08 0.2855E-03 0.2399E-08 0.6877E-02 0.2455E-08 0.1339E-02
0.2512E-08 0.2192E-03 0.2570E-08 0.2867E-02 0.2630E-08 0.2732E-03 0.2692E-08 0.7708E-02 0.2754E-08 0.2372E-02
0.2818E-08 0.3331E-02 0.2884E-08 0.2412E-02 0.2951E-08 0.8865E-03 0.3020E-08 0.3812E-02 0.3162E-08 0.2872E-02
0.3236E-08 0.2719E-02 0.3311E-08 0.7020E-02 0.3388E-08 0.7080E-02 0.3548E-08 0.4750E-02 0.3631E-08 0.1246E-02
0.3802E-08 0.7222E-02 0.3890E-08 0.3939E-02 0.3981E-08 0.2659E-02 0.4169E-08 0.2259E-02 0.4266E-08 0.8392E-02
0.4571E-08 0.3228E-03 0.4677E-08 0.3389E-02 0.4786E-08 0.7377E-03 0.4898E-08 0.2048E-04 0.5012E-08 0.5020E-03
0.5129E-08 0.1413E-02 0.5248E-08 0.3638E-04 0.5623E-08 0.3049E-02 0.5754E-08 0.1355E-02 0.5888E-08 0.1419E-02
0.6166E-08 0.7082E-03 0.6457E-08 0.5687E-03 0.6607E-08 0.4961E-03 0.6761E-08 0.6875E-03 0.6918E-08 0.2520E-02
0.7079E-08 0.8456E-03 0.7244E-08 0.3595E-03 0.7413E-08 0.1285E-02 0.7586E-08 0.2666E-02 0.7762E-08 0.4181E-02
0.7943E-08 0.2350E-02 0.8128E-08 0.1592E-02 0.8318E-08 0.1157E-02 0.8710E-08 0.2643E-02 0.8913E-08 0.6633E-03
0.9120E-08 0.4610E-02 0.9550E-08 0.3019E-02 0.1175E-07 0.6438E-03 0.1259E-07 0.4166E-03 0.1585E-07 0.6594E-03
0.1622E-07 0.1234E-03 0.1660E-07 0.1569E-02 0.1698E-07 0.2192E-03 0.1862E-07 0.7761E-03 0.1950E-07 0.6718E-03
0.1995E-07 0.8865E-03

270
0.4169E-11 0.8939E-04 0.4786E-11 0.1053E-03 0.6026E-11 0.2899E-04 0.1122E-10 0.3044E-03 0.1230E-10 0.1710E-07
0.1259E-10 0.5634E-03 0.1318E-10 0.3585E-03 0.1380E-10 0.3037E-07 0.1514E-10 0.7180E-03 0.1549E-10 0.2823E-07
0.1738E-10 0.9872E-04 0.2042E-10 0.2496E-03 0.2291E-10 0.8939E-04 0.2692E-10 0.1048E-02 0.3162E-10 0.1055E-02
0.3548E-10 0.2899E-04 0.3631E-10 0.9725E-03 0.3802E-10 0.1919E-02 0.4074E-10 0.2496E-03 0.4266E-10 0.1021E-02
0.4467E-10 0.2663E-06 0.4571E-10 0.2445E-02 0.4786E-10 0.9614E-07 0.5495E-10 0.2005E-03 0.6310E-10 0.8501E-03
0.7943E-10 0.5634E-03 0.8128E-10 0.1802E-02 0.8511E-10 0.3212E-02 0.8913E-10 0.3037E-07 0.9333E-10 0.4255E-05
0.9550E-10 0.7180E-03 0.1000E-09 0.5904E-02 0.1096E-09 0.5747E-06 0.1148E-09 0.3312E-02 0.1230E-09 0.5336E-06
0.1259E-09 0.6523E-05 0.1288E-09 0.8510E-03 0.1318E-09 0.2496E-03 0.1349E-09 0.1846E-02 0.1380E-09 0.3479E-02
0.1413E-09 0.9067E-06 0.1445E-09 0.4134E-05 0.1479E-09 0.1796E-05 0.1549E-09 0.1210E-02 0.1585E-09 0.9725E-03
0.1738E-09 0.1038E-04 0.1778E-09 0.1626E-02 0.1820E-09 0.1028E-02 0.1862E-09 0.1104E-04 0.1905E-09 0.3326E-03
0.2089E-09 0.2048E-04 0.2138E-09 0.1998E-02 0.2239E-09 0.2087E-03 0.2344E-09 0.3639E-04 0.2399E-09 0.9725E-03
0.2512E-09 0.3382E-04 0.2570E-09 0.1055E-02 0.2630E-09 0.6137E-02 0.2692E-09 0.2496E-03 0.2754E-09 0.2813E-02
0.2884E-09 0.1021E-02 0.3020E-09 0.1476E-04 0.3162E-09 0.7868E-02 0.3311E-09 0.3585E-02 0.3388E-09 0.2496E-03
0.3467E-09 0.1957E-05 0.3715E-09 0.2025E-03 0.3981E-09 0.3204E-02 0.4074E-09 0.2221E-04 0.4169E-09 0.6298E-03
0.4266E-09 0.6278E-02 0.4365E-09 0.1253E-02 0.4467E-09 0.4595E-05 0.4571E-09 0.3602E-02 0.4677E-09 0.6118E-05
0.4786E-09 0.1103E-03 0.4898E-09 0.7403E-05 0.5012E-09 0.8144E-02 0.5129E-09 0.4339E-02 0.5370E-09 0.1767E-03

0.5495E-09 0.2652E-02 0.5623E-09 0.1167E-03 0.5888E-09 0.5050E-02 0.6166E-09 0.4340E-02 0.6310E-09 0.4255E-05
0.6457E-09 0.1234E-03 0.6607E-09 0.2496E-03 0.6761E-09 0.2403E-02 0.6918E-09 0.3629E-02 0.7079E-09 0.2192E-03
0.7244E-09 0.7250E-03 0.7413E-09 0.3282E-03 0.7586E-09 0.1021E-03 0.7762E-09 0.5356E-02 0.7943E-09 0.1821E-03
0.8128E-09 0.7443E-03 0.8318E-09 0.3890E-02 0.8511E-09 0.2740E-04 0.8710E-09 0.4093E-03 0.8913E-09 0.1242E-01
0.9120E-09 0.1846E-02 0.9333E-09 0.6529E-02 0.9550E-09 0.5477E-03 0.9772E-09 0.6308E-05 0.1000E-08 0.3579E-03
0.1047E-08 0.7654E-02 0.1072E-08 0.1318E-01 0.1096E-08 0.1277E-02 0.1122E-08 0.2660E-02 0.1148E-08 0.1108E-02
0.1175E-08 0.3964E-02 0.1202E-08 0.2310E-02 0.1230E-08 0.1439E-02 0.1259E-08 0.2993E-02 0.1288E-08 0.1091E-01
0.1318E-08 0.1178E-02 0.1349E-08 0.2196E-02 0.1380E-08 0.4382E-02 0.1413E-08 0.6734E-02 0.1445E-08 0.2226E-02
0.1479E-08 0.1221E-01 0.1514E-08 0.6134E-03 0.1585E-08 0.4411E-03 0.1622E-08 0.6738E-02 0.1660E-08 0.1515E-01
0.1698E-08 0.3130E-02 0.1738E-08 0.5440E-02 0.1778E-08 0.1180E-02 0.1820E-08 0.1170E-02 0.1862E-08 0.5153E-02
0.1905E-08 0.9597E-02 0.1950E-08 0.2662E-06 0.1995E-08 0.1142E-01 0.2042E-08 0.4845E-03 0.2089E-08 0.4202E-03
0.2138E-08 0.1522E-02 0.2188E-08 0.1079E-02 0.2239E-08 0.1747E-01 0.2291E-08 0.2870E-02 0.2344E-08 0.4879E-04
0.2399E-08 0.1470E-02 0.2455E-08 0.4404E-02 0.2512E-08 0.1744E-01 0.2570E-08 0.3317E-02 0.2630E-08 0.6438E-03
0.2692E-08 0.1995E-02 0.2754E-08 0.3897E-02 0.2818E-08 0.6913E-02 0.2884E-08 0.1339E-01 0.2951E-08 0.1246E-02
0.3020E-08 0.2399E-01 0.3090E-08 0.6752E-02 0.3162E-08 0.1053E-02 0.3236E-08 0.1570E-02 0.3311E-08 0.1040E-01
0.3388E-08 0.1226E-01 0.3467E-08 0.8472E-02 0.3548E-08 0.2702E-02 0.3631E-08 0.1470E-01 0.3715E-08 0.1393E-01
0.3802E-08 0.3784E-02 0.3890E-08 0.7951E-02 0.3981E-08 0.3037E-02 0.4074E-08 0.1013E-01 0.4169E-08 0.4053E-02
0.4266E-08 0.5532E-02 0.4365E-08 0.1570E-02 0.4467E-08 0.1492E-01 0.4571E-08 0.1126E-01 0.4677E-08 0.4332E-02
0.4786E-08 0.2079E-02 0.4898E-08 0.2190E-02 0.5012E-08 0.5363E-03 0.5129E-08 0.1378E-02 0.5248E-08 0.1662E-01
0.5370E-08 0.7753E-02 0.5495E-08 0.1398E-01 0.5623E-08 0.5971E-02 0.5754E-08 0.4120E-02 0.5888E-08 0.2661E-03
0.6026E-08 0.1794E-01 0.6166E-08 0.1012E-01 0.6310E-08 0.7173E-02 0.6457E-08 0.1779E-02 0.6607E-08 0.4927E-02
0.6761E-08 0.3418E-03 0.6918E-08 0.5400E-02 0.7079E-08 0.3576E-02 0.7244E-08 0.4584E-01 0.7413E-08 0.7084E-02
0.7586E-08 0.2841E-02 0.7762E-08 0.3751E-02 0.7943E-08 0.1454E-01 0.8128E-08 0.2690E-02 0.8318E-08 0.3214E-02
0.8511E-08 0.6362E-02 0.8710E-08 0.3758E-02 0.8913E-08 0.4495E-02 0.9120E-08 0.1600E-01 0.9333E-08 0.1708E-01
0.9550E-08 0.2688E-02 0.9772E-08 0.8341E-02 0.1000E-07 0.4764E-02 0.1023E-07 0.3591E-02 0.1047E-07 0.8412E-03
0.1072E-07 0.4047E-03 0.1096E-07 0.7083E-03 0.1122E-07 0.1803E-01 0.1148E-07 0.7621E-02 0.1175E-07 0.1183E-01
0.1202E-07 0.3088E-02 0.1230E-07 0.5205E-02 0.1259E-07 0.3472E-03 0.1288E-07 0.3972E-02 0.1318E-07 0.2813E-02
0.1349E-07 0.3376E-02 0.1380E-07 0.1154E-01 0.1413E-07 0.2194E-02 0.1479E-07 0.1047E-01 0.1514E-07 0.1292E-01
0.1549E-07 0.4458E-02 0.1585E-07 0.8949E-02 0.1622E-07 0.1133E-02 0.1660E-07 0.1232E-02 0.1698E-07 0.8395E-02
0.1738E-07 0.4590E-02 0.1778E-07 0.9214E-02 0.1820E-07 0.4726E-03 0.1862E-07 0.5086E-03 0.1905E-07 0.3304E-02
0.1950E-07 0.8705E-02 0.1995E-07 0.6104E-02 0.2042E-07 0.1745E-02 0.2089E-07 0.2883E-03 0.2138E-07 0.1063E-01
0.2188E-07 0.1277E-02 0.2239E-07 0.7168E-03 0.2344E-07 0.1552E-02 0.2399E-07 0.5379E-02 0.2455E-07 0.8711E-03
0.2512E-07 0.2659E-02 0.2570E-07 0.1531E-02 0.2630E-07 0.6000E-04 0.2692E-07 0.4283E-02 0.2754E-07 0.2643E-02
0.2818E-07 0.2264E-02 0.2884E-07 0.4201E-03 0.2951E-07 0.6179E-02 0.3090E-07 0.2626E-02 0.3162E-07 0.5580E-02
0.3236E-07 0.1443E-02 0.3311E-07 0.8571E-03 0.3388E-07 0.1553E-02 0.3631E-07 0.2831E-02 0.3715E-07 0.5218E-03
0.3802E-07 0.1993E-02 0.3981E-07 0.2457E-03 0.3981E-07 0.5687E-03 0.4169E-07 0.1145E-02 0.4266E-07 0.6438E-03
0.4467E-07 0.2322E-02 0.4571E-07 0.4947E-03 0.4677E-07 0.2105E-03 0.5012E-07 0.4557E-03 0.5623E-07 0.1228E-02
0.5888E-07 0.1193E-02 0.6026E-07 0.1234E-03 0.6166E-07 0.6718E-03 0.6607E-07 0.2192E-03 0.6761E-07 0.1432E-02
235
0.4365E-10 0.8939E-04 0.4898E-10 0.1053E-03 0.5754E-10 0.2899E-04 0.6310E-10 0.1710E-07 0.6761E-10 0.5861E-07
0.9550E-10 0.5634E-03 0.1148E-09 0.7180E-03 0.1380E-09 0.3044E-03 0.1413E-09 0.9431E-03 0.1445E-09 0.1567E-06
0.1479E-09 0.2496E-03 0.1549E-09 0.3585E-03 0.1622E-09 0.1056E-02 0.1820E-09 0.2499E-03 0.1862E-09 0.9872E-04
0.1905E-09 0.9725E-03 0.1995E-09 0.5822E-07 0.2138E-09 0.1034E-06 0.2188E-09 0.9614E-07 0.2291E-09 0.1021E-02
0.2570E-09 0.1026E-02 0.2818E-09 0.4255E-05 0.2884E-09 0.8939E-04 0.2951E-09 0.2003E-03 0.3020E-09 0.3010E-02
0.3090E-09 0.1919E-02 0.3162E-09 0.5747E-06 0.3311E-09 0.1053E-03 0.3548E-09 0.2310E-02 0.3631E-09 0.2782E-02
0.3802E-09 0.2265E-04 0.3890E-09 0.2899E-04 0.3981E-09 0.8548E-05 0.4169E-09 0.4744E-04 0.4365E-09 0.9753E-03
0.4467E-09 0.4056E-04 0.4571E-09 0.4040E-02 0.4677E-09 0.8897E-05 0.4786E-09 0.8514E-03 0.4898E-09 0.3834E-02
0.5129E-09 0.3594E-02 0.5248E-09 0.9067E-06 0.5495E-09 0.2003E-03 0.5754E-09 0.4528E-02 0.5888E-09 0.8509E-03
0.6166E-09 0.3312E-02 0.6457E-09 0.5634E-03 0.6607E-09 0.3204E-02 0.6918E-09 0.1115E-02 0.7244E-09 0.4763E-02
0.7586E-09 0.4831E-02 0.7762E-09 0.7200E-03 0.7943E-09 0.1019E-03 0.8128E-09 0.3231E-02 0.8318E-09 0.5015E-02
0.8511E-09 0.3576E-05 0.8913E-09 0.1676E-02 0.9120E-09 0.1267E-03 0.9333E-09 0.8304E-04 0.9550E-09 0.4796E-02
0.9772E-09 0.1029E-01 0.1000E-08 0.8855E-03 0.1023E-08 0.1957E-05 0.1047E-08 0.7179E-03 0.1072E-08 0.2037E-03
0.1096E-08 0.1056E-02 0.1148E-08 0.7882E-02 0.1175E-08 0.6261E-02 0.1202E-08 0.3005E-02 0.1230E-08 0.2720E-03
0.1259E-08 0.2035E-02 0.1288E-08 0.1017E-02 0.1318E-08 0.3452E-04 0.1349E-08 0.7672E-03 0.1380E-08 0.6718E-02
0.1413E-08 0.7211E-02 0.1445E-08 0.1100E-02 0.1479E-08 0.5690E-02 0.1514E-08 0.3341E-02 0.1549E-08 0.1061E-01
0.1585E-08 0.3599E-02 0.1660E-08 0.2976E-02 0.1698E-08 0.3715E-02 0.1738E-08 0.2174E-05 0.1778E-08 0.4263E-02
0.1820E-08 0.2310E-02 0.1862E-08 0.1687E-01 0.1905E-08 0.3208E-02 0.1950E-08 0.1333E-02 0.1995E-08 0.4455E-03
0.2042E-08 0.3211E-02 0.2089E-08 0.2295E-03 0.2138E-08 0.1439E-01 0.2188E-08 0.1210E-02 0.2239E-08 0.4606E-02
0.2291E-08 0.5169E-02 0.2344E-08 0.8348E-02 0.2399E-08 0.1876E-01 0.2455E-08 0.1469E-02 0.2512E-08 0.3557E-03
0.2570E-08 0.3332E-02 0.2630E-08 0.1106E-01 0.2692E-08 0.7650E-02 0.2754E-08 0.4092E-02 0.2818E-08 0.5128E-02
0.2884E-08 0.6378E-02 0.2951E-08 0.3052E-02 0.3020E-08 0.4010E-02 0.3090E-08 0.4198E-02 0.3162E-08 0.1140E-01
0.3236E-08 0.2851E-02 0.3311E-08 0.4906E-02 0.3388E-08 0.2901E-02 0.3467E-08 0.4618E-02 0.3548E-08 0.7818E-03
0.3631E-08 0.1819E-02 0.3715E-08 0.1280E-02 0.3802E-08 0.1819E-01 0.3890E-08 0.1566E-01 0.3981E-08 0.5779E-02
0.4074E-08 0.4495E-02 0.4169E-08 0.3051E-02 0.4266E-08 0.1176E-03 0.4365E-08 0.6453E-02 0.4467E-08 0.2747E-01
0.4571E-08 0.1357E-01 0.4677E-08 0.4276E-02 0.4786E-08 0.1124E-01 0.4898E-08 0.1256E-01 0.5012E-08 0.1068E-03
0.5129E-08 0.1220E-01 0.5248E-08 0.2013E-05 0.5370E-08 0.1139E-01 0.5495E-08 0.1348E-01 0.5623E-08 0.4583E-02
0.5754E-08 0.9862E-02 0.5888E-08 0.1274E-01 0.6026E-08 0.1997E-02 0.6166E-08 0.1269E-01 0.6310E-08 0.7402E-02
0.6457E-08 0.1877E-02 0.6607E-08 0.4690E-02 0.6761E-08 0.1529E-02 0.6918E-08 0.1596E-01 0.7079E-08 0.1710E-02

0.7244E-08 0.1614E-01 0.7413E-08 0.5621E-02 0.7586E-08 0.1504E-01 0.7762E-08 0.1118E-02 0.7943E-08 0.9316E-02
0.8128E-08 0.2798E-02 0.8318E-08 0.1171E-01 0.8511E-08 0.1595E-02 0.8710E-08 0.8790E-02 0.8913E-08 0.1395E-01
0.9120E-08 0.1959E-01 0.9333E-08 0.2958E-02 0.9550E-08 0.1670E-01 0.9772E-08 0.1309E-01 0.1000E-07 0.1531E-01
0.1023E-07 0.4920E-02 0.1047E-07 0.3221E-02 0.1072E-07 0.5392E-02 0.1096E-07 0.2803E-02 0.1122E-07 0.1299E-01
0.1148E-07 0.1376E-01 0.1175E-07 0.5889E-04 0.1202E-07 0.5226E-02 0.1230E-07 0.5789E-02 0.1259E-07 0.5700E-02
0.1288E-07 0.1413E-01 0.1349E-07 0.1191E-01 0.1413E-07 0.1518E-01 0.1445E-07 0.5560E-02 0.1479E-07 0.4977E-02
0.1514E-07 0.1092E-02 0.1549E-07 0.9164E-02 0.1585E-07 0.3228E-03 0.1622E-07 0.4320E-02 0.1660E-07 0.2415E-01
0.1698E-07 0.6718E-03 0.1738E-07 0.3376E-02 0.1778E-07 0.6113E-02 0.1820E-07 0.1712E-02 0.1862E-07 0.7640E-02
0.1905E-07 0.9165E-02 0.1950E-07 0.3584E-02 0.1995E-07 0.7110E-03 0.2042E-07 0.7255E-02 0.2089E-07 0.1213E-01
0.2138E-07 0.2407E-02 0.2188E-07 0.5658E-02 0.2239E-07 0.5371E-02 0.2291E-07 0.4563E-03 0.2344E-07 0.2179E-02
0.2399E-07 0.9310E-02 0.2455E-07 0.4563E-02 0.2512E-07 0.1306E-04 0.2570E-07 0.3957E-02 0.2630E-07 0.1370E-02
0.2692E-07 0.1021E-02 0.2754E-07 0.2302E-02 0.2818E-07 0.2976E-02 0.2951E-07 0.1121E-01 0.3020E-07 0.5678E-03
0.3090E-07 0.2591E-02 0.3162E-07 0.2684E-02 0.3236E-07 0.1291E-02 0.3311E-07 0.5997E-04 0.3388E-07 0.3019E-02
0.3467E-07 0.6117E-02 0.3548E-07 0.3546E-02 0.3631E-07 0.8456E-03 0.3715E-07 0.9605E-03 0.3802E-07 0.3036E-02
0.3981E-07 0.2014E-02 0.4074E-07 0.3748E-03 0.4169E-07 0.6778E-03 0.4266E-07 0.1617E-02 0.4365E-07 0.1519E-02
0.4571E-07 0.2230E-02 0.4786E-07 0.1061E-02 0.5012E-07 0.4583E-03 0.5129E-07 0.1534E-02 0.5248E-07 0.8090E-03
0.5370E-07 0.6324E-03 0.5495E-07 0.3638E-04 0.5754E-07 0.3381E-04 0.6166E-07 0.2004E-02 0.6607E-07 0.6718E-03
0.6761E-07 0.5399E-03 0.7079E-07 0.8865E-03 0.7244E-07 0.2192E-03 0.7413E-07 0.3418E-03 0.7586E-07 0.2037E-03

Note that the distribution file is much larger, reflecting the large number of alternative hazard estimates.

Calculation of Frequency of Intersection for Kernel Density. The third approach to estimating the spatial density of volcanic events, $f(x,y)$, was to use kernel density estimates, defined by Equations (3-10) and (3-11). The required parameter is h the smoothing constant. Two approaches were used to define the parameter h . The first was for the expert to directly specify a distribution for h . Figure G-6 shows an example of the spatial density calculated using a Epanechnikov kernel with h set to 10 km. The stippled pattern encompasses the 95 percent density region.

For the case of an expert specified value of h , the annual frequency of intersection is calculated using program FKVH(v1.0). First, the program reads in the conditional probability of intersection values for the computation grid (the output of program CPDI). Then it reads in the discrete distributions for the volcanic event counts at each of the volcanic centers associated with the field. The program then uses nested loops to calculate all possible combinations of event counts associated with the field. For each possible event count a kernel density estimate of $f(x,y)$ is calculated using the specified kernel type and value of h . These spatial densities are combined with the three point distribution for the rate parameter calculated as described above. The program then performs the summation of Equation (G-1) for each rate parameter and spatial density estimate, given a specific set of events. Hidden event factors are then included in the same manner as in the calculations described above.

The following is a listing of example input and output files for program FKVH using the example shown of Figure G-6. The example presents only calculations for the homogeneous temporal model. Results for the nonhomogeneous Weibull process are obtained in exactly the same manner as in the use of program UZVH.

Input File: FKVH.IN

fk.in first individual source zone input file
 q q to quit

Input File: fk.IN

```

.\cpdi\examp.cpi output file from program CPDI
Epanechnikov kernel fix h of 10 km - homogeneous field calculation label
fk-h output file name
1 # of fields
Example Zone field label
'x' 'e' 10 1 1 0 zone boundary file for constraint of density function (x indicates no
constraint), kernel type (e - Epanechnikov, g - Gaussian), h for
major axis, unit variance for major axis of kernel, unit variance for minor
axis, azimuth of major axis
1 1 LN remaining parameters are the same as described above for input file
'x' UZ.IN used in program UZVH
1 1 NWCF
'invc.3'
1 1 SECF
'svc.4'
1 1 AG
'x'
1 1 SB
'x'
1 1 TM
'x'
1 1 BM
'x'
t 5000000 1.0 0 1 1.0 1.0
    
```

As before, the program produces three output files for each calculation.

Output File: FK-H.OUT

```

Epanechnikov kernel fix h of 10 km - homogeneous
Source SUM1 SUM2 SUM3 mambda mbeta sbeta
Example Zone 0.0000E+00 0.6123E-02 0.7261E-02 0.1509E-05 0.000 0.000
    
```

Output File: FK-H.HAZ

```

Epanechnikov kernel fix h of 10 km - homogeneous
3
1 0.0000000E+00 0.0000000E+00 0.0000000E+00 0.0000000E+00 0.0000000E+00 0.0000000E+00 0.0000000E+00
0.0000000E+00 0.0000000E+00 0.0000000E+00 0.0000000E+00 0.0000000E+00 0.0000000E+00
2 0.9241772E-08 0.2286762E-16 0.2999940E-23 0.2999940E-23 0.2999940E-23 0.2999940E-23 0.2999940E-23
0.2999940E-23 0.2999940E-23 0.2999940E-23 0.2999940E-23 0.2286762E-16
3 0.1096076E-07 0.3216559E-16 0.2459447E-23 0.2459447E-23 0.2459447E-23 0.2459447E-23 0.2459447E-23
0.2459447E-23 0.2459447E-23 0.2459447E-23 0.2459447E-23 0.2459447E-23 0.3216559E-16
    
```

Output File: FK-H.DST

```

Epanechnikov kernel fix h of 10 km - hom
3
1
0.0000E+00 0.1000E+01
3
0.2630E-08 0.1850E+00 0.8511E-08 0.6300E+00 0.1820E-07 0.1850E+00
3
0.3162E-08 0.1850E+00 0.1023E-07 0.6300E+00 0.2138E-07 0.1850E+00
    
```


g- Gaussian), starting value of h, density probability for zone boundary, minimization stopping tolerance, maximum number of iterations remaining parameters are the same as described above for input file UZ.IN used in program UZVH

```

1 1 LN
'X'
  1 1 NWCF
'nvc.3'
  1 1 SECF
'svc.4'
  1 1 AG
'X'
  1 1 SB
'X'
  1 1 TM
'X'
  1 1 BM
'X'
  t 5000000 1.0 0 1 1.0 1.0
    
```

As before, the program produces three output files for each calculation.

Output File: EK95-H.OUT

95% Epanechnikov kernel fit to Example Zone - homogeneous

Source	SUM1	SUM2	SUM3	mambda	mbeta	sbeta	mean H
Example Zone	0.0000E+00	0.3434E-04	0.1321E-02	0.1509E-05	0.000	0.000	5.215 0.000

Note the file lists the statistics of the fitted values of h

Output File: EK95-H.HAZ

95% Epanechnikov kernel fit to Example Zone - homogeneous

	1	2	3	4	5	6	7
1	0.0000000E+00						
2	0.5183692E-10	0.7194298E-21	0.0000000E+00	0.0000000E+00	0.0000000E+00	0.0000000E+00	0.0000000E+00
3	0.1994310E-08	0.1064867E-17	0.1084203E-24	0.1084203E-24	0.1084203E-24	0.1084203E-24	0.1084203E-24
4	0.1084203E-24	0.1084203E-24	0.1084203E-24	0.1084203E-24	0.1084203E-24	0.1064867E-17	

Output File: EK95-H.DST

95% Epanechnikov kernel fit to Example Z

	1	2	3	4	5	6
1	0.0000E+00	0.1000E+01				
2	0.1585E-10	0.1850E+00	0.4898E-10	0.6300E+00	0.1023E-09	0.1850E+00
3	0.5754E-09	0.1850E+00	0.1862E-08	0.6300E+00	0.3890E-08	0.1850E+00

G.2.3 Combined Hazard Calculation

The five computer programs described above calculate the frequency of intersection for specific sources and sets of parameters. The final calculation is to combine the contributions from all of the sources and calculate the hazard distribution over all of the possible models and parameters specified by the experts in their volcanic hazard model logic trees, and aggregate the distributions from all experts. This calculation is performed using computer program VHTREE(v1.0). The program consists of a set of nested loops that read in the discrete distributions for models and parameters defined by the experts and laid out in the sequence

presented on Figures 3-15 and 3-16. The program reads as input the weights assigned to the logic tree branches and the output files (with the extensions **.HAZ** and **.DST**) developed by the various calculation modules described above.

The input and output files for an example calculation are described below.

Input File: VHTREE.IN

```

Aggregated                                calculation label
'x' 'x' 'Expert' 'x' 'DLD' 'DAzm' 'TempM' 'TimeP' 'BG' 'SpaceM' 'ZoneM' 'ZoneB' 'AgeD' 'ZEgd' 'H' 'SRBase' 'SRFac' 'LW'
'NWCF' 'SECF' 'AV' 'SB' 'TM' 'BM' 'FP' 'OZEC' 'HE' 'Rate' labels for the levels of the logic tree
1 1                                        additional level of logic tree not used
1 1                                        additional level of logic tree not used
1 1 Experts                                # of experts, weight assigned to each expert
1 1 Source Types                            additional level of logic tree not used
1 1 Event Type                              # of event types, weight assigned to each event type
1 1 Dike Length Distribution                # of dike length distributions, weight assigned to each distribution
1 1 Dike Azimuth Distribution              # of dike azimuth distributions, weight assigned to each distribution
1 1 Temporal Model                         # of temporal models, weight assigned to each model
1 1 Time Period                            # of time periods, weight assigned to each time period
1 1 Backgrounds                            # of regions of interest, weight assigned to region
5 .2 .2 .2 .2 .2 Spatial Model            # of spatial models, weight assigned to each model
1 1 Zonation Model                          # of zonation models, weight assigned to each model
1 1 Zone Boundaries                        # of zone boundary alternatives, weight assigned to each alternative
1 sources                                  # of source for this spatial and zonation model
1 1 Age Dates                              # of age date sets, weight assigned to each date set
1 1 Zone Edge                              # of zone edge models, weight assigned to each model
1 1 H - Smoothing parameter                # of smoothing parameter values, weight assigned to each value
1 1 Source Rate Basis                      # of approaches to calculating zone event rate, weight assigned to
                                         each approach
1 1 Source Rate Factor                    # of source rate factors, weight assigned to each factor
.\haz\uz-h                                output fine name for first spatial model
1 1 Zonation Model                          remaining lines give the input for the other spatial models
1 1 Zone Boundaries
1 sources
1 1 Age Dates
1 1 Zone Edge
1 1 H - Smoothing parameter
1 1 Source Rate Basis
1 1 Source Rate Factor
.\haz\pf-h
1 1 Zonation Model
1 1 Zone Boundaries
1 sources
1 1 Age Dates
1 1 Zone Edge
1 1 H - Smoothing parameter
1 1 Source Rate Basis
1 1 Source Rate Factor
.\haz\fpf-h
1 1 Zonation Model
1 1 Zone Boundaries
1 sources
1 1 Age Dates
1 1 Zone Edge
1 1 H - Smoothing parameter
1 1 Source Rate Basis
1 1 Source Rate Factor
.\haz\fk-h
1 1 Zonation Model
1 1 Zone Boundaries
1 sources
    
```

- 1 1 Age Dates
- 1 1 Zone Edge
- 1 1 H - Smoothing parameter
- 1 1 Source Rate Basis
- 1 1 Source Rate Factor

.\haz\ek95-h

The program produces two primary output files.

Output File: VHTREE

total hazard:
 Aggregated

iz	enu	snu	cov	
1	0.2454167E-09	0.1016103E-08	4.140	mean, standard deviation, and coefficient of variation for the three event type measures (1 - point event, 2 - event centered dike, 3 - randomly placed dike)
2	0.6165958E-08	0.6064549E-08	0.984	
3	0.8670821E-08	0.7415725E-08	0.855	

Contributions to Variance in Hazard Rate

iz	cov	percent contribution to variance from:												
		Expert	DLD	DAzm	TempM	TimeP	BG	SpaceM	ZoneM	ZoneB	AgeD	ZEgd	H	
1	4.140	0.000	0.000	0.000	0.000	0.000	0.000	0.166	0.000	0.000	0.000	0.000	0.000	
2	0.984	0.000	0.000	0.000	0.000	0.000	0.000	0.318	0.000	0.000	0.000	0.000	0.000	
3	0.855	0.000	0.000	0.000	0.000	0.000	0.000	0.301	0.000	0.000	0.000	0.000	0.000	

SRBase	SRFac	LW	NWCF	SECF	AV	SB	TM	BM	FP	OZEC	HE	Rate
0.000	0.000	0.000	0.000	0.000	0.000	0.000	0.000	0.000	0.611	0.000	0.000	0.224
0.000	0.000	0.000	0.000	0.000	0.000	0.000	0.000	0.000	0.253	0.000	0.000	0.430
0.000	0.000	0.000	0.000	0.000	0.000	0.000	0.000	0.000	0.199	0.000	0.000	0.500

Breakdown of the total variance into the fraction arising from uncertainty at each level of the logic tree. In this example the only uncertainties are in the spatial model, the Gaussian field parameters, and the statistical uncertainty in the rate estimate.

Aggregated

probability levels calculated from distribution

iz	enu	snu	pl: 0.0500	0.1000	0.1500	0.2000	0.3000	0.4000	0.5000	0.6000
0.7000	0.8000	0.8500	0.9000	0.9500						
1	0.2463E-09	0.1017E-08	0.0000E+00							
0.8710E-10	0.1549E-09	0.1995E-09	0.3236E-09	0.1023E-08						
2	0.6158E-08	0.6057E-08	0.5248E-10	0.5248E-10	0.5248E-10	0.1023E-09	0.2512E-08	0.3715E-08	0.4677E-08	0.8511E-08
0.8511E-08	0.8511E-08	0.9772E-08	0.1514E-07	0.1820E-07						
3	0.8674E-08	0.7386E-08	0.8913E-09	0.1862E-08	0.1862E-08	0.2042E-08	0.3715E-08	0.5129E-08	0.6607E-08	0.1023E-07
0.1023E-07	0.1318E-07	0.1380E-07	0.1862E-07	0.2455E-07						

Fractiles of the discrete distribution for frequency of intersection

Output File: VHTREE.DST

Aggregated

3	
284	
0.0000E+00	0.6109E+00
0.4365E-11	0.1941E-03
0.4898E-11	0.4262E-05
0.5495E-11	0.1510E-03
0.3981E-11	0.3981E-11
0.1109E-02	0.1109E-02
0.4074E-11	0.4074E-11
0.2384E-02	0.2384E-02
0.4169E-11	0.4169E-11
0.2059E-02	0.2059E-02
0.4266E-11	0.4266E-11
0.2343E-03	0.2343E-03
0.4786E-11	0.4786E-11
0.1700E-03	0.1700E-03
0.5370E-11	0.5370E-11
0.8670E-06	0.8670E-06
0.6166E-11	0.6166E-11
0.4475E-05	0.4475E-05

0.6310E-11 0.3914E-06 0.6607E-11 0.6883E-05 0.6761E-11 0.4338E-07 0.7079E-11 0.2546E-06 0.7244E-11 0.1324E-02
0.7413E-11 0.8228E-03 0.7586E-11 0.4438E-06 0.7762E-11 0.9436E-03 0.7943E-11 0.7860E-04 0.8318E-11 0.4528E-05
0.8511E-11 0.5726E-05 0.8710E-11 0.1592E-04 0.8913E-11 0.2864E-03 0.9333E-11 0.6490E-04 0.9772E-11 0.6574E-03
0.1023E-10 0.8866E-03 0.1047E-10 0.2236E-03 0.1072E-10 0.1787E-04 0.1096E-10 0.5724E-05 0.1122E-10 0.2416E-03
0.1202E-10 0.6652E-04 0.1230E-10 0.2106E-04 0.1259E-10 0.2310E-04 0.1288E-10 0.6110E-03 0.1380E-10 0.1681E-05
0.1413E-10 0.1916E-02 0.1445E-10 0.1086E-04 0.1479E-10 0.6488E-03 0.1514E-10 0.5796E-05 0.1585E-10 0.2880E-06
0.1622E-10 0.2442E-02 0.1660E-10 0.2352E-04 0.1738E-10 0.4900E-04 0.1778E-10 0.2500E-04 0.1862E-10 0.1652E-04
0.1905E-10 0.7620E-04 0.1950E-10 0.1019E-02 0.1995E-10 0.5644E-08 0.2042E-10 0.9404E-04 0.2089E-10 0.1088E-02
0.2138E-10 0.6072E-08 0.2188E-10 0.6786E-05 0.2239E-10 0.2182E-02 0.2291E-10 0.5656E-04 0.2344E-10 0.1733E-04
0.2455E-10 0.3748E-02 0.2512E-10 0.5776E-03 0.2570E-10 0.5724E-03 0.2951E-10 0.1389E-05 0.3020E-10 0.1186E-02
0.3162E-10 0.6116E-03 0.3236E-10 0.2338E-02 0.3311E-10 0.1258E-03 0.3388E-10 0.7932E-04 0.3467E-10 0.6416E-03
0.3548E-10 0.1200E-04 0.3631E-10 0.3082E-03 0.3715E-10 0.2514E-03 0.3890E-10 0.3890E-10 0.2268E-02 0.3981E-10 0.2038E-04
0.4266E-10 0.7062E-03 0.4365E-10 0.1661E-04 0.4467E-10 0.4384E-04 0.4677E-10 0.8838E-03 0.4786E-10 0.6956E-04
0.4898E-10 0.1716E-03 0.5012E-10 0.6436E-03 0.5129E-10 0.3712E-01 0.5248E-10 0.2420E-04 0.5370E-10 0.1204E-03
0.5495E-10 0.5112E-03 0.5623E-10 0.1053E-03 0.5754E-10 0.1922E-07 0.5888E-10 0.3202E-03 0.6026E-10 0.9166E-04
0.6166E-10 0.4184E-02 0.6310E-10 0.2068E-07 0.6761E-10 0.6984E-03 0.6918E-10 0.1726E-03 0.7244E-10 0.4502E-02
0.7413E-10 0.5324E-03 0.7943E-10 0.8920E-04 0.8128E-10 0.6416E-03 0.8511E-10 0.2390E-03 0.8710E-10 0.2936E-02
0.9120E-10 0.4900E-04 0.9333E-10 0.2104E-02 0.9550E-10 0.2208E-02 0.9772E-10 0.4284E-03 0.1000E-09 0.2552E-03
0.1023E-09 0.2184E-02 0.1047E-09 0.1034E-03 0.1072E-09 0.1993E-02 0.1096E-09 0.1792E-03 0.1122E-09 0.5644E-08
0.1148E-09 0.3778E-03 0.1175E-09 0.2492E-03 0.1202E-09 0.1084E-02 0.1230E-09 0.6072E-08 0.1259E-09 0.2228E-03
0.1288E-09 0.2042E-04 0.1349E-09 0.2258E-03 0.1380E-09 0.4938E-03 0.1413E-09 0.1448E-02 0.1445E-09 0.1484E-03
0.1479E-09 0.2232E-02 0.1514E-09 0.4114E-03 0.1549E-09 0.1261E+00 0.1622E-09 0.2818E-03 0.1698E-09 0.5198E-03
0.1778E-09 0.8388E-03 0.1820E-09 0.2442E-02 0.1862E-09 0.4336E-03 0.1950E-09 0.8508E-06 0.1995E-09 0.1248E-02
0.2042E-09 0.5110E-03 0.2089E-09 0.1017E-02 0.2138E-09 0.9054E-03 0.2188E-09 0.1813E-02 0.2239E-09 0.5882E-03
0.2291E-09 0.2208E-05 0.2344E-09 0.5886E-04 0.2399E-09 0.6048E-03 0.2455E-09 0.1075E-03 0.2512E-09 0.1887E-02
0.2570E-09 0.2328E-03 0.2630E-09 0.4290E-02 0.2692E-09 0.3090E-03 0.2754E-09 0.7904E-03 0.2818E-09 0.4384E-04
0.2884E-09 0.2790E-03 0.3020E-09 0.3098E-02 0.3090E-09 0.2190E-02 0.3162E-09 0.1109E-02 0.3236E-09 0.3705E-01
0.3311E-09 0.9072E-04 0.3388E-09 0.3204E-02 0.3467E-09 0.4800E-03 0.3715E-09 0.8488E-03 0.3802E-09 0.1486E-02
0.3890E-09 0.1729E-03 0.4074E-09 0.3540E-03 0.4169E-09 0.6014E-03 0.4266E-09 0.2014E-03 0.4365E-09 0.3306E-03
0.4467E-09 0.2412E-02 0.4571E-09 0.5874E-03 0.4677E-09 0.6496E-03 0.5012E-09 0.6844E-03 0.5248E-09 0.7496E-04
0.5370E-09 0.4882E-03 0.5495E-09 0.3074E-02 0.5623E-09 0.6072E-04 0.5754E-09 0.2690E-03 0.5888E-09 0.8738E-03
0.6026E-09 0.1135E-02 0.6310E-09 0.9690E-04 0.6457E-09 0.2030E-02 0.6761E-09 0.3778E-02 0.7079E-09 0.4044E-03
0.7244E-09 0.1613E-02 0.7413E-09 0.2412E-03 0.7586E-09 0.2826E-03 0.7762E-09 0.1315E-02 0.7943E-09 0.3718E-02
0.8128E-09 0.2514E-03 0.8318E-09 0.4070E-03 0.8511E-09 0.7656E-03 0.8710E-09 0.3422E-03 0.8913E-09 0.2264E-02
0.9120E-09 0.5930E-04 0.9333E-09 0.1064E-02 0.9550E-09 0.6360E-03 0.9772E-09 0.2538E-02 0.1000E-08 0.5306E-03
0.1023E-08 0.1750E-02 0.1047E-08 0.2410E-03 0.1072E-08 0.2266E-03 0.1096E-08 0.4638E-03 0.1148E-08 0.5186E-03
0.1175E-08 0.2372E-03 0.1202E-08 0.4650E-03 0.1230E-08 0.1953E-02 0.1259E-08 0.4580E-03 0.1288E-08 0.2454E-03
0.1318E-08 0.3368E-02 0.1349E-08 0.3670E-03 0.1413E-08 0.8458E-03 0.1445E-08 0.1323E-02 0.1514E-08 0.2840E-03
0.1622E-08 0.2370E-02 0.1660E-08 0.2960E-03 0.1698E-08 0.1867E-02 0.1738E-08 0.1834E-03 0.1778E-08 0.2068E-03
0.1820E-08 0.2978E-03 0.1862E-08 0.2036E-02 0.1905E-08 0.4938E-03 0.1950E-08 0.1773E-03 0.1995E-08 0.1017E-03
0.2042E-08 0.8486E-03 0.2089E-08 0.2298E-03 0.2138E-08 0.3928E-03 0.2188E-08 0.2528E-02 0.2291E-08 0.6296E-03
0.2344E-08 0.1705E-03 0.2399E-08 0.1375E-02 0.2455E-08 0.2678E-03 0.2512E-08 0.4384E-04 0.2570E-08 0.5734E-03
0.2630E-08 0.5464E-04 0.2692E-08 0.1542E-02 0.2754E-08 0.4744E-03 0.2818E-08 0.6662E-03 0.2884E-08 0.4824E-03
0.2951E-08 0.1773E-03 0.3020E-08 0.7624E-03 0.3162E-08 0.5744E-03 0.3236E-08 0.5438E-03 0.3311E-08 0.1404E-02
0.3388E-08 0.1416E-02 0.3548E-08 0.9500E-03 0.3631E-08 0.2492E-03 0.3802E-08 0.1444E-02 0.3890E-08 0.7878E-03
0.3981E-08 0.5318E-03 0.4169E-08 0.4518E-03 0.4266E-08 0.1678E-02 0.4571E-08 0.6456E-04 0.4677E-08 0.6778E-03
0.4786E-08 0.1475E-03 0.4898E-08 0.4096E-05 0.5012E-08 0.1004E-03 0.5129E-08 0.2826E-03 0.5248E-08 0.7276E-05
0.5623E-08 0.6098E-03 0.5754E-08 0.2710E-03 0.5888E-08 0.2838E-03 0.6166E-08 0.1416E-03 0.6457E-08 0.1137E-03
0.6607E-08 0.9922E-04 0.6761E-08 0.1375E-03 0.6918E-08 0.5040E-03 0.7079E-08 0.1691E-03 0.7244E-08 0.7190E-04
0.7413E-08 0.2570E-03 0.7586E-08 0.5332E-03 0.7762E-08 0.8362E-03 0.7943E-08 0.4700E-03 0.8128E-08 0.3184E-03
0.8318E-08 0.2314E-03 0.8710E-08 0.5286E-03 0.8913E-08 0.1327E-03 0.9120E-08 0.9220E-03 0.9550E-08 0.6038E-03
0.1175E-07 0.1288E-03 0.1259E-07 0.8332E-04 0.1585E-07 0.1319E-03 0.1622E-07 0.2468E-04 0.1660E-07 0.3138E-03
0.1698E-07 0.4384E-04 0.1862E-07 0.1552E-03 0.1950E-07 0.1344E-03 0.1995E-07 0.1773E-03
271
0.7244E-11 0.1788E-04 0.7762E-11 0.2106E-04 0.9120E-11 0.5798E-05 0.1413E-10 0.6088E-04 0.1514E-10 0.3420E-08
0.1549E-10 0.1127E-03 0.1622E-10 0.7170E-04 0.1698E-10 0.6074E-08 0.1820E-10 0.1436E-03 0.1862E-10 0.3700E-01
0.1995E-10 0.1974E-04 0.2344E-10 0.4992E-04 0.2630E-10 0.1788E-04 0.3020E-10 0.2096E-03 0.3388E-10 0.2110E-03
0.3802E-10 0.5798E-05 0.3890E-10 0.1945E-03 0.4074E-10 0.3838E-03 0.4365E-10 0.4992E-04 0.4571E-10 0.2042E-03
0.4786E-10 0.5326E-07 0.4898E-10 0.4890E-03 0.5129E-10 0.1923E-07 0.5248E-10 0.1260E+00 0.5888E-10 0.4010E-04
0.6761E-10 0.1700E-03 0.8511E-10 0.1127E-03 0.8710E-10 0.1003E-02 0.8913E-10 0.6074E-08 0.9333E-10 0.8510E-06
0.9550E-10 0.1436E-03 0.1000E-09 0.1181E-02 0.1023E-09 0.3700E-01 0.1096E-09 0.1149E-06 0.1148E-09 0.6624E-03
0.1230E-09 0.1067E-06 0.1259E-09 0.1305E-05 0.1288E-09 0.1702E-03 0.1318E-09 0.4992E-04 0.1349E-09 0.3692E-03
0.1380E-09 0.6958E-03 0.1413E-09 0.1813E-06 0.1445E-09 0.8268E-06 0.1479E-09 0.3592E-06 0.1549E-09 0.2420E-03
0.1585E-09 0.1945E-03 0.1738E-09 0.2076E-05 0.1778E-09 0.3252E-03 0.1820E-09 0.2056E-03 0.1862E-09 0.2208E-05
0.1905E-09 0.6652E-04 0.2089E-09 0.4096E-05 0.2138E-09 0.3996E-03 0.2239E-09 0.4174E-04 0.2344E-09 0.7278E-05
0.2399E-09 0.1945E-03 0.2512E-09 0.6764E-05 0.2570E-09 0.2110E-03 0.2630E-09 0.1227E-02 0.2692E-09 0.4992E-04
0.2754E-09 0.5626E-03 0.2884E-09 0.2042E-03 0.3020E-09 0.2952E-05 0.3162E-09 0.1574E-02 0.3311E-09 0.7170E-03
0.3388E-09 0.4992E-04 0.3467E-09 0.3914E-06 0.3715E-09 0.4050E-04 0.3981E-09 0.6408E-03 0.4074E-09 0.4442E-05

0.4169E-09 0.1260E-03 0.4266E-09 0.1256E-02 0.4365E-09 0.2506E-03 0.4467E-09 0.9190E-06 0.4571E-09 0.7204E-03
0.4677E-09 0.1224E-05 0.4786E-09 0.2206E-04 0.4898E-09 0.1481E-05 0.5012E-09 0.1629E-02 0.5129E-09 0.8678E-03
0.5370E-09 0.3534E-04 0.5495E-09 0.5304E-03 0.5623E-09 0.2334E-04 0.5888E-09 0.1010E-02 0.6166E-09 0.8680E-03
0.6310E-09 0.8510E-06 0.6457E-09 0.2468E-04 0.6607E-09 0.4992E-04 0.6761E-09 0.4806E-03 0.6918E-09 0.7258E-03
0.7079E-09 0.4384E-04 0.7244E-09 0.1450E-03 0.7413E-09 0.6564E-04 0.7586E-09 0.2042E-04 0.7762E-09 0.1071E-02
0.7943E-09 0.3642E-04 0.8128E-09 0.1489E-03 0.8318E-09 0.7780E-03 0.8511E-09 0.5480E-05 0.8710E-09 0.8186E-04
0.8913E-09 0.2484E-02 0.9120E-09 0.3692E-03 0.9333E-09 0.1306E-02 0.9550E-09 0.1095E-03 0.9772E-09 0.1262E-05
0.1000E-08 0.7158E-04 0.1047E-08 0.1531E-02 0.1072E-08 0.2636E-02 0.1096E-08 0.2554E-03 0.1122E-08 0.5320E-03
0.1148E-08 0.2216E-03 0.1175E-08 0.7928E-03 0.1202E-08 0.1202E-08 0.1230E-08 0.1230E-08 0.1230E-08 0.5986E-03
0.1288E-08 0.2182E-02 0.1318E-08 0.2356E-03 0.1349E-08 0.4392E-03 0.1380E-08 0.8764E-03 0.1413E-08 0.1347E-02
0.1445E-08 0.3745E-01 0.1479E-08 0.2442E-02 0.1514E-08 0.1227E-03 0.1585E-08 0.8822E-04 0.1622E-08 0.1348E-02
0.1660E-08 0.3030E-02 0.1698E-08 0.6260E-03 0.1738E-08 0.1088E-02 0.1778E-08 0.2360E-03 0.1820E-08 0.2340E-03
0.1862E-08 0.1031E-02 0.1905E-08 0.1919E-02 0.1950E-08 0.5324E-07 0.1995E-08 0.2284E-02 0.2042E-08 0.9690E-04
0.2089E-08 0.8404E-04 0.2138E-08 0.3044E-03 0.2188E-08 0.2158E-03 0.2239E-08 0.3494E-02 0.2291E-08 0.5740E-03
0.2344E-08 0.9758E-05 0.2399E-08 0.2940E-03 0.2455E-08 0.8808E-03 0.2512E-08 0.3488E-02 0.2570E-08 0.6634E-03
0.2630E-08 0.7413E-01 0.2692E-08 0.3990E-03 0.2754E-08 0.7794E-03 0.2818E-08 0.1383E-02 0.2884E-08 0.2678E-02
0.2951E-08 0.2492E-03 0.3020E-08 0.4798E-02 0.3090E-08 0.1350E-02 0.3162E-08 0.2106E-03 0.3236E-08 0.3140E-03
0.3311E-08 0.2080E-02 0.3388E-08 0.2452E-02 0.3467E-08 0.1694E-02 0.3548E-08 0.5404E-03 0.3631E-08 0.2940E-02
0.3715E-08 0.2786E-02 0.3802E-08 0.7568E-03 0.3890E-08 0.1590E-02 0.3981E-08 0.6074E-03 0.4074E-08 0.2026E-02
0.4169E-08 0.8106E-03 0.4266E-08 0.1106E-02 0.4365E-08 0.3140E-03 0.4467E-08 0.2984E-02 0.4571E-08 0.2252E-02
0.4677E-08 0.1269E+00 0.4786E-08 0.4158E-03 0.4898E-08 0.4380E-03 0.5012E-08 0.1073E-03 0.5129E-08 0.2756E-03
0.5248E-08 0.3324E-02 0.5370E-08 0.1551E-02 0.5495E-08 0.2796E-02 0.5623E-08 0.1194E-02 0.5754E-08 0.8240E-03
0.5888E-08 0.5322E-04 0.6026E-08 0.3588E-02 0.6166E-08 0.2024E-02 0.6310E-08 0.1435E-02 0.6457E-08 0.3558E-03
0.6607E-08 0.9854E-03 0.6761E-08 0.6836E-04 0.6918E-08 0.1080E-02 0.7079E-08 0.7152E-03 0.7244E-08 0.9168E-03
0.7413E-08 0.1417E-02 0.7586E-08 0.5682E-03 0.7762E-08 0.7502E-03 0.7943E-08 0.2908E-02 0.8128E-08 0.5380E-02
0.8318E-08 0.6428E-03 0.8511E-08 0.2533E+00 0.8710E-08 0.7516E-03 0.8913E-08 0.8990E-03 0.9120E-08 0.3200E-02
0.9333E-08 0.3416E-02 0.9550E-08 0.5376E-03 0.9772E-08 0.3867E-01 0.1000E-07 0.9528E-03 0.1023E-07 0.7182E-03
0.1047E-07 0.1682E-03 0.1072E-07 0.8094E-04 0.1096E-07 0.1417E-03 0.1122E-07 0.3606E-02 0.1148E-07 0.1524E-02
0.1175E-07 0.2366E-02 0.1202E-07 0.6176E-03 0.1230E-07 0.1041E-02 0.1259E-07 0.6944E-04 0.1288E-07 0.7944E-03
0.1318E-07 0.5626E-03 0.1349E-07 0.6752E-03 0.1380E-07 0.2308E-02 0.1413E-07 0.4388E-03 0.1479E-07 0.2094E-02
0.1514E-07 0.2584E-02 0.1549E-07 0.8916E-03 0.1585E-07 0.1790E-02 0.1622E-07 0.2266E-03 0.1660E-07 0.2464E-03
0.1698E-07 0.1679E-02 0.1738E-07 0.9180E-03 0.1778E-07 0.3884E-01 0.1820E-07 0.3709E-01 0.1862E-07 0.1017E-03
0.1905E-07 0.6608E-03 0.1950E-07 0.1741E-02 0.1995E-07 0.1221E-02 0.2042E-07 0.3490E-03 0.2089E-07 0.5766E-04
0.2138E-07 0.2126E-02 0.2188E-07 0.2554E-03 0.2239E-07 0.1434E-03 0.2344E-07 0.3399E-03 0.2399E-07 0.1076E-02
0.2455E-07 0.1742E-03 0.2512E-07 0.5318E-03 0.2570E-07 0.3062E-03 0.2630E-07 0.1200E-04 0.2692E-07 0.8566E-03
0.2754E-07 0.5286E-03 0.2818E-07 0.4528E-03 0.2884E-07 0.8402E-04 0.2951E-07 0.1236E-02 0.3090E-07 0.5252E-03
0.3162E-07 0.1116E-02 0.3236E-07 0.2886E-03 0.3311E-07 0.1714E-03 0.3388E-07 0.3106E-03 0.3631E-07 0.5662E-03
0.3715E-07 0.1044E-03 0.3802E-07 0.3986E-03 0.3981E-07 0.4914E-04 0.4074E-07 0.1137E-03 0.4169E-07 0.2290E-03
0.4266E-07 0.1288E-03 0.4467E-07 0.4644E-03 0.4571E-07 0.9894E-04 0.4677E-07 0.4210E-04 0.5012E-07 0.9114E-04
0.5623E-07 0.2456E-03 0.5888E-07 0.2386E-03 0.6026E-07 0.2468E-04 0.6166E-07 0.1344E-03 0.6607E-07 0.4384E-04
0.6761E-07 0.2864E-03

237

0.4677E-10 0.1788E-04 0.5248E-10 0.2106E-04 0.6166E-10 0.5798E-05 0.6761E-10 0.3420E-08 0.7244E-10 0.1172E-07
0.9550E-10 0.1127E-03 0.1148E-09 0.1436E-03 0.1380E-09 0.6088E-04 0.1413E-09 0.1886E-03 0.1445E-09 0.3134E-07
0.1479E-09 0.4992E-04 0.1549E-09 0.7170E-04 0.1622E-09 0.2112E-03 0.1820E-09 0.4998E-04 0.1862E-09 0.1974E-04
0.1905E-09 0.1945E-03 0.1995E-09 0.1164E-07 0.2138E-09 0.2068E-07 0.2188E-09 0.1923E-07 0.2291E-09 0.2042E-03
0.2570E-09 0.2052E-03 0.2818E-09 0.8510E-06 0.2884E-09 0.1788E-04 0.2951E-09 0.4006E-04 0.3020E-09 0.6020E-03
0.3090E-09 0.3838E-03 0.3162E-09 0.1149E-06 0.3311E-09 0.2106E-04 0.3548E-09 0.4620E-03 0.3631E-09 0.5564E-03
0.3802E-09 0.4530E-05 0.3890E-09 0.5798E-05 0.3981E-09 0.1710E-05 0.4169E-09 0.9488E-05 0.4365E-09 0.1951E-03
0.4467E-09 0.8112E-05 0.4571E-09 0.8080E-03 0.4677E-09 0.1779E-05 0.4786E-09 0.1703E-03 0.4898E-09 0.7668E-03
0.5129E-09 0.7188E-03 0.5248E-09 0.1813E-06 0.5495E-09 0.4006E-04 0.5754E-09 0.3791E-01 0.5888E-09 0.1702E-03
0.6166E-09 0.6624E-03 0.6457E-09 0.1127E-03 0.6607E-09 0.6408E-03 0.6918E-09 0.2230E-03 0.7244E-09 0.9526E-03
0.7586E-09 0.9662E-03 0.7762E-09 0.1440E-03 0.7943E-09 0.2038E-04 0.8128E-09 0.6462E-03 0.8318E-09 0.1003E-02
0.8511E-09 0.7152E-06 0.8913E-09 0.3352E-03 0.9120E-09 0.2534E-04 0.9333E-09 0.1661E-04 0.9550E-09 0.9592E-03
0.9772E-09 0.2058E-02 0.1000E-08 0.1771E-03 0.1023E-08 0.3914E-06 0.1047E-08 0.1436E-03 0.1072E-08 0.4074E-04
0.1096E-08 0.2112E-03 0.1148E-08 0.1576E-02 0.1175E-08 0.1252E-02 0.1202E-08 0.6010E-03 0.1230E-08 0.5440E-04
0.1259E-08 0.4070E-03 0.1288E-08 0.2034E-03 0.1318E-08 0.6904E-05 0.1349E-08 0.1534E-03 0.1380E-08 0.1344E-02
0.1413E-08 0.1442E-02 0.1445E-08 0.2200E-03 0.1479E-08 0.1138E-02 0.1514E-08 0.6682E-03 0.1549E-08 0.2122E-02
0.1585E-08 0.7198E-03 0.1660E-08 0.5952E-03 0.1698E-08 0.7430E-03 0.1738E-08 0.4348E-06 0.1778E-08 0.8526E-03
0.1820E-08 0.4620E-03 0.1862E-08 0.1294E+00 0.1905E-08 0.6416E-03 0.1950E-08 0.2666E-03 0.1995E-08 0.8910E-04
0.2042E-08 0.3764E-01 0.2089E-08 0.4590E-04 0.2138E-08 0.2878E-02 0.2188E-08 0.2420E-03 0.2239E-08 0.9212E-03
0.2291E-08 0.1034E-02 0.2344E-08 0.1670E-02 0.2399E-08 0.3752E-02 0.2455E-08 0.2938E-03 0.2512E-08 0.7114E-04
0.2570E-08 0.6664E-03 0.2630E-08 0.2212E-02 0.2692E-08 0.1530E-02 0.2754E-08 0.8184E-03 0.2818E-08 0.1026E-02
0.2884E-08 0.1276E-02 0.2951E-08 0.6104E-03 0.3020E-08 0.8020E-03 0.3090E-08 0.8396E-03 0.3162E-08 0.3928E-01
0.3236E-08 0.5702E-03 0.3311E-08 0.9812E-03 0.3388E-08 0.5802E-03 0.3467E-08 0.9236E-03 0.3548E-08 0.1564E-03
0.3631E-08 0.3638E-03 0.3715E-08 0.2560E-03 0.3802E-08 0.3638E-02 0.3890E-08 0.4013E-01 0.3981E-08 0.1156E-02
0.4074E-08 0.3790E-01 0.4169E-08 0.6102E-03 0.4266E-08 0.2352E-04 0.4365E-08 0.1291E-02 0.4467E-08 0.5494E-02
0.4571E-08 0.2714E-02 0.4677E-08 0.8552E-03 0.4786E-08 0.2248E-02 0.4898E-08 0.2512E-02 0.5012E-08 0.2136E-04

0.5129E-08 0.2440E-02 0.5248E-08 0.4026E-06 0.5370E-08 0.2278E-02 0.5495E-08 0.2696E-02 0.5623E-08 0.9166E-03
0.5754E-08 0.1972E-02 0.5888E-08 0.2548E-02 0.6026E-08 0.3994E-03 0.6166E-08 0.2538E-02 0.6310E-08 0.1480E-02
0.6457E-08 0.3754E-03 0.6607E-08 0.1269E+00 0.6761E-08 0.3058E-03 0.6918E-08 0.3192E-02 0.7079E-08 0.3420E-03
0.7244E-08 0.3228E-02 0.7413E-08 0.1124E-02 0.7586E-08 0.3008E-02 0.7762E-08 0.2236E-03 0.7943E-08 0.1863E-02
0.8128E-08 0.5596E-03 0.8318E-08 0.2342E-02 0.8511E-08 0.3190E-03 0.8710E-08 0.1758E-02 0.8913E-08 0.2790E-02
0.9120E-08 0.3918E-02 0.9333E-08 0.5916E-03 0.9550E-08 0.3340E-02 0.9772E-08 0.2618E-02 0.1000E-07 0.3062E-02
0.1023E-07 0.1270E+00 0.1047E-07 0.6442E-03 0.1072E-07 0.1078E-02 0.1096E-07 0.5606E-03 0.1122E-07 0.2598E-02
0.1148E-07 0.2752E-02 0.1175E-07 0.1178E-04 0.1202E-07 0.1045E-02 0.1230E-07 0.1158E-02 0.1259E-07 0.1140E-02
0.1288E-07 0.2826E-02 0.1318E-07 0.1260E+00 0.1349E-07 0.2382E-02 0.1380E-07 0.3700E-01 0.1413E-07 0.3036E-02
0.1445E-07 0.1112E-02 0.1479E-07 0.9954E-03 0.1514E-07 0.2184E-03 0.1549E-07 0.1833E-02 0.1585E-07 0.6456E-04
0.1622E-07 0.8640E-03 0.1660E-07 0.4830E-02 0.1698E-07 0.1344E-03 0.1738E-07 0.6752E-03 0.1778E-07 0.1223E-02
0.1820E-07 0.3424E-03 0.1862E-07 0.1528E-02 0.1905E-07 0.1833E-02 0.1950E-07 0.7168E-03 0.1995E-07 0.1422E-03
0.2042E-07 0.1451E-02 0.2089E-07 0.2426E-02 0.2138E-07 0.3748E-01 0.2188E-07 0.1132E-02 0.2239E-07 0.1074E-02
0.2291E-07 0.9126E-04 0.2344E-07 0.4358E-03 0.2399E-07 0.1862E-02 0.2455E-07 0.9126E-03 0.2512E-07 0.2612E-05
0.2570E-07 0.7914E-03 0.2630E-07 0.2740E-03 0.2692E-07 0.2042E-03 0.2754E-07 0.3746E-01 0.2818E-07 0.5952E-03
0.2951E-07 0.2242E-02 0.3020E-07 0.1136E-03 0.3090E-07 0.5182E-03 0.3162E-07 0.5368E-03 0.3236E-07 0.2582E-03
0.3311E-07 0.1199E-04 0.3388E-07 0.6038E-03 0.3467E-07 0.1223E-02 0.3548E-07 0.7092E-03 0.3631E-07 0.1691E-03
0.3715E-07 0.1921E-03 0.3802E-07 0.6072E-08 0.3981E-07 0.4028E-03 0.4074E-07 0.7496E-04 0.4169E-07 0.1356E-03
0.4266E-07 0.3234E-03 0.4365E-07 0.3038E-03 0.4571E-07 0.4460E-03 0.4786E-07 0.2122E-03 0.5012E-07 0.9166E-04
0.5129E-07 0.3068E-03 0.5248E-07 0.1618E-03 0.5370E-07 0.1265E-03 0.5495E-07 0.7276E-05 0.5754E-07 0.6762E-05
0.6166E-07 0.4008E-03 0.6607E-07 0.1344E-03 0.6761E-07 0.1080E-03 0.7079E-07 0.1773E-03 0.7244E-07 0.4384E-04
0.7413E-07 0.6836E-04 0.7586E-07 0.4074E-04

The discrete distributions for frequency of intersection in the same format used for each of the calculation modules listed above.

G.3 REFERENCE

Press, W.H., Flannery, B.P., Teukolsky, S.A., and Vetterling, W.T., 1992, Numerical Recipes, the Art of Scientific Computing, Cambridge University Press, 818 p.

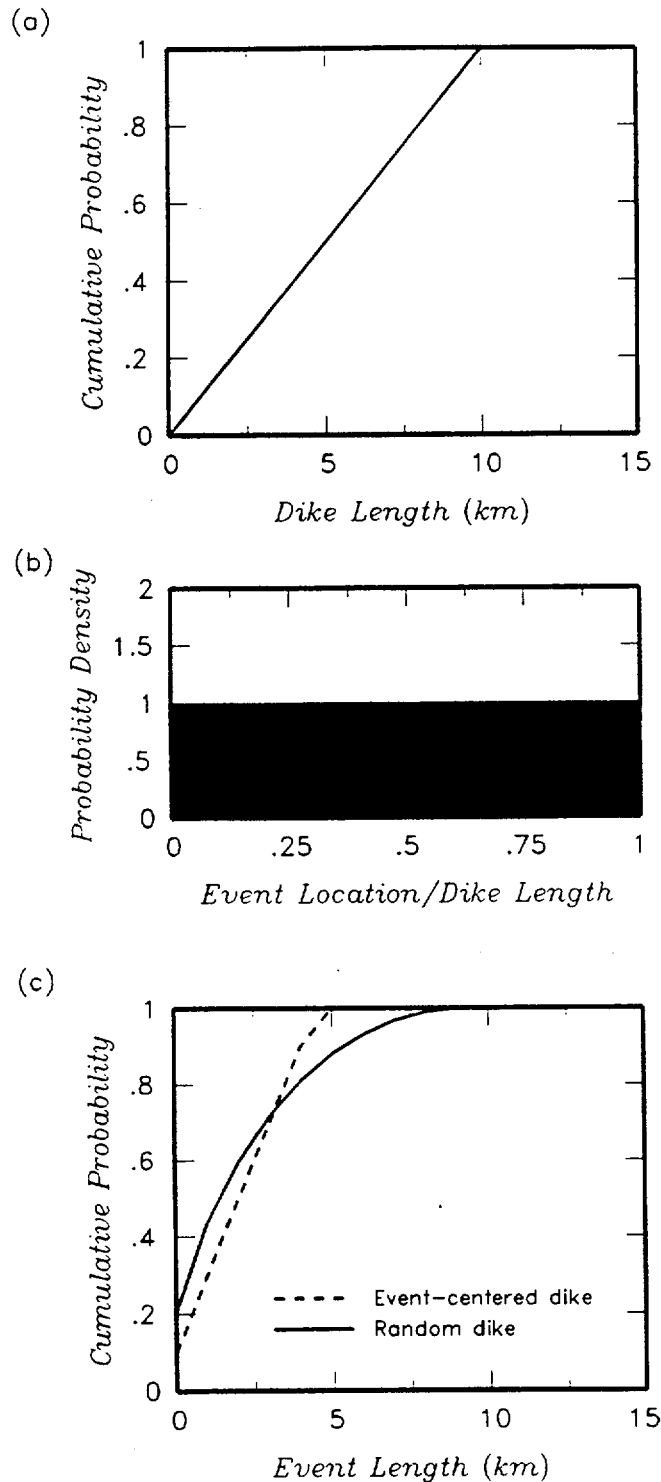


Figure G-1 Development of event length distributions. (a) Expert specified cumulative distribution for total dike length. (b) Expert specified distribution for location of point event on dike. (c) Derived distributions for event length.

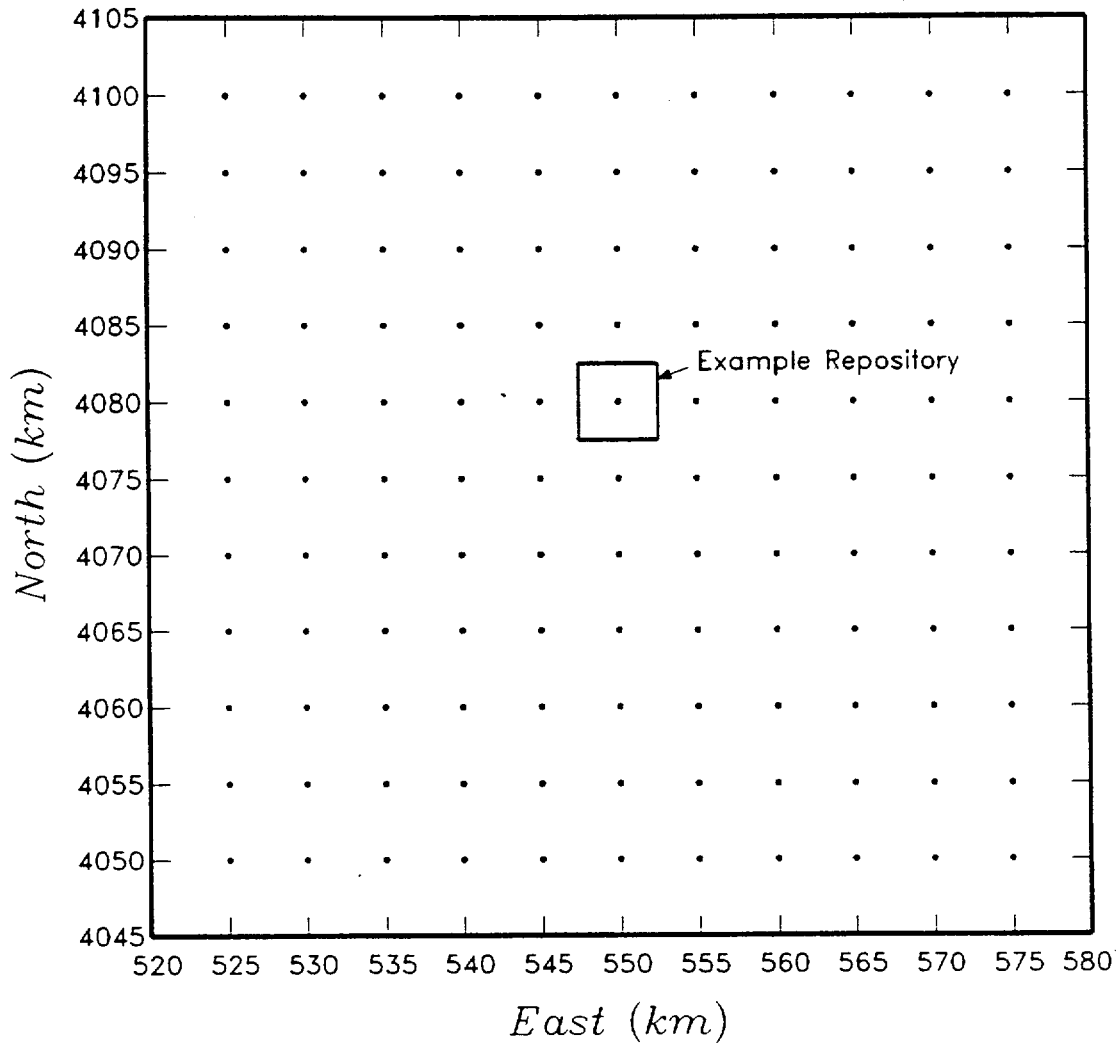


Figure G-2 Example calculation grid with $\Delta x = \Delta y = 5$ km.

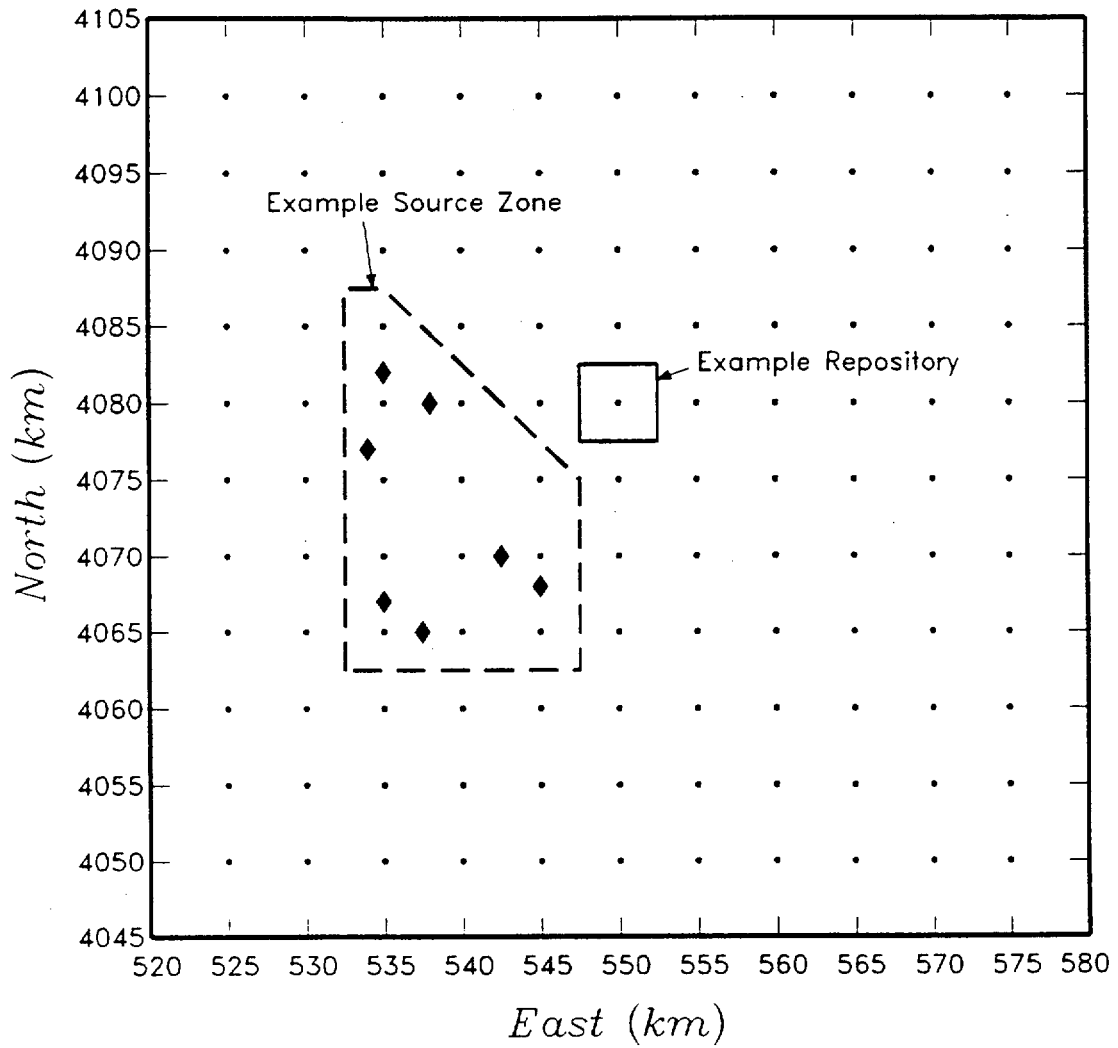


Figure G-3 Example source zone. Diamonds show locations of events, separated into a northern group of three and a southern group of four.

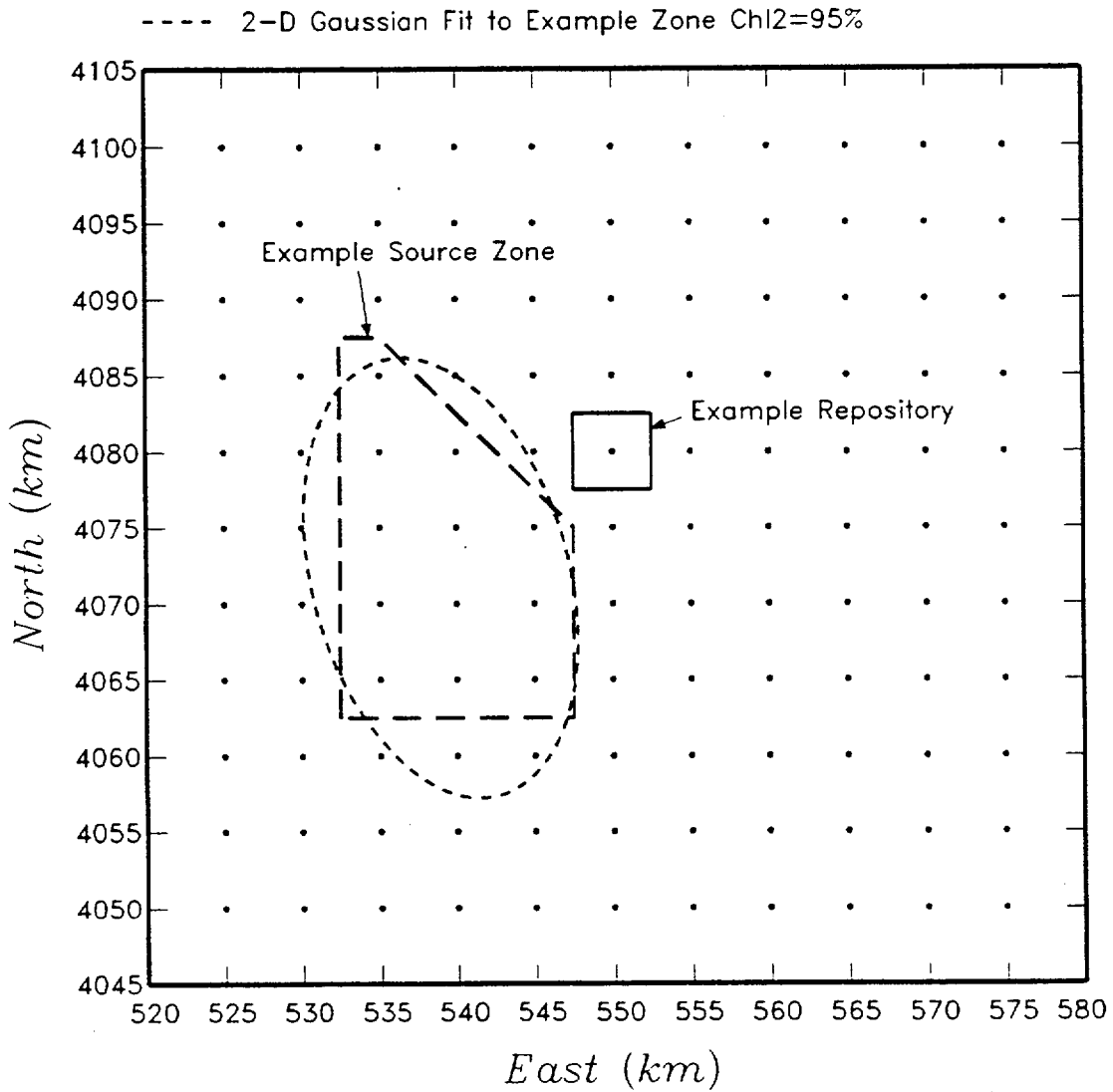


Figure G-4 Fit of a bivariate Gaussian field shape to the example source zone boundary assuming the boundary is an approximate 95 percent density contour.

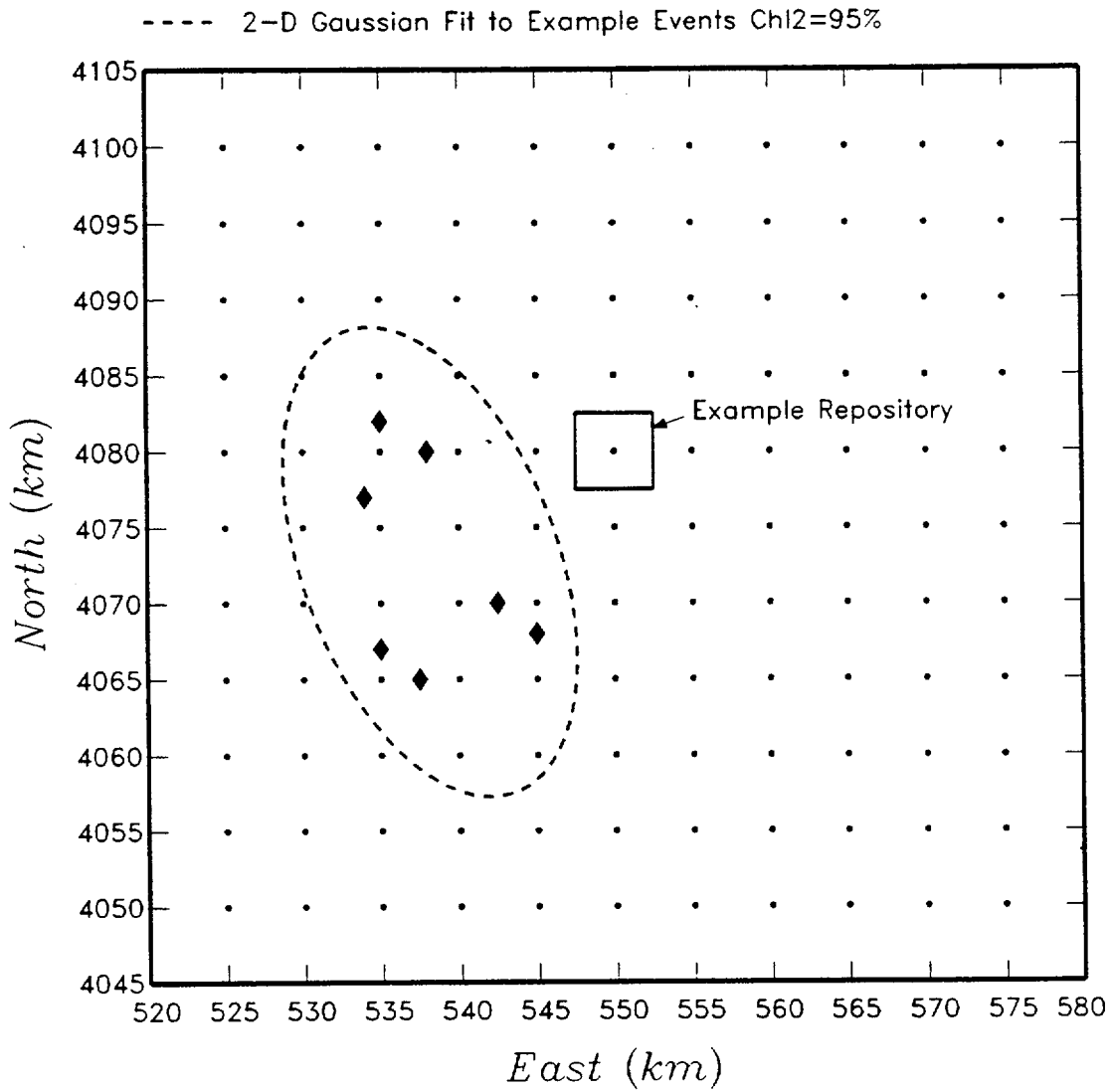


Figure G-5 Fit of a bivariate Gaussian field shape to the events shown on Figure G-3. The ellipse defines the 95-percent density contour.

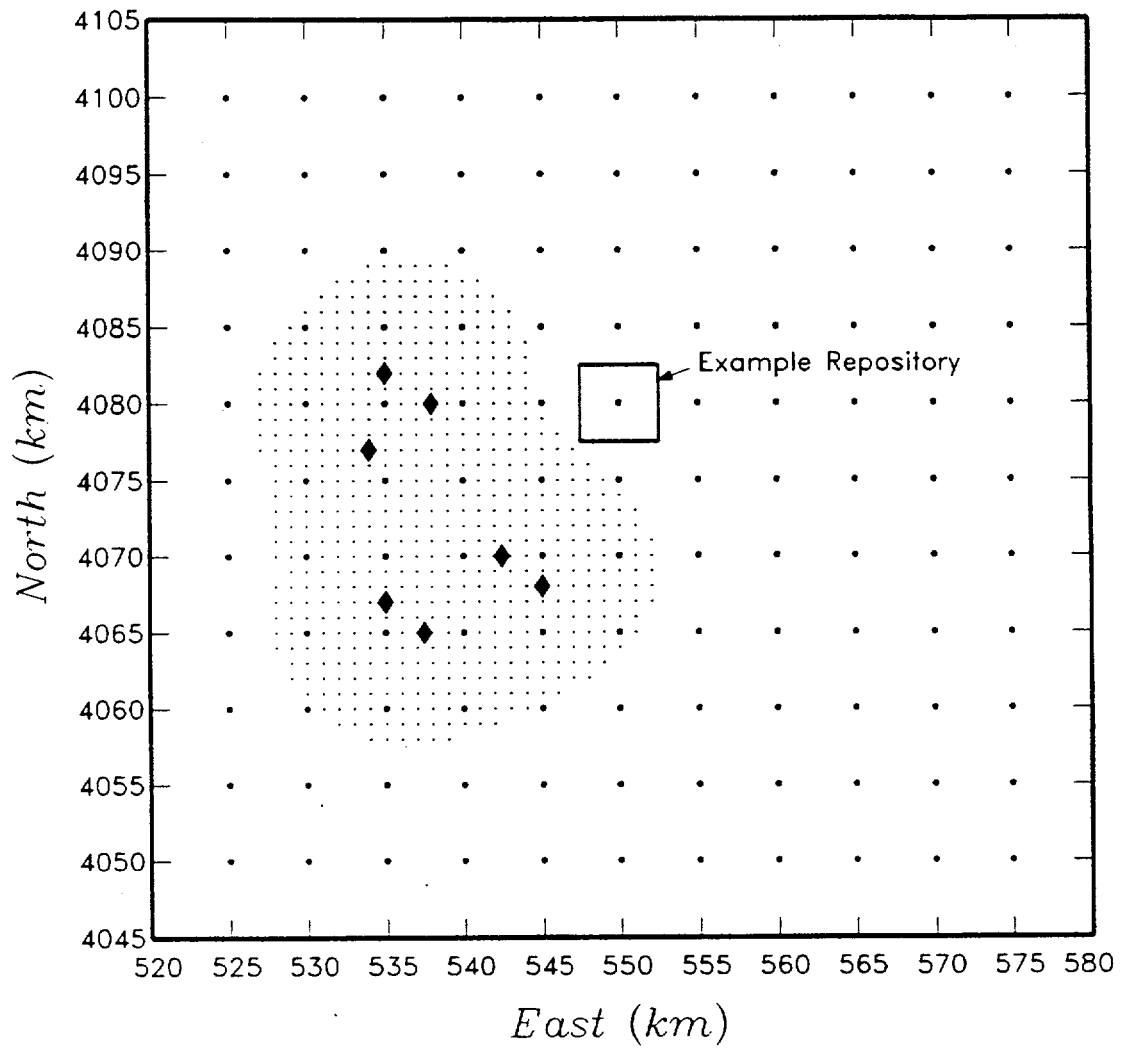


Figure G-6 Example kernel density estimation with fixed h . Stippled area defines the 95 percent density contour computed with an Epanechnikov kernel and $h = 10$ km.

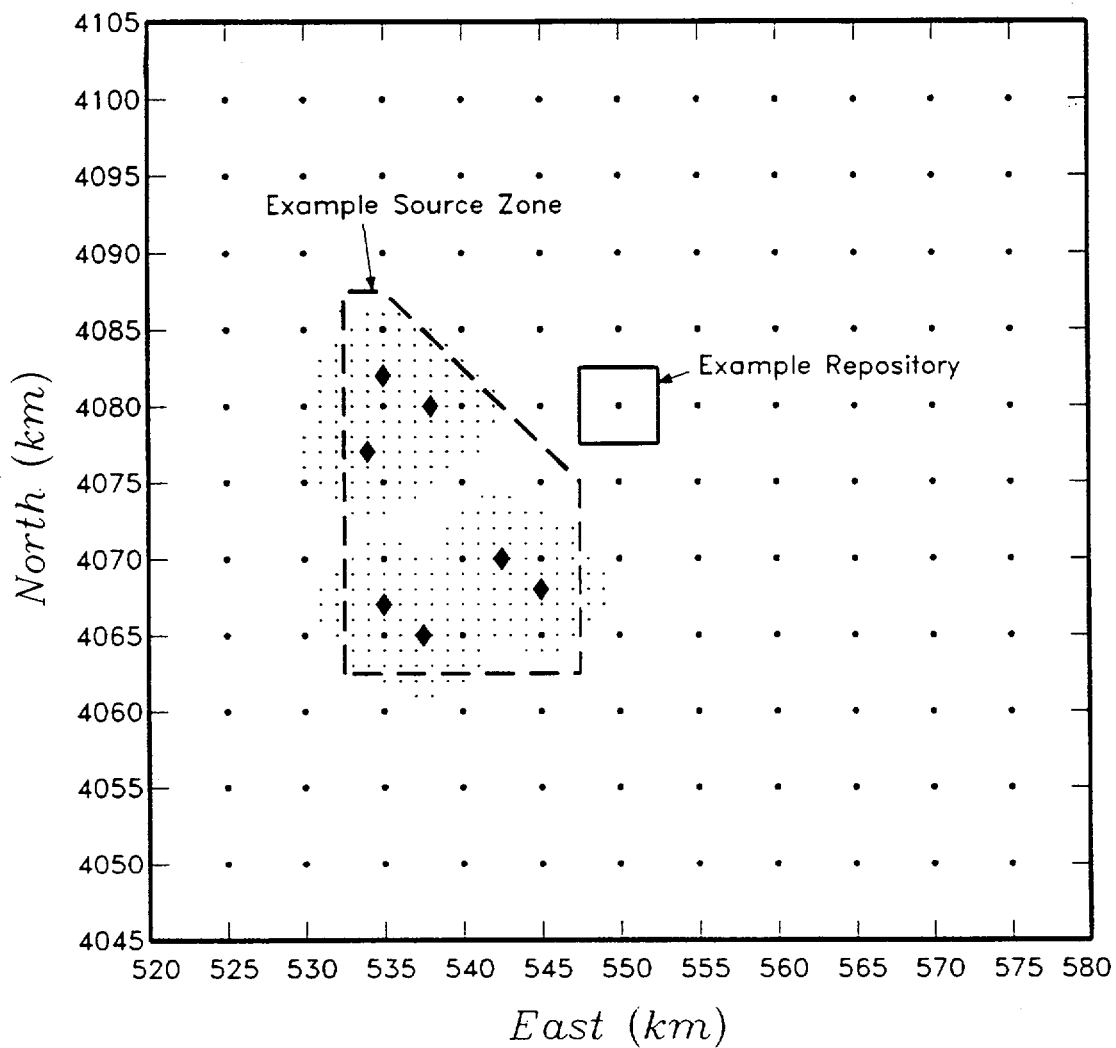


Figure G-7 Fit of a kernel density function to the example source zone boundary assuming the boundary is an approximate 95 percent density contour. The resulting value of h is 5.2 km.

APPENDIX H
QUALITY ASSURANCE

APPENDIX H QUALITY ASSURANCE

The OCRWM Quality Assurance program is applicable to this document. Preparation of the document was consistent with Civilian Radioactive Waste Management System Management and Operating Contractor (M&O) Quality Administrative Procedure (QAP) QAP-3-5, Revision 6, "Development of Technical Documents." This procedure defines the requirements for preparation of technical documents that are subject to the requirements of the Quality Assurance Requirements and Description (QARD; DOE/RW-0333P, Revision 5). QAP-3-5 is the QA program vehicle used to control and document the PVHA task. This appendix to the Probabilistic Volcanic Hazard Analysis (PVHA) presents the relevant discussion of the QA program requirements from Section 5.2.C of the procedure which are not specifically addressed in other sections of the document.

An M&O QAP-2-0, "Control of Activities," Activity Evaluation was prepared specifically for the PVHA task and is maintained as a controlled document under Document Identifier B00000000-01717-2200-00112. This Activity Evaluation described the purpose of the PVHA, evaluated the applicability of the QARD, and established the procedures that applied to this task. "Classification of Permanent Items," M&O QAP-2-3, does not apply to this activity since the report does not address any permanent items as defined under this procedure. No determination of importance evaluations were necessary under M&O Nevada Line Procedure (NLP) NLP-2-0 as the PVHA involved only analysis of existing data which was generated during previous activities.

Qualification of PVHA Inputs and Outputs

Section 5.2.C.4 of QAP-3-5 requires identification of unqualified design input and data. As is summarized in Section 2.1.1 of the report, the required inputs for the PVHA task are any available pertinent or corroborating data, regardless of source. The sources of all input used in

the PVHA are identified as standard scientific bibliographic citations in the references sections. The data themselves do not provide an interpretation of the volcanic hazard at the site. Rather, it is the expert elicitation process that evaluates, integrates and interprets the data (inputs), and results in a qualified analysis of the hazard. Therefore, it is unnecessary to discriminate between qualified data and unqualified data in this report.

As discussed in Section 2.1.2, formal guidance for the expert elicitation process has been developed and established, and the methods have been successfully applied in other comparable analyses. The expert elicitation methods developed and applied in this analysis are clearly and carefully documented in Section 2.0 of the report.

The purpose of the expert elicitation was to characterize uncertainties in the hazard analysis. The results of the PVHA describe the expected annual frequency of a volcanic event intersecting the potential Mined Geological Disposal System repository footprint. Despite variations in interpretations and analytical assumptions between the experts, the hazard estimates are consistent among the experts.